Concurrent Aeroservoelastic Design and Optimization of Wind Turbines

Tibaldi, Carlo

Publication date:
2015

Document Version
Publisher's PDF, also known as Version of record

Concurrent Aeroservoelastic Design and Optimization of Wind Turbines

Carlo Tibaldi

DTU Wind Energy

January 2015

Author: Carlo Tibaldi

Title: Concurrent aeroservoelastic design and optimization of wind turbines

Department: DTU Wind Energy

This dissertation is submitted to the Technical University of Denmark, in partial fulfillment of the requirements for the obtainment of the PhD degree from the PhD School DTU Wind Energy.
The PhD project was carried out in the years 2011-2015 at the Aeroelastic Design Section of DTU Wind Energy, Department of Wind Energy (formerly RisøDTU, Wind Energy Department). The dissertation was submitted in January 2015.

Main Supervisor:
Christian Bak, DTU Wind Energy
Co-Supervisor:
Lars C. Henriksen, DTU Wind Energy

DTU Wind Energy
PhD-0059(EN)
January 2015

ISBN:978-87-93278-79-0

pages: 193
tables: 2
figures: 23
references: 62

Technical University of Denmark
DTU Wind Energy
RisøCampus
Frederiksborgvej 399
Building 114
DK-4000 Roskilde
tlbl@dtu.dk
www.vindenergi.dtu.dk

Abstract

This work develops and investigates methods to integrate controllers in the wind turbine design process and to perform wind turbine optimization. These techniques can exploit the synergy between wind turbine components and generate new design solutions.

Two frameworks to perform wind turbine optimization design are presented. These tools handle workflows to model a wind turbine and to evaluate loads and performances under specific conditions.

Three approaches to evaluate loads are proposed and integrated in the optimization codes. The first method is based on time domain simulations, the second exploits a linear model to evaluate fatigue damage loads in frequency domain, and the third allows avoiding resonant conditions that could lead to excessive fatigue damage. The first technique exploits nonlinear time domain aeroservoelastic simulations, here computed with HAWC2, and the other two approaches are based on a high-order aeroservoelastic linear model implemented in HAWCStab2. The limitations and advantages of each method are illustrated and discussed.

Methods to systematically tune wind turbine controllers are improved and presented. This work focuses on basic controllers for wind turbine regulation under normal operation, therefore no controller for load reduction is considered. The approaches presented are based on a pole-placement technique and loads minimization. Two methods allow the tuning of the proportional integral gains of the pitch controller. A third approach, based on time domain simulations, allows the selection of any controller parameter.

The methods to evaluate loads and the pole-placement technique are then employed to carry out wind turbine optimization design from an aeroservoelastic prospective. Several analysis of the NREL 5 MW Reference Wind Turbine and the DTU 10 MW Reference Wind Turbine are carried out to illustrate the validity and limitations of these approaches. In some of the test cases, the method reduces the blade mass and increases the annual energy production.

Resumé

I dette arbejde er metoder udviklet og undersøgt for at integrere styringer i vindmølle design processen og til at udføre vindmølleoptimering. Disse teknikker kan udnytte synergien mellem vindmøllekomponenter og generere nye designs.

To simuleringsværktøjer til at optimere vindmøller med præsenteres. Disse værktøjer håndterer workflows til at modellere en vindmølle og evaluere belastninger og ydeevne under særlige betingelser.

Tre metoder til at vurdere belastninger foreslås og integreres i optimeringsværktøjerne. Den første metode er baseret på tidsdomæne simuleringer, den anden udnytter en lineær model til evaluering udmattelses- belastninger i frekvens domænet, og den tredje undgår resonans, der kan føre til større udmattelsesskader. Den første teknik udnytter ulineære tidsdomæne aeroservoelastiske simuleringer, her beregnet med HAWC2, og de to andre fremgangsmåder er baseret på en højere-ordens aeroservoelastisk lineær model implementeret i HAWCStab2. Begrænsninger og fordele ved hver metode er illustreret og diskuteret.

Metoder til systematisk at tune en vindmøllestyring forbedres og vises. Dette arbejde fokuserer kun på grundlæggende styringer til vindmølleregulering under normal drift. Metoderne er baseret på pol-placerings teknik og belastninger, der er evalueret i tids- og frekvensdomænet. Pol-placeringen og frekvensdomæne metoden tillader tuning af proportional og integral leddene i forstærkningen af pitch-styringen. Tidsdomæne metoden gør det muligt at udvælge enhver styrings parameter.

De beskrevne metoder anvendes derefter til at udføre optimeringer på vindmøller. Flere analyser af NREL 5 MW Reference Wind Turbine og DTU 10 MW reference Wind Turbine udføres for at vise styrkerne og svaghederne ved hver af disse metoder.

Preface

This dissemination is submitted to the Technical University of Denmark, in partial fulfillment of the requirements for the obtainment of the PhD degree from the PhD School DTU Wind Energy. The PhD project was carried out from November 2011 till January 2015 at the Aeroelastic Design Section of the Department of Wind Energy at DTU. The project has been supervised by Senior Scientist Morten Hartvig Hansen from the beginning till January 2013 and by Christian Bak from February 2013 till the end of the project. Co-supervision has been carried-out by Scientist Lars Henriksen.

The dissertation is organized as a collection of papers. The first part of the thesis gives a synopsis of the investigation. The second part contains a collection of seven papers and one report. All the publications are part of the dissertation, and they illustrate in detail the methods developed during the project and the results.

During the PhD studies I have followed courses for 30 ECTS. I took part in one commercial project, I taught at two courses concerning the linear aeroservoelastic stability tool HAWCStab2, and I contributed to the controller lesson of the aeroelastic code HAWC2 on-line course. I attended and presented part of my work at the TORQUE 2012 conference, the 32nd ASME Wind Energy Symposium at the AIAA SciTech 2014 conference, the Vestas-ASCE research symposium in 2012, and the 8th PhD Seminar on Wind Energy in Europe in 2012. From mid January 2014 till mid April 2014 I visited the National Wind Technology Center of the National Renewable Energy Laboratory (NREL) in Boulder Colorado, USA, as part of my external research stay.

A list of publications that I contributed to during the last three years follows below. Only the publications with a boldface reference are part of the dissertation and are included in the second part of the thesis. These boldface references are used in the synopsis.

List of publications

Peer-reviewed articles

- [**Article I**] Tibaldi C, Kim T, Larsen TJ, Rasmussen F, de Rocca Serra R, Sanz F. An investigation on wind turbine resonant vibrations. *Under Review* 2014;

- [**Article II**] Tibaldi C, Henriksen L, Hansen MH, Bak C. Wind turbine fatigue damage evaluation based on a linear model and a spectral method. *Under Review* 2014;

- [**Article III**] Tibaldi C, Hansen MH, Henriksen LC. Optimal tuning for a classical wind turbine controller. *In Proceedings of the Science of Making Torque from Wind 2012*, Oldenburg, Germany, 2012.

Conference articles

- [**Article IV**] Tibaldi C, Henriksen LC, Hansen MH, Bak C. Effects of gain-scheduling methods in a classical wind turbine controller on wind turbine aero-servo-elastic modes and loads. *32nd ASME Wind Energy Symposium*. American Institute of Aeronautics and Astronautics, 2014, doi: 10.2514/6.2014 − 0873.

- [**Article V**] Tibaldi C, Henriksen LC, Bak C. Investigation of the dependency of wind turbine loads on the simulation time. *European Wind Energy Conference and Exhibition 2014, EWEA* 2014.

- [**Article VI**] Tibaldi C, Hansen MH, Henriksen LC. Concurrent aero-servo-elastic design of a wind turbine operating in partial load region. *In Proceedings of 8th PhD Seminar on Wind Energy in Europe*, ETH Zurich, Switzerland, 2012.

- [**Article VII**] Zahle F, Tibaldi C, Verelst DR, Bak C, Bitsche R, Blasques JP Aero-Elastic Optimization of a 10 MW Wind Turbine *33rd ASME Wind Energy Symposium*. American Institute of Aeronautics and Astronautics, 2015, doi: 10.2514/6.2015 − 0491.

- Pavese C, Tibaldi C, Kim T. Controller tuning of wind turbines with backward swept blades *33rd ASME Wind Energy Symposium*. American Institute of Aeronautics and Astronautics, 2015, doi: 10.2514/6.2015 − 1211.

Reports

- **[Report I]** Tibaldi C, Hansen MH, Zhale F Methods for systematic tuning of wind turbine controllers DTU Wind Energy Report.

- The Light Rotor project, EUDP-2010-I: Final Report. Edited by Bak C, Zahle F. DTU Wind Energy Report.

Contents

Part I

Synopsis

CHAPTER 1

Introduction

To increase the competitiveness of wind energy, as a source of electricity in the global market, an ongoing effort has been spent to reduce its cost of energy. As a result of this, the size of wind turbines has significantly increased in the last decade, leading to a high level of system complexity.

Despite the large design improvements during the recent years, it is believed, that new methods and approaches are required to obtain a significant further enhancements. Therefore, new design techniques are currently under investigation.

A promising method to reduce the cost of energy is the design of wind turbines with a holistic approach. Wind turbines are composed of several different subsystems that are traditionally designed independently. This procedure suggests to design wind turbines as a single comprehensive system, where several components are designed at the same time, within the same process. The method captures and exploits the high interaction between the different components improving their design within the system. This approach is expected to generate new design solutions and identify different trade-offs in components design. As a result of this, a further reduction in the cost of energy should be achieved.

On modern variable-speed pitch regulated wind turbines, controllers are an essential part of the system because they are responsible for regulating the turbine to operate within an operational envelope. Controllers need to be tuned according to the desired performances of the specific wind turbine. Different tunings can generate significantly different wind turbine dynamic responses and therefore different loads on the structure. These dependencies make the wind turbine and the controller design subject to each other.

The state-of-the-art design approach consists of few iterations between the rotor design and the tuning of the controller. These processes are performed in series as two independent design procedures. One reason for this separation is the difference in the modeling details needed in aeroelastic design and control design. The former usually requires a highly detailed description of the structural and aerodynamic components of the turbine, while the latter is normally based on low order models to guarantee low computational time. However, the state-of-the-art design approach can limit the overall wind turbine performance due to the insufficient ability to capture the synergy between the aeroelastic and the controller systems.

A concurrent design of the rotor and the controller is expected to improve the design of the two systems leading to a reduction in the cost of energy. With a holistic approach each change of the rotor design would generate a suited controller tuning and vice versa, ensuring that the right gains are selected for each design evaluation. Figure 1.1 gives a schematic representation of the differences between the state-of-the-art approach (left side) and the new holistic approach (right side).

To integrate the controller and the rotor design, methods to systematically tune the controller are required, and a framework to perform the holistic optimization design needs to be developed.

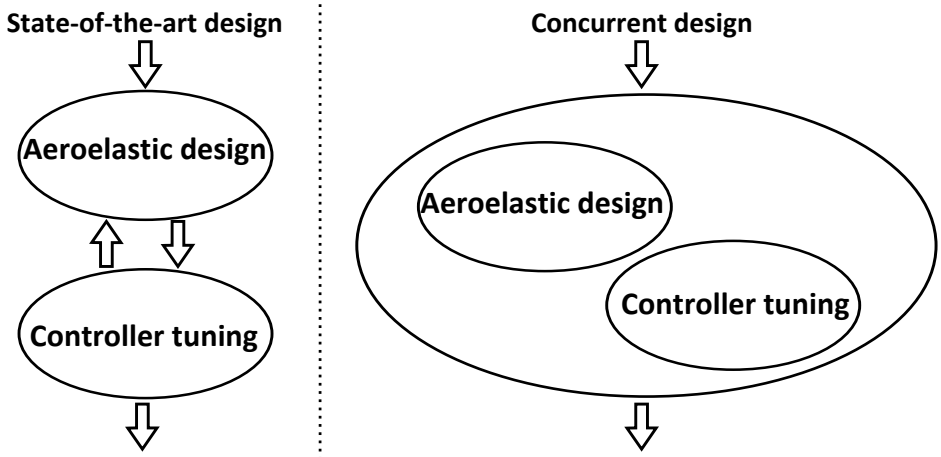

Figure 1.1: Diagram representing the state-of-the-art design approach with iterations performed in series (left) and the concurrent design approach (right).

1.1 Controller design

Wind turbines controllers have been investigated extensively in the last years, and several controller strategies and algorithms for wind turbine regulations have been proposed, see for instance Leithead et al. [1], Leith and Leithead [2], Wright and Fingersh [3], Bottasso and Croce [4], Henriksen et al. [5], and Bossanyi et al. [6]. Despite the existence of advanced controller strategies, basic proportional integral (PI) controllers are still the most used.

Once the controller architecture is selected, the controller design consists of the controller tuning. Tuning a controller means that gains and parameters of the controller have to be selected to obtain the desired performances.

Tuning of a controller is not a straightforward process due to contrasting results of the gains. It is always necessary to identify a trade-off according to the requirements. For instance, when tuning the pitch controller, a compromise between tower loads and rotor speed regulation needs to be identified because an aggressive controller leads to high loads and low rotor speed variations and a milder controller generates lower tower loads but higher rotor speed oscillations. Controllers can significantly alter dampings of wind turbine modes, and a wrong tuning can even lead to instabilities, as shown by Riziotis et al. [7, 8], Buhl et al. [9], and Markou et al. [10].

Tuning a PI controllers can be performed using several methods, among them pole-placement technique, tuning by means of optimization procedures, and trial-and error approaches.

Pole-placement methods have the advantage of being model based, therefore they are based on a physical system. In these methods, the gains are selected to set the frequency and damping of the dynamic response of a simplified model of the controlled system to desired values. However, simplified models are not always available or easy to obtain.

Øye, in the work by Hansen et al. [11], proposes a single degree of freedom wind turbine model to perform the pole-placement and therefore tune a controller.

Trial and error approaches require several iterations and can also be very time consuming depending on the type of the controller and the number of tuning parameters. To improve the selection of the controller parameters, tuning by means of numerical optimization has been investigated in previous works.

In the work by Hansen et al. [11] the gains of a classical PI controller are computed to minimize the standard deviation of the blade root flapwise bending moment. The load is evaluated with several simulations at different mean wind speeds above rated. In the investigation a reduction of the standard deviation of the blade root flapwise bending moment up to 2% is achieved.

Bottasso and Croce [4] describe an approach to perform a goal-oriented optimization of the tuning parameters. In their work they describe a possible coupling between an optimization and an aeroservoelastic software. They also focus on the multi-objective nature of the tuning problem showing two approaches, one based on a combined scalar objective function and one based on a multi-objective Pareto-front optimization.

Ashuri et al. [12] developed a framework to perform concurrent wind turbine aeroservoelastic design by means of numerical optimization. In the investigation the design variables include controller parameters for different operational regions, blade twist, and servo-motor performances. The quality of the solutions is evaluated with a scalar cost function that represents the cost of energy based on annual energy production and fatigue loads computed with time-domain aeroelastic simulations.

1.2 Wind turbine optimization design

The first relevant works on wind turbine optimization design are described by Fuglsang [13], Selig and Coverstone-Carrol [14], and Fuglsang and Madsen [15].

Further developments of the first generation approaches can be found in Fuglsang and Madsen [16] and Fuglsang and Thomsen [17]. In this method, the blade shape design is addressed taking into account aerodynamic calculations, structural calculations, time-domain aeroelastic calculations, extreme loads calculation, and estimation of aerodynamic noise. To reduce the computational effort, a semi-empirical method to compute the gradients and a wind turbine model with 20 degrees of freedom is used. The method shows relevant reductions in the cost of energy, even if it relies on simple models and assumptions. In a test case, the cost of energy of a 1.5 MW stall regulated wind turbine is reduced.

Fuglsang et al. [18] developed a method for site-specific wind turbine design. The method is based on time domain aeroelastic simulations. To limit the computational time, the number of load cases and the simulation length are reduced. The reduction of the cases is performed selecting only those simulations that generate design-driving loads. A check on the simulations to consider, among a larger set, is performed every five iterations.

Bottasso et al. [19] present a design framework that includes aerodynamic and detailed structural design. The method assumes that the wind turbine aeroelastic loads do not change significantly for small changes in the structural design. This assumption allows to split the aeroelastic load evaluation and the structural optimization in two nested design loops, and thereby to avoid the computation of the aeroelastic loads for each structural parameter variation.

The method can therefore evaluate a large set of design load cases without compromising significantly the computational time. Bottasso et al. [20] apply the design method from the previous work to perform a parametric investigation where they identify a trade-off between active and passive load control. This work gives a first and clear idea of the potential of concurrent aeroservoelastic design.

Ashuri et al. [21] present a framework that can address aerodynamic and structural design. The method is based on a multidisciplinary feasible architecture that couples different tools. The framework does not include any nested design loop or model simplification, therefore, to contain the computational time, the number of load cases evaluated is limited to 72 simulations. The cases include normal operation and extreme conditions. The method uses 14 parallel computational nodes to speed up the computation. The controller tuning is not included in the work.

Merz et al. [22] developed a method to perform fast computation based on frequency domain load calculations, for stall-regulated wind turbines. Their work focuses on the aerodynamic modeling and the linearization of the dynamic stall model. The rotating turbulence power spectra are computed from Fourier transformations of analytical correlation functions. Deterministic contributions, e.g. wind shear and tower shadow, are added afterwards to the spectra as spikes at the multiple frequencies of the rotational speed frequency. The structural model, used for the analysis, is composed of an isolated blade rigidly mounted at the root and rotating at a fixed rotational speed. The Dirlik's method is then used to estimate the fatigue damage based on the power spectra. The method presented by Merz is then used in [23, 24] to design three different multi-megawatt stall-regulated wind turbines. The assumptions made in the model allow to estimate loads only on one blade. Furthermore, the model cannot handle variations in the rotational speed, torsional deformations, large blade deflections, controller dynamic and interactions between the wind turbine components.

Fischer et al. [25] presents a framework to perform aerodynamic and structural blade design. The tool parametrizes the airfoils that are evaluated with a panel code. Loads are then retrieved with a Blade Element Momentum code and fed into a structural code to estimate blade mass and stiffness. No structural deflections are considered. A Multi-Objective Tabu Search is used to solve an optimization problem with 16 design variables.

1.3 Scope and outline

The scope of the investigation is to develop methods to integrate the controller into the wind turbine design and hence overcome the limitations of the serial state-of-the-art design approach. The focus is on developing tools to perform wind turbine optimization design suitable for concurrent aeroservoelastic design and to demonstrate the potential of these new methods in reducing the cost of energy.

The contributions of this work can be divided into:

- development of optimization frameworks to perform concurrent design;
- development of methods to estimate wind turbine loads tailored to optimization design applications;
- extension of techniques to systematically tune wind turbine controllers;
- analysis of wind turbine response in open and closed loop.

The controller used in the investigation is based on a classical algorithm, therefore, no advanced controllers or controllers for load mitigation are addressed in this dissertation. However, some of the methods developed can be directly applied to any type of controller without significant changes.

The definition of an accurate cost function is outside the scope of this project. Different cost functions have been used during the project depending on the application and the information available at that moment. The connection between these models and the actual cost of energy has not been established. For this reason, the test cases that are illustrated later in the dissertation do not, as such, result in a new design, but they aim at showing the potential and capabilities of these design techniques. Furthermore, when results from optimizations are presented, no emphasis is put on the optimization parameters, algorithm, and exit criteria because the intention is to focus more on the method than the result itself.

Two optimization frameworks have been developed to interconnect different tools that model the wind turbine and allow loads evaluations. The first framework is implemented in Matlab and the second in OpenMDAO, a python based tool. Chapter 2 introduces these frameworks, the aeroservoelastic models, and the wind turbine models used in the investigation.

Three techniques to estimate wind turbine loads have been investigated and integrated in the optimization frameworks, described in Chapter 3, one based on time domain simulations, one on frequency domain response, and one on modal analysis considerations. These techniques can all be used for preliminary design, and their applications are presented with different design test cases.

Chapter 4 introduces methods to systematically tune a wind turbine controller. In this chapter, a model based method to tune the wind turbine controller is extended to improve the placement of the pole associated with the dynamic response of the wind turbine controller for regulation above rated. Moreover, two numerical techniques to tune the controller are discussed.

Chapter 5 gives a series of test cases, where the different methods implemented and described in the previous chapters are applied to perform wind turbine optimization design.

Finally, Chapter 6 summarizes the conclusions and findings of this work and suggests topics for possible future investigations.

CHAPTER 2

Simulation Environments and Models

This chapter introduces the simulation environments and the wind turbine models used in the dissertation.

Two in-house environments for wind turbine simulations are used throughout the whole project, HAWCStab2 and HAWC2. The first code is employed for linear analysis, the latter for nonlinear load evaluation. Two different frameworks are used to perform optimization. The frameworks have been developed at different stages of the project, and therefore they appear in different articles that are part of the dissertation.

Several wind turbine are applied for the numerical simulations. The most used models are the NREL 5MW Reference Wind Turbine and the DTU Wind Energy 10MW Reference Wind Turbine. Only in article [Article I] different models, than the two just mentioned, are used. These models are not described in this chapter.

2.1 Linear model

The linear high-order aeroservoelastic model implemented in HAWCStab2 [26] (Horizontal Axis Wind turbine Code for Stability analysis, 2nd generation) is used to retrieve steady-state parameters and linearized models of the wind turbine. HAWCStab2 is an improved version of HAWCStab [27] with different kinematics. A detailed description is provided by Hansen [28].

The model is based on an analytical linearization of a linear finite element beam model in a nonlinear corotational formulation. The wind turbine model

is composed by different bodies. Each body is an assembly of Timoshenko beam elements with six degrees-of-freedom at each node. Pitch and shaft bearings are included with frictionless bearing.

The structural model is coupled with an unsteady blade element momentum model of the blade aerodynamics. The aerodynamic model considers shed vorticity and dynamic stall. A model of the dynamic inflow has been added by fellow PhD student Georg Pirrung during the course of the project. The dynamic inflow is therefore included in the manuscripts [Article II], [Article IV], [Article VII], and [Report I], while in [Article I] frozen wake is assumed.

The analytical linearization is performed around steady-state conditions. The steady states are obtained to balance elastic, aerodynamic, and inertial forces. This computation does not include gravitational forces nor flexible tower and shaft. In the computation of the steady states, the multi-body formulation allows to capture nonlinear effects due to large deflections and rotations.

A linearized model of the controller, described in Section 2.4, is given in [Article II].

An extensive validation and analysis of the open-loop performances of the tool without dynamic inflow are provided by Sønderby and Hansen [29].

A validation of the performances in closed-loop are shown in [Article II] and [Article IV].

2.2 Nonlinear model

The nonlinear aeroservoelastic model implemented in HAWC2 [30] (Horizontal Axis Wind turbine Code, 2nd generation) is used for calculating the wind turbine response in time domain. The code couples a structural model, an aerodynamic model, and a controller system.

The structural part is based on a multi-body formulation. The wind turbine model is composed of bodies connected by constraints. Each body is an assembly of Timoshenko beam elements [31], with six degrees-of-freedom at each node. The deformations of the elements are obtained, with respect to a local reference system, with the linear assumption of small deflections and rotations. This general formulation allows to account for nonlinear effects from large deflections and rotations.

The aerodynamic model is based on the blade element momentum theory. The unsteady aerodynamic forces and moments are computed using 2D models. The aerodynamic model is extended to handle dynamic inflow, dynamic stall, skew inflow, and shear effects on the induction [32, 33].

The controller system is included through a DLL (Dynamic Link Library). The controller used throughout the project is described in Section 2.4.

Extensive validations of the code are presented in [34–38].

The three-dimensional Mann turbulence model [39] is used in all the simulations with turbulent wind.

A manual of the code can be found in [40].

2.3 Optimization framework

During the course of the project two different optimization frameworks have been developed and used.

The frameworks handle all the required operations in the optimization workflow to compute the cost function and constraint outputs for given design parameters. The frameworks interact with different codes, connects their inputs and outputs, and perform pre and post-processing operations. The frameworks are then connected to optimization algorithms to perform the actual optimization.

In the following sections the two frameworks are briefly described.

Matlab framework

A first framework was developed using the numerical computing environment Matlab [41] and its optimization toolbox. The framework combines a set of functions to write HAWC2 input files, launch the simulations on a cluster, read the logfiles for errors, read the results files, and perform the post-processing to compute the cost function and the constraints.

The development and use of this framework stopped approximately one year and five months after the beginning of the project. At that stage, the focus shifted to a new framework more flexible and also employed in other projects in the DTU Wind Energy Department.

The Matlab framework is employed and described in [Article III] and [Article VI].

OpenMDAO framework

Approximately one year and a half after the beginning of the project, a new framework started to be developed. This second framework is based on the open-source tool OpenMDAO (Open-source Multidisciplinary Design, Analysis, and Optimization framework) [42–45]. The reason of the change of

platform is mainly found in the more flexible and versatile environment. Furthermore, the development of the framework was already ongoing in other projects in the Wind Energy Department at DTU.

OpenMDAO is based on Python and it provides an interface and tools to help setting up MDAO problems. It handles the definition of the optimization problem, workflow, dataflow, and parallelization of simulation cases.

OpenMDAO has an interface to PyOpt [46, 47] which has wrappers for several optimization algorithms. The gradient-based sequential quadratic programming optimizer SNOPT [48, 49] is used in all the investigations with this framework.

The contribution to the OpenMDAO framework has been carried out developing an OpenMDAO plug-in. The plug-in is able to handle the input/output interface to HAWCStab2 and HAWC2.

Within the department several other plug-ins have been developed to connect other softwares to the framework, among them BECAS [50–52] and a preprocessor tool to parametrize the blade design. BECAS is a finite element cross sectional tool used to predict the structural and mass properties and to retrieve stresses along the blades. BECAS is used in [Article VII].

The framework can run on the clusters available at the DTU Wind Energy Department.

This framework is used and described more in detail in [Article VII] and [Report I].

2.4 Controller

The Basic DTU Wind Energy controller [53] is used to regulate the turbine in the nonlinear time domain simulations.

The controller is meant for variable-speed pitch regulated wind turbines. It comprehends basic regulation capabilities, switching functions between the different operational regions, and start-up and shut-down procedures.

The regulation is divided into three different strategies: variable speed and variable torque, constant speed and variable torque, and constant speed and constant power or torque. The first strategy is used in Region 2, the second in Region 1 and 3, and the third in Region 4. Figure 2.1 shows the four different operational regions of the NREL 5MW Reference Wind Turbine [54]. The figure illustrates also the steady-state pitch angle, rotor speed, and power.

The following sections introduce the controllers used to regulate the turbine

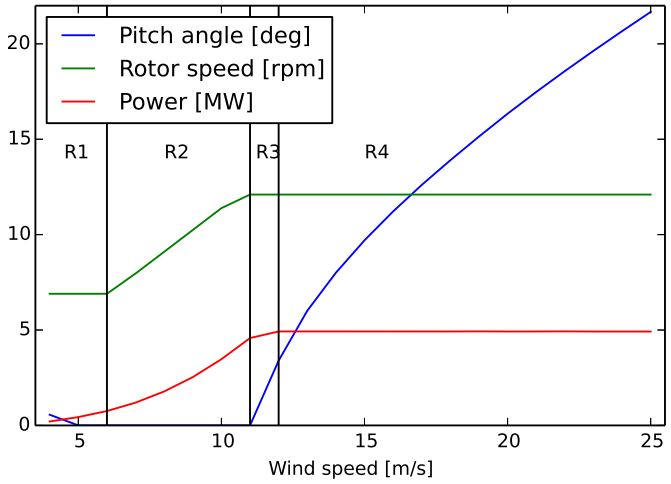

Figure 2.1: Operational regions of the NREL 5 MW Reference Wind Turbine. Region 1 (R1), Region 2 (R2), Region 3 (R3), and Region 4 (R4).

according to the different strategies. The techniques of switching between regions are not described. A detailed description of these techniques can be found in the report [53].

Variable speed, variable torque

The pitch is kept constant at the angle β^* and the generator torque is used to regulate the rotational speed Ω to track a constant tip-speed-ratio. The value of the torque is set to

$$Q_{ref} = k\Omega^2 \tag{2.1}$$

to balance the aerodynamic torque. The constant k is a parameter that needs to be tuned to obtain the desired tip-speed-ratio.

Constant speed, variable torque

When the wind turbine is operating at the minimum rotor speed (Ω_{min}) or rated Ω_R, the controller keeps the rotational speed constant. In the Basic DTU Wind Energy controller, the regulation is performed with a proportional integral (PI) controller on the generator torque while the blade pitch is kept constant. The reference torque is set as

$$Q_{ref} = k_p^Q(\Omega_f - \Omega_{set}) + k_i^Q \int_0^t (\Omega_f(\tau) - \Omega_{set})d\tau \tag{2.2}$$

Ω_f is a low-pass second order filtered rotational speed, Ω_{set} is either the minimum rotor speed or the rated speed rotor speed Ω_R, k_p^Q and k_i^Q are the proportional and the integral gains of the rotor speed error PI feedback.

Constant speed, constant power

When the power reaches the rated value, the controller has to guarantee constant power and constant rotational speed. This regulation is obtained with a PI controller on the pitch angle

$$\beta_{ref} = k^{\beta}_{p,\Omega}\eta_k(\Omega_f - \Omega_R) + k^{\beta}_{p,P}\eta_k(P_{ref} - P_R) + \tag{2.3}$$

$$+ \eta_k \int_0^t [k^{\beta}_{i,\Omega}(\Omega_f - \Omega_R) + k^{\beta}_{i,P}(P_{ref} - P_R)]d\tau \tag{2.4}$$

β_{ref} is the reference pitch, $k^{\beta}_{p,\Omega}$ and $k^{\beta}_{i,\Omega}$ are the proportional and integral gains for the rotor speed error feedback, and η_k is a gain scheduling factor. In the pitch controller there are also a proportional and an integral term depending on the error between the reference power and the rated power, P_{ref} and P_R. These terms are introduced to improve the transition between the different regions. The power reference is obtained multiplying the reference torque with the unfiltered rotor speed. The two integral terms share a saturated integrator ensuring minimum pitch in the variable speed region and a fast action when the power is increasing.

The measured rotor speed is also filtered with a second-order band stop filter to remove the contents at the drivetrain mode frequency.

2.5 NREL 5MW Reference Wind Turbine

The analyses presented in [Article II], [Article III], [Article IV], [Article V], and [Article VI] are performed with the NREL 5MW Reference Wind Turbine (RWT). The conceptual design has been carried out at the National Renewable Energies Laboratories, Golden USA, and it is available in the report by Jonkman et al. [54]. The turbine is a variable-speed pitch regulated with a three-bladed upwind rotor. It has 5 MW rated power, a rated rotational speed of 12.1 rpm, a rotor diameter of 126 m, and a hub height of 90 m. In the entire project, the model is used in the on-shore configuration.

2.6 DTU 10MW Reference Wind Turbine

The analyses presented in [Article VII] and [Report I] are performed with the DTU 10MW Reference Wind Turbine. The design is presented by Bak et al. [55, 56], and the model can be downloaded at [57]. The turbine is variable-speed pitch regulated with a three-bladed upwind rotor. It has a rated power of 10 MW, a rated rotational speed of 9.6 rpm, a rotor diameter of 178.3 m, a prebend of 3 m, and a hub height of 119 m. In the entire project, the model is used in the on-shore configuration.

CHAPTER 3

Loads Estimation Methods

The estimation of the loads level is an essential part in a wind turbine design process. Loads are required to verify the solidity and robustness of a designed structure during its entire operational life and to estimate if the turbine can operate within the desired load envelope. Loads can therefore be a direct indication of the performance and quality of a new design.

This chapter introduces methods to estimate loads on a wind turbine for preliminary design. Applications of these techniques are given in the following two chapters.

Three methods are introduced: the first approach evaluates the loads based on time domain simulations, the second estimates fatigue loads based on power spectral densities, which is in the frequency domain, and the third method allows to estimate loads from general considerations on the dynamic response based on the modal properties of the wind turbine.

The methods have very different levels of accuracy, but they all can be exploited in wind turbine design procedures.

3.1 Time domain method

Nonlinear time domain aeroservoelastic simulations are certainly the most accurate tool to estimate loads on a wind turbine. From post-processing of the simulated time series, parameters can be extracted and used as part of a cost function and constraints. When this technique is used in a design procedure, the quality of the final design depends only on the representativeness of the simulations of the wind turbine life-time conditions. Theoretically, if the set of simulations that is used in the design procedure represents and describe

any possible event and load condition, the design obtained satisfies all the requirements. On the other hand, a small set of simulated cases leads to a solution that needs to be verified and eventually modified, since the loads that the wind turbine will experience during its life are not fully considered during the design. A large set of simulations needs to be accounted for to obtain a reliable and robust design but, since aeroservoelastic simulations are time consuming, a trade-off between accuracy and computational time has to be selected by the designer.

When a set of simulations is selected, the nonlinear nature of aeroservoelastic models, combined with the stochastic wind input due to turbulence, can lead to numerical problems in the optimization. When a gradient based algorithm is used, each design parameter is perturbed to identify its effect on the cost function. However, when turbulent wind simulations are performed, the loads highly depend on the selected set of turbulence seeds. Therefore, when the gradients are computed, it is impossible to distinguish between the effects of the parameter variation on the loads and the effects due to a different wind hitting the turbine. Even when the same turbulence boxes are used, a change in a design parameter leads to a different response of the turbine that, therefore, experiences a different wind. This issue can be overcome increasing the number of simulations cases at the price of a higher computational time.

Figure 3.1 and Figure 3.2 show the dependency of blade root flapwise bending moment and of the tower base longitudinal bending moment on the number of turbulent seeds for the NREL 5MW RWT. The dependency is estimated increasing the number of turbulence seeds used for the loads evaluation from 1 to 20, and repeating the load evaluation using 5 different turbulence realizations.

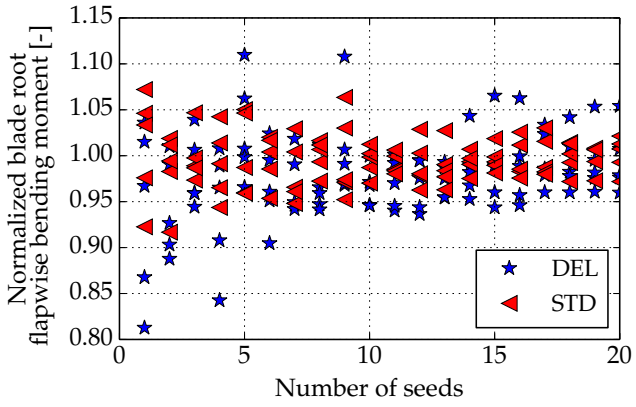

Figure 3.1: Dependency of blade root flapwise bending moment on the number of turbulent seeds. Comparison of damage equivalent load (DEL) and standard deviation (STD).

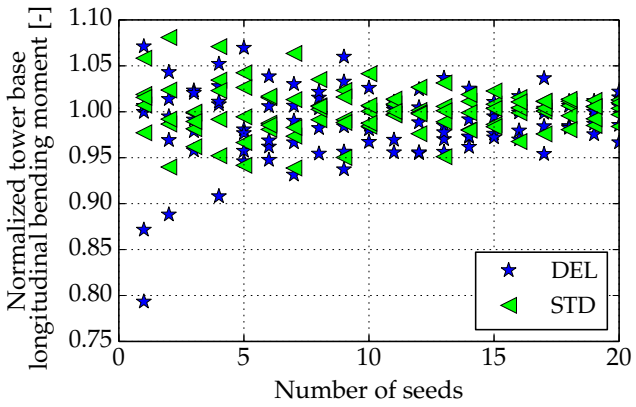

Figure 3.2: Dependency of tower base longitudinal bending moment on the number of turbulent seeds. Comparison of damage equivalent load (DEL) and standard deviation (STD).

Each marker, therefore, represents a load evaluated from a set of simulations with a defined number of turbulent seeds. The parameters analyzed are the damage equivalent load (DEL) and standard deviation (STD). The plots show that even with a high number of turbulence seeds, the dependency of the parameters, on the set of wind realizations used in the simulations, is still high. At the blade root and tower base, when using 20 turbulence seeds the scatter of the loads is about $\pm 3\,\%$. This means that even with 20 turbulence seeds the wind is not fully described and the loads depend on the set of seeds selected.

Figure 3.3 and Figure 3.4 show the dependency of loads variations on the number of turbulence seeds due to a change in the controller tuning. The comparison is performed on the damage equivalent load and standard deviation of the tower base longitudinal bending moment and on the rotor speed standard deviation. The variations of the loads are important because they give an estimation of the numerical gradients computed by the optimization algorithm. Also in this case, the scatter of the estimated parameters is high even with 20 turbulence seeds. At the tower base, for the case investigated, at least nine turbulence seeds need to be used to understand if the controller tuning change leads to an increase or decrease of loads. The variations of the rotor speed standard deviation are more consistent because even with few seeds it is clear that the change in the tuning leads to an increase in the parameter. On the other hand, the amplitude of the variation is not estimated with precision even with a high number of turbulence seeds.

In conclusion, time domain method to estimate loads has the advantage of being accurate but only when a significantly large set of simulations is considered for the loads estimation. Such large set can be impractical for large

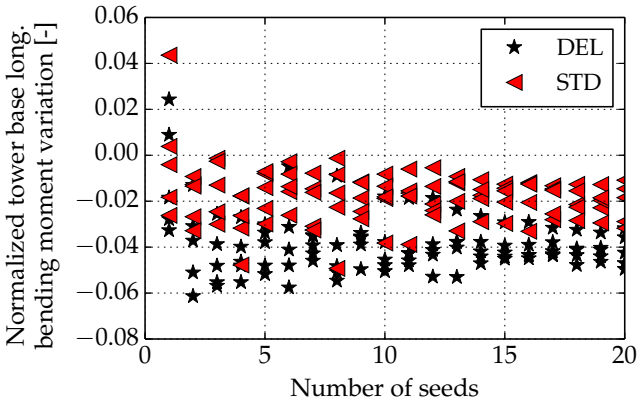

Figure 3.3: Dependency on the number of turbulent seeds of tower base longitudinal bending moment variations due to a change in the controller tuning. Wind speed of 15 m/s. Comparison of damage equivalent load (DEL) and standard deviation (STD).

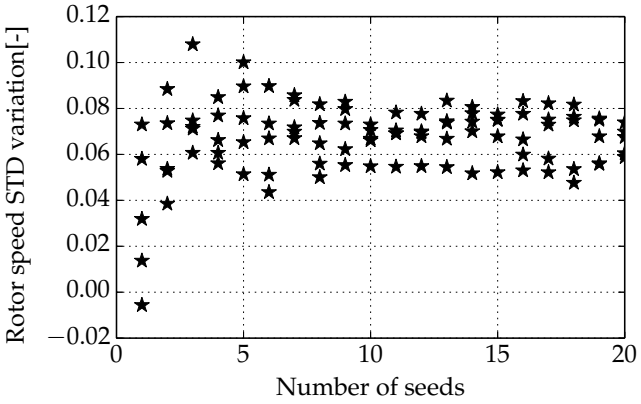

Figure 3.4: Dependency on the number of turbulent seeds of the rotor speed standard deviation variations due to a change in the controller tuning. Wind speed of 15 m/s.

optimization design applications.

The detailed investigation on the effects of the number of turbulent seeds on wind turbine loads and the loads gradients are given in [Article V].

3.2 Frequency domain method

This section introduces a method to evaluate fatigue loads in frequency domain. The approach has been developed and implemented to obtain a faster method to evaluate fatigue loads than time domain simulations. This technique enables the evaluation of the fatigue loads for each design variable change allowing a better exploitation of wind turbine components synergies.

Fatigue analysis is an essential part of the design process. In a preliminary design procedure, the fatigue estimation can be evaluated in the frequency domain so that time domain simulations are avoided. Spectral methods can be used to estimate the fatigue damage from the power spectral density (PSD) of a wind turbine. Analyses in the frequency domain are generally faster than in the time domain and, therefore, preferable when a large number of evaluations are required. This procedure cannot completely substitute completely time domain analysis but it can be exploited to obtain overall load variations more efficiently.

In [Article II] a method to evaluate wind turbine fatigue damage in the frequency domain is described in detail, and it is validated against time domain rainflow-counting. The method exploits a high-order wind turbine linear model to compute the PSD of the response of wind turbine sensors, and it uses a spectral method to estimate the fatigue damage from the PSD.

Figure 3.5 shows a diagram of the workflow to compute the PSD of a load sensor, starting from the wind sampling and the linear wind turbine system equations, given by the state-space system matrices $\mathbf{A}_{ase}, \mathbf{B}_{ase}$, $\mathbf{C}_{ase}, \mathbf{D}_{ase}$. First, the wind input, $\mathbf{U}_w(\omega)$, has to be obtained. Throughout the project, the wind input is computed from sampling of results from time-domain simulations, $\mathbf{u}_{w,bf}$, and Fourier transformation. From the linearized wind turbine system equations, the transfer function of the closed-loop model needs to be evaluated as $\mathbf{H}_{ase}(\omega)$. Joining the wind input and the wind turbine transfer functions, the turbine response is obtained in the ground-fixed reference frame, $\mathbf{Y}_{gf}(\omega)$. If a signal on the blades is required, a transformation in the frequency-domain, $\mathbf{B}(\omega)$, must be performed to transform a signal in the blade-fixed reference frame. The PSD of any wind turbine output is then computed and used to estimate the fatigue damage by the spectral method presented by Benasciutti and Tovo [58, 59].

The wind input time series depend on the wind turbine model only for the rotational speed and the position of the aerodynamic sections along the blade. Therefore, in an optimization design procedure, the wind sampling and the computation of the wind input can be performed only once, at the beginning. Alternatively, if a model of the wind turbulence in the rotating frame is used, e.g. as shown by [60, 61], the wind sampling can be skipped and the PSD of

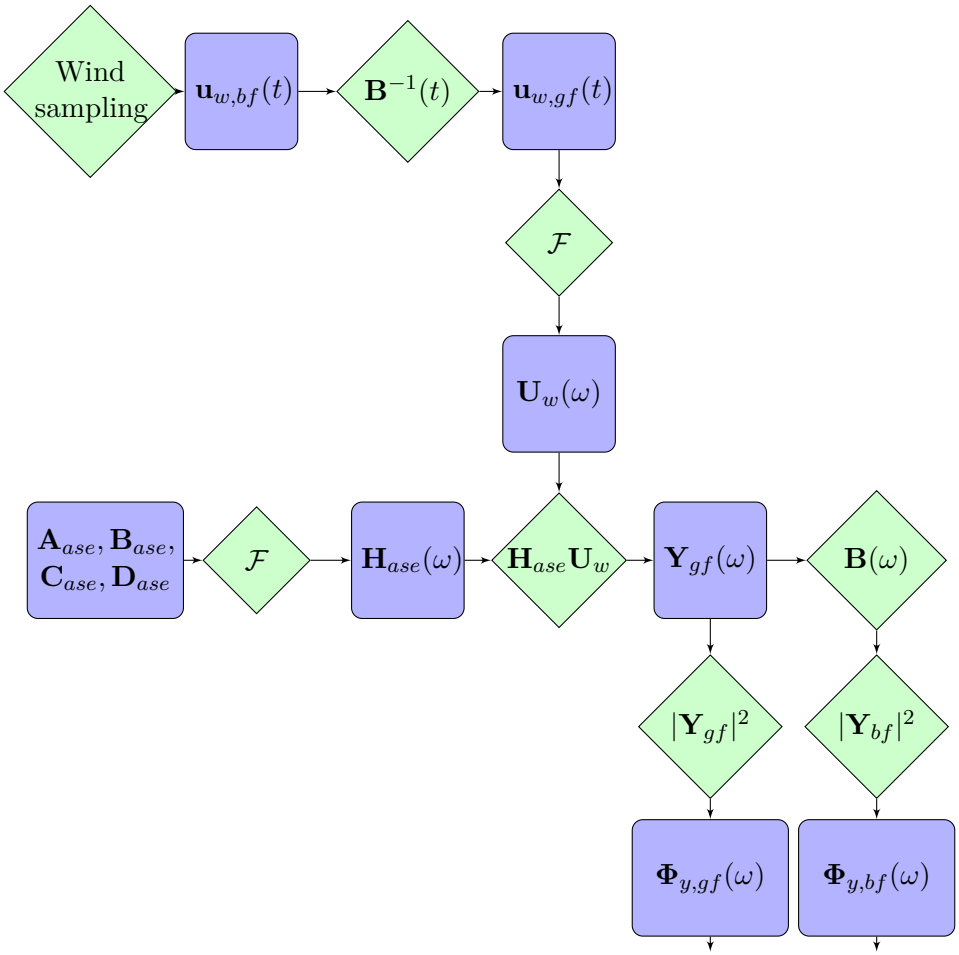

Figure 3.5: Block diagram of the workflow to compute the PSD of the output starting from the linear system equations and the sampled wind.

the wind input can be directly obtained.

3.3 Indirect method based on modal analysis

Rough estimations on the load level experienced by a wind turbine during normal operation can be obtained by looking at results of modal analysis. Wind turbine aeroelastic frequencies and dampings, retrieved with modal analysis, are generally correlated with fatigue loads through the wind turbine dynamic response. The damping of a mode affects the amplitude of the response at that mode frequency, hence, an analysis of the damping variations during the design can give a first indication on the fatigue loading. Constraining the minimum value of the wind turbine aeroelastic damping can be a fast approach to avoid an increase in the fatigue loads and to ensure that the design does

not have unstable modes at the design operational points. Furthermore, the knowledge of the position of the wind turbine aeroelastic frequencies can be exploited to avoid resonance problems of low damped modes that lead to high fatigue damage. The analysis of resonances is a critical aspect in wind turbine design, and therefore, constraints that avoid low damped mode frequencies to coincide with external excitation frequencies should always be accounted for.

Wind turbine resonant frequencies

A numerical analysis of the wind turbine response to an artificial external excitation gives an overview of the critical frequencies, where no resonance should be present. This section presents results of an investigation performed on a multi-megawatt wind turbine.

Two types of excitations placed at the blade tip are considered to simply represent real-life conditions: one acting in a global reference system and one in a local reference system. The former excitation moves with the blade, and it is always aligned with the ground. This force can be related to wind turbine excitations such as those generated by gravity, large scale turbulence, and wakes. The force acting in the local reference frame does not change orientation as seen from the blade, hence it changes orientation with respect to the ground. This excitation can be associated with excitations due to small scale turbulence and distributed actuators on the blades, e.g. trailing edge flaps.

Figure 3.6 shows the amplitude of the tower base lateral bending moment due to a harmonic external excitation placed at the blade tip and acting in a lateral direction in the global reference system. This type of excitation leads to a high response at the frequencies of the wind turbine modes (first lateral tower model and first blade edgewise forward and backward whirling modes), and it does not directly excite the blade edgewise mode.

Figure 3.7 shows the amplitude of the tower base lateral bending moment due to a harmonic external excitation placed at the blade tip and acting in a lateral direction in the local reference system. In this second case, the frequencies that lead to the highest response are not those associated with the wind turbine modes but they are shifted by $\pm 1P$ (with P equals to the rotational frequency) from the wind turbine modes frequencies. This external excitation can, therefore, directly excite the blade edgewise frequency and reflection about the first tower lateral mode frequency.

Since an excitation during operation is a combination of the global and local excitations, a general design recommendation is to place the edgewise frequency at standstill at 3.5, 4.5, ..., N.5 P which ensures the smallest risk of resonance of any of the edgewise modes and edgewise whirling modes, and

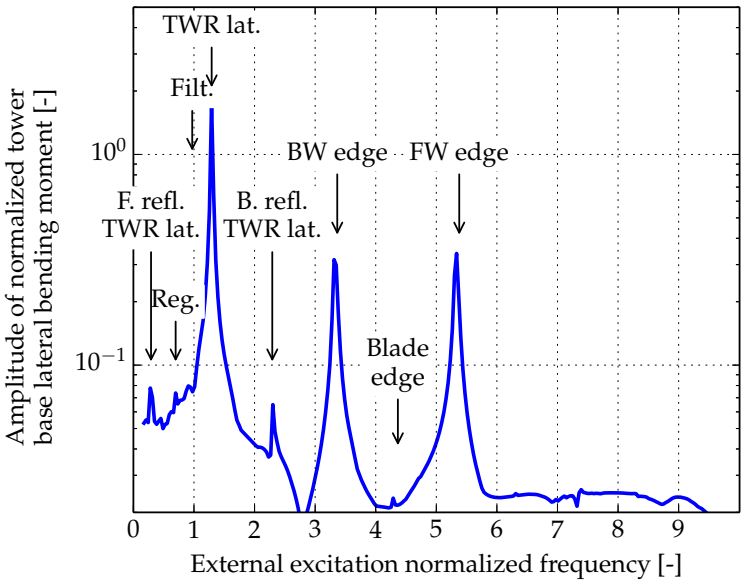

Figure 3.6: Amplitude of tower base lateral bending moment due to a harmonic external excitation of varying frequency placed at the blade tip and acting in the lateral direction in the global reference system. Wind speed: 10 m/s

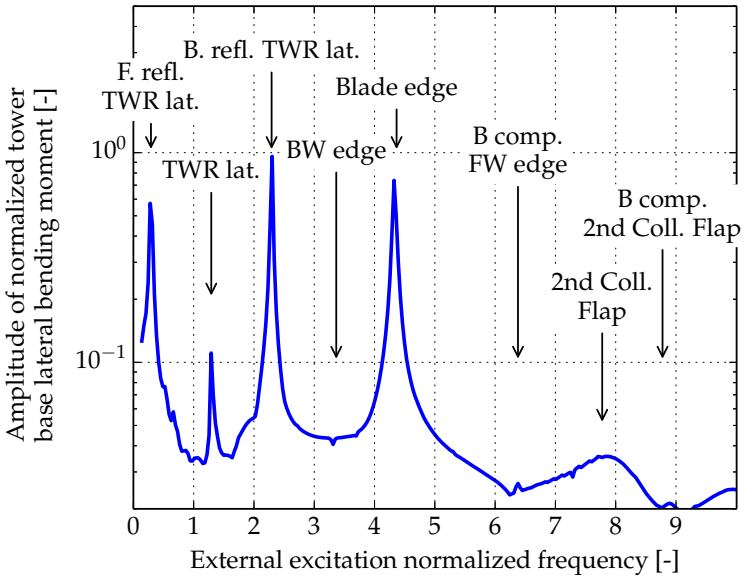

Figure 3.7: Amplitude of tower base lateral bending moment due to a harmonic external excitation of varying frequency placed at the blade tip and acting in the lateral direction in the local reference system. Wind speed: 10 m/s

leads to the lowest response level.

In [Article I] a detailed investigation of wind turbine resonance conditions is presented.

3.4 Remarks

In this chapter three different methods to estimate loads have been presented and discussed. Remarks about each method and their possible role within an optimization design procedure can be summarized as:

- **Time domain method**:
  1. Long time simulations are required;
  2. Used for all kind of loads: ultimate and fatigue;
  3. Requires a large amount of simulations to avoid uncertainty of results (even with 20 seeds for each wind speed the loads are not precisely estimated and gradients can be incorrect);
  4. Not recommended for inner loops of an optimization, where the cost function is evaluated at each parameter variation;
  5. Can be used in outer loops of an optimization to verify the design and update constraints.

- **Frequency domain method**:
  1. Faster than time domain;
  2. It predicts only fatigue loads;
  3. Wind spectra can be computed in the preprocessor of the optimization, so high detailed representation of the wind is obtained without compromising computational time;
  4. It is based on a linear model, so loads due to nonlinearities are not captured;
  5. Can be used in an inner loop of an optimization.

- **Modal analysis method**:
  1. Very fast, especially when a linear model is already available in the workflow;
  2. Gives indications on designs that could lead to high fatigue loads;
  3. It is not a direct indication of the loads, so the final design needs to be verified;
  4. The estimation does not depend on the wind conditions;
  5. Highly recommended to avoid resonant conditions and unstable modes.

CHAPTER 4

Automatic Controller Tuning

This chapter presents three different methods to perform automatic controller tuning.

Controller tuning is a first step towards the integration of controller and rotor designs. When a controller is tuned, the dynamic of the controller is modified such that the response of the wind turbine system achieves the desired behavior. A tuning highly depends on the wind turbine dynamic properties, and it needs to be set accordingly. Therefore, there is a strong bond between a controller tuning and a specific wind turbine design.

An automatic controller tuning procedure has the advantage of allowing designers not to perform time consuming manual iterations. Furthermore, an automatic approach can be connected to a framework that performs rotor design, hence leading to the integration of controllers into the wind turbine design.

Three methods are presented here, a model based method for the tuning of the PI pitch controller, a time domain method for the tuning of any controller parameter, and a frequency based method to tune the gains of the PI pitch controller.

4.1 Model based method

In the model based method presented here, the controller tuning is chosen to obtain a desired dynamic response of a simplified model of the controlled wind turbine. The dynamic response is imposed by selecting target values of the frequency and damping of the mode associated with the controller, the regulator mode. To retrieve the frequency and damping of the regulator

mode, a linearized model of a wind turbine is used. Depending on the order of the wind turbine model, different tunings can be achieved due to the different model dynamics. When a very simple model is used, an analytical formulation can be derived to obtain the gains, while with a high-order model numerical optimization has to be used.

In this dissertation the dynamic of the controller is selected to be uniform throughout all the operational region. Hence, the same frequency and damping are required at all wind speeds above rated wind speed. The reason or this choice is to obtain a consistent controller response. However, different strategies could also be investigated.

Model based techniques have the advantage of allowing fast tuning with a physical perception of the problem, but they require the selection of certain parameters a priori. In the cases investigated here, the aimed dynamic of the regulator mode has been selected arbitrarily based on experience and not on loads considerations. Furthermore, the model used for the tuning does not contain all the parameters required by the nonlinear implementation of the Basic DTU Wind Energy controller, therefore these parameters cannot be tuned with this approach.

In the following sections two approaches are described. These two methods differ in the order of the model used for the tuning. These techniques are employed to tune the PI pitch controller of the Basic DTU Wind Energy controller.

Simplified model

The method that is presented here is an extension of a pole-placement method first developed by Øye [11] and improved by Hansen [62].

The original method consists of a pole-placement technique of the solid-body rotation of the wind turbine rotor. The wind turbine is modeled with a linear system where the only degree of freedom is the rotation of the rotor. All the structural components are therefore assumed rigid and the aerodynamic steady. This simplified model has two external torques acting on it, the aerodynamic torque Q and the generator torque Q_g. When operating above rated wind speed the aerodynamic torque is a function of the wind speed V, the rotor speed Ω, and the pitch angle θ. The pitch angle can be expressed as a function of the rotor speed variation and its integral, $\dot{\phi}$ and ϕ respectively. This simplified controller model neglects the effects due to possible filters on the measured rotor speed. Substituting the pitch angle expression into the wind turbine simplified model, the formulation of the wind turbine in closed-

loop formulation is obtained as

$$I\ddot{\phi} + \Big(\frac{\partial Q_g}{\partial \Omega} - \frac{\partial Q}{\partial \Omega} - k_P \frac{\partial Q}{\partial \theta}\Big)\dot{\phi} - k_I \frac{\partial Q}{\partial \theta}\phi = 0. \tag{4.1}$$

I is the total drivetrain inertia including rotor, shaft, gearbox and generator and k_P and k_I are the PI controller gains including the gain-scheduling factor.

The pole-placement method consists of selecting the controller gains k_I and k_P such that the eigenvalues of the system in Equation (4.1) have frequency and damping decided a priori. The aerodynamic gain $\dfrac{\partial Q}{\partial \theta}$ and the aerodynamic damping $\dfrac{\partial Q}{\partial \Omega}$ change in the operational region, therefore a parametrization of the gains is required to obtain the same pole-placement at the different wind speeds. The parametrization is called gain-scheduling. In the original work by Øye the gain-scheduling is a polynomial function of the pitch angle and the coefficients of the polynomial are obtained with a linear fitting of the aerodynamic gain. Later, Hansen [28] suggested to perform a quadratic fitting to better capture the changes of the aerodynamic characteristics. However, in both works the effects of the aerodynamic damping $\dfrac{\partial Q}{\partial \Omega}$ are neglected.

The new suggested method includes also the effects of the aerodynamic damping $\dfrac{\partial Q}{\partial \Omega}$. The inclusion of this parameter leads to a new formulation of the gain-scheduling. This method is described and presented in details in [Article IV].

The new gain-scheduling technique has been implemented in the Basic DTU Wind Energy controller and in its linearization in HAWCStab2. In [Article IV] the two implementations are compared analyzing time domain responses due to step changes in the wind speed on high-order models, with gains obtained with the simplified model. Furthermore, the article contains an analysis of the frequencies and dampings of the placed regulator mode. The analysis shows that the interaction with other wind turbine components and the more complex dynamics of a high order model lead to a different frequency and damping compared to the desired one. Generally, the damping of the regulator mode is significantly lower than expected. The filter on the measured rotational speed plays a major role in the reduction of the damping of the regulator mode when the filter frequency is too low.

Figure 4.1 shows the damped natural frequency and the damping ratio of the rotor speed regulator mode of the NREL 5MW RWT when tuned using three different gain-scheduling. The techniques illustrated are the linear approach suggested by Øye [11] (*Lin.*), the quadratic improvement suggested by Hansen [62] (*Quad.*), and the new method (*Quad.+Damp.*). In this investigation the dynamic inflow model is not included. The plots show that the

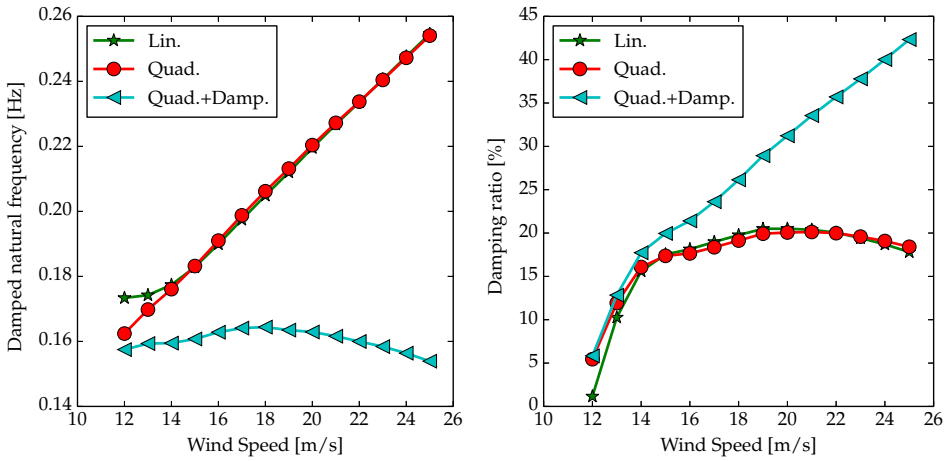

a) Damped natural frequency. *b) Damping ratio.*

Figure 4.1: Damped natural frequency and damping ratio of the rotor speed regulator mode using a high-order model of the wind turbine. Comparison of the linear approach suggested by Øye [11] (*Lin.*), the quadratic improvement suggested by Hansen [62] (*Quad.*), and the new method (*Quad.+Damp.*).

frequency and dampings of the regulator mode are not constant throughout the operational region. However, the location of the frequency of *Quad.+Damp.* is significantly improved compared to the two other methods. Therefore, in this case, the position of the regulator mode frequency is closer to the one required by the designer with the pole-placement. On the other hand, the values of the damping ratio are still considerably lower than required, especially at low wind speeds.

High-order model

When a high-order model is used for the pole-placement technique, numerical optimization is required to solve the problem because a closed analytical formulation that links the gains and the frequencies and dampings cannot be obtained. This method can be applied with the same approach to any different level of model order.

The optimization problem is defined as a minimization of the error between the actual regulator mode frequency and damping and the target ones. The design variables are the normalized controller gains.

[Report I] describes this method in detail, and it presents results on four different models with increasing order. The models are all based on the DTU Wind Energy 10MW RWT. The different models are used to obtain the tuning within the optimization procedure, and the final tuning is then evaluated on

a linear full high-order model. The models investigated are:

SDOF single degree of freedom or two states model of the rigid rotor rotation as described by Øye [11];

Model 1 twelve states model including: the rigid rotor rotation, the second-order low pass filter on the rotor speed feedback, the second order band stop filter on the drivetrain frequency, and three second order models of the pitch actuators;

Model 2 same as *Model 1* with the addition of degrees of freedom for blade flexibility;

Model 3 same as *Model 2* with the addition of state variables for the unsteady blade aerodynamics;

Model 4 same as *Model 3* with the addition of state variables for dynamic inflow.

All the gains are computed numerically, except for *SDOF* model.

Figure 4.2 and Figure 4.3 show the frequency and damping of the regulator mode of the full high-order model obtained with the different tunings. The figure includes the results of models *SDOF*, *Model 1*, *Model 2*, *Model 3*, and *Model 4*. Despite the increasing order, none of the models achieves performances that are uniform throughout the operational region. The reason of these poor performances rely partially on the inability of the gain-scheduling to fit

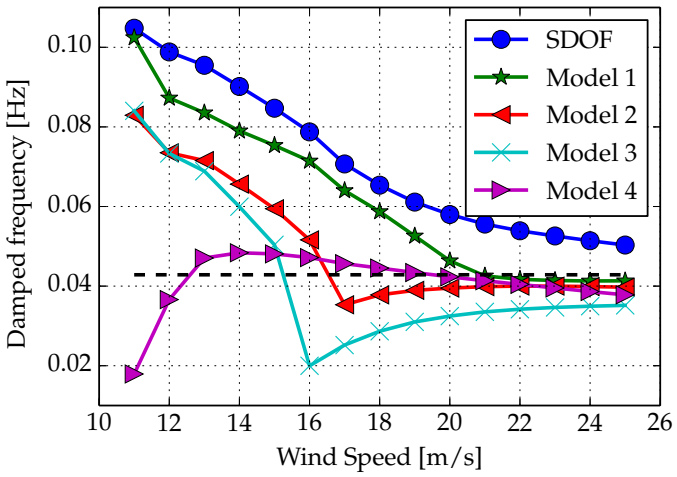

Figure 4.2: Regulator mode damped frequency of the full high-order model. Comparison between the tuning obtained with models *SDOF* (rigid turbine), *Model 1* (rigid turbine and filters), *Model 2* (filters and flexible rotor), *Model 3* (filters, flexible rotor, and unsteady aerodynamic), and *Model 4* (filters, flexible rotor, unsteady aerodynamic, and dynamic inflow).

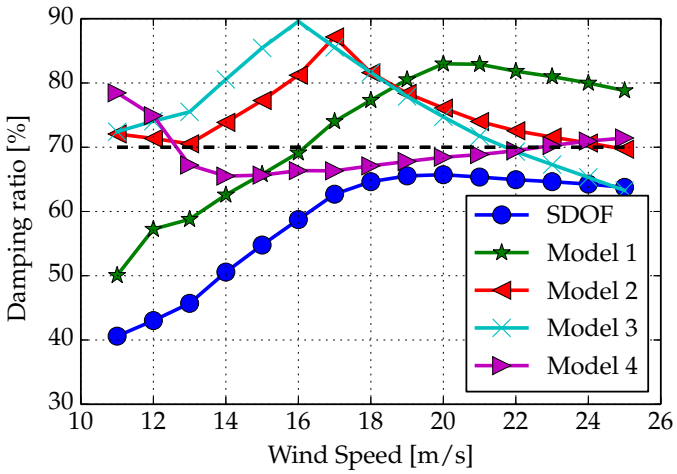

Figure 4.3: Regulator mode damping ratio of the full high-order model. Comparison between the tuning obtained with models *SDOF* (rigid turbine), *Model 1* (rigid turbine and filters), *Model 2* (filters and flexible rotor), *Model 3* (filters, flexible rotor, and unsteady aerodynamic), and *Model 4* (filters, flexible rotor, unsteady aerodynamic, and dynamic inflow).

the changes in the aeroelastic characteristics of the wind turbine and on the differences that each of the model has compared to the full high-order model. The pole-placement technique with the model that includes also the rotor speed filter improves the placement of the pole compared to *SDOF* since the minimum damping ratio incraeses. Furthermore, this model does not compromise the computational time since the model is still fairly small.

From the investigation in [Report I], it appears that the dynamic inflow model, highly interacts with the regulator mode, affecting significantly the controller frequency and damping. Furthermore, if the dynamic inflow model is included in the tuning procedure, as for *Model 4*, the identification of the regulator mode among all the aeroservoelastic modes becomes non-trivial. Further effort should be spent to better understand the dynamics of the controller and dynamic inflow interaction and, therefore, better exploit this tuning technique.

4.2 Time domain method

This section presents a method to tune a controller based on load estimations from time domain simulations. This approach is subject to the considerations and limitations due to the uncertainty of the results, stated in Section 3.1.

With an optimization framework a cost function based on wind turbine loads and annual energy production is minimized with respect to controller tuning

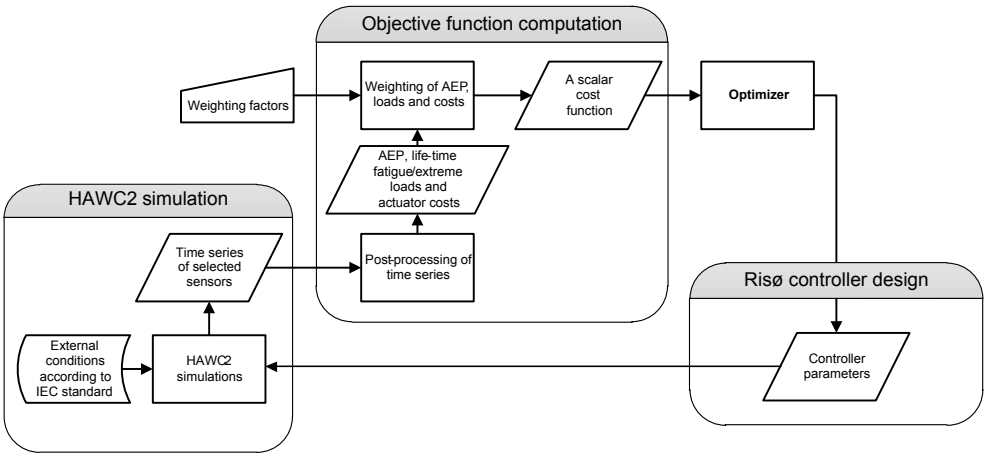

Figure 4.4: Work-flow diagram of the numerical optimization procedure.

parameters. The method is described in detail in [Article III].

Figure 4.4 shows the workflow of the optimization procedure. First, the optimization algorithm selects a controller tuning. Nonlinear time domain simulations are then performed with HAWC2 with the new set of tunings. Finally specific loads are post-processed to define a scalar cost function.

The cost function, used for this investigation, is based on annual energy production, actuator duty cycle, and fatigue loads. Loads at different positions on the wind turbine are considered to better capture the effect of the different optimization parameters on the cost.

The optimization test case leads to a reduction of the cost function of 2 %. The reduction is achieved reducing the gains of the torque controller and the integral gain of the pitch controller. The change of the integral gain of the torque controller smoothens the transition between the constant speed constant power region and the constant speed variable torque region.

The main advantage of controller tuning based on time domain simulations is that it allows to tune any controller parameter. Because it is based on a nonlinear high-order model of the wind turbine and the controller, gains, filters frequencies, and switching parameters can be identified with this method. On the other hand, the optimization requires a large number of computationally expensive cost function evaluations. Furthermore, optimization results depend on the definition of the cost function making therefore general considerations difficult.

4.3 Frequency domain method

This section presents a method to tune a controller based on fatigue load estimations in frequency domain based on a linear model. This approach utilizes the method introduced in Section 3.2.

The controller gains are selected with an optimization procedure that tries to minimize the fatigue damage load at the tower base in the longitudinal direction, without increasing the variations of the rotor speed and limiting the maximum value of the regulator mode damping ratio of a simplified model. This case is presented in detail in [Report I]. The DTU 10MW RWT is employed in this investigation.

Figure 4.5 shows the tower base longitudinal bending moment and rotor speed fatigue damage variation with respect to the reference solution *SDOF*. These loads are evaluated with nonlinear time domain simulations using the tuning obtained from the optimizations. The variations in the tower loads are small and not uniform. *Tuning 2* achieves a load reduction that on average is 1 %, while *Tuning 1* almost does not affect the loads. On the other hand, the rotor speed variations are more significant. *Tuning 1* satisfies the constraint on the rotor speed in all the operational region, on the other hand *Tuning 2* has higher rotor speed variations in the first part of the region. These increases are not captured by the linear model used for the tuning. *Tuning 1* is faster (it has a lower damping ratio) compared to *Tuning 2* because it has a higher proportional gain, especially below 20 m/s. On the other hand, both tunings have lower integral gain, which means lower frequency of the regulator mode and, therefore, less aggressive regulation. The obtained loads are the result of

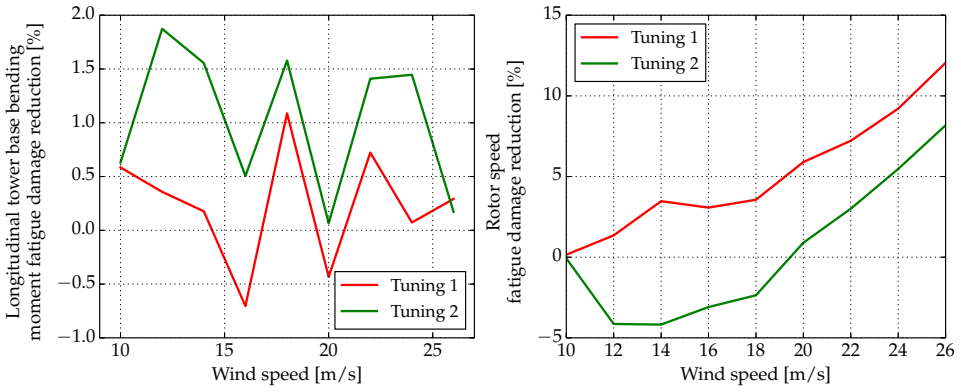

a) Tower base. *b) Rotor speed.*

Figure 4.5: Tower base longitudinal bending moment and rotor speed damage equivalent load evaluated with HAWC2. Load variation of *Tuning 1* and *Tuning 2* with respect to the reference tuning.

a balance between these behaviors.

4.4 Remarks

In this chapter three methods to automatically tune the controller have been presented and discussed. These techniques can help estimating a controller tuning to achieve desired wind turbine dynamic responses. Considerations and conclusions about the methods can be summarized as:

- **Model based**: a model based method to tune the controller by placing the pole of the regulator mode has been improved by:
  1. extending the gain-scheduling scheme with an additional quadratic function;
  2. developing a technique to perform the tuning with a model with a higher order than available in the literature.

  This technique can only be used to tune a PI controller, and parameters chosen a priori need to be identified. The new gain-scheduling has shown to improve the placement of the pole when it is tuned analytically with the technique available in the literature.
  Employing a high-order model for the pole-placement has shown the following:
  1. the placement of the regulator mode is not significantly improved despite the higher order model;
  2. the quadratic shape of the gain-scheduling is not able to capture the variation of the aerodynamic characteristics in the full load operational region, hence the poor performances despite the higher order;
  3. adding only the filter on the rotor speed in the tuning model improves the damping of the regulator mode and does not compromise the computational time to obtain a tuning;
  4. the poles associated with the dynamic inflow highly interact with the controller pole. A deeper understanding of this interaction should be addressed in future investigation.

- **Time domain**: this is a method to tune a controller based on load estimations from time domain simulations.
  1. It is based on time domain aeroservoelastic simulations;
  2. The approach is highly flexible and it can be employed to tune any wind turbine controller parameter;
  3. It is a slow procedure, and high computational time is required;
  4. It can be subject to uncertainty in the results due to limited turbulent wind realizations;
  5. It does not require parameters chosen a priori but a cost function to find the trade-off between performances.

- **Frequency domain**: this is a a method to tune a controller based on fatigue load estimations in the frequency domain based on a linear model.
    1. It is a faster method because it does not require time domain simulations;
    2. It can be less accurate because it is based on a linear model;
    3. It cannot be used for all the controller parameters and cannot capture behavior associated with nonlinear components of the controller;
    4. It does not require parameters chosen a priori but a cost function to find the trade-off between performances.

CHAPTER 5

Wind Turbine Optimization Design Applications

This chapter presents applications of the methods and frameworks presented in the previous chapters. Different wind turbine designs are presented to illustrate the validity and limitations of the methods developed.

The cases shown are divided into three groups according to the method that are used to evaluate the loads, as described in Chapter 3.

5.1 Time domain loads

The results shown in this section are obtained with the optimization framework implemented in Matlab, see Section 2.3. The baseline model, used as reference in the comparisons and as initial design guess, is the NREL 5MW RWT.

Blade sweep and partial load region controller gains

A simple test case of concurrent aeroservoelastic design with loads evaluated in time domain is presented in [Article VI]. The blade backward sweep, the minimum pitch angle, and the controller gain that defines the operative tip-speed-ratio in partial load (k in Equation (2.1)) are optimized. The cost function includes ultimate and fatigue loads on different wind turbine components. The loads are computed with 16 nonlinear simulations during normal operation at wind speeds below rated. In eight iterations the cost function is reduced by almost 12 %. The cost reduction is achieved reducing the loads on the blade and on the tower. The blade sweep increases while the tip-speed-

ratio is increased. The pitch angle decreases to compensate the reduction in power production due to the sweep of the blade.

This simple test case achieves a relevant reduction of the cost function within few iterations. The results however are highly dependent on the small set of simulations considered in the problem. The optimization did not suffer from issues related to the uncertainty of the gradients evaluations, as described in Section 3.1, probably due to the simple set up and to the high sensitivity of the design variables on the cost function.

Blade sweep and partial and full load regions controller gains

The test case of the previous section is extended to take into account also the full load region. As a consequence of this, the proportional gain k_P and the integral gain k_I of the PI pitch controller are added to the optimization variables. On the other hand, the pitch angle is removed. A constraint on the rotor overspeed is included to avoid too soft controller action. The cost function and the problem formulation are identical to those described in the previous section and illustrated in detail in [Article VI].

Figure 5.1 shows the variations of the cost function throughout the first ten optimization iterations. Also the rotor speed constraint variation is illustrated. The constraint remains always below zero meaning that it is always satisfied. After four iterations, where the cost function is reduced, the algorithm increases the cost for the following four iterations. This abrupt change in the optimization trend has been attributed to the uncertainty of the results, described in Section 3.1. Since all the constraints are satisfied, there is no reason for the algorithm to increase the cost function, therefore, the motivation for this behavior can be the inaccuracy and low reliability of the numerical gradient estimations.

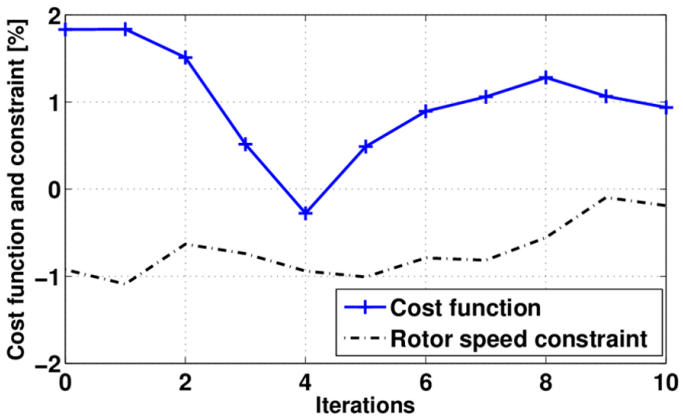

Figure 5.1: Evolution of the cost function and constraint at each iteration.

Figure 5.2 shows the evolution of the design variables during the optimization. When the cost function starts to increase, only a small variation in the design variables occurs supporting the hypothesis of the uncertain gradients estimation.

5.2 Frequency domain loads

The results shown in this section are obtained with the optimization framework based on OpenMDAO, see Section 2.3. The baseline model, used as reference in the comparisons and as initial design guess, is the DTU 10MW RWT.

Shape and structural optimization with fatigue constraint

This application includes both shape and structural design variables. All the aeroelastic calculations are performed based on steady-state calculations with a linear model. The blade sectional properties are evaluated with the finite element code BECAS [50]. The problem formulation and extended results are shown in [Article VII].

The peculiarity of this test case is that it has one constraint on the fatigue damage of the tower bottom longitudinal bending moment and one constraint on the fatigue damage of the rotor speed. The fatigue is evaluated with the method presented in Section 3.2. A reduction of the tower base load can be beneficial for the design of an offshore wind turbine sub-structure and therefore it can reduce the cost of energy. The constraint on the fatigue of

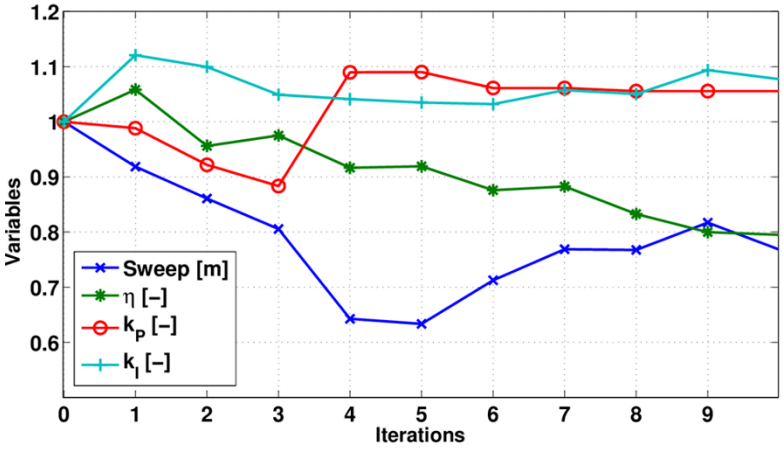

Figure 5.2: Evolution of the design variables at each iteration. Blade sweep, controller gain to set the tip-speed-ratio (η), and proportional and integral gains of the pitch controller (k_P and k_I).

the rotor speed is included to avoid that the rotor speed variations increase. The fatigue constraint on the tower load imposes a lower fatigue damage than the one of the baseline design multiplied by a factor lower than one. Therefore, this constraint is violated at the beginning of the optimization. The linear model is in closed-loop configuration and therefore, it includes the wind turbine controller. In this test case, the tuning of the controller is not modified, and the tuning of the reference model is used throughout the optimization. Two cases are tested with two different level of tower base fatigue damage reduction: 5% and 10%. The constraint on the rotor speed is set so that rotor speed variations do not increase compare to the reference design ones. These cases are labeled *Fatigue 5%* and *Fatigue 10%* respectively. The fatigue is constrained only at 11 and $14m/s$.

Figure 5.3 shows the evolution of the optimizations in term of AEP and blade mass. These two parameters are part of the objective function. The results are compared with respect to solutions obtained without the fatigue constraint and with different weights between the AEP and the blade mass in the cost function. The value of the weight is indicated in the label of the models. Both designs with the fatigue constraint fall inside the Pareto front obtained with unconstrained optimizations and changing the weight factor. This effect shows that when the fatigue constraint is included, it limits the mass reduction and the increase in AEP. *Fatigue 5%* has lower mass and lower AEP compared to *Fatigue 10%*, as the designs of the Pareto front with a weight that favors the structural design to the aerodynamic one.

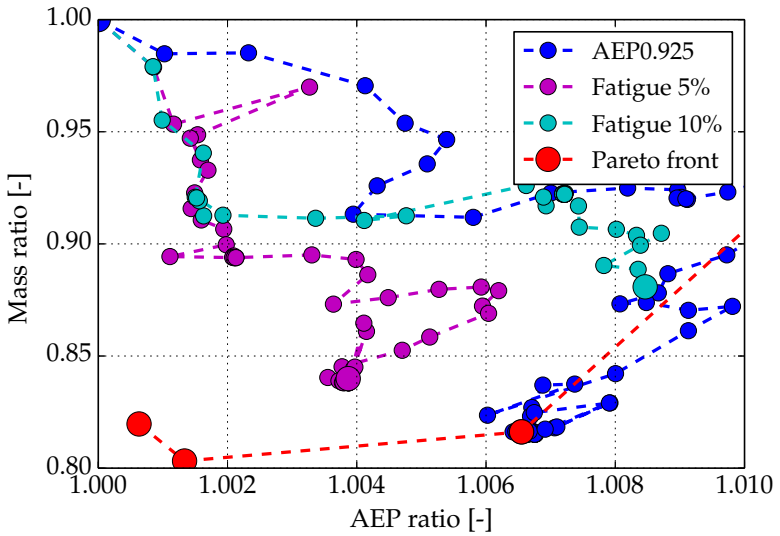

Figure 5.3: Evolution of the AEP and blade mass at each iteration with respect to the Pareto front obtained with unconstrained optimizations.

Figure 5.4 shows the reduction of the tower base longitudinal bending moment at each major iteration. Both optimizations terminate before the target fatigue constraint is achieved, however the error is lower than 1.5 % in both cases.

Figure 5.5 shows the reduction of the fatigue damage of the longitudinal tower base bending moment evaluated with time domain nonlinear simulations. The values shown in the plot confirm the results estimated with the simplified method used in the optimization framework. The reduction in fatigue achieved with the method based on the spectral method and a linear model is therefore confirmed with nonlinear aeroservoelastic simulations.

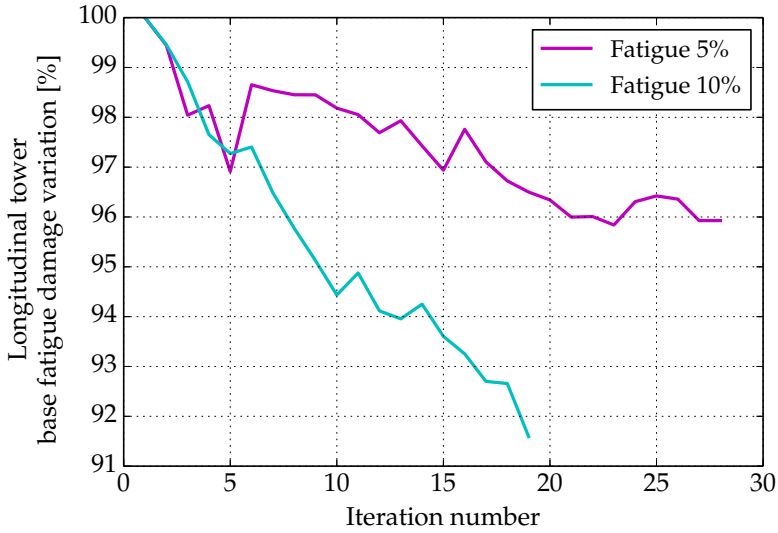

Figure 5.4: Evolution of the tower base longitudinal bending moment fatigue damage variation at each iteration.

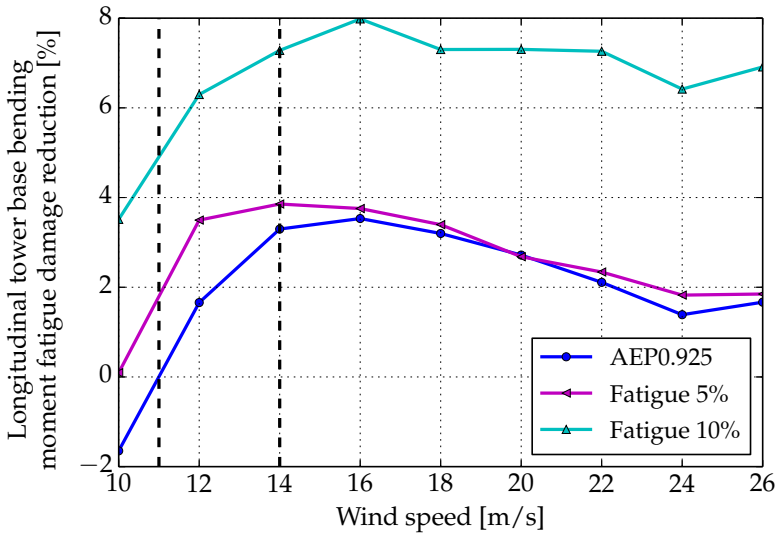

Figure 5.5: Tower base longitudinal bending moment fatigue reduction with respect to the reference design. Values evaluated with nonlinear time domain simulations. Dashed vertical lines indicate the wind speed where the constraint is present in the optimization.

Shape and structural optimization with fatigue constraint and controller tuning

This test case is based on the same set-up as the one in the previous section. Here, the constraint on the fatigue damage at the tower base is set to achieve a reduction of 8 %. Results of two optimizations are compared:

- **W/o tuning** the controller tuning is not updated when the turbine design is modified;
- **With tuning** the controller tuning is updated at each design variable change. The pole-placement technique described in Section 4.1 is used.

The aim of this test case is to identify the influence of the controller tuning on the design.

Both optimizations have been interrupted after approximately 10 days of computations. Despite a similar execution time, the optimization with the controller tuning performed less iterations, meaning that more line searches have been required by the algorithm. This behavior is an indication that a feasible solution is more difficult to be obtained when the controller tuning is included in the design process.

Figure 5.6 shows the evolution of the blade mass for each iteration. Both cases achieve a blade mass reduction close to 10 %.

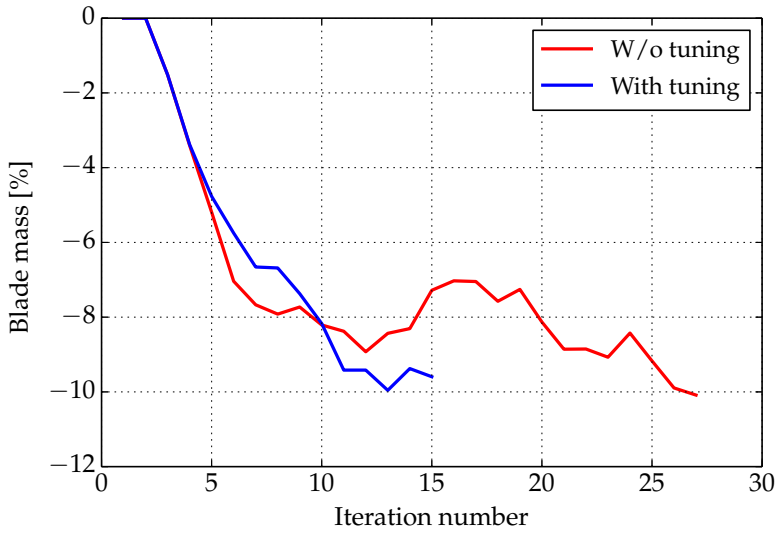

Figure 5.6: Evolution of the blade mass at each iteration. Comparison between a design without controller tuning and with controller tuning.

Figure 5.7 shows the evolution of the annual energy production for each iteration. The case without controller tuning reaches an increase in performance of almost 0.7 % while when the tuning is updated it is only of 0.35 %.

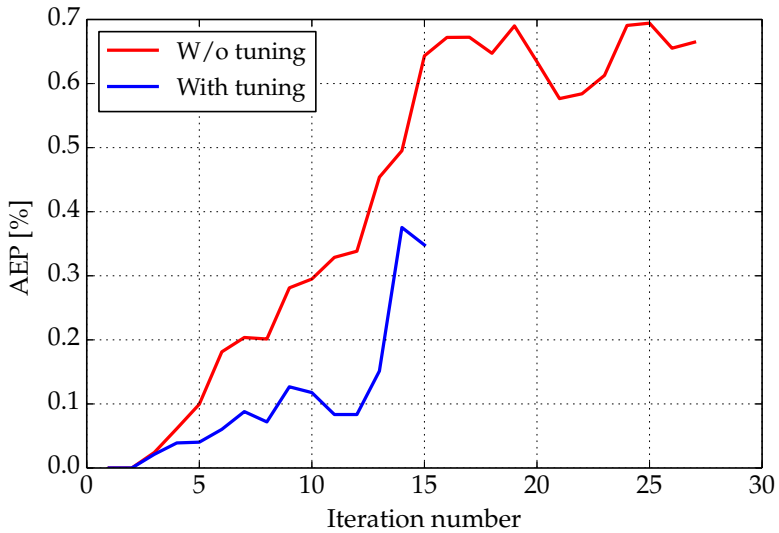

Figure 5.7: Evolution of the annual energy production at each iteration. Comparison between a design without controller tuning and with controller tuning.

Figure 5.8 shows the evolution of the tower base longitudinal bending moment. The fatigue damage of the optimization with the updated gains always lays at higher values than the other case. After 15 iterations, it reaches a reduction of almost 2 %, while case *W/o tuning* almost reaches a solution that satisfies the constraint.

Table 5.1 contains the controller gains of the two models at the final iteration. The gains of *W/o tuning* do not change during the optimization and they are also the gains of the first iteration of *With tuning*. The gains of *With tuning* are significantly different from those of *W/o tuning* meaning that the changes in the wind turbine design do actually affect the controller tuning. The proportional gain of *With tuning* is higher than the one of the other model, indicating a lower regulator mode damping and faster response. This difference in the tuning justifies the lower loads at the tower base of model *W/o tuning*.

From this test case, it appears that the controller tuning highly affects the performances of the optimization and therefore the design through the constraint on the fatigue damage. Updating the controller gains at each cost function evaluation guarantees that the same controller performances are achieved, and therefore it does not allow for a load reduction simply due to a less aggressive controller strategy.

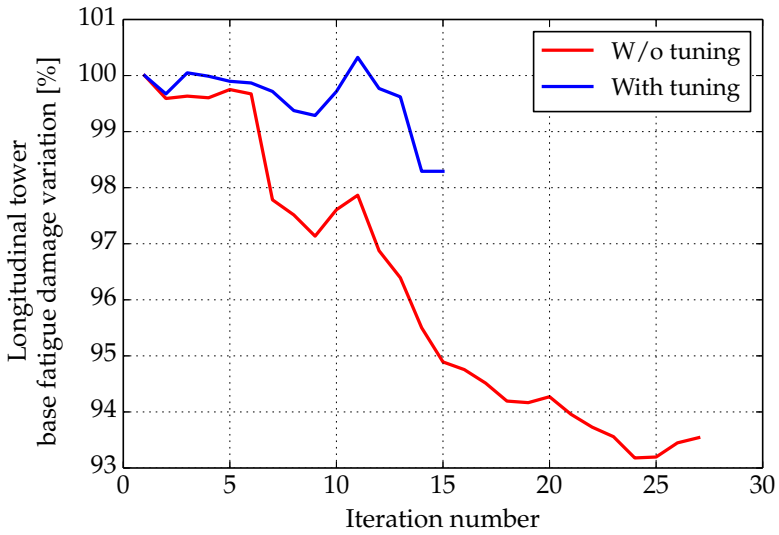

Figure 5.8: Evolution of the tower base longitudinal bending moment fatigue damage variation at each iteration. Comparison between a design without controller tuning and with controller tuning.

Table 5.1: Controller gains used in the optimization at the last iteration. Comparison between *W/o tuning* and *With tuning*.

	$k_{P,0}$ $[rad/(rad/s)]$	$k_{I,0}$ $[rad/rad]$	$k_{P,0,\Omega}$ $[Nm\,s/rad]$	
W/o tuning	1.489	0.401	0.005	
With tuning	1.639	0.441	0.019	
	K_1 $[deg]$	K_2 $[deg^2]$	$K_{1,\Omega}$ $[deg]$	$K_{2,\Omega}$ $[deg^2]$
W/o tuning	8.813	459.686	-0.432	-2.050
With tuning	8.774	402.228	-2.259	-7.640

5.3 Frequency domain loads and frequency placement

The results shown in this section are obtained with the optimization framework based on OpenMDAO, see Section 2.3. The baseline model, used as reference in the comparisons and as initial design guess, is the DTU 10MW RWT.

Shape and structural optimization with frequency constraint

This test case includes both shape and structural design variables and it is based on the same set-up as the cases of the previous section. The problem formulation and extended results are shown in [Article VII]. Constraint on the position of the first forward whirling (FW) edgewise mode frequency, to avoid resonant conditions with the external excitations, and a constraint on the minimum damping of the backward whirling (BW) edgewise mode are added in the optimization problem. The constraint on the aeroelastic frequencies can ensure that the final design will not be subject to resonant conditions, and therefore, the final design will not experience high blade loading. The constraint is implemented as a minimum distance that the frequency of the FW edgewise mode has to have from the 6P external excitation frequency. The minimum distance is 7%. The constraint on the mode damping is included to avoid designs with a very low damped edgewise mode that would lead to high fatigue damage loading. The damping ratio is set to be higher than 1%. Both constraints are applied at 14 and $25m/s$. The obtained solution is denoted *Freq. constr.*.

This new design locates far from the Pareto front (introduced in the previous section) but still it reaches a 10% reduction of the blade mass, and does not compromise the AEP.

Figure 5.9 shows the wind turbine aeroelastic frequencies close to the 6P ex-

ternal excitation of designs DTU 10MW RWT, AEP0.8, AEP0.925, and *Freq. constr.*. The designs AEP0.8 and AEP0.925 are also included because they represent significant limits on the Pareto front. They are obtained with optimizations without the frequency constraint and with different weights in the cost function between mass and AEP. In the plot the first collective flapwise mode (Coll. flap.), the first FW flapwise mode (FW flap.), and the first FW and BW edgewise modes (FW edge and BW edge) can be seen. All the optimized models have a significant reduction in the values of the aeroelastic frequencies compared to the reference design. The frequency of the FW edgewise mode of AEP0.8 is overlapping the frequency of 6P external excitation above rated wind speed. AEP0.925 has the frequency of the FW edgewise mode that is sufficiently reduced to be lower than the 6P frequency. The frequency of *Freq. Constr.* hits the constraint at $25m/s$ and it is not further reduced.

Even if the constraint is based on the distance between the mode and the excitation frequency, and therefore it does not impose the mode frequency to be higher than the 6P frequency, the algorithm is not able to find a solution with a frequency lower than the 6P. This limitation is intrinsic of a gradient

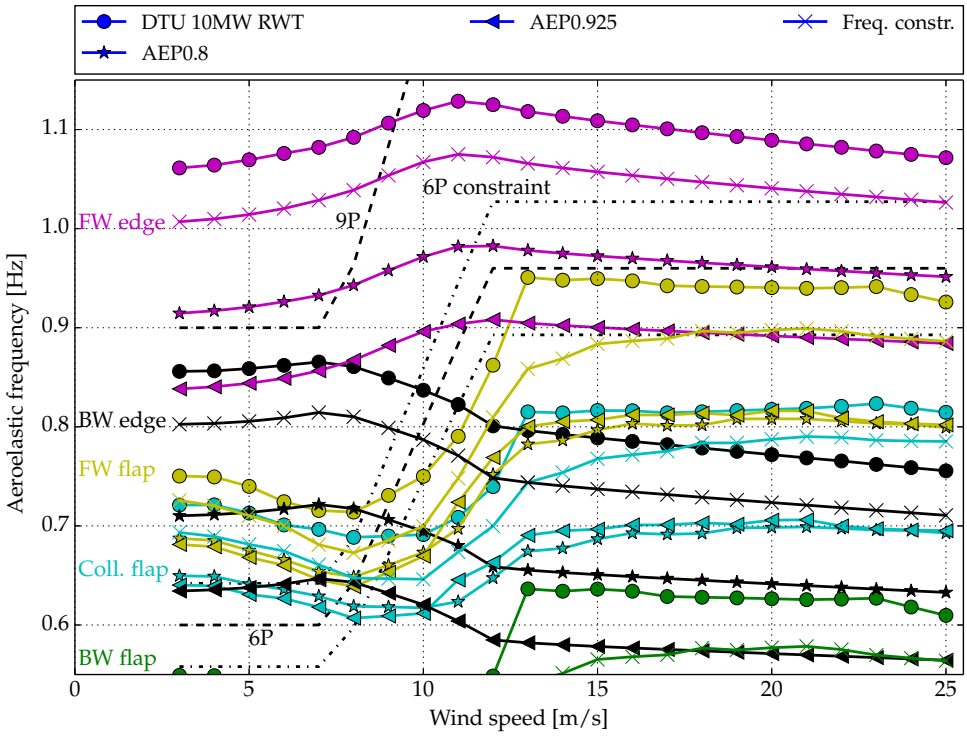

Figure 5.9: Wind turbine aeroelastic frequencies close to the 6P external excitation. Comparison between DTU 10MW RWT, AEP0.8, AEP0.925, and *Freq. Contr.*.

based algorithm, unless large steps are allowed. To further improve the design a different formulation of the constraint should be identified, or a design with $w = 0.8$ should be started from the design of $AEP0.925$, so that the frequency is already lower than the 6P frequency.

5.4 Remarks

Remarks and conclusions about the results shown in this chapter can be summarized as:

1. Optimization based on loads evaluated in time domain can perform poorly when the problem complexity increases due to inaccuracy of the gradient evaluation;
2. Optimization based on loads evaluated in time domain are significantly time consuming even when simulations are parallelized;
3. The frequency based method for fatigue estimation allows to obtain designs with same AEP and lower loading. The load reduction has been verified with time domain simulations;
4. Including the controller tuning in the design process affects the design and limits the reduction of the fatigue damage. Therefore, concurrent aeroservoelastic design can lead to different solutions compared to the state-of-the-art aeroelastic approach;
5. Adding constraints to regulate the position of the aeroelastic frequencies helps avoiding designs with resonant conditions. When a linear model is already available in the workflow, a check on the frequencies and damping does not increase the computational time but can significantly improve the final design;
6. An improved formulation of the mode frequency constraint should be investigated so that the mode frequency could move so that it could be both lower than and greater than the external excitation frequency.

CHAPTER 6

Conclusions and Future Work

New design approaches are required to further reduce the cost of energy by better exploitation of the synergy between wind turbine components.

This work presented methods and techniques to integrate wind turbine controllers in the wind turbine design process and to perform concurrent aeroservoelastic optimization design.

Two optimization frameworks have been developed to perform optimization design. These tools handle workflows that model a wind turbine and evaluate loads and performances under specific conditions. Three approaches to evaluate wind turbine loads have been proposed and integrated in the optimization codes. The first method is based on time domain simulations, the second exploits a linear model to evaluate fatigue damage loads in the frequency domain, and the third allows to avoid resonant conditions that could lead to excessive fatigue damage. The first technique exploits nonlinear time domain aeroservoelastic simulations, here computed with HAWC2, and the other two methods are based on a high-order aeroservoelastic linear model implemented in HAWCStab2. The methods have been employed to perform wind turbine optimization design.

Methods to automatically tune a wind turbine controller have been improved and introduced. A first approach is based on a pole-placement technique with models of different order. Two other methods based on loads evaluated in the time domain and the frequency domain have been described.

Several analyses with a 5MW and a 10MW wind turbine have been carried out to demonstrate the validity and limitations of these approaches. The method showed the ability of reducing the blade mass and increase the annual energy production. The analysis leads to the following conclusions in the listed topics:

- **Systematic controller tuning**:
  - Numerical pole-placement approaches with high-order models did not improve significantly the positioning of the regulator mode. This was partially due to the scheduling function of the controller used in the investigation;
  - Pole-placement with a model that includes the filter on the rotor speed feedback improved the performances increasing the damping and it did not compromise computational cost;
  - Tuning based on time domain simulations allowed selecting any controller parameter and estimating both ultimate and fatigue loads. On the other hand, it could be subject to uncertainty and unreliability of the results due to a limited turbulent wind realization;
  - Tuning based on fatigue evaluated in the frequency domain allowed for faster tuning compared to time domain. However, this approach had the limitation that it could not estimate gains related to nonlinear components of the controller;
  - The dynamic inflow affected significantly the placement of the regulator mode. Interaction between the dynamic inflow and regulator poles had been identified.
- **Wind turbine optimization design**:
  - Optimization based on loads evaluated in time domain performed poorly when the problem complexity increased. Time domain aeroservoelastic simulations should not be employed in a cost function because they require too high computational time. Uncertainty related with the nonlinearity of the models and the stochastic wind input compromised the evaluation of the gradients, affecting the obtained results;
  - Fatigue damage evaluated with a linear model in frequency domain allowed faster loads evaluation, making it suitable for optimization applications. However, the lower accuracy of the model required that the solution was verified with time domain analysis. The method allowed to obtain new designs with lower fatigue damage that had been confirmed with time domain simulations;
  - Constraints on the position of low damped aeroelastic modes frequencies could avoid resonant conditions that can lead to high vi-

brations. This technique improved the final design without affecting the computational cost since a linear model was already available in the optimization workflow;

– Retuning the controller at each cost function evaluation before the loads are evaluated, affected the design because it guaranteed a consistent controller strategy throughout the design process. Therefore, concurrent aeroservoelastic design led to a different solution than an aeroelastic approach;

– The optimization tool is able to reduce the blade mass and increase the annual energy production within the constraints, for the selected test cases.

6.1 Future work

Recommendations for future works are:

- New scheduling functions should be investigated to improve the pole-placement. Different strategies, than having constant frequency and damping along the full load region, should be tested to improve the trade-off between loads and rotor speed regulation;

- Further analysis of the interaction between the regulator mode and the dynamic inflow should be performed to better understand the dynamic inflow effects on the controller tuning;

- Adopt as reference tuning the one obtained from pole-placement with a model that includes the filter on the rotor speed feedback. This solution has shown better performances compared to the state-of-the-art approach and it can still generate a solution within few seconds;

- More concurrent aeroservoelastic designs should be performed to estimate better the effects of the controller tuning on the wind turbine design;

- It is highly recommended not to use loads evaluated with time domain simulations in a cost function that is computed for each design variable. Time domain load evaluations should be integrated in the optimization framework as an outer-loop to verify the obtained solutions and update constraints based on nonlinear loads;

- Improve the formulation of the constraint on the mode frequency placement so that it could be both lower than and greater than the external

excitation frequency.

- Extend the analysis including controllers for load alleviation in the design process. This advancement should illustrate the actual effects of these controller strategies on the turbine design.

Acknowledgements

I would like to express my gratitude to my supervisors Christian, Morten, and Lars. Thank you for the trust, support, and guidance throughout these years. I really appreciated your patience and help.

Special thanks to the AED section for being a great working environment. In particular, thanks to Frederik for all the help with the HAWC2 wrapper and Taeseong, Torben, and Flemming for all the discussions about resonances.

I would like to thanks the office mates: Leo, Georg, Joachim, Sri, David, Witold, and Ivan. Thanks for all the serious and less-serious discussions, the technical and moral support, and all the very cheerful moments.

I would also like to acknowledge all those that supported and helped me outside work: my Danish Family, the Adventure Gang, and the Roomies. Thanks for all the great moments and the patience in the not-so-great days. Thanks to you these years have been a wonderful life experience.

Finally, many thanks to my family: Mamma, Papà, Dinda, Giordi, and Agnese. Grazie mille per aver accetato la mia scelta di spostarmi al nord e per il vostro supporto ed affetto anche quando sono lontano.

Thank you all.

Carlo

Roskilde, January 2015.

Bibliography

[1] Leithead WE, De La Salle SA, and Reardon D. Classical control of active pitch regulation of constant speed horizontal axis wind turbines. *International Journal of Control* 1992; **55**(4):845–876, doi:10.1080/00207179208934263.

[2] Leith DJ and Leithead WE. Implementation of wind turbine controllers. *International Journal of Control* 1997; **66**(3):349–380, doi:10.1080/002071797224621.

[3] Wright AD and Fingersh LJ. Advanced control design for wind turbines; part i: Control design, implementation, and initial tests. *Technical Report NREL/TP500-42437*, NREL/NWTC, 2008.

[4] Bottasso CL and Croce A. Advanced control laws for variable-speed wind turbines and supporting enabling technologies. Technical Report DIA-SR 09-01, Dipartimento di Ingegneria Aerospaziale, Politecnico di Milano, Milano, Italy, 2009.

[5] Henriksen LC, Poulsen NK, and Hansen MH. Nonlinear model predictive control of a simplified wind turbine. *In proceedings of the 18th IFAC World Congress* 2011; 551-556, doi:10.3182/20110828-6-IT-1002.02070.

[6] Bossanyi E, Savini B, Iribas M, Hau M, Fischer B, Schlipf D, van Engelen T, Rossetti M, and Carcangiu CE. Advanced controller research for multi-MW wind turbines in the UPWIND project. *Wind Energy* 2012; **15**(1):119–145, doi:10.1002/we.523.

[7] Riziotis VA, Politis ES, Voutsinas SG, and Chaviaropoulos PK. Stability analysis of pitch-regulated, variable-speed wind turbines in closed loop operation using a linear eigenvalue approach. *Wind Energy* 2008; **11**(5):517–535, doi:10.1002/we.276.

[8] Riziotis VA. Stability analysis of pitch-regulated, variable speed wind turbines in closed loop operation using a linear eigenvalue approach. *In Proceedings of the Science of Making Torque from Wind 2007*, 2007.

[9] Mogensen TS, Larsen AJ, Poulsen NK, Politis ES, Riziotis V, van Engelen TG, Buhl T, Thomsen K, Markou H. Design guidelines for integrated aeroelastic control of wind turbines - task-12 report. *Technical Report 87-550-3550-7*, Risø National Laboratory, 2007.

[10] Markou H, Hansen MH, Buhl T, van Engelen T, Politis ES, Riziotis V, Poulsen NK, Larsen AJ, Mogensen TS, Holierhoek JG. Aeroelastic stability and control of large wind turbines - main results. *Proceedings of EWEA 2007 - European Wind Energy Conference and Exhibition*, 2007.

[11] Hansen MH, Hansen A, Larsen TJ, Øye S, Sørensen P, Fuglsang P. Control design for a pitch-regulated, variable speed wind turbine. *Technical Report Risø-R-1500(EN)*, Risø National Laboratory, 2005.

[12] Ashuri T, van Bussel GJW, Zaayer MB, van Kuik GAM. Controller design automation for aeroservoelastic design optimization of wind turbines. *TU Delft: Aerospace Engineering: Aerodynamics, Wind Energy & Propulsion* 2010.

[13] Fuglsang P. Optimization of stall regulated rotors. *IEA Joint Action. 8. Symposium on Aerodynamics of Wind Turbines*, 333–351, 1994.

[14] Selig MS and Coverstone-Carroll VL. Application of a genetic algorithm to wind turbine design. *Journal of Energy Resources Technology* 1996, **118**(1):22–28, doi:10.1115/1.2792688.

[15] Fuglsang P, Aagaard MH. A design study of a 1 MW stall regulated rotor. *Technical Report 87-550-2057-7* , Risø National Laboratory, 1995.

[16] Fuglsang P, Madsen H. Optimization method for wind turbine rotors. *Journal of Wind Engineering and Industrial Aerodynamics* 1999; **80**(12):191–206, doi:10.1016/S0167-6105(98)00191-3.

[17] Fuglsang P, Thomsen K. Site-specific design optimization of 1.5-2.0 MW wind turbines. *Journal of Solar Energy Engineering* 2001; **123**(4):296, doi:10.1115/1.1404433.

[18] Fuglsang P, Bak C, Schepers JG, Bulder B, Cockerill TT, Claiden P, Olesen A, van Rossen R. Site-specific design optimization of wind turbines. *Wind Energy* 2002; **5**(4), 261–279, doi:10.1002/we.61.

[19] Bottasso CL, Campagnolo F, Croce A. Multi-disciplinary constrained optimization of wind turbines. *Multibody System Dynamics* 2012; **27**(1):21–53, doi:10.1007/s11044-011-9271-x.

[20] Bottasso CL, Campagnolo F, Croce A, Tibaldi C. Optimization-based study of bendtwist coupled rotor blades for passive and integrated passive/active loadalleviation. *Wind Energy* 2013; **16**(8):1149–1166, doi: 10.1002/we.1543.

[21] Ashuri T, Zaaijer MB, Martins JRRA, van Bussel GJW, van Kuik GAM. Multidisciplinary design optimization of offshore wind turbines for minimum levelized cost of energy. *Renewable Energy* 2014; **68**:893–905, doi:10.1016/j.renene.2014.02.045.

[22] Merz KO, Muskulus M, Moe G. A simple frequency-domain method for stress analysis of stall-regulated wind turbines. *Wind Energy* 2012; **15**(5):773–798, doi:10.1002/we.504.

[23] Merz KO. Rapid optimization of stall-regulated wind turbine blades using a frequency-domain method: Part 1, loads analysis. *Wind Energy* 2014; doi:10.1002/we.1786.

[24] Merz KO. Rapid optimization of stall-regulated wind turbine blades using a frequency-domain method: Part 2, cost function selection and results. *Wind Energy* 2014; doi:10.1002/we.1738.

[25] Fischer GR, Kipouros T, Savill AM. Multi-objective optimization of horizontal axis wind turbine structure and energy production using aerofoil and blade properties as design variables. *Renewable Energy* 2014; **62**(0):506 – 515, 2014, doi:10.1016/j.renene.2013.08.009.

[26] HAWCStab2 - Aeroservoelastic Analysis Code. http://hawcstab2.vindenergi.dtu.dk.

[27] Hansen MH. Aeroelastic stability analysis of wind turbines using an eigenvalue approach. *Wind Energy* 2004; **7**(2):133–143, doi:10.1002/we.116.

[28] Hansen MH. Aeroelastic properties of backward swept blades. *49th AIAA Aerospace Sciences Meeting including the New Horizons Forum and Aerospace Exposition*. American Institute of Aeronautics and Astronautics, 2011, doi:10.2514/6.2011-260.

[29] Sønderby I, Hansen MH. Open-loop frequency response analysis of a wind turbine using a high-order linear aeroelastic model. *Wind Energy* 2014; **17**: 1147–1167, doi:10.1002/we.1624.

[30] Welcome to HAWC2!. http://www.hawc2.dk.

[31] Kim T, Hansen AM, Branner K. Development of an anisotropic beam finite element for composite wind turbine blades in multibody system. *Renewable Energy* 2013; **59**:172–183, doi:10.1016/j.renene.2013.03.033.

[32] Hansen MH, Gaunaa M, Madsen HA. A beddoes-leishman type dynamic stall model in state-space and indicial formulations. *Technical Report Risø-R-1354(EN)*, Risø National Laboratory, 2004.

[33] Madsen HA, Riziotis V, Zahle F, Hansen M, Snel H, Grasso F, Larsen T, Politis E, Rasmussen F. Blade element momentum modeling of inflow with shear in comparison with advanced model results. *Wind Energy* 2012; **15**(1), 63–81, doi:10.1002/we.493

[34] Passon P, Kühn M, Butterfield S, Jonkman J, Camp T, Larsen TJ. OC3 benchmark exercise of aero-elastic offshore wind turbine codes. *Journal of Physics: Conference Series* 2007, **75**(1):012071, doi:10.1088/1742-6596/75/1/012071.

[35] Jonkman J, Musial W. Offshore code comparison collaboration (OC3) for IEA wind task 23 offshore wind technology and deployment. *Technical Report NREL/TP-5000-48191*, NREL/NWTC, 2010.

[36] Popko W, Vorpahl F, Zuga A, Kohlmeier M, Jonkman J, Robertson A, Larsen TJ, Yde A, Sætertrø K, Okstad KM, *et al.*. Offshore code comparison collaboration continuation (OC4), phase i - results of coupled simulations of an offshore wind turbine with jacket support structure. *Proceedings of the International Offshore and Polar Engineering Conference 2012*; Rhodes, Greece 2012; 337–346.

[37] Vorpahl F, Strobel M, Jonkman JM, Larsen TJ, Passon P. Verification of aero-elastic offshore wind turbine design codes under IEA wind task XXIII. *Wind Energy* 2013, doi:10.1002/we.1588.

[38] Larsen TJ, Aagaard MH, Larsen GC, Hansen KS. Validation of the dynamic wake meander model for loads and power production in the Egmond aan Zee wind farm. *Wind Energy* 2013; **16**(4): 605–624, doi:10.1002/we.1563.

[39] Mann J. Wind field simulation. *Probabilistic Engineering Mechanics* 1998; **13**(4):269–282, doi:10.1016/S0266-8920(97)00036-2.

[40] Larsen TJ, Hansen MA. How 2 HAWC2, the user's manual. *Technical Report Risø-R-1597(ver. 4-4)(EN)*, Risø National Laboratory, 2014.

[41] MATLAB (2011) Release 2011b, Natick, Massachusetts: The MathWorks Inc..

[42] OpenMDAO. http://openmdao.org.

[43] Moore KT, Naylor B, Gray JS. The development of an open-source framework for multidisciplinary analysis and optimization. *10th AIAA/ISSMO Multidisciplinary Analysis and Optimization Conference*. American Institute of Aeronautics and Astronautics, 2008.

[44] Gray JS, Moore KT, Naylor BA. OPENMDAO: An open source framework for multidisciplinary analysis and optimization. *13th AIAA/ISSMO Multidisciplinary Analysis and Optimization Conference*, American Institute of Aeronautics and Astronautics, 2010.

[45] Heath CM, Gray JS. OpenMDAO: Framework for flexible multidisciplinary design, analysis, and optimization methods. *8th AIAA Multidisciplinary Design Optimization Specialist Conference*, American Institute of Aeronautics and Astronautics, 2012.

[46] pyOpt. http://pyopt.org.

[47] Perez RE, Jansen PW, Martins JRRA. pyOpt: a python-based object-oriented framework for nonlinear constrained optimization. *Structural and Multidisciplinary Optimization* 2012; **45**(1), 101–118. doi:10.1007/s00158-011-0666-3

[48] Gill PE, Murray W, Saunders MA. SNOPT: An SQP algorithm for large-scale constrained optimization (reprinted from SIAM journal optimization, vol 12, pg 979-1006, 2002). *Siam Review* 2005; **47**(1):99–131, doi:10.1137/S0036144504446096.

[49] Gill PE, Murray W, Saunders MA. SNOPT 7 user's guide. *Technical Report Numerical Analysis Report NA 04-1*, Department of Mathematics, University of California, 2008.

[50] BECAS. http://becas.dtu.dk.

[51] Blasques JP. User' s manual for BECAS: a cross section analysis tool for anisotropic and inhomogeneous beam sections of arbitrary geometry. *Technical Report Risø-R-1785(EN)*, Risø National Laboratory, 2012.

[52] Blasques JP, Stolpe M. Multi-material topology optimization of laminated composite beam cross sections. *Composite Structures* 2012, **94**(11):3278 – 3289, 2012, doi:10.1016/j.compstruct.2012.05.002.

[53] Hansen MH, Henriksen LC. Basic DTU Wind Energy controller. *Technical Report E-0028*, DTU Wind Energy, 2013.

[54] Jonkman J, Butterfield S, Musial W, Scott G. Definition of a 5-MW reference wind turbine for offshore system development. *Technical Report NREL/TP-500-38060*, NREL/NWTC, 2009.

[55] Bak C, Zahle F, Bitsche R, Kim T, Yde A, Henriksen LC, Andersen PB, Natarajan A, Hansen MH Design and performance of a 10 MW wind turbine. *To be submitted* 2013.

[56] Bak C, Bitsche R, Yde A, Kim T, Hansen MH, Zahle F, Gaunaa M, Blasques JPAA, Døssing M, Wedel Heinen JJ, Behrens T. Light rotor: The 10-MW reference wind turbine. *Proceedings of EWEA 2012 - European Wind Energy Conference and Exhibition*, 2012.

[57] The DTU 10MW Reference Wind Turbine project site. http://dtu-10mw-rwt.vindenergi.dtu.dk.

[58] Benasciutti D, Tovo R. Spectral methods for lifetime prediction under wide-band stationary random processes. *International Journal of Fatigue* 2005; **27**(8):867–877, doi:10.1016/j.ijfatigue.2004.10.007.

[59] Benasciutti D, Tovo R. Comparison of spectral methods for fatigue analysis of broad-band gaussian random processes. *Probabilistic Engineering Mechanics* 2006; **21**(4):287–299, doi:10.1016/j.probengmech.2005.10.003.

[60] Connell JR. The spectrum of wind speed fluctuations encountered by a rotating blade of a wind energy conversion system. *Solar Energy* 1982; **29**(5):363–375, doi:10.1016/0038-092X(82)90072-X.

[61] Dragt J. Atmospheric turbulence characteristics in the rotating frame of reference of a wecs rotor. *European Community Wind Energy Conference*, Madrid, Spain, 1990; 274–278.

[62] Hansen MH. Aeroelastic optimization of MW wind turbines. *Technical Report Risø-R-1803(EN)*, Risø National Laboratory, 2011.

Part II

Publications

Article I: An Investigation on Wind Turbine Resonant Vibrations.

This article was submitted for publication to the *Wind Energy* journal in May 2014.

WIND ENERGY
Wind Energ. 2014; **00**:1–14
DOI: 10.1002/we

RESEARCH ARTICLE

An investigation on wind turbine resonant vibrations

C. Tibaldi[1], T. Kim[1], T. J. Larsen[1], F. Rasmussen[1], R. de Rocca Serra[2], and F. Sanz[2]

[1] Technical University of Denmark, Department of Wind Energy
[2] Alstom Renovables S.L.

ABSTRACT

In this paper wind turbine resonant vibrations are investigated on the basis of aeroelastic simulations both in frequency and time domain. The investigation focuses on three different aspects: the need of a precise modeling when a wind turbine is operating close to resonant conditions; the importance of estimating wind turbine loads also at low turbulence intensity wind conditions to identify the presence of resonances; and the wind turbine response due to external excitations. In the first analysis, three different wind turbine models are analyzed with respect to the frequency and damping of the wind turbine aeroelastic modes. The fatigue damage loads on the same wind turbine models are then investigated with two different turbulence intensities, to analyze the wind turbine response. In the second analysis, a wind turbine model is excited with an external force placed at different locations on a wind turbine. This analysis helps identifying the modes that might be excited, and therefore the frequencies at which minimal external excitation should be present during operations. The study shows that significant edgewise blade vibrations can occur on modern variable-speed pitch-controlled wind turbines even if the aeroelastic damping of the edgewise modes is positive. When operating close to resonant conditions, small differences in the modeling can have a large influence on the vibration level, and more detailed information on especially the blade properties may be required than otherwise necessary. The edgewise vibrations are less visible in high turbulent conditions and they may be difficult to identify in a normal design approach. Using simulations with low level turbulence intensity will ease this identification and could potentially avoid a redesign. Furthermore, depending on the type of external excitation different aeroelastic modes can be excited. The investigation is performed using aeroelastic models corresponding to a 1.5 MW class wind turbine with slight variations in blade properties.

KEYWORDS

Wind turbine, resonance, aeroelastic damping, edgewise vibrations, structural pitch

Correspondence
T. Kim, Technical University of Denmark, Department of Wind Energy, RisøCampus, Frederiksborgvej 399, DK-4000 Roskilde, Denmark

E-mail: tkim@dtu.dk

Received . . .

1. INTRODUCTION

The most important contribution to wind turbine loads is the periodic excitation from turbulence denoted rotational sampling. The location of the frequency excitations are denoted 1P, 2P, ..., NP. The main sources of these excitations are gravity, tower shadow, wind shear, rotor imbalance, atmospheric turbulence, and wakes from other upstream turbines. Resonant conditions are more likely to occur with increased wind turbine size because the frequencies of wind turbine aeroelastic modes are lower, hence the gap between the frequencies is smaller. Furthermore, larger turbines have corresponding lower rotor rotational speed, and therefore the distance between the excitation frequencies is lower. For these reasons, on modern large-scale wind turbines, aeroelastic modal frequencies have a high risk of coinciding with one of the most energetic harmonics of the external excitations. Therefore, a better understanding of the wind turbine response under resonant conditions is required.

The importance of avoiding resonant conditions is well established in the wind energy community [1, 2, 3], however few studies have investigated the details and impact of this phenomenon on wind turbines.

One of the most common wind turbine resonant condition occurs when the 3P frequency coincides with the tower frequencies [4]. After the wind turbine starts-up, the rotor speed increases, and the 3P frequency crosses the tower natural frequencies, before the turbine reaches the rated rotor rotational speed. This resonance problem can be easily solved imposing a fast transition through the rotor speed, where the 3P frequency coincides with the first tower mode frequencies [5, 6, 7, 8]. With this approach, the resonant condition does not lead to high loading as the vibrations do not have time to build up.

It is also well known that a resonance condition between 1P and the first side-side tower mode should be avoided [9]. This rotor excitation mainly origins from either mass or aerodynamic imbalance.

Sullivan [10] investigated the resonant response of two two-bladed horizontal-axis wind turbines both analytically and experimentally. In the study he concluded that resonance with the external excitations up to the 5P, with the first blade edgewise mode frequency, can lead to high vibrations. When a resonance with a blade flapwise mode occurs, this does not lead to large vibrations because of the large aerodynamic damping. Furthermore, a resonance with the tower modes does not affect blade vibrations.

Fleming et al. [11] investigated resonant conditions on the CART3 wind turbine. The vibrations arose after a conversion of the turbine from two-bladed to three-bladed. In the paper, two vibration conditions due to resonance are addressed. The first vibration occurred on the high-speed shaft, when a not-defined mode frequency crossed the gear meshing frequency and the 2P frequency. This resonance was not considered critical because the vibration level was acceptable. The second resonance was measured on the nacelle accelerometer. This resonant condition was caused by the coincidence of a gear meshing frequency, at rated wind speed, and the natural frequency of the inertial measurement unit mount. This second resonance was solved stiffening the mount.

This article investigates the effects of resonant conditions on a three-bladed pitch regulated wind turbine in the MW size. The investigation focuses on three different aspects. First, the effect of structural pitch on resonant blade edgewise vibrations is analyzed. This analysis shows the importance of detailed modeling to evaluate the wind turbine response when operating close to a resonant condition. Secondly, the need of evaluating low turbulence intensity wind conditions, to better identify the presence of resonance, is pointed out. The relevance of wind conditions is addressed looking at first blade edgewise vibrations and second lateral tower vibrations. Finally, the wind turbine response to harmonic excitation in the lateral direction is simulated and discussed. This investigation is performed to identify the most energetic resonant conditions. The aim is to improve the understanding of where a wind turbine mode frequency should be placed, during the design phase, to obtain the lowest level of vibrations.

The paper focuses only on edgewise and lateral vibrations because the damping of longitudinal and flapwise modes is usually sufficiently high to limit the vibrations.

The investigation is carried out as a case study where three different blade configurations are analyzed and compared. The analysis is performed using a nonlinear aeroservoelastic model, implemented in HAWC2, and a linearized aeroservoelastic model, implemented in HAWCStab2.

2. WIND TURBINE AEROSERVOELASTIC MODELS

Three different 1.5 MW-class wind turbines are considered in this investigation. The blades have no pre-bend and no flatback airfoils. They are denoted **REF**, **SP5**, and **STIF**.

REF is the reference model. REF and SP5 differ only in the amount of structural pitch of the blades. In REF the structural pitch is 0 deg along the whole blade, while in SP5 it is 5 deg along the whole blade. STIF has a different structural design with increased mass and stiffness properties and an increased first blade edgewise natural frequency, compared to the REF model. The flapwise frequency is lower because of this change. The structural pitch of STIF is 0 deg along the whole blade. Each wind turbine is analyzed both with a nonlinear aeroelastic model and with a linear aeroelastic model.

The first blade edgewise natural frequencies of REF and SP5 are close to the 4P excitation frequency. STIF has a higher first blade edgewise natural frequency, to avoid the resonant condition. Table I shows the first four isolated blade structural

	REF	SP5	STIF
1st Flap	2.36	2.36	2.15
1st Edge	3.93	3.92	4.31
2nd Flap	7.53	7.54	7.13
2nd Edge	13.13	13.13	14.09
2nd Tower lateral	9.08	9.08	9.08

Table I. Frequencies of the first two isolated blade structural modes and of the second lateral tower wind turbine structural mode normalized with the 1P frequency at rated.

Wind Energ. 2014; **00**:1–14 © 2014 John Wiley & Sons, Ltd.
DOI: 10.1002/we
Prepared using weauth.cls

frequencies. The frequencies are computed at standstill, therefore without aerodynamics. The values of the frequencies are normalized with respect to the 1P frequency at rated, as all the frequencies shown throughout the paper. The table shows that the frequencies of REF and SP5 are almost identical. STIF has higher edgewise mode frequencies caused by an increased stiffness-to-mass ratio. The second lateral tower mode frequencies are close to the 9P excitation.

2.1. Nonlinear model

The nonlinear aeroservoelastic model implemented in HAWC2 [12] is used for calculating wind turbine response in time domain. The structural part of the model is based on a multi-body formulation, where each body is an assembly of Timoshenko beam elements [13]. The aerodynamic model is based on the blade element momentum theory. The model is extended to handle dynamic inflow, dynamic stall, skew inflow, shear effects on the induction, and effects from large deflections. A validation of the model can be found in [14], [15], and [16].

The Basic DTU Wind Energy controller [17] is used to regulate the wind turbine in the nonlinear simulations.

All the nonlinear simulations are performed using a Newmark integration method with a time-step of 0.02 s.

2.2. Linear model

The linear high-order aeroelastic model, implemented in HAWCStab2, is used to compute the frequency and damping of the wind turbine aeroelastic modes. The model is based on an analytical linearization of a linear finite beam element model in a nonlinear corotational formulation. The structural model is coupled with an unsteady aerodynamic blade element momentum model. The aerodynamic model considers model contributions from shed vorticity and dynamic stall. Frozen wake is assumed with respect to induction. A detailed description of the model is provided by Hansen [18, 19]. An extensive validation and analysis of the open-loop performance of the tool is provided by Sønderby and Hansen [20].

The frequencies and damping computed with HAWCStab2 are of particular interest because they include aeroelastic effects of the rotating rotor. Therefore, it is possible to identify those modes that are generated from the splitting of the rotor tilt-yaw and vertical-lateral modes, for an increasing rotational speed (Ω) due to gyroscopic effects, best known as whirling modes. These modes are observed on a ground fixed frame. The mode that diverges with a value of $-\Omega$ is called backward whirling (BW) mode, while the mode that diverges with a value of $+\Omega$ is called forward whirling (FW) mode [21, 22, 23].

2.3. Wind turbine aeroelastic modes frequencies and dampings

An analysis of the wind turbine aeroelastic modes frequencies gives a first insight on the presence of resonant conditions.

Figure 1 shows the normalized frequencies of the first seven aeroelastic modes of the three wind turbine linear models. The figure shows also the 3P and 6P frequencies. When the rotor is balanced, all external excitations, seen by the wind turbine rotor in a ground-fixed reference frame, have peak frequencies at the harmonics of the 3P frequency.

The most important thing to notice is that the first edgewise BW mode frequencies of models REF and SP5 are very close to the 3P external excitation, above rated wind speed. The frequency of the mode is slightly above the 3P frequency at 10 m/s and decreases slowly for increasing wind speed. A resonant condition of the second lateral tower mode (not shown in the figure, but shown in Table I) is also present at the 9P excitation. The frequency of this mode is fairly constant throughout the wind speeds.

Other resonances can also be identified below the 9P frequency. REF and SP5 have the frequency of the first flapwise BW mode coinciding with the 3P excitation below 5 m/s. All the models crosses the 3P excitation with the first flapwise symmetric mode and the 6P excitations with the first edgewise FW mode. Both conditions are not considered critical, the first one because the flapwise mode is highly damped due to the aerodynamics, the second one because the vibrations are unlikely to build up due to the variable rotational speed. STIF has the frequency of the second flapwise BW mode close to the 6P excitation, above 9 m/s. REF has the frequency of the second flapwise symmetric mode that crosses the 9P frequency at 23 m/s. All the resonant conditions involving flapwise modes are not critical as the modes have high damping.

Figure 2 shows the damping ratio of the first three least damped wind turbine aeroelastic modes of the three linear models. The two first blade edgewise whirling modes are the least damped modes. All the aeroelastic modes have positive damping, therefore no modes are unstable. Even if the damping is positive, the resonant conditions of the first edgewise BW mode can lead to high vibrations since the damping is low.

The linear and nonlinear models differ, to some extent, due to the different model implementation and assumptions. Therefore, the aeroelastic frequencies of the two models might also differ. To better analyze and understand results of the nonlinear time domain simulations, the value of the first edgewise BW mode frequency is also identified with the nonlinear model at a wind speed of 10 m/s. The mode frequency is identified with modal excitation and spectral analysis. The identification shows that the frequencies of this mode are lower than the 3P frequency. Their values are 2.97 P and 2.99 P for model REF and SP5 respectively. The frequencies obtained with the linear model are then corrected to match the values identified with the nonlinear model at 10 m/s. The correction leads to a maximum difference between the original and corrected frequencies of 1.3 %.

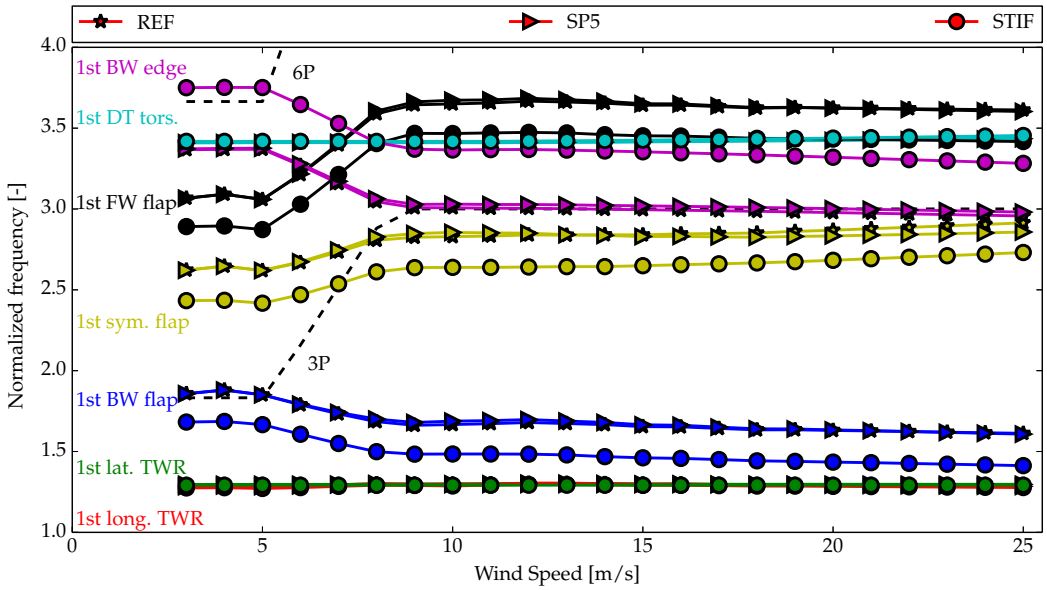

Figure 1. Frequencies of the first seven wind turbine aeroelastic modes normalized with normalized with the 1P frequency at rated. Comparison between the three wind turbine models, REF (stars), SP5 (triangles), and STIF (circles). The external excitations with frequencies of 3P and 6P are also shown (dashed lines). The frequencies are obtained with the linear model.

Figure 3 shows the normalized aeroelastic frequency of the first edgewise BW mode evaluated with the linear model and corrected with the nonlinear model identification. Only REF and SP5 are shown. Around rated wind speed, SP5 has the mode frequency that is very close to the 3P frequency. For increasing wind speed the frequency slowly decreases causing a greater margin to the 3P excitation frequency.

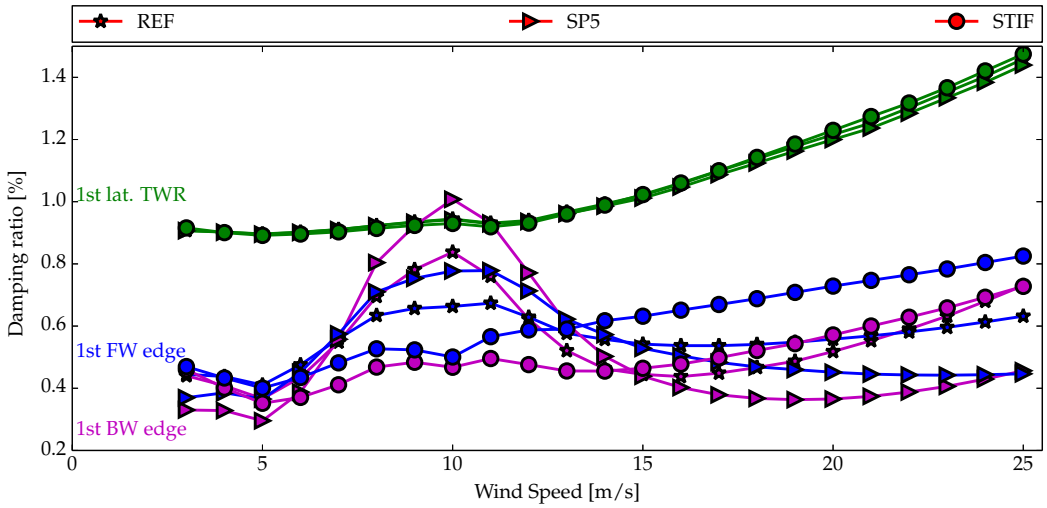

Figure 2. Damping ratio of the first three least damped wind turbine aeroelastic modes. Comparison between the three wind turbine models, REF (stars), SP5 (triangles), and STIF (circles). These values are obtained with the linear model.

Wind Energ. 2014; **00**:1–14 © 2014 John Wiley & Sons, Ltd.
DOI: 10.1002/we
Prepared using weauth.cls

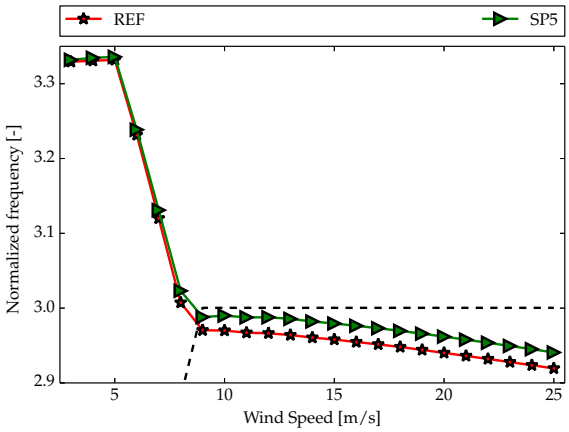

Figure 3. Normalized aeroelastic frequency of the first edgewise backward whirling mode evaluated with the linear model and corrected with the nonlinear model identification.

2.4. Structural pitch

The structural pitch is the angle between the reference system aligned with the chord and the one aligned with the principal axes of bending. A structural pitch different from zero creates an increasing coupling between the flapwise and the edgewise deflections. The structural pitch is of interest because it may have an effect on the aeroelastic frequencies, while it does not change the structural frequencies significantly. Figure 3 shows this effect. At low wind speeds the aeroelastic mode frequency of REF and SP5 are almost identical. On the other hand, at rated wind speed and above, the frequencies of the two models differ. Therefore, two blades, that have a similar elastic behavior, can have different aeroelastic responses, caused by differences in the aeroelastic frequencies. When changing the structural pitch, the aeroelastic damping is also modified. The difference can be seen between model REF and SP5 in Figure 2 on both the first edgewise BW and FW modes. When the structural pitch is increased, the damping decreases at low wind speed and above 15 m/s, while it increases around rated wind speed. The damping differences between the models are due to a different direction of vibration of the edgewise mode, in accordance with the findings in [21, 24].

In the next chapter, more detailed investigations about the aeroelastic responses by changing the aeroelastic frequency and damping due to the structural pitch will be addressed.

3. TURBULENT WIND SIMULATIONS

This section introduces results from nonlinear time simulations during operation. Section 3.1 shows a case with reference turbulence intensity of 16 %, whereas Section 3.2 shows a case with reference turbulence intensity of 2 %. The Mann turbulence model [25] is used in these simulations. The loads are obtained from six different ten minutes simulations with different turbulence seed for each wind speed.

Fatigue damage equivalent loads are evaluated for the tower base lateral bending moment and the blade root edgewise bending moment. The moments are normalized with the steady-state value of the tower base lateral bending moment at 10 m/s and the blade mass moment of REF, respectively. Power spectral densities (PSD) of the time series are shown to identify the modes that contribute the most to the vibrations.

3.1. Normal turbulence intensity

Figure 4 shows the damage equivalent load of the normalized tower base lateral bending moment and of the normalized blade root edgewise bending moment. The loads are compared for the three wind turbine models at wind conditions with a reference turbulence intensity of 16%. At the tower base, Figure 4a, the loads have similar amplitudes between the three models in the whole wind speed range. No model shows a significant increase in the loads compared to the others, even if the edgewise BW modes of REF and SP5 are close to the 3P excitation. The loads at the blade root differs between the models. STIF has higher loads at very low wind speeds due to the higher blade mass. SP5 has higher loads around rated wind speed, due to operation close to the 3P excitation (see Figure 3). STIF has higher loads at wind speeds above 18 m/s.

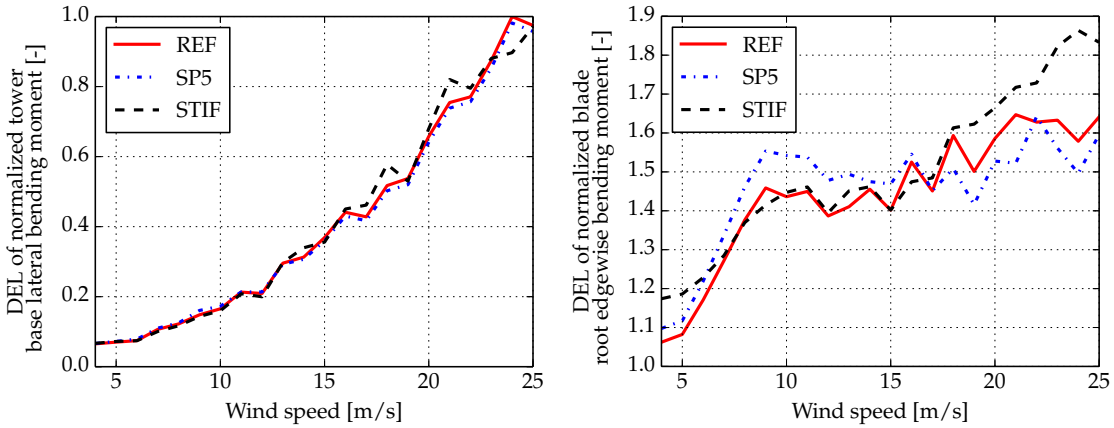

a) Tower base lateral *b) Blade root edgewise*

Figure 4. Damage equivalent load of bending moments. Reference turbulence intensity 16%. Comparison between REF (red solid line), SP5 (blue dash-dot line), and STIF (black dashed line).

In Figure 5 the PSD of the tower base lateral bending moment at 10 m/s and 20 m/s is shown. At both wind speeds, the peak at the tower lateral frequency has the highest energy. At 10 m/s, the second highest peak is the one associated with the first edgewise BW mode. REF and SP5 have the mode frequency very close to the 3P excitation while for STIF it is slightly higher. The peak of STIF has less energy compared to the others. On the other hand, STIF has a higher peak at the frequency of the first forward edgewise whirling mode compared to the other two models. The overall vibrations lead to a similar damage, as shown in Figure 4a. The differences between the variance of the signals, computed as the integral of the power spectra, are less than 5 %. At 20 m/s the peak at 9P has similar amplitude to the peak at the 3P. These vibrations occur due to the proximity of the frequency of the second tower lateral mode with the 9P excitation. When the wind speed increases, the damage at the tower base is dominated by vibrations at the first tower mode frequency.

Figure 6 shows the PSD of the blade root edgewise bending moment at 10 m/s and 20 m/s. At both wind speeds the highest peak occurs at 1P. STIF has higher energy at 1P due to the higher blade mass. The second highest peak, at both wind speeds, is the one at the first blade edgewise frequency. The peak magnitude at the blade frequency of SP5 is slightly higher than for the other models. This difference explains the fatigue damage difference noticed in Figure 4b around rated wind speed. STIF has higher loads above 18 m/s due to the higher mass of the blade (1P from gravity) and due to the

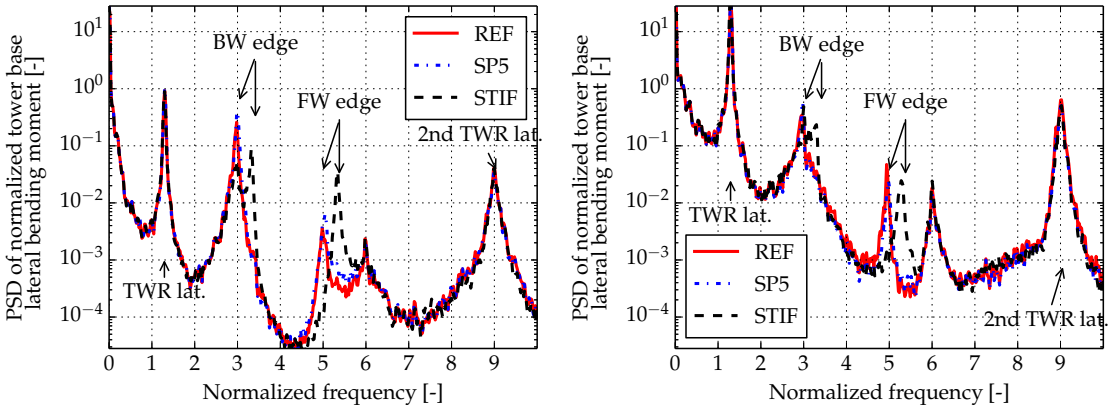

a) 10 m/s *b)* 20 m/s

Figure 5. Tower base lateral bending moment power spectral densities comparison. Reference turbulence intensity 16%.Comparison between REF (red solid line), SP5 (blue dash-dot line), and STIF (black dashed line).

Wind Energ. 2014; **00**:1–14 © 2014 John Wiley & Sons, Ltd.
DOI: 10.1002/we
Prepared using weauth.cls

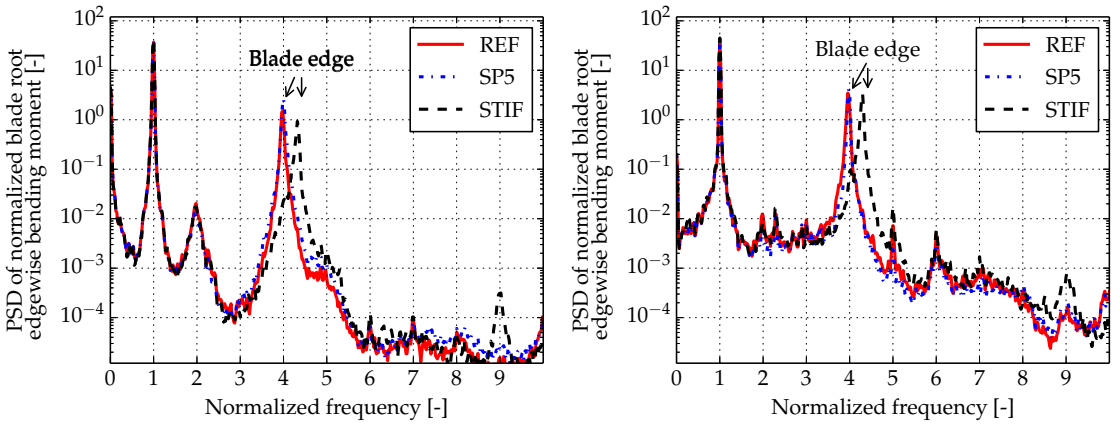

a) 10 m/s *b)*20 m/s

Figure 6. Blade root edgewise bending moment power spectral densities comparison. Reference turbulence intensity 16%.Comparison between REF (red solid line), SP5 (blue dash-dot line), and STIF (black dashed line).

increase of vibrations at the blade edgewise frequency. Comparing the amplitudes of the first edgewise mode at 10 m/s with those at 20 m/s, STIF shows larger increases in the vibration energy than the other two models.

3.2. Low turbulence intensity

Figure 7 shows the damage equivalent load of the normalized tower base lateral bending moment and of the normalized blade root edgewise bending moment. The wind turbulence intensity is selected based on a reference turbulence intensity of 2%. The loads at the tower base do not show remarkable differences except that SP5 has higher loads around rated wind speed, while REF has higher loads above 15 m/s. On the other hand, at the blade root, Figure 7b, the loads are significantly different. SP5 shows an exceptional increase in the loads starting from 8 m/s till 17 m/s. REF has a peak around 10 m/s, but of a lower amplitude. Despite STIF is heavier, it has the same fatigue damage load as REF, at 10 m/s. This similarity indicates that REF has higher vibrations at the first blade edgewise natural frequency. At all the other wind speeds, STIF has higher loads than REF due to the higher weight.

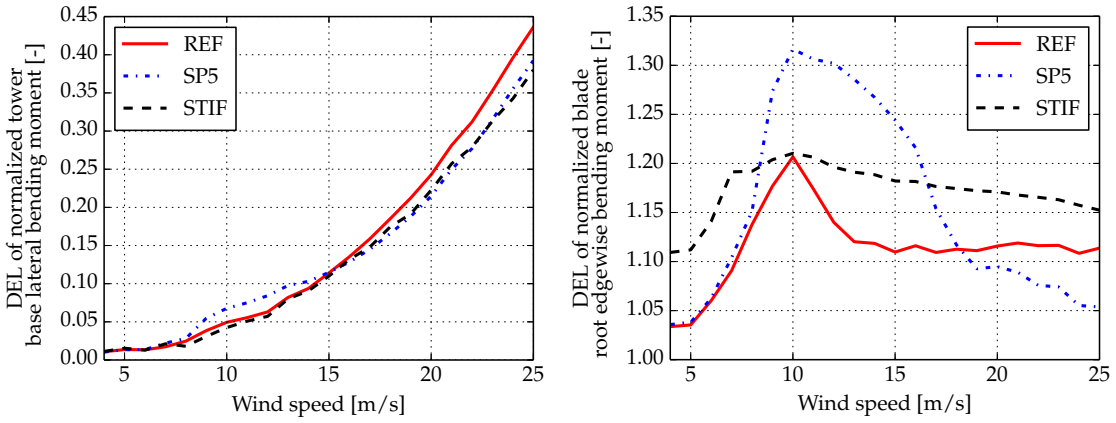

a) Tower base lateral *b) Blade root edgewise*

Figure 7. Damage equivalent load of bending moments. Reference turbulence intensity 2%.Comparison between REF (red solid line), SP5 (blue dash-dot line), and STIF (black dashed line).

Figure 8 shows the PSD of the tower base lateral bending moment at 10 m/s and 20 m/s. At 10 m/s, the frequency with the higher energy is 3P. REF and SP5 have a 3P peak significantly higher than the peak at the tower lateral natural frequency. This behavior can be an indication of the presence of a blade edgewise resonance because the tower is expected to vibrate mainly at its first mode frequency. The peak of the first edgewise BW mode of STIF is lower than those of REF and SP5. The contribution of the peak at 9P, due to the second lateral tower mode, has also a noticeable energy level. The differences of the peak at 3P explain the loads differences seen in Figure 7a. Indeed, SP5 has the highest fatigue damage and the highest peak, while STIF the lowest. The response does not contain significant contributions due to the edgewise FW mode. This behavior reflects that a wind turbine mode is mainly excited by a harmonic of the 3P frequency when the rotor has no imbalances. At 20 m/s the vibrations with the highest amount of energy are those at 9P, indicating the presence of resonance with the second tower mode. At low turbulence intensity wind conditions, the vibration that contributes the most to the fatigue damage is different from the one at high turbulence intensity. Therefore, the low turbulence intensity simulations show more clearly these resonant conditions.

Figure 9 shows the PSD of the blade root edgewise bending moment at 10 m/s and 20 m/s, at the low turbulence intensity wind conditions. The peak of the first edgewise natural frequency is significantly lower for STIF, while they are similar with normal turbulence intensity (see Figure 6). At 10 m/s SP5 has a higher peak at 4P than REF. However, they have

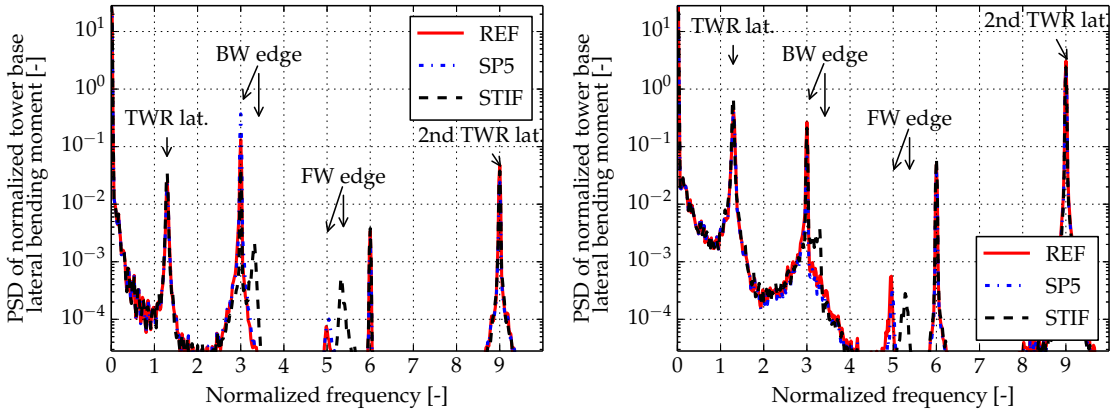

a) 10 m/s *b)* 20 m/s

Figure 8. Tower base lateral bending moment power spectral densities comparison. Reference turbulence intensity 2%.Comparison between REF (red solid line), SP5 (blue dash-dot line), and STIF (black dashed line).

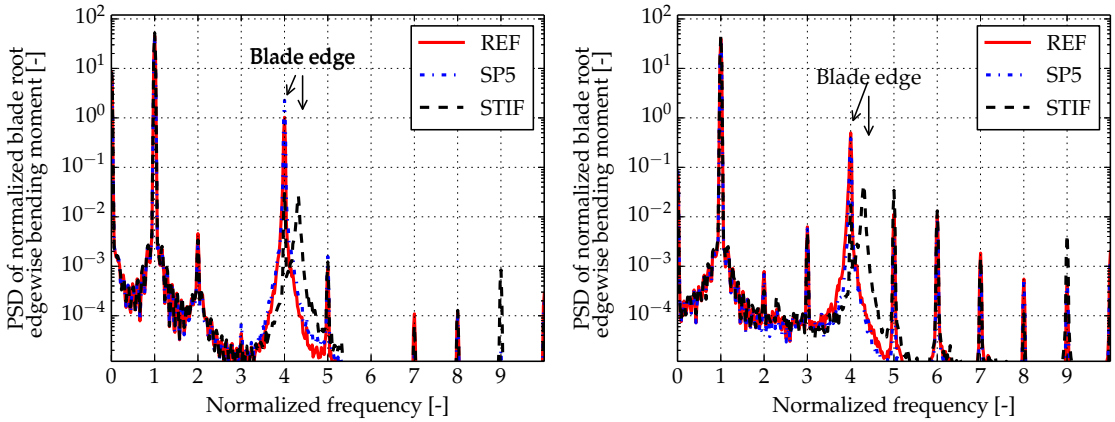

a) 10 m/s *b)* 20 m/s

Figure 9. Blade root edgewise bending moment power spectral densities comparison. Reference turbulence intensity 2%.Comparison between REF (red solid line), SP5 (blue dash-dot line), and STIF (black dashed line).

DOI: 10.1002/we
Prepared using weauth.cls

similar energy at 20 m/s for the same frequency. Results from this analysis show that the high blade loads of SP5, seen in Figure 7b, are due to vibrations at the blade frequency due to the resonance of the first edgewise BW mode.

Figure 10 shows an extract from the time series of the normalized blade root edgewise bending moment, for both turbulence intensities at 13 m/s. The responses are all dominated by the gravitational contribution at 1P, at both turbulence intensities. At low turbulence intensity, REF and STIF have almost no contribution at the blade frequency. The response of these two modes is indeed very close to a sinusoidal signal. On the other hand, SP5 has more visible contribution at the blade edgewise mode frequency. This contribution leads to a load variation for SP5 higher than for STIF even though SP5 has lighter blades. At high turbulence intensity, all models show a significant load contribution at the blade edgewise frequency, however, the high turbulence intensity hides the presence of the resonance, making its identification nontrivial.

The differences between the *REF* and *SP*5 models clarify the effect of the structural pitch on the wind turbine response. When operating close to resonance, a change of 5 deg leads to an increase of almost 10 % in the maximum blade damage equivalent load. The change in aeroelastic frequency, due to the structural pitch, is responsible for the large loads variation. The loads increase despite an increase in the aerodynamic damping of the first edgewise BW mode is also present. Furthermore, the difference in the response appears when analyzing loads estimated at low turbulence intensity wind conditions. With low turbulence intensity, the wind speed variations do not lead to significant changes in the rotor speed. The external excitation frequencies can therefore be constant over a long period of time, allowing resonant vibrations to build up. With high turbulence intensity the wind turbine operates in and out of the resonant conditions, hence the identification of the resonance can be difficult.

Even though the resonant vibration level seen on SP5 at low turbulence intensity is increased, it is in this particular case not design driving. However, in combination with other aero and structural properties, the level of vibrations could potentially increase beyond design limits. For instance if the torsional stiffness was increased by 20 %, the difference in vibration level due to the structural pitch difference of 5deg would be more pronounced , see Figure 11. The figure shows a comparison of the blade edgewise vibrations between SP5 and a modified version of SP5 with higher torsional stiffness.

4. WIND TURBINE RESPONSE TO A HARMONIC EXTERNAL EXCITATION

To improve the understanding of the turbine response a special study is conduced in time domain simulations. An external harmonic force is applied on a wind turbine to reproduce operational external excitations with different frequencies. Amplitude responses are then measured at the blade root and tower base. The turbine model STIF is used and three different cases are investigated:

- Case 1: an external harmonic force is placed at the tip of one blade. The force acts in the edgewise direction in a global coordinate system, hence in the lateral direction in the rotor plane. This case represents excitations such as gravity, large scale turbulence, and wakes.
- Case 2: the force is placed at the tip of one blade in the edgewise direction, in a local blade coordinate system. This case represents excitations such as small scale turbulence and trailing edge flaps.

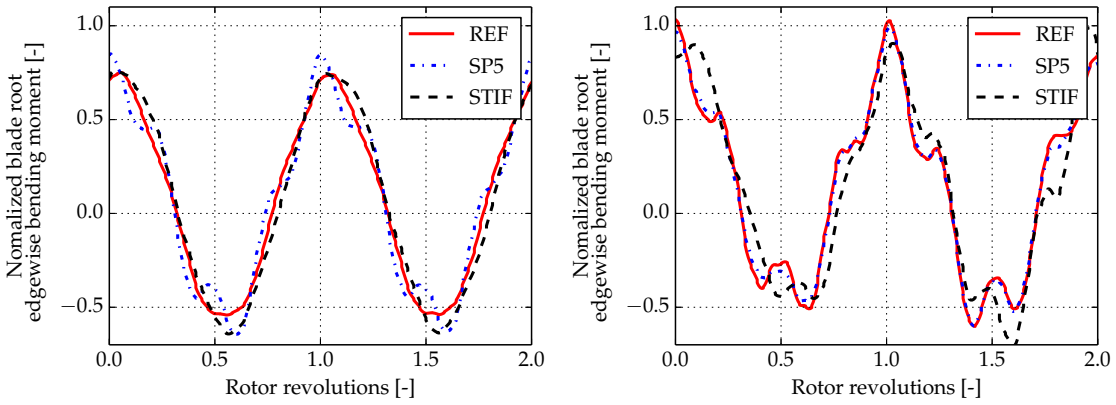

a) Low turbulence intensity *b) High turbulence intensity*

Figure 10. Extract from time series of normalized blade root edgewise bending moment at 13 m/s. Reference turbulence intensity of 2% and 16%. Comparison between REF (red solid line), SP5 (blue dash-dot line), and STIF (black dashed line).

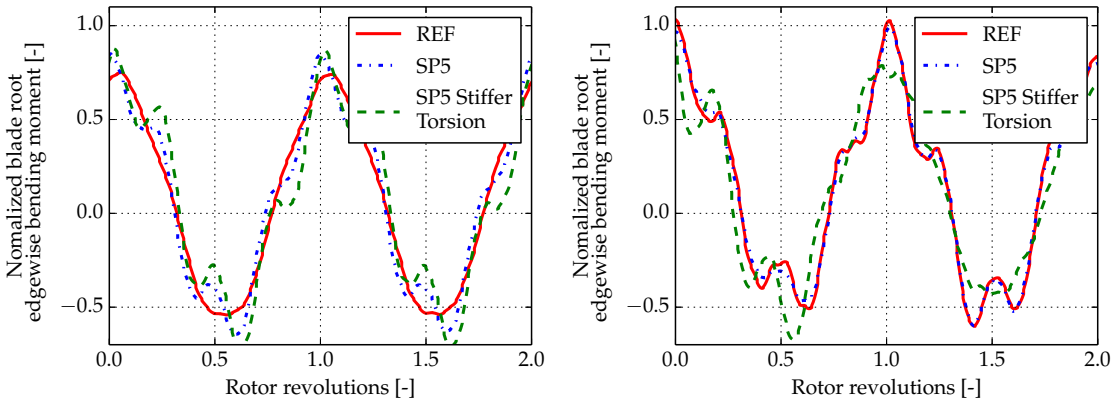

a) Low turbulence intensity *b) High turbulence intensity*

Figure 11. Extract from time series of normalized blade root edgewise bending moment at 13 m/s. Reference turbulence intensity of 2% and 16%. Comparison between REF (red solid line), SP5 (blue dash-dot line), and a modified version of SP5 with a higher torsional stiffness (green dashed line).

- Case 3: the force is placed at the tower top in the lateral direction, in the global coordinate system.

When the external excitation is placed on the blade, the point of excitation rotates and follows the rotating blade. In Case 1, the excitation maintains the same orientation as seen from an observer on the ground. In Case 2, the direction also rotates with the blade. Figure 12 shows a schematic representation of the three excitation cases.

The wind turbine response is evaluated measuring the amplitude of the tower base lateral bending moment and of the blade root edgewise bending moment. The measurement of the amplitude is performed after all the transients are damped out. The amplitude of the tower base lateral bending moment is normalized with the steady-state value of the tower base lateral bending moment at 10 m/s. The amplitude of the blade root edgewise bending moment is normalized with the blade mass moment. To avoid interference with other external excitations, uniform inflow, no gravity, and no tower shadow are considered in the simulations. Nonlinear time simulations are performed with increasing external excitation frequencies to cover the first 10 harmonics of the rotational frequency. The wind condition is set at 10 m/s. At this wind speed, the rotational speed has reached rated value, and the pitch angle is at the minimum fixed value.

Figure 13 shows the blade root edgewise bending moment amplitude and the tower base lateral bending moment amplitude for Case 1. At the blade root (Figure 13a), the frequency response is dominated by two large peaks at the frequencies of the first BW edgewise mode and of the first FW edgewise mode. The two modes show a similar response in amplitude, because they have equal damping, as shown in Figure 2. No response is present in the proximity of the first

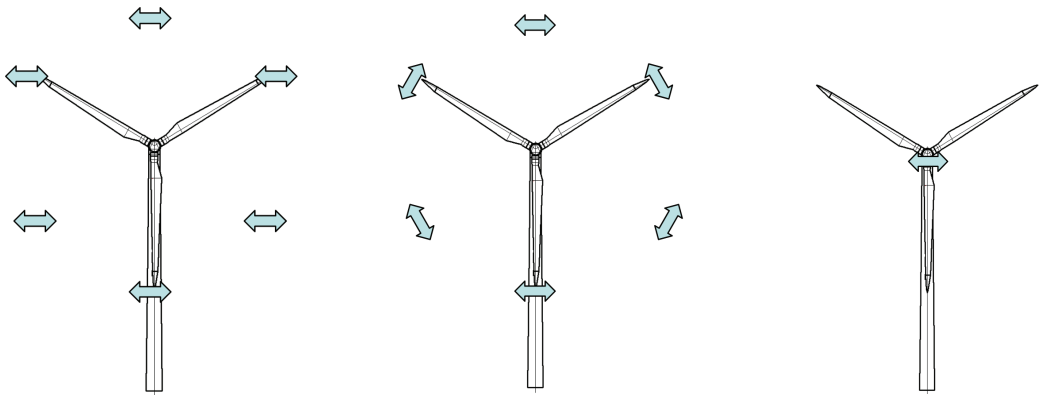

Case 1 *Case 2* *Case 3*

Figure 12. Representation of the thee excitation cases. Ground fixed, blade fixed, and tower top external excitations.

Wind Energ. 2014; **00**:1–14 © 2014 John Wiley & Sons, Ltd.
DOI: 10.1002/we
Prepared using weauth.cls

isolated blade edgewise natural frequency. The isolated blade mode is thus not excited, when the excitation is acting in a global reference frame. A small response is also present at the first tower lateral mode frequency, at the regulator mode frequency, and at the rotor speed filter frequency. These last two modes are due to the presence of the controller in the wind turbine model. A small peak is also noticed around 2.4P. This peak is due to the reflection of the first tower lateral mode. At the tower base (Figure 13b), the dominating response corresponds to the first tower lateral bending mode. The response of the two blade edgewise whirling modes is seen at 3.3P and 5.3P, respectively. A small peak at the isolated blade edgewise frequency is present. Furthermore two reflections around the tower bending mode frequency are present. The reflections are due to the rotating external excitation. As a blade mode has two whirling components and a symmetric component, when seen in a ground-fixed reference frame, the tower frequency has three reflections, if seen on a rotating reference frame. Hence, a rotating external excitation can also excite the tower mode at frequencies equal to $\pm$1P around the frequency of the tower mode.

Figure 14 shows the blade root edgewise bending moment amplitude and the tower base lateral bending moment amplitude for Case 2. At the blade root (Figure 14a), the response is dominated by one mode, the blade edgewise mode.

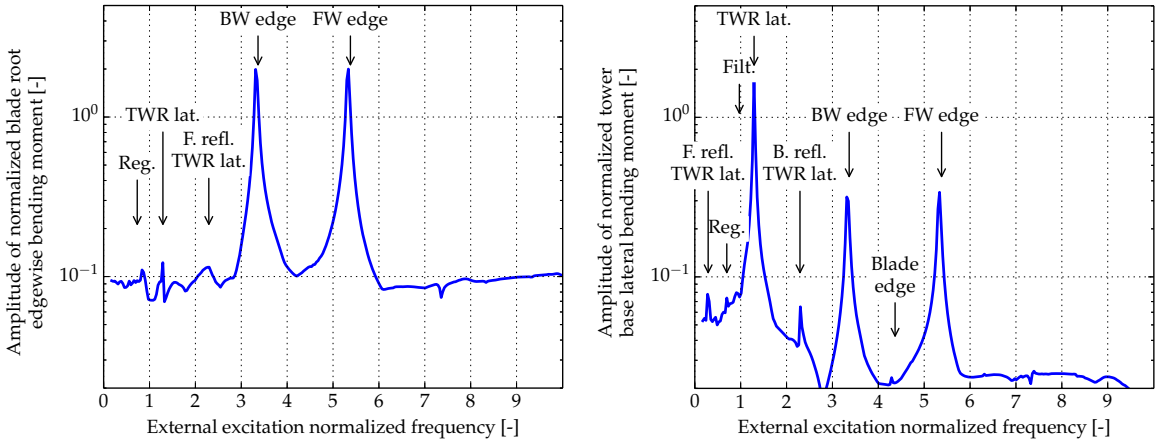

a) Blade root edgewise *b) Tower base lateral*

Figure 13. Case 1: amplitude of bending moments due to a harmonic external excitation of varying frequency placed at the blade tip and acting in the lateral direction in the global reference system. Wind speed 10 m/s

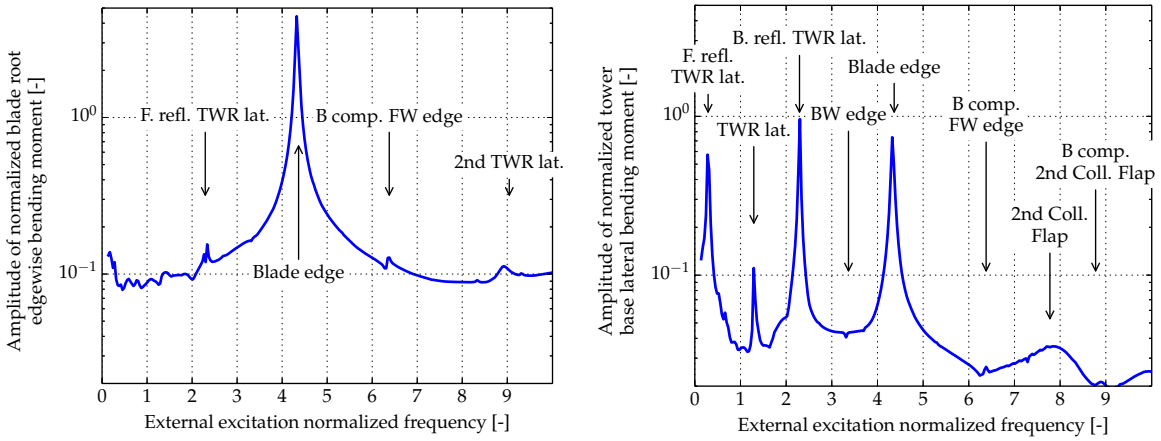

a) Blade root edgewise *b) Tower base lateral*

Figure 14. Case 2: amplitude of bending moments due to a harmonic external excitation of varying frequency placed at the blade tip and acting in the edgewise direction in local blade reference system. Wind speed 10 m/s

Other peaks of small amplitudes are also visible. These peaks are due to the forward reflection of the tower lateral mode, the backward reflection of the FW edgewise mode, and the second lateral tower mode. At the tower base (Figure 14b), the modes giving the maximum response are not wind turbine aeroelastic modes, but their reflections. The mode generating the most energetic response is the backward reflection of the first lateral tower mode. A peak close to the forward reflection of the first tower lateral mode frequency is also present at low frequency. The response at the blade edgewise mode frequency has also significant amplitude. Above the 7P frequency a peak corresponding to the excitation of the second collective flap mode is present.

Figure 15 shows the tower base lateral bending moment amplitude for Case 3. The response is dominated by the first tower lateral mode. Effects due to the whirling edgewise modes and the second tower lateral mode are also present. The amplitudes of the responses of these three modes are similar.

This analysis has shown that depending on the location of the external excitation and on its reference system, different responses arise. When the excitation is in a global reference system, only the wind turbine modes are excited. If the excitation is in a blade-fixed reference frame, the maximum amplitude response on a blade is at its natural frequency. The same excitation has a high response on the tower at the blade frequency and at the reflections of the tower lateral mode. The modes that are excited on a blade lead to a high response also at the tower base. The frequency at which the maximum excitation occurs is not always the frequency at which the blade or the tower are vibrating. If the external excitation is in the local frame, the blade vibrates at the same frequency of the external excitation and the tower at the relative $\pm$1P frequency values. If the excitation is in the fixed reference frame, the tower vibrates at the same frequency as the excitation while the blade at the relative $\pm$1P frequency values. Since the most common excitations, e.g. gravity, large scale wind turbulence, shear, tower shadow, and wakes, are in a ground fixed reference frame, they will excite the wind turbines at the frequencies of the wind turbines modes. Hence, a wind turbine blade cannot be excited by one of these excitations at its natural frequencies, but at the corresponding wind turbines modes frequencies. Nevertheless, the blade will vibrate at its natural frequency, but due to an excitation at $\pm$1P around it. The case of an excitation in a local reference frame is interesting mainly for controller purposes. When individual pitch control or flaps are used, the excitation is on a local reference frame. In these conditions, the modes that are excited are not the wind turbines modes, but their reflections. Extra care should be considered when using these controller solutions because different modes from the wind turbine modes can be excited.

5. CONCLUSIONS

In this work an investigation on resonant wind turbine conditions has been carried out. The main results of the investigation are:

- Distinctive edgewise blade vibrations could occur on modern variable-speed pitch-controlled wind turbines. The vibrations can be critical, due to resonant conditions, even if the aeroelastic dampings of the edgewise modes are

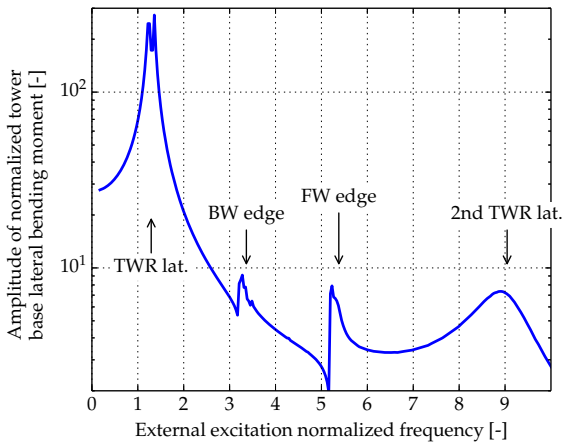

Figure 15. Case 3: amplitude of tower base lateral bending moment due to a harmonic external excitation of varying frequency placed at the tower top and acting in the lateral direction in the global reference system. Wind speed 10 m/s.

Wind Energ. 2014; **00**:1–14 © 2014 John Wiley & Sons, Ltd.
DOI: 10.1002/we
Prepared using weauth.cls

positive. In the presented example, the edgewise vibrations are caused by a resonance between 3P and the first edgewise backward whirling mode.

- When operating close to resonant conditions, small differences in the characteristics can have a large influence on the vibrations level. In this investigation, the structural pitch has been investigated. This parameter does not affect the structural frequency, i.e. the frequencies at stand still, however it does change the aeroelastic frequency during operation, and thereby it affects the vibration level.
- It could be highly relevant to include low turbulence intensity simulation in the evaluation and test of wind turbine loads. Low turbulence intensity conditions lead to operational conditions with more constant rotational speed, giving time to resonant vibration to build up. High turbulence causes higher rotor speed variation, and therefore the turbine will be in and out of resonance, lowering the vibrations. Therefore, only when performing low turbulence intensity simulations, it is possible to easily identify the presence of resonant conditions.
- Depending on whether an external excitation is acting in a blade-fixed reference frame, e.g. trailing edge flaps, or in a ground-fixed reference frame, e.g. gravity, wakes, and large scale turbulence, the wind turbine response differs, and different modes can be excited.
- In the case of a local tangential blade excitation, the excitation excites only blade modes and the $\pm$1P reflections of the tower modes.
- In the case of edgewise blade excitation in a ground-fixed reference frame, the whirling modes and the tower modes are excited.
- Resonance with blade edgewise modes and wind turbine edgewise whirling modes should be avoided. A large margin between the aeroelastic and the excitations frequencies should be kept because a detailed model is required to predict the loads with sufficient confidence. As a result of this, a general design recommendation is to place the edgewise frequency at standstill at 3.5, 4.5, ..., N.5 P which ensures the smallest risk of resonance of any of the edgewise modes and edgewise whirling modes, and leads to the lowest response level.

REFERENCES

1. Manwell JF, McGowan JG, Rogers AL. *Wind Energy Explained: Theory, Design and Application, Second Edition*. John Wiley & Sons, Ltd, 2010, doi:10.1002/9781119994367.
2. Burton T, Jenkins N, Sharpe D, Bossanyi E. *Wind Energy Handbook, Second Edition*. John Wiley & Sons, Ltd, 2011, doi:10.1002/9781119992714.
3. Brøndsted P, Nijssen R. *Advances in Wind Turbine Blade Design and Materials*. Woodhead Publishing, 2013, doi: 10.1533/9780857097286.
4. Hu WH, Thöns S, Said S, Rücker W. Resonance phenomenon in a wind turbine system under operational conditions. *Proceedings of the 9th International Conference on Structural Dynamics, EURODYN 2014* 2014; Porto, Portugal.
5. Bossanyi EA. The design of closed loop controllers for wind turbines. *Wind Energy* 2000; **3**(3):149–163, doi: 10.1002/we.34.
6. Bossanyi E. Wind turbine control for load reduction. *Wind Energy* 2003; **6**(3):229–244, doi:10.1002/we.95.
7. Schaak P, Corten G, van der Hooft EL. Crossing resonance rotor speeds of wind turbines. *Proceedings of European Wind Energy Conference 2003*; Madrid, Spain, 2003.
8. Licari J, Ekanayake J, Jenkins N. Investigation of a speed exclusion zone to prevent tower resonance in variable-speed wind turbines. *IEEE Transactions on Sustainable Energy* Oct 2013; **4**(4):977–984, doi:10.1109/TSTE.2013.2257899.
9. DEA Dansk Ingenirforenings og Ingenir-Sammenslutningens norm for last og sikkerhed for vindmllekonstruktioner (Code of practice for loads and safety of wind turbines construction) DS 472 *Danish Energy Agency* 1992
10. Sullivan TL. A review of resonance response in large, horizontal-axis wind turbines. *Solar Energy* 1982; **29**(5):377–383, doi:10.1016/0038-092X(82)90073-1.
11. Fleming P, Wright A, Fingersh LJ, van Wingerden JW. Resonant Vibrations Resulting from the Re-Engineering of a Constant-Speed 2-Bladed Turbine to a Variable-Speed 3-Bladed Turbine. *49th AIAA Aerospace Sciences Meeting including the New Horizons Forum and Aerospace Exposition*. American Institute of Aeronautics and Astronautics, 2011, doi:10.2514/6.2011-634.
12. Larsen TJ, Hansen MA. How 2 HAWC2, the user's manual. *Technical Report Risø-R-1597(ver. 3-1)(EN)*, Risø National Laboratory, 2007. www.hawc2.dk
13. Kim T, Hansen AM, Branner K. Development of an anisotropic beam finite element for composite wind turbine blades in multibody system. *Renewable Energy* 2013; **59**:172–183, doi:10.1016/j.renene.2013.03.033.
14. Vorpahl F, Strobel M, Jonkman JM, Larsen TJ, Passon P. Verification of aero-elastic offshore wind turbine design codes under IEA wind task XXIII. *Wind Energy* 2013, doi:10.1002/we.1588.
15. Popko W, Vorpahl F, Zuga A, Kohlmeier M, Jonkman J, Robertson A, Larsen TJ, Yde A, Sætertrø K, Okstad KM, *et al.*. Offshore code comparison collaboration continuation (OC4), phase i - results of coupled simulations of an

offshore wind turbine with jacket support structure. *Proceedings of the International Offshore and Polar Engineering Conference 2012*; Rhodes, Greece 2012; 337–346.
16. Larsen TJ, Aagaard MH, Larsen GC, Hansen KS. Validation of the dynamic wake meander model for loads and power production in the Egmond aan Zee wind farm. *Wind Energy* 2013; **16**(4): 605–624, doi:10.1002/we.1563.
17. Hansen MH, Henriksen LC. Basic DTU Wind Energy controller. *Technical Report E-0028*, DTU Wind Energy, 2013.
18. Hansen MH. Aeroelastic stability analysis of wind turbines using an eigenvalue approach. *Wind Energy* 2004; **7**(2):133–143, doi:10.1002/we.116.
19. Hansen MH. Aeroelastic properties of backward swept blades. *49th AIAA Aerospace Sciences Meeting including the New Horizons Forum and Aerospace Exposition*. American Institute of Aeronautics and Astronautics, 2011, doi: 10.2514/6.2011-260.
20. Sønderby I, Hansen MH. Open-loop frequency response analysis of a wind turbine using a high-order linear aeroelastic model. *Wind Energy* 2014; **17**: 1147–1167, doi:10.1002/we.1624.
21. Hansen MH. Aeroelastic instability problems for wind turbines. *Wind Energy* 2007; **10**(6): 551–577, doi:10.1002/we. 242.
22. Pedersen JT, Thomsen K, Madsen HA. Local blade whirl and global rotor whirl interaction. *Technical Report Risø-R-1067(EN)*, Risø National Laboratory, 1998.
23. Hansen MH. Improved Modal Dynamics of Wind Turbines to Avoid Stall-induced Vibrations. *Wind Energy* 2003; **6**(2): 179–195, doi:10.1002/we.79.
24. Rasmussen F, Petersen JT, Madsen HA. Dynamic Stall and Aerodynamic Damping *Journal of Solar Energy Engineering* 1999; **121**(3): 150–155, doi:10.1115/1.2888426.
25. Mann J. Wind field simulation. *Probabilistic Engineering Mechanics* 1998; **13**(4):269–282, doi:10.1016/ S0266-8920(97)00036-2.

Article II: Wind Turbine Fatigue Damage Evaluation Based on a Linear Model and a Spectral Method

This article was submitted for publication to the *Wind Energy* journal in October 2014.

WIND ENERGY
Wind Energ. 0000; **00**:1–17
DOI: 10.1002/we

Wind turbine fatigue damage evaluation based on a linear model and a spectral method

C Tibaldi, LC Henriksen, MH Hansen and C Bak

Department of Wind Energy, Technical University of Denmark

ABSTRACT

Wind turbine multidisciplinary design optimization is currently the focus of several investigations because it has showed potential in reducing the cost of energy. This design approach requires fast methods to evaluate wind turbine loads with a sufficiently high-level of fidelity. This paper presents a method to estimate wind turbine fatigue damage suited for optimization design applications. The method utilizes a high-order linear wind turbine model. The model comprehends a detailed description of the wind turbine and the controller. The fatigue is computed with a spectral method applied to power spectral densities of wind turbine sensors responses to turbulent wind. In this paper the model is validated both in time-domain and frequency-domain with a nonlinear aeroservoelastic model. The approach is compared quantitatively against fatigue damage obtained from the power spectra of time series evaluated with nonlinear aeroservoelastic simulations and qualitatively against rainflow-counting. Results are presented for three cases: load evaluation at normal operation in the full wind speed range, load changes evaluation due to two different controller tunings at normal operation at three different wind speeds above rated, and load dependency on the number of turbulence seeds used for their evaluation. For the full range normal operation, the maximum difference between the two frequency-domain based estimates of the tower base lateral fatigue moments is 36 %, whereas the differences for the other sensors are less than 15 %. For the loads variations evaluation, the maximum difference of the tower base longitudinal bending moment variation is 22 %. Such large difference occurs only when the change in controller tuning has a low effect on the loads. Furthermore, results show that loads evaluated with the presented method are less dependent on the turbulent wind realization, therefore less turbulence seeds are required compared to time-domain simulations to remove the dependency on the wind realization used to estimate loads.

KEYWORDS
Wind turbine, aeroelasticity, fatigue damage, spectral method, wind turbine control, multidisciplinary design optimization, linear model

Correspondence
C Tibaldi, tlbl@dtu.dk. Department of Wind Energy, DTU RisøCampus, Frederiksborgvej 399, DK-4000 Roskilde, Denmark

Received . . .

1. INTRODUCTION

In the recent years, holistic wind turbine design has considerably grown in importance, to further reduce the cost of energy. Designing wind turbine components, not as individual systems but as parts of more general and comprehensive systems, can lead to lighter and more efficient designs. Multidisciplinary design optimization methods are well suited to perform holistic design. These methods are very general and they can be applied to different level of model complexity. One of the main challenges in designing multidisciplinary design frameworks is to guarantee a sufficiently high-detailed model and limit the computational cost.

The first relevant multidisciplinary design optimization framework applied to wind turbine is the one described by Fuglsang and Madsen [1] and Fuglsang and Thomsen [2]. In this method, the blade shape design is addressed by taking into account aerodynamic calculations, structural calculations, time-domain aeroelastic calculations, extreme loads calculation, and estimation of aerodynamic noise. To reduce the computational effort, they use a semi-empirical method to compute the gradients and a wind turbine model with 20 degrees of freedom. The method shows relevant reductions in the cost of energy, even if it relies on simple models and assumptions.

Fuglsang et al. [3] developed a method for site-specific wind turbine design. The method is based on time-domain aeroelastic simulations. To limit the computational time, the number of load cases and the simulation length are reduced.

Prepared using weauth.cls [Version: 2010/06/17 v1.00]

The reduction of the cases is performed selecting only those simulations that generate design-driving loads. A check on the simulations to consider, among a larger set, is performed every five iterations.

Bulder and Schepers [4] also describe a method for site-specific wind turbine optimization design. The approach consists of two optimization modules. The first module does not require the evaluation of derivatives of the cost function. The second module uses derivatives of an approximation of the cost function that can be evaluated quickly. The combination of these two modules allows for few objective functions evaluations leading to a faster optimization procedure.

Bottasso et al. [5, 6, 7] present a design framework that includes aerodynamic and detailed structural design. The method assumes that the wind turbine aeroelastic loads do not change significantly for small changes in the structural design. This assumption allows to split the aeroelastic load evaluation and the structural optimization in two nested design loops, and thereby to avoid the computation of the aeroelastic loads for each structural parameter variation. The method can therefore evaluate a large set of design load cases without significantly compromising the computational time.

Ashuri et al. [8, 9] present a framework that can address aerodynamic and structural design. The framework does not include any nested design loop or model simplification, therefore, to limit the computational time, the number of load cases evaluated is limited to 72 simulations. The cases include normal operation and extreme conditions.

Merz et al. [10] developed a method to perform fast computations based on frequency-domain load computations, for stall-regulated wind turbines. Their work focuses on the aerodynamic modeling and the linearization of the dynamic stall model. The rotating turbulence power spectra are computed from Fourier transformations of analytical correlations functions. Deterministic contributions, e.g. wind shear and tower shadow, are added to the spectra as spikes at the multiple frequencies of the rotational speed frequency. The structural model, used for the analysis, is composed of an isolated blade rigidly mounted at the root and rotating at a fixed rotational speed. Dirlik's method [11] is then used to estimate the fatigue damage based on the power spectra. The method presented by Merz is then used in [12, 13] to design three different multi-megawatt stall-regulated wind turbines. The assumptions made in the model allow to estimate loads only on one blade. Furthermore, the model cannot handle variations in the rotational speed, torsional deformations, large blade deflections, and interactions between the wind turbine components.

These works use three main strategies to reduce the computational cost: employing a simplified model, limiting the amount of simulation cases, and including nested optimization loops. A simplified wind turbine model does not capture the physics of the problem accurately and the corresponding interactions, therefore it can limit the potential of the holistic design. Moreover, it does not allow to extract loads on each wind turbine component, limiting the definition of the cost function and constraints. The selection of few simulations for the fatigue and extreme loads evaluation leads to the use of loads that are not representative of the entire wind turbine operational life, hence it is not guaranteed that the final design satisfies all the design requirements, stated in the IEC standards [14]. Furthermore, the wind turbine loads highly depend on the wind realization used for their evaluation, as shown by Thomsen [15] and Natarajan and Verelst [16]. This dependency can lead to a wrong evaluation of the gradients, when a gradient-based algorithm is used in the optimization, even when the same wind field is used in the simulations [17]. A nested optimization loop can significantly simplify the optimization problem, however it can limit the improvement in the design because the optimization algorithm does not have a direct overview of the consequences of parameters variations. This limitation can be more severe at the beginning of the design process, when large parameters variations are performed. Furthermore, the simplification of nested design loops cannot be applied to all the wind turbine parameters. For instance, when including also the controller tuning in the design process, no hypothesis can be made to avoid the computation of the aeroservoelastic simulations each time a controller parameter is changed. There are methods to auto-tune PI controllers based on simplified models [18, 19], but this auto-tuning does not ensure that the controller parameters are optimal in a holistic sense. With more advanced controller strategies, e.g. LQR or MPC, gains or weights must be identified based on results of aeroservoelastic simulations.

In this work, an approach to evaluate wind turbine fatigue loads is presented. The method exploits a high-order linear aeroservoelastic wind turbine model to compute the frequency response of loads due to a turbulent wind input. The high-order model allows for a detailed description of the wind turbine enabling to capture aeroservoelastic effects and components interactions. The fatigue loads are computed using a spectral method from the power spectral density (PSD) of the responses of selected load sensors. The method allows using a high-detailed wind realization without increasing the computational cost. Therefore, the method can be used in an optimization design procedure to evaluated fatigue loads, guaranteeing a more efficient evaluation of the gradients compared to time-domain simulations. The application of this method cannot be extended to ultimate loads because it is based on a linear model.

The linearized model used in this investigation is obtained with the aeroservoelastic code HAWCStab2 [20]. The linear model is compared with results from nonlinear simulations obtained with the multibody aeroservoelastic code HAWC2 [21]. The Basic DTU Wind Energy controller, described by Hansen and Henriksen [22], is selected for the HAWC2 simulations. The spectral method presented by Benasciutti and Tovo [23, 24] is used to evaluate the fatigue damage from the PSDs of the loads sensors at the tower base in the longitudinal and lateral directions and at the blade root in the in-plane and out-of-plane directions. The presented results are based on the NREL 5 MW Reference Wind Turbine [25].

Wind Energ. 0000; **00**:1–17 © 0000 John Wiley & Sons, Ltd.
DOI: 10.1002/we
Prepared using weauth.cls

Section 2 describes the wind turbine model used is this investigation. Section 3 introduces the method to compute the fatigue damage from the linear model. In this section, the approach to evaluate the PSD and the spectral method are described. Section 4 shows the comparison of the linear and the nonlinear models. The comparison is carried out looking at both wind step responses and PSDs of sensors during normal operation. Section 5 presents the fatigue damages obtained with the method for three case studies. The results obtained with the linear model are compared with those obtained with the nonlinear one. Finally, the conlusions of the presented results are given.

2. LINEAR MODEL

This section contains the description of the linear high-order model. First the open-loop wind turbine and the controller models are described. Finally, the equations of the closed-loop aeroservoelastic model are introduced.

2.1. Wind turbine model

The open-loop wind turbine model is obtained with HAWCStab2, a tool developed at DTU Wind Energy. HAWCStab2 is an improved version of HAWCStab [26] with a different kinematic formulation. The model is an analytical linearization of a nonlinear finite beam element model. The beam model is coupled with an unsteady blade element momentum model of the blade aerodynamic. The aerodynamic model includes shed vorticity, dynamic stall, and dynamic inflow [20]. A validation and analysis of the open-loop performances are provided by Sønderby and Hansen [27] for a version of HAWCStab2 without the present dynamic inflow model.

The wind turbine model is represented with a set of linear first-order equations for different operational point.

$$\dot{\mathbf{x}} = \mathbf{A}\mathbf{x} + \mathbf{B}(\mathbf{u} + \mathbf{u}_{pert}) + \mathbf{B}_w\mathbf{u}_w \tag{1a}$$

$$\mathbf{y} = \mathbf{C}\mathbf{x} + \mathbf{D}(\mathbf{u} + \mathbf{u}_{pert}) + \mathbf{D}_w\mathbf{u}_w \tag{1b}$$

$$\mathbf{z} = \mathbf{E}\mathbf{x} + \mathbf{F}(\mathbf{u} + \mathbf{u}_{pert}) + \mathbf{F}_w\mathbf{u}_w \tag{1c}$$

The states vector $\mathbf{x}$, with dimension N_x, includes the structural and the aerodynamic states. The input signal includes the N_u controller inputs $\mathbf{u}$ and their perturbations $\mathbf{u}_{pert}$. The input $\mathbf{u}_w$ represents the wind inputs to the system. Two different equations are considered to represent the system outputs, $\mathbf{y}$ and $\mathbf{z}$. The first includes a set of N_y general output sensors. The second only includes the N_z outputs that are used for the feedback to the controller. The system matrix $\mathbf{A}$, actuation matrix $\mathbf{B}$, observation matrices $\mathbf{C}$ and $\mathbf{E}$, feed-through matrices $\mathbf{D}$ and $\mathbf{F}$, and the wind input matrices $\mathbf{B}_w$, $\mathbf{D}_w$, and $\mathbf{F}_w$ are all computed with HAWCStab2 at any operational point.

The high-order model used in this investigation is composed of 998 states, including structural and aerodynamic degrees of freedom.

2.2. Controller model

The linearized controller equations are also obtained with HAWCStab2. The controller model is a simplified linearization of the Basic DTU Wind Energy Controller, described by Hansen and Henriksen [22]. A description and validation of part of the controller is performed in [28] and [19]. The controller comprehends three different sub-controllers to operate in four different operational regions. The regions are: Region 1, with minimum constant rotational speed and variable torque, Region 2 with variable torque and variable rotational speed, Region 2½ with variable torque and constant rotational speed, and Region 3 with constant power or constant torque and constant rotational speed.

The controller is described, at each operational point, with a linear first-order system

$$\dot{\mathbf{x}}_c = \mathbf{A}_c\mathbf{x}_c + \mathbf{B}_c\mathbf{u}_c \tag{2a}$$

$$\mathbf{y}_c = \mathbf{C}_c\mathbf{x}_c + \mathbf{D}_c\mathbf{u}_c \tag{2b}$$

In the system equations, $\mathbf{x}_c$ are the N_{xc} controller states, $\mathbf{u}_c$ represents the N_{uc} input signals to the controller, and $\mathbf{y}_c$ are the N_{yc} output from the controller. The controller matrices $\mathbf{A}_c$, $\mathbf{B}_c$, $\mathbf{C}_c$, and $\mathbf{D}_c$ are dependent on the operational region, and for Region 3 the gain-scheduling of the pitch feedback also varies the $\mathbf{C}_c$ matrix. The controller inputs are the rotor speed and the collective pitch angle. The controller outputs are the reference generator torque and the reference collective pitch angle.

The following sections describe the controllers of each operational region.

2.2.1. Region 1 and Region 2½

The controllers in Region 1 and Region 2½ are the same. The controller is composed of a PI controller that regulates the generator reference torque based on a filtered rotor speed error. This filter is a second-order low-pass filter with natural

angular frequency $\omega_{lp,\Omega}$ and damping ratio $\zeta_{lp,\Omega}$. An integrator is included to compute the integral of the rotor speed error. The $\mathbf{A}_c$ and $\mathbf{B}_c$ matrices of the linearized controller equations are:

$$\mathbf{A}_c = \begin{bmatrix} \mathbf{A}_{lp,\Omega} & \mathbf{0}_{(2,1)} \\ 1 \quad 0 & 0 \end{bmatrix}, \qquad \mathbf{B}_c^T = \begin{bmatrix} 0 & \omega_{lp,\Omega}^2 & 0 \\ 0 & 0 & 0 \end{bmatrix} \tag{3}$$

where $\mathbf{0}_{(2,1)}$ is a $2x1$ zero vector and $\mathbf{A}_{lp,\Omega}$ is the matrix describing the rotor speed low-pass filter

$$\mathbf{A}_{lp,\Omega} = \begin{bmatrix} 0 & 1 \\ -\omega_{lp,\Omega}^2 & -2\zeta_{lp,\Omega}\,\omega_{lp,\Omega} \end{bmatrix} \tag{4}$$

The matrices $\mathbf{C}_c$ and $\mathbf{D}_c$ are

$$\mathbf{C}_c = \begin{bmatrix} k_{P,Q} & 0 & k_{I,Q} \\ 0 & 0 & 0 \end{bmatrix} \quad \text{and} \quad \mathbf{D}_c = \mathbf{0} \tag{5}$$

In the matrix $\mathbf{C}_c$ the parameters $k_{P,Q}$ and $k_{I,Q}$ are the proportional and the integral gain of the PI controller respectively.

2.2.2. Region 2

In Region 2 the controller is composed of a rotor speed filter, as the one in Equation (4), and a term proportional to the square of the rotor speed. This second term sets the reference generator torque. The matrices of the linearized system are

$$\mathbf{A}_c = \begin{bmatrix} \mathbf{A}_{lp,\Omega} \end{bmatrix}, \qquad \mathbf{B}_c^T = \begin{bmatrix} 0 & \omega_{lp,\Omega}^2 \\ 0 & 0 \end{bmatrix}, \tag{6}$$

$$\mathbf{C}_c = \begin{bmatrix} 2K\Omega_0 & \mathbf{0}_{(1,2)} \\ 0 & \mathbf{0}_{(1,2)} \end{bmatrix}, \quad \text{and} \quad \mathbf{D}_c = \mathbf{0} \tag{7}$$

The parameter K is the constant of the $K\Omega^2$ controller and Ω_0 is the rotational speed at the operational point of linearization.

2.2.3. Region 3

In Region 3, a PI controller adjusts the pitch angle, based on filtered rotational speed measurements. A gain-scheduling method is included to compensate the variations of the aerodynamic properties, and achieve uniform controller performances in all the region [19]. The measured rotational speed is filtered with two filters. A band-stop notch filter, $\mathbf{A}_{bs,\Omega}$, characterized by the parameters $\xi_{bs,\Omega}$, $\zeta_{bs,\Omega}$, and $\omega_{bs,\Omega}$, to remove the component of the signal with the frequency of the drive-train mode, and the second-order low-pass filter in Equation (4). The matrices of the controller $\mathbf{A}_c$ and $\boldsymbol{B}_c$ for the Region 3 are

$$\mathbf{A}_c = \begin{bmatrix} \mathbf{A}_{lp,\Omega} & \mathbf{O}_{(2,1)} & \mathbf{O}_{(2,1)} & \mathbf{A}_{lp,bs} \\ 1 \quad 0 & 0 & 0 & 0 \\ \mathbf{O}_{(2,3)} & & \mathbf{A}_{bs,\Omega} & \end{bmatrix} \quad \text{and} \quad \mathbf{B}_c^T = \begin{bmatrix} 0 & \omega_{lp,\Omega}^2 & \mathbf{0}_{(1,2)} & 1 \\ 0 & 0 & \mathbf{0}_{(1,2)} & 0 \end{bmatrix}, \tag{8}$$

where

$$\mathbf{A}_{bs,\Omega} = \begin{bmatrix} 0 & 1 \\ -\omega_{bs,\Omega}^2 & -2\zeta_{bs,\Omega}\,\omega_{bs,\Omega} \end{bmatrix}, \qquad \mathbf{A}_{lp,bs} = \begin{bmatrix} 0 \\ 2\omega_{lp,\Omega}^2\omega_{bs,\Omega}(\xi_{bs,\Omega} - \zeta_{bs,\Omega}) \end{bmatrix}, \tag{9}$$

$$\mathbf{C}_c = \begin{bmatrix} 0 & 0 & 0 & \mathbf{0}_{(1,2)} \\ \eta_K k_{P,0} & 0 & \eta_K k_{I,0} & \mathbf{0}_{(1,2)} \end{bmatrix}, \quad \text{and} \quad \mathbf{D}_c = \begin{bmatrix} -\frac{\partial Q_g}{\partial \Omega} & 0 \\ 0 & 0 \end{bmatrix}, \text{where } \frac{\partial Q_g}{\partial \Omega} = \begin{cases} 0 & \text{constanst torque} \\ -\frac{P_r}{\Omega_r^2} & \text{constant power} \end{cases} \tag{10}$$

The parameters $k_{P,0}$ and $k_{I,0}$ are the proportional and integral gains respectively, η_K is the gain-scheduling parameter. The gain-scheduling parameter is a function of the pitch angle at steady-state. The gain-scheduling affects the controller parameters only when the operational point is changed, through a different pitch angle.

In this paper, the controller is tuned using a pole-placement technique implemented in HAWCStab2 [28, 19]. Table I shows the values of the controller parameters used in this investigation. Constant torque control is used in Region 3, whereby $\mathbf{D}_c = \mathbf{0}$.

Wind Energ. 0000; **00**:1–17 © 0000 John Wiley & Sons, Ltd.
DOI: 10.1002/we
Prepared using weauth.cls

Table I. Controller tuning parameters for the NREL 5-MW Reference Wind Turbine.

Rated power	P_r =5 MW	Rated rotor speed	Ω_r =12.1 rpm
Minimum rotor speed	7.1 rpm		
Low-pass filter	$\omega_{lp,\Omega} = 3.77$ rad/s	$\zeta_{lp,\Omega} = 0.7$	
Band-stop filter	$\xi_{bs,\Omega} = 0.01$	$\zeta_{bs,\Omega} = 0.1$	$\omega_{bs,\Omega} = 10.19$ rad/s
Region 1 and 3	$k_{P,Q}$ = 1.93×10^7 Nm s/rad	$k_{I,Q} = 4.33 \times 10^6$ Nm/rad	
Region 2	$K = 2.10 \times 10^6$		
Region 4	$k_{P,0}$ = 1.36 s	$k_{I,0}$ = 0.67	

2.3. Closed-loop system

To obtain the closed-loop equations, the input of the wind turbine model $\mathbf{u}$ has to be connected to the output of the controller model $\mathbf{y}_c$, and the output of the wind turbine model $\mathbf{z}$ has to be connected to the input of the controller model $\mathbf{u}_c$.

$$\begin{cases} \mathbf{u}_c = \mathbf{z} \\ \mathbf{u} = \mathbf{y}_c \end{cases} \tag{11}$$

With these two new conditions, the systems (1a) and (2a) and the output equations (1b) can be written as a single closed-loop aeroservoelastic system. The system and the output equations are:

$$\dot{\mathbf{x}}_{\text{ase}} = \mathbf{A}_{\text{ase}}\mathbf{x}_{\text{ase}} + \mathbf{B}_{\text{ase}}\mathbf{u}_{\text{pert}} + \mathbf{B}_{w,\text{ase}}\mathbf{u}_w \tag{12a}$$

$$\mathbf{y} = \mathbf{C}_{\text{ase}}\mathbf{x}_{\text{ase}} + \mathbf{D}_{\text{ase}}\mathbf{u}_{\text{pert}} + \mathbf{D}_{w,\text{ase}}\mathbf{u}_w \tag{12b}$$

where the aeroservoelastic states vector is $\mathbf{x}_{\text{ase}} = \{\mathbf{x}^T\ \mathbf{x}_c^T\}^T$ with size $N_{x\text{ase}} = N_x + N_{xc}$.The aeroservoelastic system and input matrices are

$$\mathbf{A}_{\text{ase}} = \begin{bmatrix} \mathbf{A} + \mathbf{B}\mathbf{D}_c(\mathbf{I} - \mathbf{F}\mathbf{D}_c)^{-1}\mathbf{E} & \mathbf{B}\mathbf{C}_c + \mathbf{B}\mathbf{D}_c(\mathbf{I} - \mathbf{F}\mathbf{D}_c)^{-1}\mathbf{F}\mathbf{C}_c \\ \mathbf{B}_c(\mathbf{I} - \mathbf{F}\mathbf{D}_c)^{-1}\mathbf{E} & \mathbf{A}_c + \mathbf{B}_c(\mathbf{I} - \mathbf{F}\mathbf{D}_c)^{-1}\mathbf{F}\mathbf{C}_c \end{bmatrix} \tag{13a}$$

$$\mathbf{B}_{\text{ase}} = \begin{bmatrix} \mathbf{B} + \mathbf{B}\mathbf{D}_c(\mathbf{I} - \mathbf{F}\mathbf{D}_c)^{-1}\mathbf{F} \\ \mathbf{B}_c(\mathbf{I} - \mathbf{F}\mathbf{D}_c)^{-1}\mathbf{F} \end{bmatrix} \tag{13b}$$

$$\mathbf{B}_{w,\text{ase}} = \begin{bmatrix} \mathbf{B}_w + \mathbf{B}\mathbf{D}_c(\mathbf{I} - \mathbf{F}\mathbf{D}_c)^{-1}\mathbf{F}_w \\ \mathbf{B}_c(\mathbf{I} - \mathbf{F}\mathbf{D}_c)^{-1}\mathbf{F}_w \end{bmatrix} \tag{13c}$$

and the output and feed-through matrices are

$$\mathbf{C}_{\text{ase}} = \begin{bmatrix} \mathbf{C} + \mathbf{D}\mathbf{D}_c(\mathbf{I} - \mathbf{F}\mathbf{D}_c)^{-1}\mathbf{E} & \mathbf{D}\mathbf{C}_c + \mathbf{D}\mathbf{D}_c(\mathbf{I} - \mathbf{F}\mathbf{D}_c)^{-1}\mathbf{F}\mathbf{C}_c \end{bmatrix} \tag{14a}$$

$$\mathbf{D}_{\text{ase}} = \begin{bmatrix} \mathbf{D} + \mathbf{D}\mathbf{D}_c(\mathbf{I} - \mathbf{F}\mathbf{D}_c)^{-1}\mathbf{F} \end{bmatrix} \tag{14b}$$

$$\mathbf{D}_{w,\text{ase}} = \begin{bmatrix} \mathbf{D}_w + \mathbf{D}\mathbf{D}_c(\mathbf{I} - \mathbf{F}\mathbf{D}_c)^{-1}\mathbf{F}_w \end{bmatrix} \tag{14c}$$

When the feed-through matrix $\mathbf{F}$ is a zero matrix, the aeroservoelastic matrices becomes much simpler. This matrix is generally zero except in the presence of an acceleration measurement or of an inflow measurement that is used as a feed-back to flow control devices, e.g. trailing edge flaps.

The formulation of the closed-loop equations is independent on the wind turbine model and the controller model. Only the input and output matrices need to be consistent, i.e. $N_{uc} = N_z$ and $N_u = N_{yc}$. Hence, any wind turbine model and controller can be used in this application.

Table II shows the frequencies and dampings of the first ten aeroservoelastic modes of the NREL 5-MW Reference Wind Turbine controlled with the Basic DTU Wind Energy controller. The first mode denoted *Reg.* in Region 1 at 5 m/s and in Region 3 at 13 m/s is the solid body rotation of the drivetrain which is tuned to have frequencies below the tower modes. The controller in Region 2 does not add any pole related to a significant structural response to the system, it adds only poles associated with the filters. The values of the frequency and damping associated with the filters are not shown in Table II.

3. METHOD

A series of steps must be followed to compute the fatigue damage of a desired wind turbine output from a linear model. Figure 1 shows a diagram of the workflow to compute the PSD of a load sensor, starting from the wind sampling and the

Table II. Fequencies and dampings of the first ten aeroservoelastic modes of the NREL 5-MW RWT operating with the Basic DTU Wind Energy controller.

Wind Speed [m/s]	Reg.	TWR Lat.	TWR Long.	1st BW Flap.	1st Sym. Flap.	1st BW Edge.	1st FW Flap.	1st FW Edge.	2nd BW Flap.	1st DT
					Frequency [Hz]					
5.0	0.039	0.325	0.333	0.579	0.735	0.897	0.804	1.126	1.585	1.670
9.0	-	0.324	0.338	0.569	0.772	0.840	0.901	1.179	1.554	1.652
13.0	0.157	0.325	0.353	0.600	0.846	0.803	0.990	1.207	1.526	1.618
					Damping ratio [%]					
5.0	70.2	0.7	5.0	39.6	33.5	1.0	30.5	1.1	10.0	0.9
9.0	-	0.5	6.3	63.4	54.1	1.6	47.6	1.7	17.0	1.9
13.0	14.3	0.4	8.9	76.4	65.0	1.0	60.0	1.2	21.7	8.3

wind turbine system equations. First, the wind input, $\mathbf{U}_w(\omega)$, has to be obtained. In this work, the wind input is computed from sampling of results from time-domain simulations, $\mathbf{u}_{w,bf}$, and Fourier transformation. Then, the transfer function of the closed-loop model needs to be evaluated as $\mathbf{H}_{ase}(\omega)$. Joining the wind input and the wind turbine transfer functions, the turbine response is obtained in the ground-fixed reference frame, $\mathbf{Y}_{gf}(\omega)$. If a signal on the blades is required, a transformation in frequency-domain, $\mathbf{B}(\omega)$, must be performed to transform a signal to the blade-fixed reference frame. The PSD of any wind turbine output is then computed and used to estimate the fatigue damage by the spectral method of Benasciutti and Tovo [23, 24]. All the steps are described in details in the following sections.

3.1. Turbulent wind input in the ground-fixed reference frame

In the wind turbine model, described by the Equation (12), the wind speed is an input to the system through $\mathbf{B}_{w,ase}$. Hence, the wind speed can be used as a system input to evaluate the wind turbine response. The wind acts on each aerodynamic

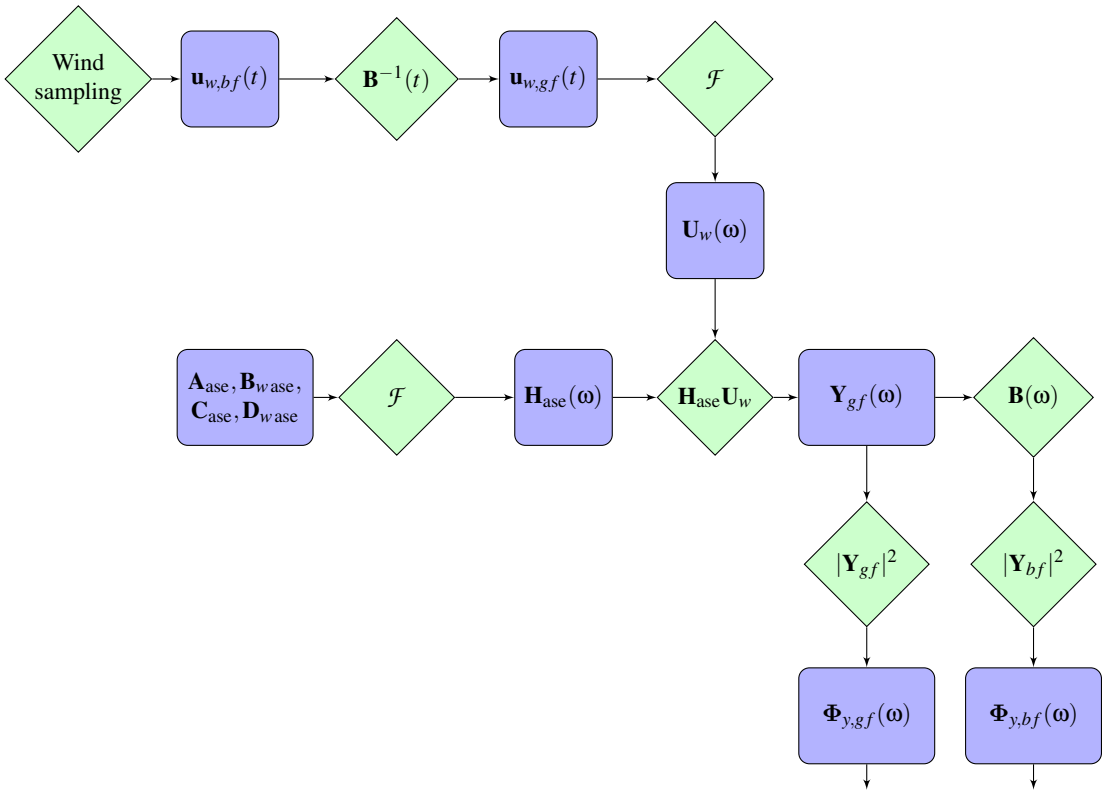

Figure 1. Block diagram of the workflow to compute the PSD of the output starting from the linear system equations and the sampled wind.

Wind Energ. 0000; **00**:1–17 © 0000 John Wiley & Sons, Ltd.
DOI: 10.1002/we
Prepared using weauth.cls

sections, positioned along the blade, in a ground-fixed reference frame. Therefore, a representation of the wind, at each aerodynamic section in a ground-fixed reference frame, is needed. Time series of the wind at each aerodynamic section are obtained in a blade-fixed reference frame from HAWC2 simulations using turbulence boxes generated with a Mann turbulence model [29]. The sensors used for the wind sampling rotate with the blade and they measure only the free wind. Hence, they do not contain any velocity contribution due to the rotor rotational speed and structural vibrations. The time series generated are then transformed into the global fixed frame of the multi-blade coordinates, with the multi-blade transformation $\mathbf{B}^{-1}$. The signals obtained are denoted $\mathbf{u}_{w,gf}(t)$. The multi-blade transformation is given by

$$\mathbf{B}^{-1} = \begin{bmatrix} \frac{1}{3} & \frac{1}{3} & \frac{1}{3} \\ \frac{2}{3}\cos(\Omega t) & \frac{2}{3}\cos(\Omega t + \frac{1}{3}\pi) & \frac{2}{3}\cos(\Omega t + \frac{2}{3}\pi) \\ \frac{2}{3}\sin(\Omega t) & \frac{2}{3}\sin(\Omega t + \frac{1}{3}\pi) & \frac{2}{3}\sin(\Omega t + \frac{2}{3}\pi) \end{bmatrix} \tag{15}$$

Given the wind speed time series in the ground-fixed reference frame, the wind speed input is computed evaluating the Fourier transform of the wind signals.

$$\mathbf{U}_w(\omega) = \mathcal{F}[\mathbf{u}_{w,gf}(t)] \tag{16}$$

This procedure allows to obtain the input in frequency domain, at each aerodynamic section of the linear model, in a ground-fixed reference frame. It is important to note that the wind input depends on the wind turbine model only for the rotational speed and the position of the aerodynamic sections along the blade. Therefore, in an optimization design procedure, the wind sampling and the computation of the wind input $\mathbf{U}_w(\omega)$ can be performed only once. Alternatively, if a model of the wind turbulence in the rotating frame is used, e.g. as shown by [30, 31], the wind sampling can be skipped.

3.2. Power spectral density of the ground-fixed response

Given the closed-loop system matrices of the wind turbine, the transfer functions between the wind speed at each aerodynamic section and any wind turbine output can be evaluated, as

$$\mathbf{H}_{ase}(\omega) = \mathbf{C}_{\text{ase}}(i\omega\mathbf{I} - \mathbf{A}_{\text{ase}})^{-1}\mathbf{B}_{w,\text{ase}} + \mathbf{D}_{w,\text{ase}} \tag{17}$$

where $i = \sqrt{-1}$ is the imaginary number, ω is the angular frequency, and $\mathbf{I}$ is the identity matrix. The wind turbine transfer function and the wind input can now be joined as

$$\mathbf{Y}_{gf}(\omega) = \mathbf{H}_{ase}(\omega)\mathbf{U}_w(\omega) \tag{18}$$

which describes the wind turbine response measured at a load sensor in the ground-fixed reference frame.

The PSD of a response in the ground-fixed reference frame can be computed as

$$\mathbf{\Phi}_{y,gf}(\omega) = |\mathbf{Y}_{gf}(\omega)|^2 \tag{19}$$

3.3. Power spectral density of the blade response

The computation of the PSD of an output in the blade-fixed reference frame requires a Coleman transformation in the frequency-domain. The multi-blade transformation (15) can be written by exponential functions of complex numbers as:

$$\mathbf{B}(t) = \mathbf{A}_0 + \mathbf{A}_1\frac{1}{2}(e^{i\Omega t} + e^{-i\Omega t}) + \mathbf{B}_1\frac{1}{2i}(e^{i\Omega t} - e^{-i\Omega t}) \tag{20}$$

where

$$\mathbf{A}_0 = \begin{bmatrix} 1 & 0 & 0 \\ 1 & 0 & 0 \\ 1 & 0 & 0 \end{bmatrix}, \quad \mathbf{A}_1 = \begin{bmatrix} 0 & 1 & 0 \\ 0 & -\frac{1}{2} & \frac{\sqrt{3}}{2} \\ 0 & -\frac{1}{2} & -\frac{\sqrt{3}}{2} \end{bmatrix}, \quad \text{and} \quad \mathbf{B}_1 = \begin{bmatrix} 0 & 0 & 1 \\ 0 & -\frac{\sqrt{3}}{2} & -\frac{1}{2} \\ 0 & \frac{\sqrt{3}}{2} & -\frac{1}{2} \end{bmatrix} \tag{21}$$

are the decomposition of the $\mathbf{B}$ matrix into the symmetric, cosine, and sine parts.

The transformation allows to project a signal $\mathbf{y}_{gf}(t)$ from the ground-fixed reference frame to the blade-fixed reference frame.

$$\begin{aligned} \mathbf{y}_{bf}(t) =& \mathbf{B}(t)\mathbf{y}_{gf}(t) \\ =& \frac{1}{2\pi}\int_{-\infty}^{\infty}\mathbf{B}(t)\mathbf{Y}_{gf}(\omega)e^{i\omega t}d\omega \end{aligned} \tag{22}$$

where $\mathbf{Y}_{gf}(\omega)$ is the Fourier transformed of $\mathbf{y}_{gf}(t)$. The frequency response of a load sensor in the rotating blade reference frame can be computed by substituting Equation (20) into Equation (22) and Fourier transformation as

$$\begin{aligned}\mathbf{Y}_{bf}(\omega) &= \int_{-\infty}^{\infty} \mathbf{y}_{bf}(t) e^{-i\omega t} dt \\ &= \mathbf{A}_0 \mathbf{Y}_{gf}(\omega) + \frac{1}{2}(\mathbf{A}_1 - i\mathbf{B}_1) \int_{-\infty}^{\infty} \mathbf{y}_{gf}(t) e^{-i(\omega-\Omega)t} dt + \frac{1}{2}(\mathbf{A}_1 + i\mathbf{B}_1) \int_{-\infty}^{\infty} \mathbf{y}_{gf}(t) e^{-i(\omega+\Omega)t} dt \\ &= \mathbf{A}_0 \mathbf{Y}_{gf}(\omega) + \frac{1}{2}(\mathbf{A}_1 - i\mathbf{B}_1)\mathbf{Y}_{gf}(\omega-\Omega) + \frac{1}{2}(\mathbf{A}_1 + i\mathbf{B}_1)\mathbf{Y}_{gf}(\omega+\Omega)\end{aligned} \tag{23}$$

Note how the backward and forward components of the response in the multi-blade coordinates are shifted in frequencies by $+\Omega$ and $-\Omega$, which is similar to the response of the turbine modes [32].

The PSD of a response on the blades can be computed as

$$\mathbf{\Phi}_{y,bf}(\omega) = |\mathbf{Y}_{bf}(\omega)|^2 \tag{24}$$

3.4. Computation of the fatigue damage rate

In the literature there are several methods to estimate the fatigue damage from the PSD of a signal. In this investigation, the method presented by Benasciutti and Tovo [23, 24] is used. This method is preferred to the one proposed by Dirlik [11] because it is not only empirical and it is supported by a theoretical background.

The method by Benasciutti and Tovo assumes a Gaussian stationary process, linear Palmgren-Miner rule [33, 34], and a S-N curve defined as

$$s^m N = C \tag{25}$$

where s is the amplitude of the signal, N is the number of cycles, m and C are constants. The method uses the information from four moments of the PSD to evaluate the rainflow-counting fatigue damage rate. Therefore, the entire spectrum is summarized by four scalar parameters. The four PSD moments required in the method are:

$$\lambda_0 = \int \Phi(f) df, \quad \lambda_1 = \int f\Phi(f) df, \quad \lambda_2 = \int f^2\Phi(f) df, \text{ and } \quad \lambda_4 = \int f^4\Phi(f) df \tag{26}$$

where f is the frequency. Two other parameters, that depend only on the moments, are also used in the method, the first and second bandwidth parameters:

$$\alpha_1 = \frac{\lambda_1}{\sqrt{\lambda_0\lambda_2}} \quad \text{and} \quad \alpha_2 = \frac{\lambda_2}{\sqrt{\lambda_0\lambda_4}} \tag{27}$$

The rainflow fatigue damage rate (D) is estimated as a weighted linear combination of the damage rate of a narrow-banded process (D_{NB}) and of a range counting damage (D_{RC}), as

$$D = b_{wgt} D_{NB} + (1 - b_{wgt}) D_{RC} \tag{28}$$

where b_{wgt} is the weight. This relationship is supported by a theoretical relation that bounds the damage rate between a range counting damage and the damage rate of of a narrow-banded process. The range counting damage is then approximated as a function of the damage of the narrow-banded process, the second bandwidth parameter α_2, and the m exponent.

$$D_{RC} \approx D_{NB}\alpha_2^{m-1} \tag{29}$$

The damage of a narrow-banded process is computed as

$$D_{NB} = \frac{\nu_0}{S_0^m} \left(\sqrt{2\lambda_0}\right)^m \Gamma(1 + 0.5m) \tag{30}$$

where Γ is the Gamma function, S_0 is the critical stress level, and ν_0 is the rate of mean upcrossings. The last parameter can be computed as

$$\nu_0 = \frac{1}{2\pi} \frac{\sqrt{\lambda_2}}{\lambda_0} \tag{31}$$

The value of the weight b_{wgt} is obtained from empirical data fitting as function of the bandwidth parameters, α_1 and α_2

$$b_{wgt} = \frac{\alpha_1 - \alpha_2}{(\alpha_2 - 1)^2} \left[1.112(1 + \alpha_1\alpha_2 - \alpha_1 - \alpha_2)e^{2.11\alpha_2} + \alpha_1 - \alpha_2\right] \tag{32}$$

Wind Energ. 0000; **00**:1–17 © 0000 John Wiley & Sons, Ltd.
DOI: 10.1002/we
Prepared using weauth.cls

In this work the power spectra are truncated at a fixed frequency. The value of 2 Hz is selected according to the findings of Bergami and Gaunaa [35]. In their work, they noted that the frequencies that contribute the most to the fatigue damage loads are those below 2 Hz, for the NREL 5 MW Reference Wind Turbine.

In this investigation the m exponent is set to 3 for loads on the tower and to 10 for loads on the blades .

Figure 2 shows a comparison between the fatigue damage rate obtained with Benasciutti and Tovo's method and the damage equivalent load obtained with the rainflow-counting. Four different sensors are reported at 15 m/s and 20 m/s: tower base lateral and longitudinal bending moments and blade root flapwise and edgewise bending moments. For each wind speed 100 different turbulent seeds are considered. All loads are normalized with respect to a reference value of the same sensor obtained with the corresponding method. The loads of the two approaches are computed with the same time series, hence the differences are only due to differences in the methods. The loads on the tower have better correlation compared to loads on the blade. Only the blade loads exceed 10% error at some turbulence seeds. The lower accuracy can be attributed to the higher m coefficient used to compute the fatigue on the blades. Benasciutti and Tovo [24] also noticed a lower accuracy of spectral methods for higher m coefficients.

3.5. Gravity contribution

The linear model does not include any gravitational acceleration, hence the fatigue damages do not contain any contribution due to the weight of the structure. However, when evaluating the blade edgewise loads, the gravity can be easily included, in the PSD, as a deterministic contribution. The PSD of the bending moment due to the weight is added to the PSD of the blade edgewise load. This approach allows to take into account the weight contribution to the fatigue damage rate. The weight component of the blade edgewise bending moment, on a non-pitching reference frame at a distance r along the blade, can be expressed as:

$$y(t,r) = g \sin(\Omega t) \int_r^R s\, m(s)\, ds \tag{33}$$

where R is the blade length, $m(s)$ is the distributed blade mass, as function of the curvilinear variable along the blade span s, and g is the gravitational acceleration.

3.6. Considerations on the computational time

The generation of the closed-loop system matrices, for the considered high-order wind turbine model, takes approximately 3 minutes for 21 given operational states, i.e. 21 different wind speeds. This operation can be parallelized, computing each operational point independently, to further reduce the computational cost. The evaluation of the fatigue damage rate of one sensor, starting from the closed-loop system matrices and the wind input in frequency domain, takes approximately 8 minutes for 21 different wind speed. Also this operation can be parallelized, evaluating the fatigue at each wind speed in parallel. As mentioned previously the computation of the wind input can be performed a priori because it does not depend on the model. The computational time of this approach is therefore lower than the time that is required to compute the time series with a nonlinear aeroservoelastic code and to evaluate the fatigue damage with the rainflow-counting.

All the above mentioned times are obtained with a standard laptop machine.

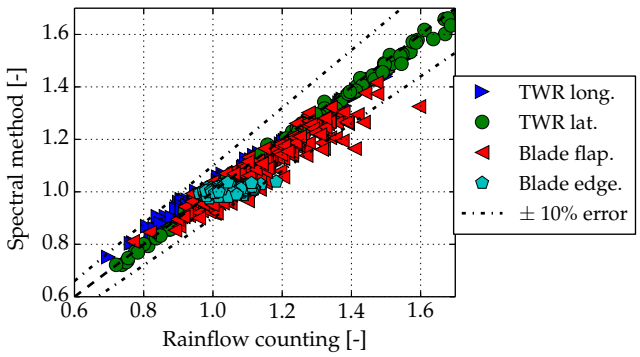

Figure 2. Comparison of normalized fatigue damage rate obtained with the spectral method and damage equivalent load obtained with rainflow-counting. Tower base longitudinal ($TWR\ long.$) and lateral ($TWR\ lat.$) bending moments and blade root flapwise ($Blade\ flap.$) and edgewise ($TWR\ lat.$) moments. Wind speeds of 15 m/s and 20 m/s. Time series obtained with nonlinear time-domain simulations. A $\pm 10\%$ error band is also plotted (dashed-dot line).

4. COMPARISON OF LINEAR AND NONLINEAR CLOSED-LOOP SYSTEMS

This section presents a comparison of the linear and nonlinear model in closed-loop configuration. The comparison is carried out in two steps. First, time responses due to wind steps are analyzed. This investigation gives a clear overview of the wind turbine models behavior, but it does not excite many aeroservoelastic modes. Secondly, PSD computed from turbulent wind simulations are addressed. This comparison gives an overview on the aeroservoelastic modes.

A modified version of the NREL 5 MW Reference Wind Turbine is used in this section. The tilt and cone angles are set to zero to remove the differences in modeling between HAWC2 and HAWCStab2, so that the nonlinear model satisfies the hypothesis of the linear one. Furthermore gravity, wind shear, and tower shadow are not included in the nonlinear time simulations. The scope of this comparison is to underly the intrinsic differences between the linear and nonlinear model that consequently affect the load evaluation method.

4.1. Response to a step in the wind speed

A comparison of wind speed step responses between the linear and the nonlinear model is performed. The response is obtained with a uniform 1 m/s wind speed step. The analysis shows the differences between the linear and the nonlinear models at different operational points. Four sensors are considered to show the performances of the linear model.

Figure 3 shows the variation of the rotor speed due to a 1 m/s wind speed step at 5, 9, and 13 m/s. The three responses are in three different operational regions 1, 2, and 4, hence they show the behavior of the three different controllers. At 5 and 13 m/s the controllers set the rotor speed variation to zero after a transient. In the first case, this is controlled adjusting the generator torque, while in the second the pitch angle. At 9 m/s the rotational speed sets to a different value, than the initial one, because the operational region has variable speed. In the three plots, only the mode associated with the controller can be clearly distinguished. The linear and nonlinear model agree on the values of the frequency and damping of the regulators mode. At 9 m/s, the rotor speed steady-state value of the linear model differs from the one of the nonlinear by 4 %. The discrepancy is associated to the increase of rotor speed at steady-state due to the variable speed region.

Figure 4 shows the variation of the tower base longitudinal bending moment due to a 1 m/s wind speed step at 5, 9, and 13 m/s. The responses are dominated by the first longitudinal tower mode. The linear and nonlinear models agree on the values of the first longitudinal tower mode frequency and damping at the different operational points. A difference of almost 10 % can be noticed in the steady-state value at 9 m/s. This difference is due to a different value of aerodynamic thrust at steady-state, due to the different rotational speed compared to the one at which the linear model is linearized.

Figure 5 shows the variation of the tower base lateral bending moment due to a 1 m/s wind speed step at 5, 9, and 13 m/s. The response is dominated by vibrations of the first tower lateral mode. The vibration amplitudes differ, however frequencies and amplitude decays are well captured.

Figure 6 shows the variation of the blade root out-of-plane bending moment variation due to a 1 m/s wind speed step at 5, 9, and 13 m/s. The loads on the blade are in a blade-fixed reference frame, hence the response of the linear model has been transformed with the inverse of Equation (15). In this case, more discrepancies are present between the linear and nonlinear model, below rated wind speed. However, the differences are acceptable for the current application because the general trend in the response is captured.

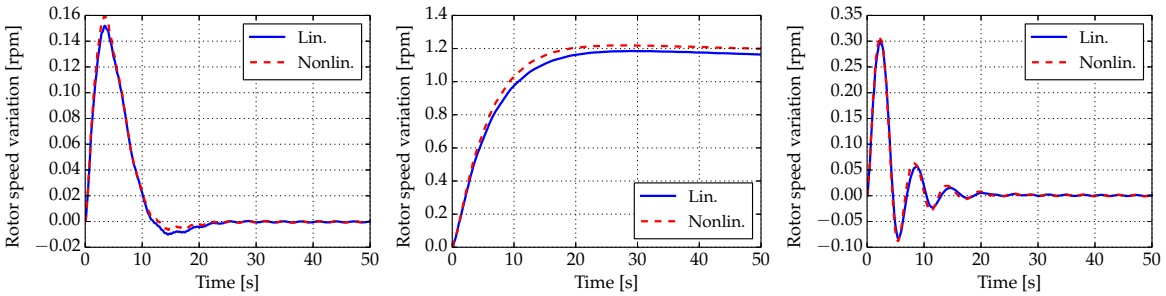

a) 5 m/s. *b)* 9 m/s. *c)* 13 m/s.

Figure 3. Rotor speed variation due to a uniform 1 m/s wind speed step. Comparison between the linear (blue solid line) and the nonlinear (red dashed line) models at 5, 9, and 13 m/s.

Wind Energ. 0000; **00**:1–17 © 0000 John Wiley & Sons, Ltd.
DOI: 10.1002/we
Prepared using weauth.cls

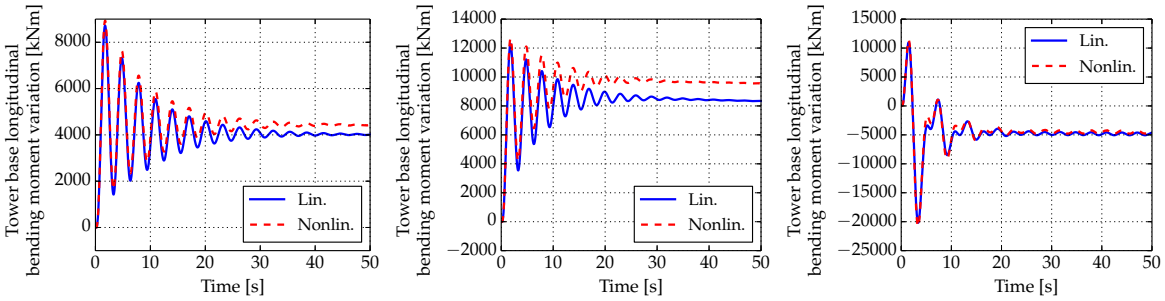

a) 5 m/s. *b)* 9 m/s. *c)* 13 m/s.

Figure 4. Tower base longitudinal bending moment variation due to a uniform 1 m/s wind speed step. Comparison between the linear (blue solid line) and the nonlinear (red dashed line) models at 5, 9, and 13 m/s.

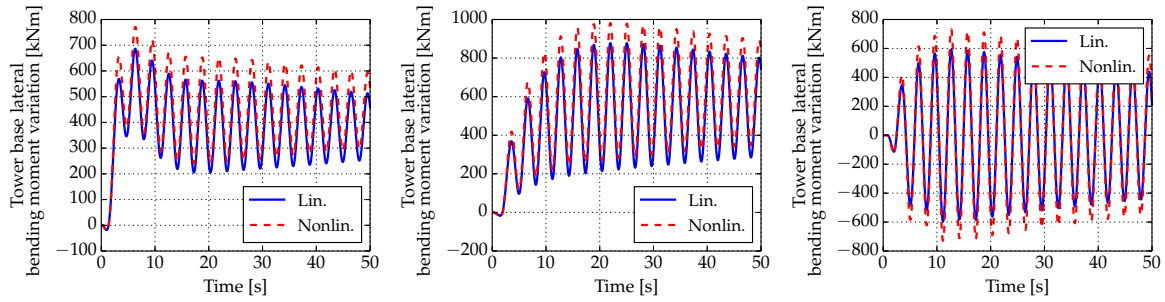

a) 5 m/s. *b)* 9 m/s. *c)* 13 m/s.

Figure 5. Tower base lateral bending moment variation due to a uniform 1 m/s wind speed step. Comparison between the linear (blue solid line) and the nonlinear (red dashed line) models at 5, 9, and 13 m/s.

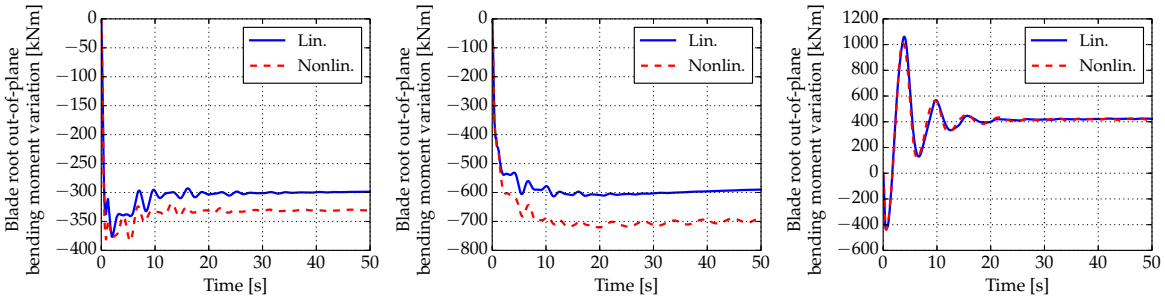

a) 5 m/s. *b)* 9 m/s. *c)* 13 m/s.

Figure 6. Blade root out-of-plane bending moment variation due to a uniform 1 m/s wind speed step. Comparison between the linear (blue solid line) and the nonlinear (red dashed line) models at 5, 9, and 13 m/s.

4.2. PSD of response to turbulent wind

This section illustrates the PSDs of different wind turbine sensors due to turbulent wind. The turbulence intensity is 1% at all wind speeds to better distinguish peaks in the PSD associated with the aeroservoelastic modes. This value of turbulence intensity is lower than the one indicated by the standards for normal operations, but it eases the models comparison. The following figures compare the linear and the nonlinear models. The plots also show the frequencies of the aeroservoelastic modes and the frequencies of the harmonics of the rotational speed. The spectra at the wind speeds of 5, 9, and 13 m/s are compared.

Figure 7 shows the PSD of the tower base longitudinal bending moment. At 5 and 13 m/s the peak with the highest energy is the one associated with the first tower longitudinal mode and at 9 m/s it is the one associated with the first backward whirling edgewise mode. The peak is higher at 5 m/s due to the proximity of the mode with the 3P frequency, equivalent to 0.353 Hz. At 13 m/s the peak associated with the regulator mode can be distinguished at about 0.2 Hz.

Figure 8 shows the PSD of the tower base lateral bending moment. Also in this case the linear model captures the main peaks and the overall energy level, as predicted by the nonlinear model.

Figure 9 shows PSD of the blade root out-of-plane bending moment. Since this results are in a blade-fixed reference frame, they are obtained with the transformation in Equation (23). The figure does not show the values of the aeroservoelastic modal frequencies, because the PSD is evaluated in a blade-fixed reference frame and the modal frequencies are computed in a ground-fixed reference frame. A good agreement between the PSD obtained with the linear and the nonlinear model is shown; frequencies and maximum power levels are predicted well, however the linear model show bigger dips than the nonlinear model.

5. FATIGUE DAMAGE

This section contains an analysis of the fatigue damage obtained with the presented method, based on three different test cases. In a first case, the fatigue damage is computed during normal operation. In the second and third cases, fatigue damage loads variations are estimated between two wind turbine models. The second and third cases differ on the wind input conditions: in the second case, the loads are evaluated with a fix number of turbulence seeds, in the third one, the number of turbulence seeds is increased to identify the dependency of the approach on the wind realization. The two models used in these cases differ in the controller tuning.

Three different results are compared in all test cases for each sensor at each wind speed:

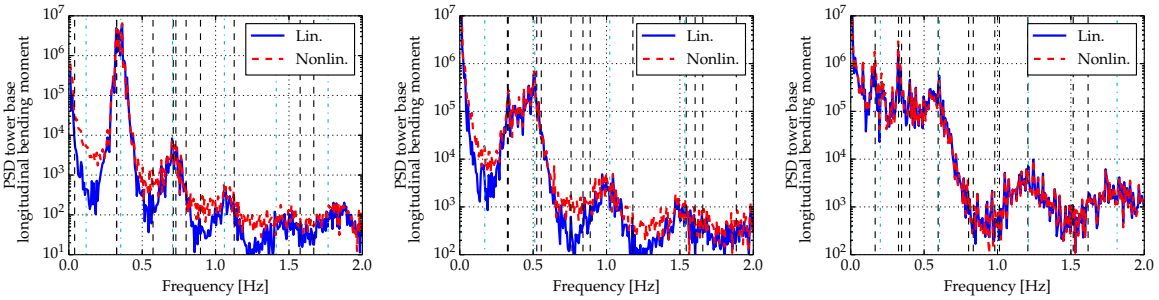

a) 5 m/s. *b)* 9 m/s. *c)* 13 m/s.

Figure 7. PSD of the tower base longitudinal bending moment. Comparison between the linear (blue solid line) and the nonlinear (red dashed line) models at 5, 9, and 13 m/s. The wind turbine aeroservoelastic mode frequencies are shown with dashed black vertical lines. The harmonics of the rotational frequency are shown with dash-dot light blue vertical lines.

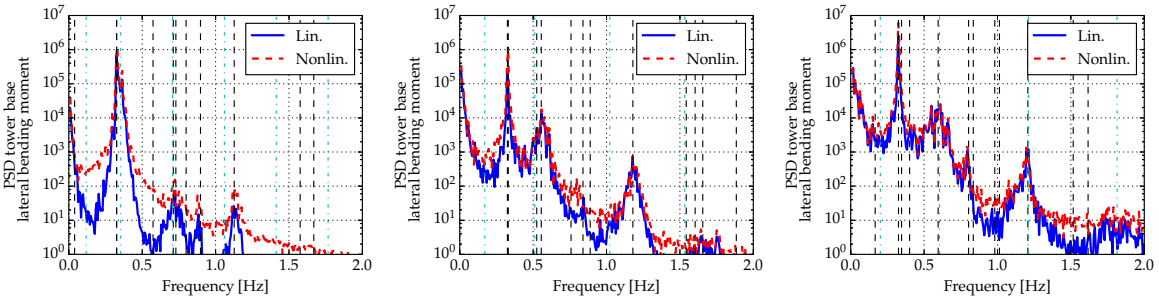

a) 5 m/s. *b)* 9 m/s. *c)* 13 m/s.

Figure 8. PSD of the tower base lateral bending moment. Comparison between the linear (blue solid line) and the nonlinear (red dashed line) models at 5, 9, and 13 m/s. The wind turbine aeroservoelastic mode frequencies are shown with dashed black vertical lines. The harmonics of the rotational frequency are shown with dash-dot light blue vertical lines.

Wind Energ. 0000; **00**:1–17 © 0000 John Wiley & Sons, Ltd.
DOI: 10.1002/we
Prepared using weauth.cls

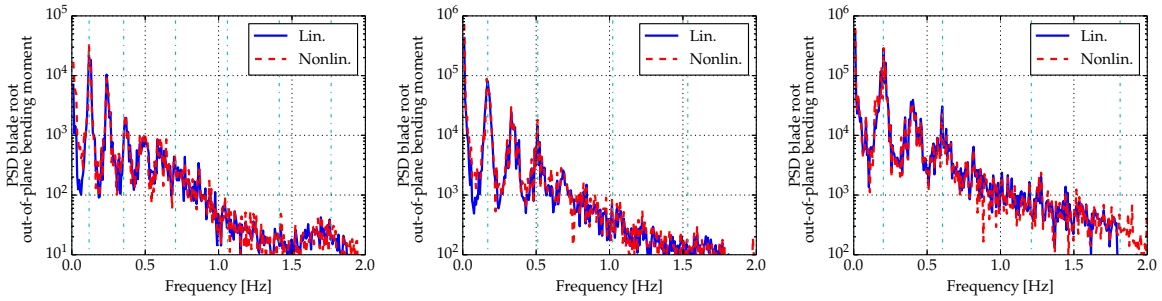

a) 5 m/s. *b)* 9 m/s. *c)* 13 m/s.

Figure 9. PSD of the blade root out-of-plane bending moment in a blade-fixed coordinate reference system. Comparison between the linear (blue solid line) and the nonlinear (red dashed line) models at 5, 9, and 13 m/s. The harmonics of the rotational frequency are shown with dash-dot light blue vertical lines.

- *Lin.*: damage rate obtained with the linear model and wind sampled from simulations.
- *Nonlin.*: damage rate obtained with the spectral method applied to the PSD of the time series computed with the nonlinear wind turbine model.
- *Rainflow*: damage equivalent load (DEL) obtained with rainflow-counting of time series computed with the nonlinear wind turbine model.

The gravitational contribution to the blade edgewise fatigue loads is included in the *Lin.* case, as described in section 3.5.

5.1. Normal operation

In this paragraph, the fatigue damage is compared during normal operation. The reference turbulence intensity is 14 % and the wind speed is between 5 and 25 m/s with 1 m/s spacing.

A normalization is performed to compare the DEL, obtained with the rainflow-counting, and the damage rate, obtained with the spectral method. The damage rates (*Lin.* and *Nonlin.*) are both normalized with the value of the damage rate of the nonlinear model (*Nonlin.*) at 5 m/s. The DELs at the different wind speeds are normalized with the DEL at 5 m/s. The comparison between the damage rates and the DELs cannot be performed on the actual values but only on the variations between the different wind speeds, because the normalization is achieved with different factors.

Figure 10 shows the normalized fatigue loads at the tower base in the longitudinal and lateral directions. The plots show the comparison between damage rate of the linear model with the wind sampled in turbulent inflow (solid blue labeled *Lin.*), damage rate of the nonlinear model (dashed red labeled *Nonlin.*), and DEL of the nonlinear model (dashed-dot green labeled *Rainflow*). Apart from the variable speed region and the high turbulence intensity, a very good agreement,

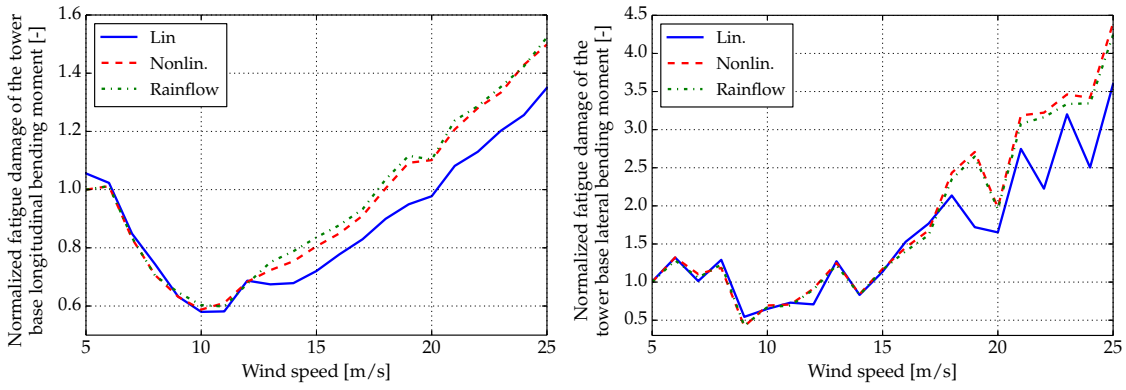

a) Longitudinal. *b) Lateral.*

Figure 10. Normalized fatigue loads at the tower base during normal operational conditions. Comparison between damage rate of the linear model with the wind sampled turbulent inflow (solid blue labeled *Lin.*), damage rate of the nonlinear model (dashed red labeled *Nonlin.*), and DEL of the nonlinear model (dashed-dot green labeled *Rainflow*).

in both longitudinal and lateral directions, is achieved at low wind speeds. Around rated wind speed, the linear model (solid lines) shows less continuity in the longitudinal loads compared to the nonlinear model (dashed lines). This can be explained by the switch between the controller regions that smears out the controller changes in the nonlinear model. Above rated, the results obtained with the linear model differ from those obtained with the nonlinear ones. The maximum difference between *Lin.* and *Nonlin.* amounts to 13 %. The difference is due to the linearizion and the differences in the model, i.e. cone angle, tilt, and gravity. In the lateral direction the loads estimated both with the linear and with the nonlinear models are less continuous with the wind speeds. The maximum difference between *Lin.* and *Nonlin.* amounts to 54 %. The differences in the lateral directions are larger than in the longitudinal because the response is more dependent on the amplitude of the wind spectrum at the frequency of the tower. Because the PSD of the tower lateral response is dominated by the sharp peak due to the low-damped tower lateral mode, a small variation in the amplitude of the input affects the response and therefore the estimated loads. This dependency can be reduced with wind sampling of longer time series or with an analytical wind spectrum. The damages obtained with the rainflow-counting (dashed-dot green labeled *Rainflow*) and the spectral method obtained from the nonlinear model (dashed red labeled *Nonlin.*) agree in all the wind speed range. This agreement indicates the effectiveness of the spectral method and the validity of the assumption to truncate the spectra at 2 Hz.

Figure 11 illustrates the normalized fatigue loads at the blade root, in the out-of-plane and in-plane directions. The figure has the same labels as Figure 10. The loads estimated with the linear model follow the trend of those evaluated with the nonlinear model. The maximum differences in the out-of-plane direction between the linear model and the nonlinear model is 10 % and in the in-plane direction is 2 %.

A larger error is present between results evaluated with the rainflow-counting (dashed-dot green labeled *Rainflow*) and those evaluated with the nonlinear model and the spectral method (dashed red labeled *Nonlin.*). This difference is intrinsic in the spectral method since the results are obtained from the same time series but with two different methods. This difference has also been shown in Section 3.4.

5.2. Parameter variation

This section contains a comparison of load variations estimated with the presented method and the rainflow-counting approach. Two cases are analyzed: first loads variations at three different wind speeds with a fix number of turbulence seeds are investigated, after loads variations estimated increasing the number of turbulent seeds at one wind speed are analyzed. The first case illustrates the accuracy of the current method to evaluate loads variations compared to the rainflow-counting, the second compares the dependency of the loads evaluated with the two approaches with respect to the wind realization. An analysis on the load variations is of interest because it reflects the accuracy of gradients estimations in an optimization design procedure.

In all cases, the load variations are obtained comparing the same sensor of two different models. The models differ in the controller tuning. The tuning is changed using a type of gain-scheduling that also includes the effects of variations in the aerodynamic torque with respect to the rotational speed [19]. The same sampled wind input $\mathbf{U}_w$ is used with both the linear models. Hence, the wind sampling is performed only once. This approach is the one that could be used in an optimization procedure, where only one set of sampled wind could be used through the design.

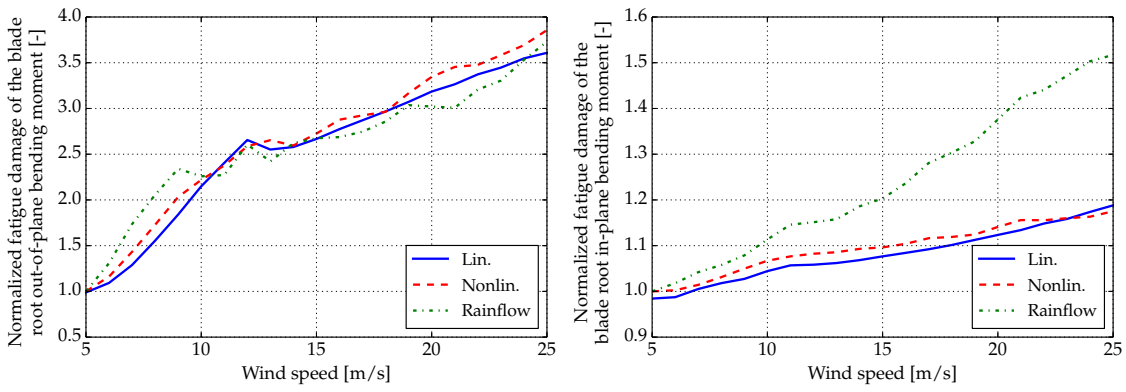

a) Out-of-plane. *b) In-plane.*

Figure 11. Normalized fatigue loads at the blade root during normal operational conditions. Comparison between damage rate of the linear model with the wind sampled turbulent inflow (solid blue labeled *Lin.*), damage rate of the nonlinear model (dashed red labeled *Nonlin.*), and DEL of the nonlinear model (dashed-dot green labeled *Rainflow*).

Wind Energ. 0000; **00**:1–17 © 0000 John Wiley & Sons, Ltd.
DOI: 10.1002/we
Prepared using weauth.cls

5.2.1. Fixed number of turbulence seeds

Here, the load variations are evaluated at three different wind speeds, 15, 20, and 25 m/s. Ten different turbulence seeds are used for each wind speed to compute the loads.

Figure 12 shows the percentage variations of the tower base longitudinal bending moment and of the rotor speed due to the change in the controller gain-scheduling. The plots show the comparison between damage rate of the linear model with the wind sampled in turbulent inflow (blue labeled *Lin.*), damage rate of the nonlinear model (red labeled *Nonlin.*), and DEL of the nonlinear model (green labeled *Rainflow*). The different gain-scheduling keeps the frequency of the speed regulator mode (the solid body rotation of the drivetrain) almost constant in the full load region, while in the reference case it increases with the wind speed because the increasing aerodynamic damping is neglected. The speed regulation is therefore less aggressive at higher wind speed with the modified gain-scheduling than with the reference one. This effect is confirmed by the load variations shown in the figure. Because the controller is less aggressive, the tower loads are reduced, and the reduction increases for increasing wind speed. On the other hand, the fluctuations of the rotor speed are increasing. The maximum error in the tower base longitudinal moment variation between *Lin.* and *Rainflow* amounts to 22 %. This difference occurs at 15 m/s, where the influence of the change in the gain-scheduling on the loads is lower. The maximum difference on the estimation of the rotor speed variation is 7 %. Overall the linear method follows correctly the trends estimated with the nonlinear simulations and the rainflow-counting.

5.2.2. Increasing number of turbulence seeds

In this case the loads are evaluated only at 15 m/s for increasing number of turbulence seeds used in the loads computation, from one to thirty. Each load variation is evaluated five different times using different wind realizations, i.e. different turbulence seeds. This analysis illustrates if the selected wind realization affects the loads or, if the number of turbulence seeds used is sufficient to fully describe the turbulent wind and therefore remove the dependency on the realization.

Figure 13 shows the percentage variations of the tower base longitudinal bending moment and of the rotor speed due to the change in the controller gain-scheduling as function of the number of turbulent seeds used in the loads evaluation. The tower base longitudinal bending moment evaluated with the linear model *Lin.* is less dependent on the wind realization compared to the one estimated with nonlinear simulations *Rainflow*. Nonlinear loads show a wide scatter depending on the wind realization, even when many turbulence seeds are used. With the nonlinear approach, the dependency on the wind condition, in some cases, significantly underestimates the effects of the different controller tuning on the loads. The rotor speed variations are generally more dependent on the wind realization with both methods. However, with more than 15 turbulence seeds, the linear approach seems to be more consistent than the nonlinear one.

Loads estimated with the spectral method are less dependent on the wind realization than when estimated with nonlinear time-domain simulations. This lower dependency can be a significant advantage in an optimization design procedure, since the final design is not affected by the selected wind input. Furthermore, the loads variations estimated with the presented method can be with more confidence attributed to the changes in the design parameters rather than on a different wind passing through the turbine.

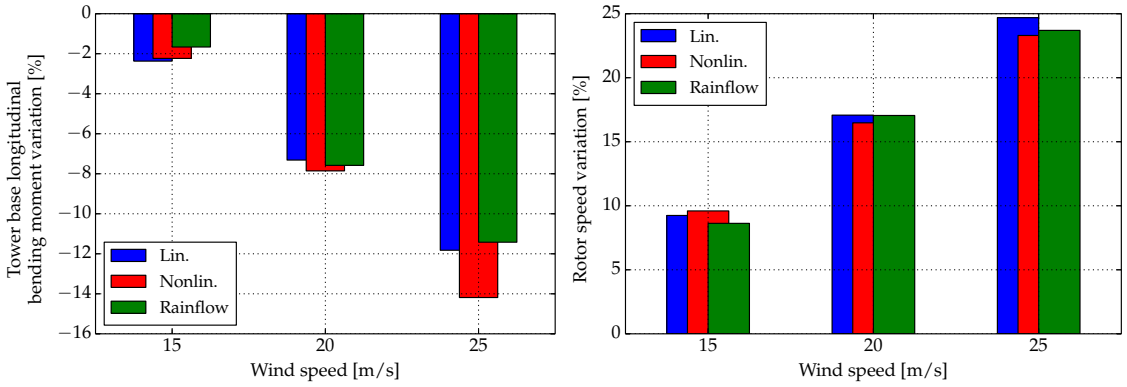

a) Tower base longitudinal. *b) Rotor speed.*

Figure 12. Percentage variation of the tower base longitudinal bending moment and of the rotor speed due to a different controller tuning. Comparison between damage rate of the linear model with the wind sampled turbulent inflow (blue labeled *Lin.*), damage rate of the nonlinear model (red labeled *Nonlin.*), and DEL of the nonlinear model (green labeled *Rainflow*). Wind speed of 15, 20, and25 m/s.

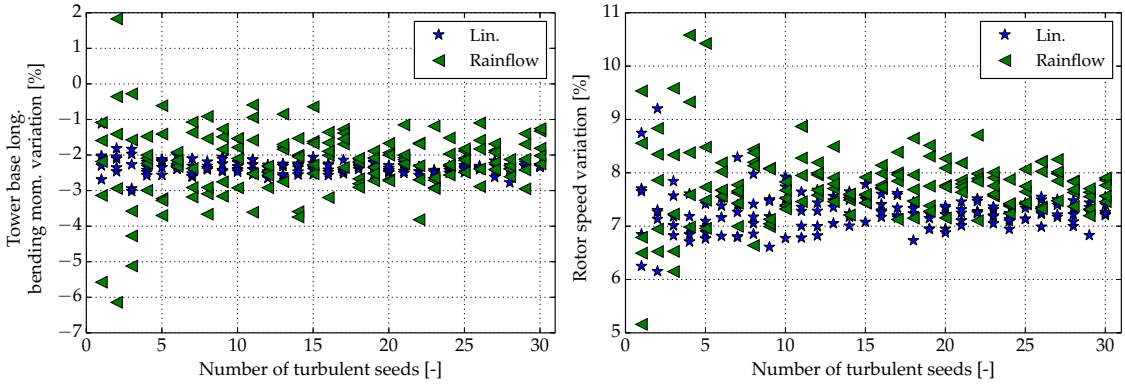

a) Tower base longitudinal. *b) Rotor speed.*

Figure 13. Percentage variation of the tower base longitudinal bending moment and of the rotor speed due to a different controller tuning. Dependency of the loads on the number of turbulence seeds used in the evaluation and on the turbulence realization. Comparison between damage rate of the linear model with the wind sampled turbulent inflow (blue labeled *Lin.*) and DEL of the nonlinear model (green labeled *Rainflow*). Wind speed of 15 m/s.

6. CONCLUSION

This paper presents a method to evaluate wind turbine fatigue loads based on a linear high fidelity wind turbine model and on a spectral method. The method has a potential for wind turbine optimization design applications because it does not require time simulations to evaluate the fatigue loads when a wind turbine parameter is changed. Furthermore, the wind input used by this method can be computed before starting the optimization, therefore a high-detailed description of the wind, i.e. high number of turbulence seeds, does not compromise the computational time. In the paper a description of the wind turbine model in closed-loop configuration is performed. The model of the controller used to regulate the wind turbine is described in details. The method to evaluate the fatigue load is first described and then analyzed through a series of comparisons with a nonlinear model, to validate the different steps it is based on. Time-domain wind step responses and power spectra are analyzed to compare the models. Two different test cases are then investigated to identify the accuracy of the loads evaluation. Results show that the method is able to estimate wind turbine loads in normal operation conditions and loads variations due to a change in the controller tuning. Furthermore, loads estimated with the presented method appear to be less dependent on the wind realization used for the evaluation.

The load estimation leads to large errors when the PSD of the response is dominated by low-damped modes. These responses are more dependent on the wind input and therefore on the sampled wind time series. These differences should be reduced with longer wind sampling or with an analytical wind input.

Future investigations should focus on a more detailed analysis of the accuracy of gradients computed with this method. The investigation should identify the dependency of results on the wind input spectra. Furthermore, an analytical formulation of the wind input should be included to avoid the wind sampling from time series.

REFERENCES

1. Fuglsang P, Madsen H. Optimization method for wind turbine rotors. *Journal of Wind Engineering and Industrial Aerodynamics* 1999; **80**(12):191–206, doi:10.1016/S0167-6105(98)00191-3.
2. Fuglsang P, Thomsen K. Site-specific design optimization of 1.5-2.0 MW wind turbines. *Journal of Solar Energy Engineering* 2001; **123**(4):296, doi:10.1115/1.04433.
3. Fuglsang P, Bak C, Schepers JG, Bulder B, Cockerill TT, Claiden P, Olesen A, van Rossen R. Site-specific Design Optimization of Wind Turbines. *Wind Energy* 2003; **5**(4):261–279, doi:10.1002/we.61.
4. Bulder BH, Schepers JG. Numerical optimization for wind turbine design, based on aeroelastic analysis. *European Wind Energy Conference and Exhibition 2001, EWEA* 2001.
5. Bottasso CL, Campagnolo F, Croce A. Multi-disciplinary constrained optimization of wind turbines. *Multibody System Dynamics* 2012; **27**(1):21–53, doi:10.1007/s11044-011-9271-x.
6. Bottasso CL, Campagnolo F, Croce A, Tibaldi C. Optimization-based study of bendtwist coupled rotor blades for passive and integrated passive/active loadalleviation. *Wind Energy* 2013; **16**(8):1149–1166, doi:10.1002/we.1543.

7. Bottasso CL, Campagnolo F, Croce A, Giuliani M. Multidisciplinary optimization of wind turbines using comprehensive aeroservoelastic models. *European and African Conference on Wind Engineering*; 2009.
8. Ashuri T, Zaaijer MB, Martins JRRA, van Bussel GJW, van Kuik GAM. Multidisciplinary design optimization of offshore wind turbines for minimum levelized cost of energy. *Renewable Energy* 2014; **68**:893–905, doi: 10.1016/j.renene.2014.02.045.
9. Ashuri T. Beyond classical upscaling: integrated aeroservoelastic design and optimization of large offshore wind turbines. *PhD Thesis*, Delft University of Technology, The Netherlands. 2012.
10. Merz KO, Muskulus M, Moe G. A simple frequency-domain method for stress analysis of stall-regulated wind turbines. *Wind Energy* 2012; **15**(5):773–798, doi:10.1002/we.504.
11. Dirlik T. Application of Computers in Fatigue Analysis. *PhD Thesis*, University of Warwick, United Kingdom; 1985.
12. Merz KO. Rapid optimization of stall-regulated wind turbine blades using a frequency-domain method: Part 1, loads analysis. *Wind Energy* 2014; doi:10.1002/we.1786.
13. Merz KO. Rapid optimization of stall-regulated wind turbine blades using a frequency-domain method: Part 2, cost function selection and results. *Wind Energy* 2014; doi:10.1002/we.1738.
14. IEC/TC88. *IEC 61400-1 Ed.3: Wind turbines - Part 1: Design requirements*. 2005.
15. Thomsen K. The statistical variation of the wind turbine fatigue loads. *Technical Report Risø-R-1063(EN)*, Risø National Laboratory, 1998. www.hawc2.dk
16. Natarajan A, Verels DR. Outlier robustness for wind turbine extrapolated extreme loads. *Wind Energy* 2012; **15**(5):679–697, doi:10.1002/we.497.
17. Tibaldi C, Henriksen LC, Bak C. Investigation of the dependency of wind turbine loads on the simulation time. *European Wind Energy Conference and Exhibition 2014, EWEA* 2014.
18. Hansen MH, Hansen A, Larsen TJ, Øye S, Sørensen P, Fuglsang P. Control design for a pitch-regulated, variable speed wind turbine. *Technical Report Risø-R-1500(EN)*, Risø National Laboratory, 2005.
19. Tibaldi C, Henriksen LC, Hansen MH, Bak C. Effects of gain-scheduling methods in a classical wind turbine controller on wind turbine aero-servo-elastic modes and loads. *32nd ASME Wind Energy Symposium*. American Institute of Aeronautics and Astronautics, 2014, doi:10.2514/6.2014-0873.
20. Hansen MH. Aeroelastic properties of backward swept blades. *49th AIAA Aerospace Sciences Meeting including the New Horizons Forum and Aerospace Exposition*. American Institute of Aeronautics and Astronautics, 2011, doi: 10.2514/6.2011-260.
21. Larsen TJ, Hansen MA. How 2 HAWC2, the user's manual. *Technical Report Risø-R-1597(ver. 3-1)(EN)*, Risø National Laboratory, 2007. www.hawc2.dk
22. Hansen MH, Henriksen LC. Basic DTU Wind Energy controller. *Technical Report E-0028*, DTU Wind Energy, 2013.
23. Benasciutti D, Tovo R. Spectral methods for lifetime prediction under wide-band stationary random processes. *International Journal of Fatigue* 2005; **27**(8):867–877, doi:10.1016/j.ijfatigue.2004.10.007.
24. Benasciutti D, Tovo R. Comparison of spectral methods for fatigue analysis of broad-band gaussian random processes. *Probabilistic Engineering Mechanics* 2006; **21**(4):287–299, doi:10.1016/j.probengmech.2005.10.003.
25. Jonkman J, Butterfield S, Musial W, Scott G. Definition of a 5-MW reference wind turbine for offshore system development. *Technical Report NREL/TP-500-38060*, NREL/NWTC, 2009.
26. Hansen MH. Aeroelastic stability analysis of wind turbines using an eigenvalue approach. *Wind Energy* 2004; **7**(2):133–143, doi:10.1002/we.116.
27. Sønderby I, Hansen MH. Open-loop frequency response analysis of a wind turbine using a high-order linear aeroelastic model. *Wind Energy* 2014; **17**: 1147–1167, doi:10.1002/we.1624.
28. Hansen MH. Aeroelastic optimization of MW wind turbines. *Technical Report Risø-R-1803(EN)*, Risø National Laboratory, 2011.
29. Mann J. Wind field simulation. *Probabilistic Engineering Mechanics* 1998; **13**(4):269–282, doi:10.1016/S0266-8920(97)00036-2.
30. Connell JR. The spectrum of wind speed fluctuations encountered by a rotating blade of a wind energy conversion system. *Solar Energy* 1982; **29**(5):363–375, doi:10.1016/0038-092X(82)90072-X.
31. Dragt J. Atmospheric turbulence characteristics in the rotating frame of reference of a wecs rotor. *European Community Wind Energy Conference*, Madrid, Spain, 1990; 274–278.
32. Hansen MH. Improved Modal Dynamics of Wind Turbines to Avoid Stall-induced Vibrations. *Wind Energy* 2003; **6**(2): 179–195, doi:10.1002/we.79.
33. Miner AM. Cumulative damage in fatigue. *Journal of Applied Mechanics* 1945; Vol. 12, Trans. ASME **67**:A159-A164.
34. Sutherland H. On the Fatigue Analysis of Wind Turbines. *Technical Report SAND99-0089*, Sandia National Laboratories, 1999.
35. Bergami L, Gaunaa M. Analysis of aeroelastic loads and their contributions to fatigue damage. *In Proceedings of the Science of Making Torque from Wind 2012*, Oldenburg, Germany, 2012.

Article III: Optimal Tuning for a Classical Wind Turbine Controller

The article was presented at the 4th EAWE conference *The Science of Making Torque from Wind*, Oldenburg, Germany, 9-11 October 2012. The proceedings are published in the *Journal of physics: conference series*.

Optimal tuning for a classical wind turbine controller

C Tibaldi, M H Hansen and L C Henriksen

DTU Wind energy, Roskilde, Denmark

E-mail: tlbl@dtu.dk

Abstract. Fine tuning of controllers for pitch-torque regulated wind turbines is an opportunity to improve the wind turbine performances and reduce the cost of energy without applying any changes to the design. For this purpose, a method for automatically tune a classical controller based on numerical optimization is developed and tested. To have a better understanding of the problem a parametric analysis of the wind turbine performances due to changes in the controller parameters is first performed. Thereafter results obtained with the automatic tuning show that is possible to identify a finer controller tuning that improves the wind turbine performances. For the case study selected in this work, a 2% cost function reduction is achieved with seven iterations.

1. Introduction

Most of the controllers that have been presented for pitch-torque controlled variable speed wind turbines require a set of gains or weights that have to be selected to obtain the desired behavior of wind turbine. With the continuous growth in the rotors sizes and the rated powers, the role of the controller is more central in the wind turbine design, where the abilities of active controllers to reduce the loads are essential in the pursuit of reducing the cost of energy.

Tuning of a controller is not a straightforward process because often the gains lead to contrasting performances. It is always necessary to identify a trade-off according to the requirements. Fine controller tuning requires several iterations and can also be very time consuming depending on the type of controller and the number of tuning parameters. To improve the selection of the controller parameters tuning by means of numerical optimization has been investigated in previous works. In the work by Hansen et al. [1] the gains of a classical PI controller are computed to minimize the standard deviation of the blade root flapwise bending moment. The load is evaluated with several simulations at different mean wind speeds above rated. In the investigation a reduction of the standard deviation of the blade root flapwise bending moment up to 2% is achieved. Bottasso and Croce [2] describe an approach to perform a goal-oriented optimization of the tuning parameters. In their work they describe a possible coupling between an optimization and an aero-servo-elastic software. They also focus on the multi-objective nature of the tuning problem showing two approaches, one based on a combined scalar objective function and one based on a multi-objective Pareto-front optimization.

In this paper, a study to identify a tuning of the controller with a parametric analysis and a numerical optimization is presented. The aim is to investigate a possible improvement in the wind turbine performances adjusting the controller parameters according with the loads computed during power production simulations. To identify the quality of the performances, a cost function is first proposed and then used both in the parametric analysis and in the

optimization. The controller selected for this work is a classical regulator based on two proportional integral (PI) controllers, one for the constant speed-variable torque region, and one for the constant speed and constant power region. In the variable speed region a torque regulation proportional to the square of the measured rotational speed is used. No advanced loops for active load reduction are present in the controller.

Results of the investigation here presented show that with an optimized controller tuning the cost function can be reduced for the specific wind conditions considered.

A classical regulator framework for power production regulation is selected, despite the existence of more advanced control approaches, because they are the most used to control variable-speed pitch-torque regulated wind turbines due to their easily implementation, reliability and robustness. The wind turbine used in this work is the NREL 5MW reference turbine [3]. The method developed in this paper is also valid for more advanced controllers, and most of the considerations and conclusions may apply also to different wind turbines.

In Section 2 the controller used for the investigation is described. The numerical optimization, the cost function and the constraints are introduced in Section 3. Section 4 contains a parametric analysis of the effect of each controller parameter on the wind turbine performances. In Section 5 the results of an optimization are shown and commented.

2. Controller description and classical tuning

The controller used here is inspired by Bossanyi [4]. It is divided into four different sub controllers, each for a different operational region. The four regions are:

- constant minimum rotor speed variable torque
- variable rotor speed, variable torque region;
- constant rated rotor speed, variable torque region;
- constant rated rotor speed, constant power region.

In the following each region controller is described to show the parameters of the optimization problem. The techniques of switching between regions are not described. It follows the ideas of Bossanyi [4] and is not part of the optimization problem.

2.1. Variable speed, variable torque region

The pitch is kept constant at the angle β^* and the generator torque is used to regulate the rotational speed Ω to track a constant tip-speed-ratio. The value of the torque is set to $Q_{ref} = k\Omega^2$ to balance the aerodynamic torque. The constant k can be computed as

$$k = \eta \frac{1}{2} \rho \pi \frac{R^5}{\lambda^{*3}} C_p(\beta^*, \lambda^*), \tag{1}$$

where ρ is the air density, R is the rotor radius, β^* and λ^* are the pitch angle and the tip-speed-ratio that maximize the power coefficient C_p, and $\eta \leq 1$ is an efficiency factor used to increase the tip-speed-ratio. Setting $\eta = 1$ the torque balance will ensure optimal tip-speed-ratio λ^* in steady state. However, due to turbulence and large rotor inertia, the controller actions is not quick enough to keep the tip-speed-ratio constant after a change in the wind speed. Variations in the tip-speed-ratio mean that, if λ and β are selected to maximize the power coefficient, the operating point will drop on one side of the $C_p(\lambda)$ curve creating a drop in power production. Moreover, if the tip-speed-ratio decreases for an increase in the wind speed while operating at the top of the C_p curve the flow on the blade will stall and the turbine may risk stall-induced vibrations. In the work by Johnson [5] he suggests to select η between 80% and 95% to increase the value of the tip-speed-ratio. This solution is a good guideline but it may not be the optimal for all wind turbines due to different wind conditions.

2.2. Constant speed, variable torque regions
When the wind turbine is operating at the minimum rotor speed (Ω_{min}) or rated Ω_R, the controller has to keep the rotational speed constant. In these regions, the regulation is performed with a PI controller on the generator torque while the blade pitch is kept constant. The reference torque is set as

$$Q_{ref} = k_p^Q(\Omega_f - \Omega_{set}) + k_i^Q \int_0^t (\Omega_f(\tau) - \Omega_{set})d\tau$$

where Ω_f is a low-pass second order filtered rotational speed, Ω_{set} is either the minimum rotor speed or the rated speed Ω_R, k_p^Q and k_i^Q are the proportional and the integral gains of the rotor speed error PI feedback.

2.3. Constant speed, constant power region
When the power reaches the rated value, the controller has to guarantee constant power and constant rotational speed. This regulation is obtained with a PI controller on the pitch angle

$$\beta_{ref} = k_{p,\Omega}^\beta \eta_k(\Omega_f - \Omega_R) + k_{p,P}^\beta \eta_k(P_{ref} - P_R) + \eta_k \int_0^t [k_{i,\Omega}^\beta(\Omega_f - \Omega_R) + k_{i,P}^\beta(P_{ref} - P_R)]d\tau$$

where β_{ref} is the reference pitch, $k_{p,\Omega}^\beta$ and $k_{i,\Omega}$ are the proportional and integral gains for the rotor speed error feedback, and η_k is a gain scheduling factor. In the pitch controller there are also a proportional and integral term depending on the error between the reference power and the rated power, P_{ref} and P_R. These terms are introduced to improve the transition between the different regions. The power reference is obtained multiplying the reference torque with the unfiltered rotor speed. The two integral terms share a saturated integrator ensuring minimum pitch in the variable speed region and a fast action when the power is increasing.

There are several techniques and methods to select the tuning parameters for PI controllers but they are based on simplified or linearized models and they do not take into account factors such as turbulence. This deficiency means that once the tuning is tested on a real machine or on an advanced model, it does not always show the desired behavior.

A possible strategy to tune the PI controllers is with a pole placement technique [1, 6, 7]. It may ensure that the frequency of the drivetrain rigid body mode is below the tower frequency to avoid a controller induced instability with the fore-aft tower mode, and sufficiently high to avoid large rotor speed variations. The main problems related with the pole placement approach for the constant rotational speed region are that this approach has the uncertainty to be based on a one degree of freedom model [7], and that the designer still have to identify the optimal position of the pole.

3. Optimization problem

The design variables for the given controller are the six gains of the PI controllers, the efficiency factor and the natural frequency and damping ratio of the second order low-pass filter on the measured generator speed.

Figure 1 shows a route diagram of the numerical optimization procedure. Simulations are performed with the multi-body aero-servo-elsastic code HAWC2 [8] according to the IEC standards [9] for a given set of controller parameters. When the simulations are terminated a post processing procedure extracts the equivalent fatigue loads, the ultimate loads and the power production performances. These values are used to compute a scalar cost function and evaluate the fulfillment of the constraints, which goes into the optimization routine that computes new design variables. A gradient based optimization algorithm implemented in the Matlab function

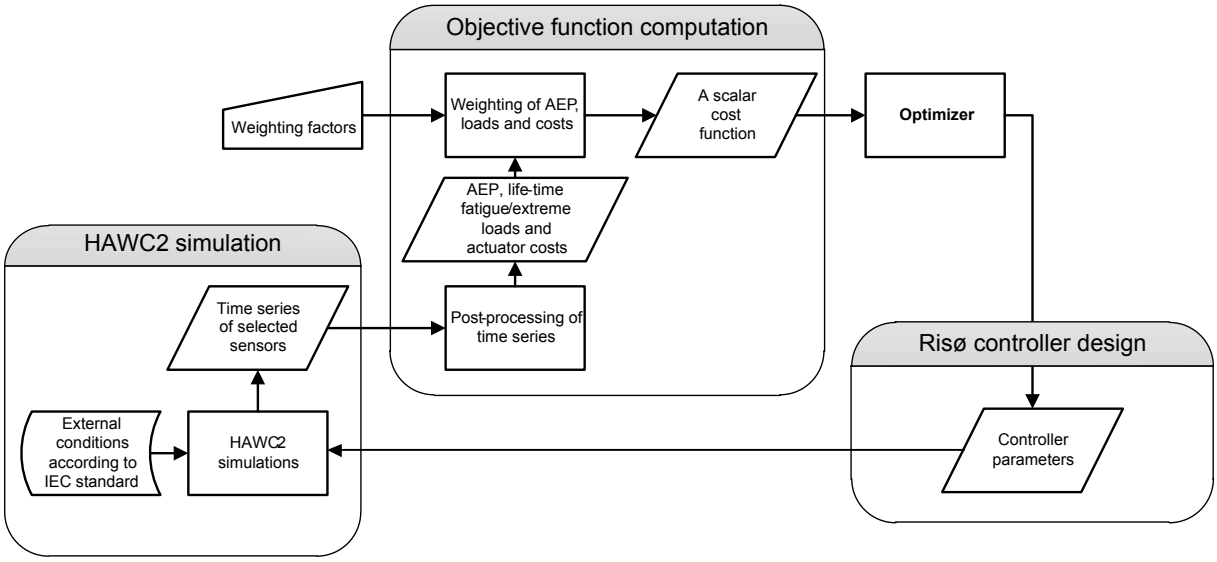

Figure 1. Route diagram of the numerical optimization procedure.

`fmincon` [10] has been used here. The procedure can be easily adapted to other algorithms and optimization platforms.

The cost function is based on loads l computed during simulations:

$$J = \sum_i w_i c_i(l) \tag{2}$$

were $c_i(l)$ are the costs of the wind turbine components and w_i are weights. The cost of the blade, the tower and the drivetrain are computed with an average between fatigue and ultimate loads divided by the annual energy production, while the cost of the pitch system (mechanism and bearings) is computed as the ratio between the normalized actuator duty cycle and the annual energy production.

$$c_i = \frac{1}{2}\frac{\hat{l}_{fatigue} + \hat{l}_{ultimate}}{\widehat{AEP}} \tag{3}$$

$$c_{pitch} = \frac{\widehat{ADC}}{\widehat{AEP}} \tag{4}$$

where $\hat{l}_{fatigue}$ is the normalized life-time damage equivalent load, $\hat{l}_{ultimate}$ is the normalized maximum load computed during the simulations, $\widehat{ADC}$ is the normalized actuator duty cycle and $\widehat{AEP}$ is the normalized annual energy production. The parameters $\hat{l}_{fatigue}$, $\hat{l}_{ultimate}$, $\widehat{ADC}$ and $\widehat{AEP}$ are normalized with respect to the corresponding value of a reference solution. The loads used for the tower and the blade are the resultant of the root section in-plane moments. The load used for the drivetrain is the torque on the shaft at the generator side. The ADC is defined as

$$ADC = \sum_j F(V_j)\frac{1}{T}\int_0^T \frac{\dot{\beta}(t, V_j)}{\dot{\beta}_{max}} dt \tag{5}$$

where $F(V_j)$ is the value of the life time Weibull probability function for the wind speed V_j, T is the length of a simulation, $\dot{\beta}$ is the pitch rate and $\dot{\beta}_{max}$ is the maximum allowable pitch

Table 1. Reference solution parameters value

Component	Fatigue	Ultimate
Blade root in-plane mom. res. [kNm]	7006.766	16108.847
Tower base in-plane mom. res. [kNm]	12464.805	73104.907
Shaft torque [kNm]	672.022	-
ADC [-]	0.042	
AEP [GWh]	10.566	

rate. The values of the loads obtained from the reference solution are shown in Table 1. The weights used in Equations (2) are shown in Table 2. These values are computed dividing an estimated cost of the component by an estimated cost of the wind turbine. The estimated costs are obtained using the method showed in [11].

To ensure tower-blade clearance and sufficient small variations of rotor speed to avoid emergency shutdowns in normal operations, two constraints are included. The first constrained parameter is the maximum blade tip deflection and the second is the maximum rotor speed. The constraints are defined in the optimization algorithm as inequality constraints:

$$m_i - m_{i,max} = \gamma_i \leq 0 \tag{6}$$

where m_i and $m_{i,max}$ are the normalized measured and the normalized maximum allowable value of the constrained parameter i and γ_i is the constraint feasibility. The parameters are normalized with respect to the reference solution. Table 3 shows the maximum allowable value of the two constraints.

The simulations used to compute the loads are in accordance with the DLC 1.2 [9]. Twelve different mean wind speeds are selected, and four different turbulent seeds are used for each of the mean wind speeds. To weight the effect of each wind speeds on the life time loads a Weibull distribution function is used.

All the results presented in the next sections are shown with respect to a reference solution for the 5MW NREL reference wind turbine. This solution is obtained tuning the controller with a classical approach. The controller parameters are

- Pitch angle and efficiency factor for the variable speed region: $\beta = 0°$ and $\eta = 1$;

Table 2. Cost function weights, w.

Component	c
Blade	0.311
Tower	0.122
Drivetrain	0.231
Pitching system	0.042

Table 3. Constraints.

Max tip deflection	5 m
Max rotor speed	$1.1\,\Omega_R$

- Proportional and integral gains of the pitch PI controller: $k^{\beta}_{p,\Omega} = 0.925\,\mathrm{rad/(rad/s)}$ and $k^{\beta}_{i,\Omega} = 0.207\,\mathrm{rad/rad}$ corresponding to a closed-loop pole of the rigid body drivetrain mode with frequency 0.05 Hz and damping 0.7;

- Proportional and integral gains of the torque PI controller: $k^{Q}_{p} = 2.022\,\mathrm{MNm/rpm}$ and $k^{Q}_{i} = 4.330$ MNm/rad corresponding to a closed-loop pole of the rigid body drivetrain mode with frequency 0.05 Hz and damping 0.7;

- Natural frequency and damping ratio of the second order low-pass filter on the measured generator speed: frequency 0.6 Hz and damping ratio 0.7. The free drivetrain frequency is about 1.65 Hz

4. Parametric analysis

The parametric analysis is performed to investigate how the tuning of the main controller parameters affects the behavior of the wind turbine. In the parametric analysis the four PI gains of the rotor speed error feedback, the efficiency factor of the torque controller and the natural frequency of the second order low pass filter are analyzed.

4.1. Proportional gain of the pitch PI controller

Figure 2 shows the variations of the normalized total cost and of the rotational speed constraint feasibility γ due to the proportional gain of the pitch controller. The total cost of the wind turbine decreases when the gain is decreased, while the maximum rotational speed increases. The damping of the drivetrain speed regulator mode is lower for reduced gains, hence the controller responds slower to the wind speed changes. A slower response leads to higher rotational speed variations and so to a higher maximum value. The solution becomes unfeasible ($\gamma > 1$) when the gain is 0.75 rad/(rad/s). In Figure 3, the costs variation of each wind turbine component are plotted for the same changes in the proportional gain. An aggressive pitch controller with high proportional gain leads to a higher pitch and tower cost. For faster control of the rotor speed the pitch action has to be higher leading to higher variations in the aerodynamic thrust and thereby larger tower oscillations. At low gain, the generator cost is higher because the torque has to counteract the large rotor speed variations to guarantee constant power.

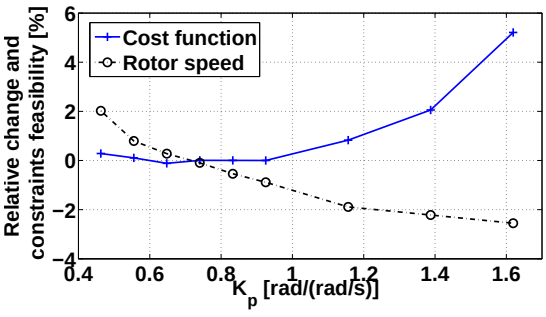

Figure 2. Variations of the normalized total cost and of the rotational speed constraint feasibility γ due to changes in the proportional gain of pitch controller.

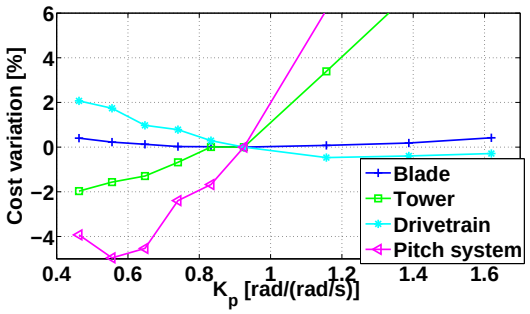

Figure 3. Variations of normalized component-cost due to changes in the proportional gain of pitch controller.

4.2. Integral gain of the pitch PI controller

Figure 4 shows the variations of the normalized total cost and of the rotational speed constraint feasibility due to the integral gain of the pitch controller. The total cost is not significantly affected by changes in the integral gain of the pitch controller, whereas the variations of the maximum rotational speed are more significant. As for the proportional gain, a low gain leads to larger rotor speed variations. A lower frequency of the drivetrain speed regulator mode is equivalent to a reduction in the stiffness that keeps the rotor speed at its set-point, hence the larger rotor speed variations. Figure 5 shows the cost of the components. Larger integral feedback leads to larger cost variation for the pitch actuator, whereas low gains leads to lower blade cost. The cost variation is clearly not convex, hence the gradient-based optimization may fail identifying the global minimum.

4.3. Proportional gain of the torque PI controller

Variations of the normalized total cost and of the rotational speed constraint feasibility due the proportional gain of torque controller are plotted in Figure 6. Again, the cost decreases when reducing the proportional gain. The maximum value of the rotational speed is not significantly affected because overspeeds occur at a higher wind speed, where the pitch is used for the regulation. Figure 7 shows the components cost variations. The blade and the tower are subject to lower loads when the torque controller is less aggressive. Even if the torque

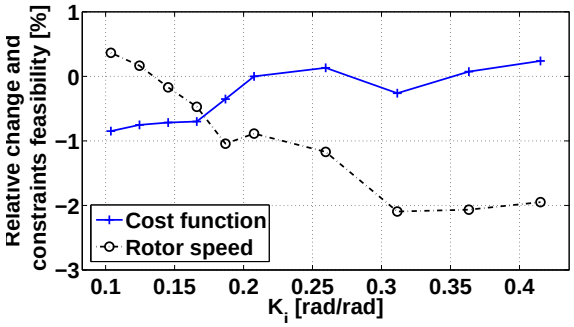

Figure 4. Variations of the normalized total cost and of the rotational speed constraint feasibility γ due to changes in the integral gain of pitch controller.

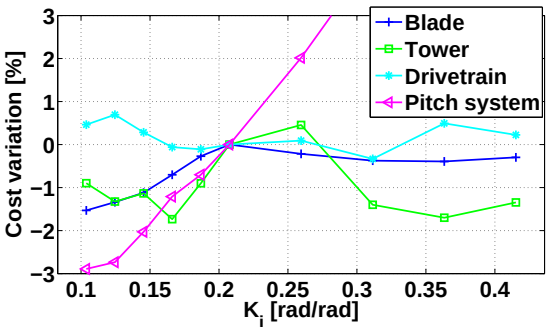

Figure 5. Variations of normalized component-cost due to changes in the integral gain of pitch controller.

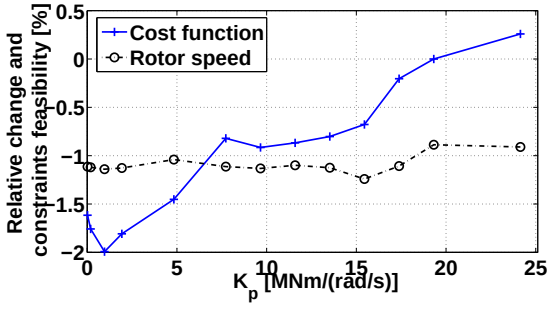

Figure 6. Variations of the normalized total cost and of the rotational speed constraint feasibility γ due to changes in the proportional gain of torque controller.

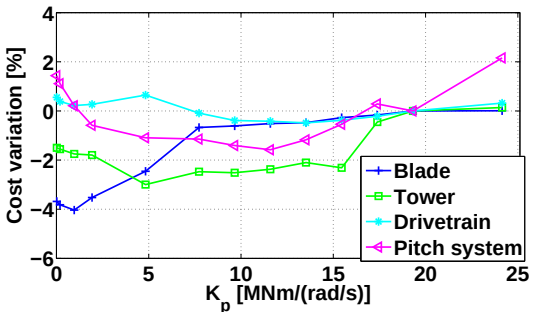

Figure 7. Variations of normalized component-cost due to changes in the proportional gain of torque controller.

controller is active in a small region, it significantly affects the cost function due to the wind speed probability distribution. Because the variable torque constant rotor speed region is small, in turbulent wind the loads might also depend on the switching conditions.

4.4. Integral gain of the torque PI controller

Figure 8 shows the total cost variation due to changes in the integral gain of the torque controller. The integral gain of the torque controller has a similar effect on the total cost as the proportional one. In Figure 9 the costs of the components are shown. When reducing the gain the tower cost decreases up to a value where it starts increasing again. The tower cost reduction is due to lower maximum loads, because a lower gain generates a slower controller and a less aggressive action after a switch between two regions.

4.5. Efficiency factor for torque controller

Figure 10 shows the variations of the total costs and of the constraint feasibility due to the efficiency factor η of the $k\Omega^2$ controller, whereas Figure 11 shows the components costs variation. The plots show that there is a significant cost reduction for low values of η. The total cost reduction is mainly driven by the tower and the blade costs. Reducing the value of η the mean value of the rotational speed increases. A higher rotational speed increases the gap between

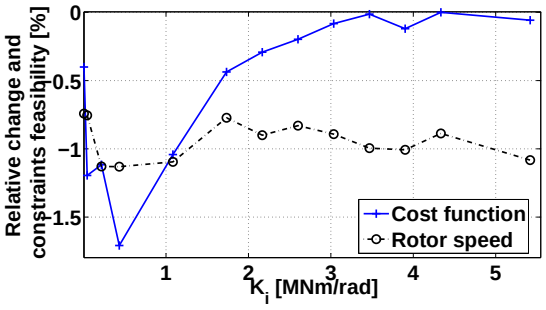

Figure 8. Variations of the normalized total cost and of the rotational speed constraint feasibility γ due to changes in the integral gain of torque controller.

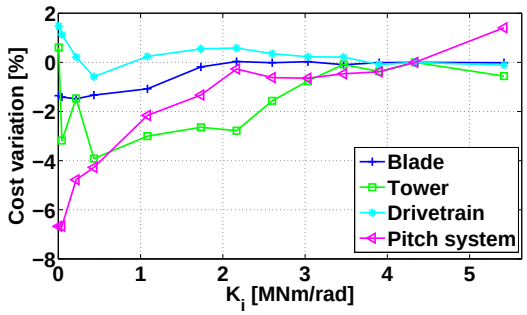

Figure 9. Variations of normalized component-cost due to changes in the integral gain of torque controller.

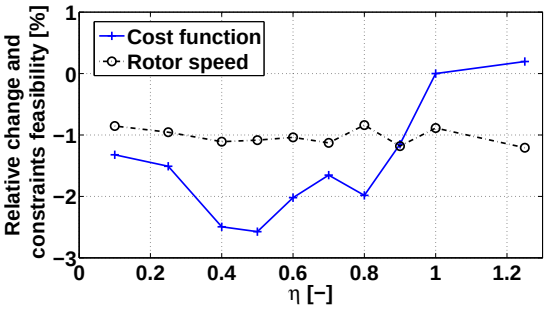

Figure 10. Variations of the normalized total cost and of the rotational speed constraint feasibility γ due to changes in the efficiency factor of the $k\Omega^2$ torque controller.

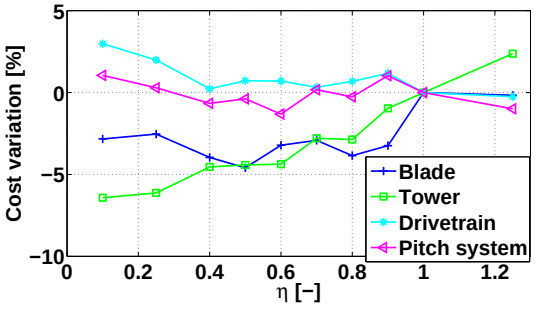

Figure 11. Variations of normalized component-cost due to changes in the efficiency factor of the $k\Omega^2$ torque controller

the 3P frequency and the tower first natural frequency reducing the tower vibrations, hence the fatigue loads. For example, an efficiency factor of 80% increases the distance between the 3P and the first tower natural frequency of 7%. For very low efficiency factors the cost increases due to the reduction in the annual energy production.

4.6. Rotational speed low-pass filter natural frequency

Figure 12 shows the variations of the normalized total cost and of the rotational speed constraint feasibility due to changes in the natural frequency of the second order low-pass filter on the measured generator speed. If the frequency is low the control action is too soft, hence the performances are lower. For too high filter frequencies the response of the low-damped free-free drive train mode is not sufficiently attenuated in the feed-back measurement, therefore the loads on the drive train and the pitch actuator are higher. In Figure 13 the components cost variations are shown. The plot shows that the components more influenced by the low-pass filter frequency are the drive train and the pitch system.

5. Automatic tuning

In this investigation only the four gains on the rotor speed feedback error are selected as optimization variables. The initial solution, required by the gradient based algorithm, is the reference solution described in Section 3. In Figure 14 the changes of the cost function in the first seven iterations are shown, where it is reduced by 2%. The cost reduction achieved with the optimization is close to the maximum reductions shown in the parametric analysis for the same parameters. This similarity in cost changes may mean that the optimization has stopped at a local minimum or that it is not possible to obtain a further reduction when optimizing with more variables at the same time. In Figure 14 also the changes in the feasibility of the constrains on the maximum tip deflection and the maximum rotational speed are plotted. The constraints are not significantly changed and they do not approach the feasibility limit. Only a small increase of the rotational speed constraint feasibility occurs, due to the reduction of integral gain of the pitch controller. Figure 15 shows the optimization variables variation with respect to the reference solution at the different iterations. During the optimization most of the parameters are reduced, in accordance with the results shown in the parametric analysis. Only the pitch proportional gain increases leading to a more aggressive controller in the full load region. The variable that has the largest variation is the integral gain of the torque controller. Indeed, from

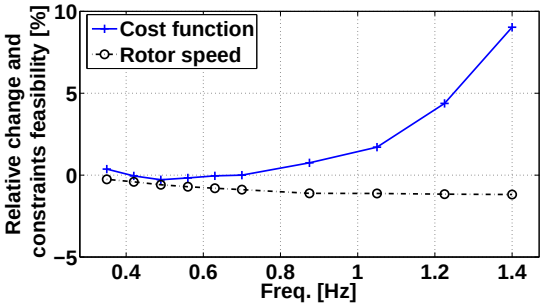

Figure 12. Variations of the normalized total cost and of the rotational speed constraint feasibility γ due to changes in the natural frequency of the second order low-pass filter on the measured generator speed.

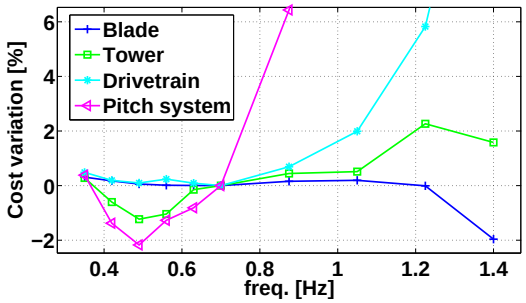

Figure 13. Variations of normalized component-cost due to changes in the natural frequency of the second order low-pass filter on the measured generator speed.

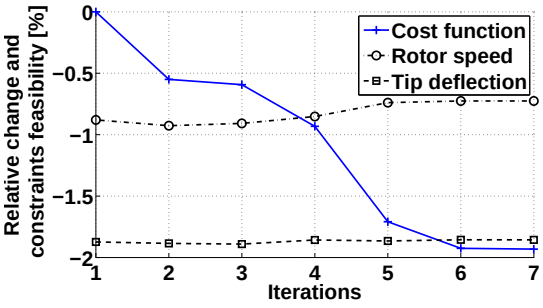

Figure 14. Automatic tuning: variations of the normalized total cost and of the rotational speed constraint feasibility γ.

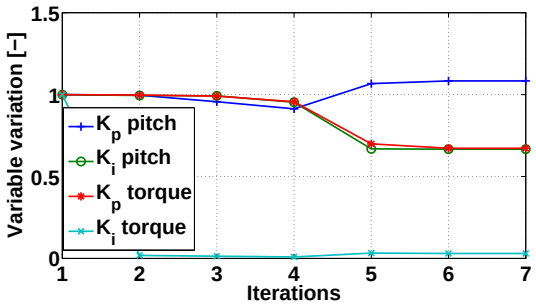

Figure 15. Automatic tuning: optimization variables variation with respect to the reference solution.

the parametric analysis, it was evident that the gains of the torque controller allow larger cost reductions compared to the gains for the pitch controller. As in the parametric analysis the component that drives the reduction of the integral gain of the torque controller is the tower. The lower integral gain generates a less sharp corner in the mean wind speed versus mean rotor speed curve, making the switch less aggressive and reducing the loads on the tower. The CPU time needed for this optimization is approximately of 4000 hours.

6. Conclusions

In this work a method to tune a wind turbine controller using a numerical optimization has been presented. A parametric analysis of the main controller parameter has shown how the tuning affects the performances and the cost of the wind turbine. This study has highlighted the complexity of the tuning process showing the contrasting behavior of some parameters on the loads. The results from the numerical optimization have shown that is possible to achieve a fine tuning that can improve the wind turbine performances leading to a lower cost of energy. In seven iterations the cost of the energy has been reduced by 2%. The cost reduction has been achieved reducing the gains of the torque controller and the integral gain of the pitch controller. The integral gain of the torque controller has been reduced to a few percent of its original value to smooth the transition between the constant speed constant power region and the constant speed variable torque region.

Further investigations should focus on repeating the numerical optimization changing the initial guess. This study should identify if the gradient based algorithm has found a local minimum and if the cost can be further reduced. Furthermore an analysis on the robustness of the solution obtained should be performed. The study should be on the dependency of the solution obtained on the wind conditions and on the wind turbine model. Future works may also focus on the improvement of the cost function and on the selection of a more suited optimization algorithm. A more realistic cost function could give more reliable and factual results while a more advanced algorithm, e.g. based on global optimization, could further improve the cost reduction identifying the global minimum.

References

[1] Hansen M H, Hansen A, Larsen T J, Øye S, Sørensen P and Fuglsang P 2005 Control design for a pitch-regulated, variable speed wind turbine. *Risø-R-1500(EN)*, Risø National Laboratory, Denmark

[2] Bottasso C L and Croce A 2009 Advanced control laws for varibale-speed wind turbines and supporting enabling techologies. *DIA-SR 09-01*, Dipartimento di Ingegneria Aerospaziale, Politecnico di Milano, Italy

[3] Jonkman J, Butterfield S, Musial W and Scott G 2009 Definition of a 5-MW reference wind turbine for offshore system development. *NREL/TP-500-38060*, National Renewable Energy Laboratory, USA

[4] Bossanyi E 2009 Controller for 5MW reference turbine. *GH report 11593/BR/04*
[5] Johnson K, Fingersh L, Balas M and Pao L 2004 Methods for increasing region 2 power capture on a variable speed wind turbine. *Journal of Solar Energy Engineering.* **126** 1092-1100
[6] Burton T, Sharpe D, Jenkins N and Bossanyi E 2001 *Wind Energy Handbook.* John Wiley And Sons Ltd chapter 8 pp 493-499
[7] Hansen M H 2011 Aeroelastic Optimization of MW Wind Turbines. *Risø-R-1803(EN)*, Risø National Laboratory, Denmark chapter 5 pp 35-54
[8] Larsen T J and Hansen A M 2007 How 2 HAWC2, the user's manual. *Risø-R-1597(EN)*, Risø National Laboratory, Denmark
[9] IEC/TC88 2005 IEC 61400-1 Ed.3: Wind turbines - Part 1: Design requirements. International Electrotechnical Commission
[10] MATLAB Version 7.13.0 2011 Natick, Massachusetts: The MathWorks Inc.
[11] Fingersh L, Hand M and Laxson A 2006 Wind turbine design cost and scaling model. *NREL/TP-500-40566*, National Renewable Energy Laboratory, USA

Article IV: Effects of Gain-scheduling Methods in a Classical Wind Turbine Controller on Wind Turbine Aeroservoelastic Modes and Loads

The article was presented at the *32nd ASME Wind Energy Symposium* during the *SciTech 2014* conference organized by the American Institute of Aeronautics and Astronautics in National Harbor, Maryland, USA, 13-17 January 2014.

Effects of gain-scheduling methods in a classical wind turbine controller on wind turbine aeroservoelastic modes and loads

Tibaldi C*, Henriksen LC, Hansen MH and Bak C
Department of Wind Energy, Technical University of Denmark

The effects of different gain-scheduling methods for a classical wind turbine controller, operating in full load region, on the wind turbine aeroservoelastic modes and loads are investigated in this work. The different techniques are derived looking at the physical problem to take into account the changes in the aerodynamic characteristics as a function of the wind speed. The modal analysis is performed with a high-order linear aeroservoelastic model computed with the frequency based stability tool HAWCStab2. The time series of the wind turbines loads are computed with the non-linear time domain tool HAWC2. Results show changes in the natural frequency and in the damping ratio of the speed regulator mode and of the tower longitudinal mode when using the different gain-scheduling schemes.

I. Introduction

In this paper a comparison of different gain-scheduling techniques for a classical Proportional Integral (PI) collective pitch wind turbine controller is performed. In the above-rated region, where the PI controller is active to set the blades pitch angle, the aerodynamic characteristics of wind turbines are subject to significant variations. These differences are due to the changing wind speed, mean blade pitch angle, and blade deformation. Hence, a gain-scheduling technique that can compensate and take into account for these changes is needed to obtain uniform performances of the speed regulator.

Gain-scheduling techniques have been presented by different authors. These approaches differ mainly on the variable used for the parametrization and on the methodology to compute the coefficients of the gain-scheduling function. Øye[1] presented a method to account for the different sensitivity of the aerodynamic torque to pitch angle variations occurring at different wind speeds. In the method suggested by Øye the gains are changed linearly with the pitch angle. The gains of the PI controller and the coefficients used for the gain-scheduling are derived with the pole placement of the rigid body drivetrain mode. This approach has also been used by Wright.[2] Bossanyi[3] also suggests a linear gain-scheduling with respect to the pitch angle. In his works he also states that, since the thrust sensitivity varies in a different way, a different parametrization may be required to ensure good performances at all wind speeds. A previous investigation by Hansen[4] has shown that the linear interpolation suggested by Øye does not guarantee the correct placement of the speed regulator mode for all the operational range. For high wind speeds the gain-scheduling method is not able to ensure the location of the pole and the value of the frequency increases for increasing wind speeds. Furthermore, the damping of the resultant regulator mode differs from the value set with the placement technique. Therefore, the need of a better gain-scheduling to guarantee a better location of the pole in all the operational range exists.

The purpose of this work is to characterize the performances of some gain-scheduling techniques. To achieve this a high-order linear aeroservoelastic model of a wind turbine is used to perform closed-loop modal analysis. The analysis is performed to take into account the possible coupling between the controller and the structure as shown in previous works.[4,5] In this investigation the method suggested by Øye[1] is considered as a baseline. This method is then extended as suggested by Hansen[4] with a quadratic parametrization of the derivative of the aerodynamic torque with respect to the pitch angle. Finally, a modified gain-scheduling

*tlbl@dtu.dk

is introduced to compensate the changes in the derivative of the aerodynamic torque with respect to the rotational rotor speed. The performances of the gain-scheduling techniques are evaluated by looking at the frequency and damping of the speed regulator mode and at relevant wind turbines loads. The investigation is performed using HAWCStab2[8,9,10] to generate a high-order linear aeroservoelastic model of the wind turbine and to perform the closed-loop modal analysis. HAWC2[6] is exploited to validate with a non-linear multi-body aeroservoelastic model the results obtained with HAWCStab2 and to identify how loads and performances are affected. The 5 MW NREL reference turbine[7] is used in the investigation. The new gain-scheduling method shows an improvement in the positioning of the speed regulator mode, especially at high wind speeds. The frequency of the mode decreases getting closer to the intended value. Hence, higher rotor speed excursions and lower tower loads occur at high wind speeds compared to the traditional approach.

This paper is structured as follows. In the first part of this investigation three gain-scheduling are derived based on the same simplified model. The methods are then used with a single degree of freedom wind turbine model to evaluate the position of the speed regulator mode. Rotor speed responses to wind steps of the single degree of freedom linear model are compared with those obtained with HAWC2 with a fully stiff turbine. The gain-scheduling methods are then compared closing the loop with a high-order model. The analysis is performed comparing frequencies and damping of the different aeroservoelastic wind turbine modes. A comparison with HAWC2 is also performed with this model. Finally, the gain-scheduling are compared looking at their influence on some wind turbine loads.

II. Linear aeroservoelastic wind turbine model

The linearized model, used for the investigation is obtained with the in-house developed tool HAWCStab2. HAWCStab2 is an improved version of HAWCStab [8] and it includes a different kinematics. The model is based on an analytical linearization of a non-linear finite beam element model coupled with an unsteady blade element momentum model of the blade aerodynamic. The aerodynamic model includes shed vorticity and dynamic stall. The model does not include dynamic inflow and assumes frozen wake. A detailed description of the model is provided by Hansen.[9] An extensive validation and analysis of the open-loop performances of the tool are provided by Sønderby and Hansen.[10] The controller used to close the loop is a simplified linearization of the controller described by Hansen and Henriksen.[11] The controller included in HAWCStab2 regards only the above-rated region. In this region the primary controller objectives are to maintain constant rotational speed and constant power or torque. The linearized controller includes the PI pitch controller, a second-order filter of the rotor speed feedback and a first-order filter of the measured pitch angle. The filtered pitch angle is required by the gain-scheduling. The linearized controller is described in detail by Hansen.[4] The closed-loop high fidelity model used for the investigation is composed by 834 dynamic states, 336 aerodynamic and 498 structural.

III. Controller tuning and gain-scheduling techniques

In this section the method to perform the controller tuning is shown and the different gain-scheduling schemes are introduced.

The tuning of the proportional and integral gains (k_P and k_I) of the PI controller is based on pole placement of the rigid body drivetrain mode introduced by Øye.[1] The method assumes rigid turbine, quasi-steady aerodynamics, no rotor speed filters, and no pitch actuators. Under these assumptions the open-loop system can be described with a single degree of freedom second-order system

$$I\dot{\Omega} = Q(V, \Omega, \theta) - Q_g(\Omega) \tag{1}$$

where $\dot{\Omega}$ is the first time derivative of the rotational speed, I is the total drivetrain inertia including rotor, shaft, gearbox and generator, Q_g is the controlled generator torque that for the given control law depends on the rotor speed, and Q is the aerodynamic torque that depends on the wind speed V, the rotor speed, and the pitch angle θ. After linearizing Eq. (1) around the operational steady states, the second-order system can be written as

$$I\ddot{\phi} + \Big(\frac{\partial Q_g}{\partial \Omega} - \frac{\partial Q}{\partial \Omega}\Big)\dot{\phi} - \frac{\partial Q}{\partial \theta}\delta\theta = 0 \tag{2}$$

where $\dot{\phi}$ is the rotor speed variation relative to the rated rotor speed $\dot{\phi} = \Omega - \Omega_R$, $\delta\theta$ is the pitch angle variation, $\frac{\partial Q_g}{\partial \Omega}$ is the partial derivative of the generator torque with respect to the rotor speed and $\frac{\partial Q}{\partial \Omega}$ and

$\frac{\partial Q}{\partial \theta}$ are the partial derivatives of the aerodynamic torque with respect to the rotor speed and the pitch angle respectively. The last two terms, $\frac{\partial Q}{\partial \Omega}$ and $\frac{\partial Q}{\partial \theta}$, can also be referred to as aerodynamic damping and aerodynamic gain respectively. The dependency on the wind speed of the aerodynamic damping has been neglected since the focus is on the homogeneous system to perform eigenvalue analysis. The linearized equations of the PI pitch controller are

$$\delta\theta = k_P\dot{\phi} + k_I\phi \tag{3}$$

where ϕ is the integral of the of the rotor speed variation $\dot{\phi}$. If the controller is included in the system the resulting closed-loop equation is

$$I\ddot{\phi} + \Big(\frac{\partial Q_g}{\partial \Omega} - \frac{\partial Q}{\partial \Omega} - k_P\frac{\partial Q}{\partial \theta}\Big)\dot{\phi} - k_I\frac{\partial Q}{\partial \theta}\phi = 0. \tag{4}$$

The pole placement is performed imposing the natural frequency ω_Ω and damping ratio ξ_Ω to the second-order system in Eq. (4).

$$\omega_\Omega^2 = -\frac{k_I}{I}\frac{\partial Q}{\partial \theta} \qquad\qquad \xi_\Omega = -\frac{\frac{\partial Q_g}{\partial \Omega} - \frac{\partial Q}{\partial \Omega} - k_P\frac{\partial Q}{\partial \theta}}{2k_I\frac{\partial Q}{\partial \theta}} \tag{5}$$

The two equations in Eq. (5) can be solved for the two PI gains

$$k_P = -\frac{2\xi_\Omega\omega_\Omega I - \frac{\partial Q_g}{\partial \Omega} + \frac{\partial Q}{\partial \Omega}}{\frac{\partial Q}{\partial \theta}} \qquad\qquad k_I = -\frac{\omega_\Omega^2 I}{\frac{\partial Q}{\partial \theta}} \tag{6}$$

The gains obtained with this approach depend only on the frequency and damping of the speed regulator mode, the drivetrain inertia, the derivative of the generator torque with respect to the rotational speed, and the gradient of the aerodynamic torque. The frequency and the damping ratio of the speed regulator mode are usually selected to be lower than the first longitudinal tower mode frequency to avoid resonance conditions but high enough to avoid large rotor speed excursions. The derivative of the generator torque with respect to the rotational speed depends whether the wind turbine is regulated for constant torque ($\frac{\partial Q_g}{\partial \Omega} = 0$) or constant power ($\frac{\partial Q_g}{\partial \Omega} = \frac{P_r}{\Omega^2}$ where P_r is the rated power). In this work constant torque is selected, therefore $\frac{\partial Q_g}{\partial \Omega}$ is set to zero. The rotor inertia, for a fixed rotor, depends only on the changes in rotor diameter due to steady static blade deformations. For the 5 MW NREL reference turbine the maximum variation of the inertia is 0.1 %. For this reason the drivetrain inertia can be approximated as constant. Both the aerodynamic gain and the aerodynamic damping depend on the operational conditions, hence the necessity to have a gain-scheduling scheme.

In this work the aerodynamic gains and damping are approximated with a polynomial approximation as functions of the pitch angle Θ. The value of the pitch angle used for the gain-scheduling is obtain filtering with a first-order filter the measured pitch angle. In this investigation the time constant of the first-order filter is set to a high value to neglect its dynamic. If a quadratic fit is selected, the approximations are

$$\frac{\partial Q}{\partial \theta} \approx \frac{\partial Q}{\partial \theta}\Big|_0\Big(1 + \frac{\Theta}{K_1} + \frac{\Theta^2}{K_2}\Big) = \frac{\partial Q}{\partial \theta}\Big|_0\frac{1}{\eta_K} \qquad \frac{\partial Q}{\partial \Omega} \approx \frac{\partial Q}{\partial \Omega}\Big|_0\Big(1 + \frac{\Theta}{K_{1,\Omega}} + \frac{\Theta^2}{K_{2,\Omega}}\Big) = \frac{\partial Q}{\partial \Omega}\Big|_0\eta_{K,\Omega} \tag{7}$$

where the parameters K_1, K_2, $K_{1,\Omega}$ and $K_{2,\Omega}$ can be computed from fitting of quasi-steady calculations. In this investigation the polynomials are fitted to the gradient computed with HAWCStab2 using a least-squares method. In the work by Øye[1] and Hansen[9] the influence of the aerodynamic damping is neglected for the tuning while the aerodynamic gain is approximated with a linear and quadratic fit respectively. Figures 1 and 2 on the following page show the aerodynamic gain and the aerodynamic damping. Values computed with HAWCStab2 and a linear and quadratic polynomial fitting are plotted. The figures show how the fitting is improved when using a quadratic approximation compared to the linear.

Substituting the approximations in Eq. (7) into the gains in Eq. (6) the gains can be written as

$$k_P = k_{P,0}\eta_K + k_{P,0,\Omega}\eta_K\eta_{K,\Omega} \qquad\qquad k_I = k_{I,0}\eta_K \tag{8}$$

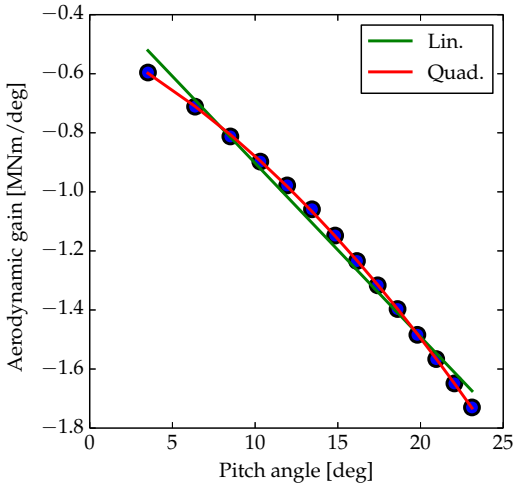

Figure 1. Partial derivative of the aerodynamic torque with respect to the pitch angle $\frac{\partial Q}{\partial \theta}$. Circles: HAWCStab2 computations. Curves: linear and quadratic least-squares fit.

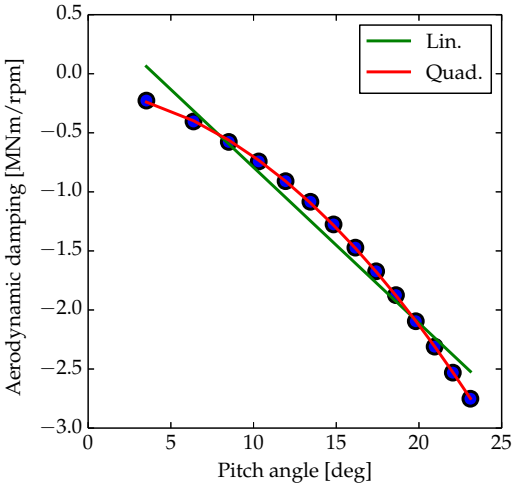

Figure 2. Partial derivative of the aerodynamic torque with respect to the rotor speed $\frac{\partial Q}{\partial \Omega}$. Circles: HAWCStab2 computations. Curves: linear and quadratic least-squares fit.

where

$$k_{P,0} = -\frac{2\xi_\Omega \omega_\Omega I - \dfrac{\partial Q_g}{\partial \Omega}}{\left.\dfrac{\partial Q}{\partial \theta}\right|_0}, \quad k_{P,0,\Omega} = -\frac{\left.\dfrac{\partial Q}{\partial \Omega}\right|_0}{\left.\dfrac{\partial Q}{\partial \theta}\right|_0} \quad and \quad k_{I,0} = -\frac{\omega_\Omega^2 I}{\dfrac{\partial Q}{\partial \theta}} \tag{9}$$

Depending on whether a linear or quadratic polynomial approximation is selected and whether the aerodynamic damping is neglected, different gain-scheduling solutions can be obtained.

A. PI gains

In this work three different gain-scheduling schemes are compared:

- **Lin.** assumes a linear variation of the aerodynamic gain and no aerodynamic damping,
- **Quad.** assumes a quadratic variation of the aerodynamic gain and no aerodynamic damping,
- **Quad.+Damp** assumes a quadratic variation of the aerodynamic gain and damping.

Due to the different gain-scheduling the PI gains will differ from each other at each wind speed. Figure 3 on the next page shows the proportional and integral gains computed with the different gain-scheduling methods. A natural frequency $f_{n,\Omega}$ of 0.1 Hz and damping ratio ξ_Ω of 0.7 are assigned to the rotor speed regulator mode. A reference value is also shown where no gain-scheduling is used but the gains are computed using for each operational point the actual values of the gradient computed with HAWCStab2. This comparison allows evaluating how the different approaches perform compared to ideal reference values. Using a quadratic instead of a linear approximation for the aerodynamic gain does not significantly affect the controller gains. The larger difference is noticed at low pitch angles, at the beginning of the above-rated region. Here the linear fitting leads to higher proportional and integral gains compared to the reference values and those obtained with a quadratic fitting. Neglecting the aerodynamic damping only affects the proportional gain, as seen in Eq. (8). The differences can be noticed for increasing pitch angles. Without the aerodynamic damping the proportional gain results to be even more than twice the reference value. This first comparison shows that the linear approximation of the aerodynamic gain has poor agreement for low pitch angles with the reference values. Neglecting the aerodynamic damping $\frac{\partial Q}{\partial \Omega}$ penalizes the gains at higher wind speeds. The proportional gain is the most affected by the choice of gain-scheduling, consequently different performances are expected especially for the damping of the regulated mode.

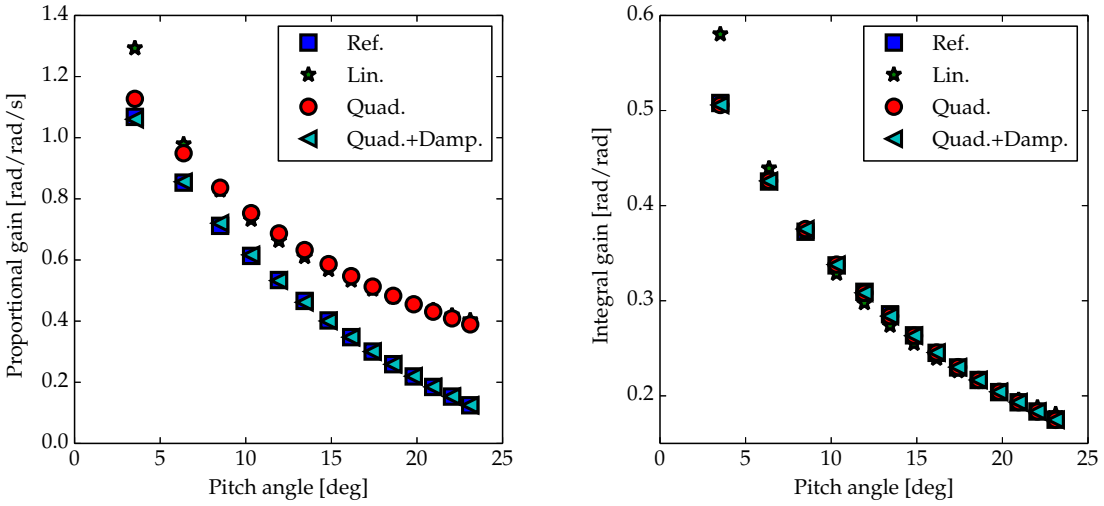

a) Proportional gain. *b) Integral gain.*

Figure 3. Comparison of the proportional and integral gains computed with the different gain-scheduling methods. The reference gains are obtained without gain-scheduling and using the actual values of the gradient of the aerodynamic torque.

IV. Results

In this section results from the closed-loop analysis are shown. First the investigation is carried out on a single degree of freedom model and then on a high-order model.

A. Single degree of freedom

In this section the three gain-scheduling methods are compared closing the loop with a single degree of freedom model of a wind turbine. The model used is the same as the one used for the tuning, hence the pole placement depends only on the gain-scheduling and it is not affected by the influence of other modes. Figure 4 on the following page shows the natural frequency and the damping ratio of the rotor speed regulator mode. The results obtained with the three gain-scheduling methods are compared with those obtained with the reference gains. The reference gains place the regulator mode exactly where it is desired to, $f_n = 0.1\,\mathrm{Hz}$ and $\xi = 0.7$. Even when using a single degree of freedom model significant differences can be noticed between the results obtained with the different techniques. If a quadratic fitting of the aerodynamic gain is selected an improvement in the frequency location can be noticed, Figure 4 on the next page *a)*. The linear fitting generates a frequency that is almost 7 % higher than the reference one at low pitch angles. With the quadratic fitting of the aerodynamic gain the natural frequency has a maximum discrepancy compare to the reference value of less than 0.5 %. Different results appear for the damping ratio in Figure 4 *b)*. If the aerodynamic damping is neglected in the gain-scheduling the damping ratio of the regulator mode differs from the placed value. The mode damping increases with the pitch angle and becomes over-damped for a pitch angle of 17 deg. When including the aerodynamic damping the resultant damping ratio is almost overlapped to the reference value. Figure 5 on the following page shows the trajectory of the regulator mode poles as function of the wind speed when a linear fitting of the aerodynamic gain is used and no aerodynamic damping is considered for the gain-scheduling. At low wind speeds the poles are complex-conjugate, hence the mode is undamped. When the wind speed increases the poles approach the real axis. Between 20 m/s and 21 m/s the poles become real and therefore the mode becomes over-damped. The distance between the poles keeps increasing for increasing wind speed leading to a further increase in the damping of the mode.

1. Comparison of the linear and non-linear model

The results obtained with the single degree of freedom model are here compared with HAWC2 simulations. The comparison is performed looking at the time response of the rotational speed to a step in the wind

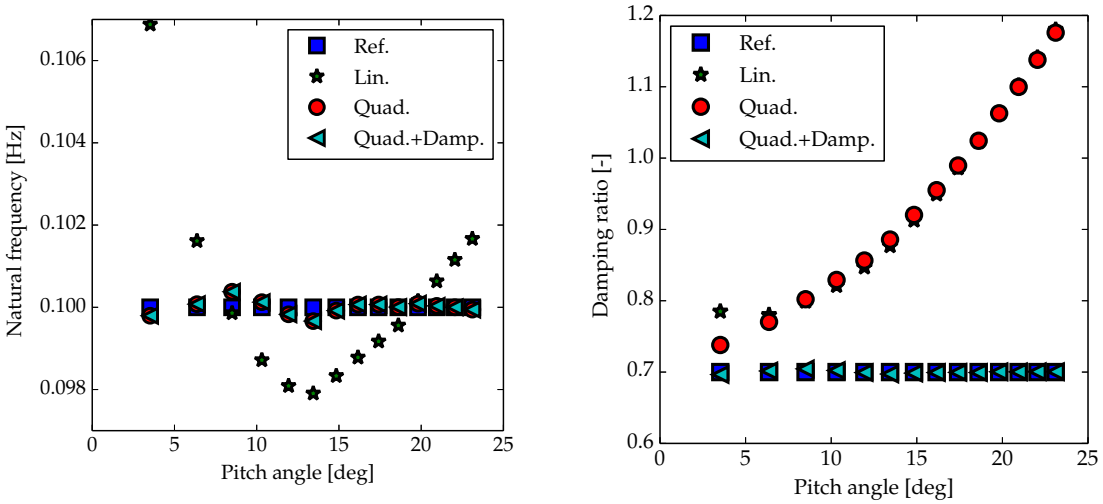

a) Natural frequency. *b) Damping ratio.*

Figure 4. Natural frequency and the damping ratio of the rotor speed regulator mode using a single degree of freedom model of the wind turbine.

speed. The comparison aims at identifying if the two different codes agree on the location of the regulator mode. Here the aim is not to investigate the limit of the linear approximation with respect to the non-linear model. To have the same model assumptions as in the linear model, the structure in the HAWC2 model is made stiff and the dynamic stall model is disabled. Here the linear model is obtained with HAWCStab2. The wind speed step is of 0.5 m/s. For the HAWC2 simulations the wind step reaches the declared wind speed, e.g. the wind step at 15 m/s goes from 14.5 to 15 m/s. For the HAWCStab2 responses the linear model at the final wind speed is used. In Figure 6 on the next page the rotor speed variation due to a wind speed step is compared between HAWC2 and HAWCStab2 at 15, 20, and 25 m/s. The gain-scheduling *Lin.* and *Quad.+Damp.* are shown. The time response of the two models appears to be of good agreement. The maximum amplitude of the overspeed, the time at which the maximum overspeed occurs and the time the system needs to reach the steady state give an indication that the two models agree on the values of the regulator mode frequency and damping. When using the gain-scheduling *Lin.* the system appears to be slower at regaining the steady state speed for increasing wind speed, indicating an increase of the damping.

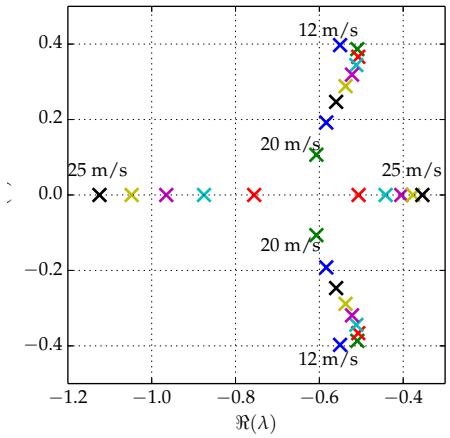

Figure 5. Trajectory of the pole associated with the speed regulator mode for increasing wind speed. Poles obtained with a linear fitting of the aerodynamic gain and without aerodynamic damping (*Lin.*).

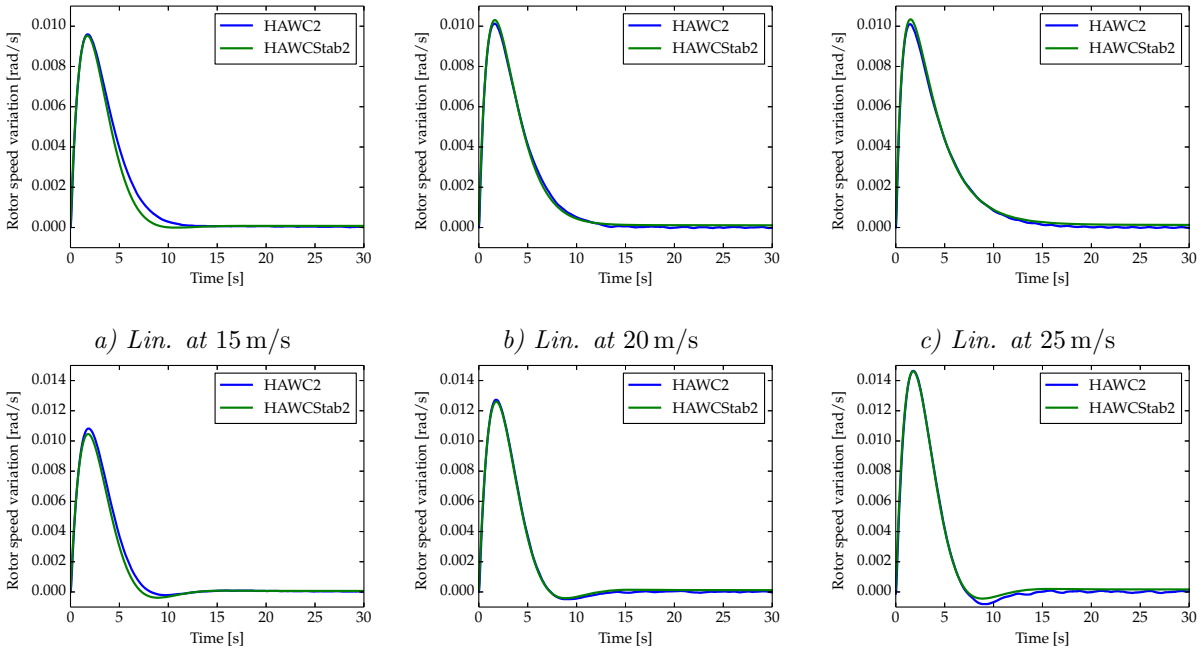

Figure 6. Rotor speed variation due to a wind speed step. Comparison between HAWC2 and HAWCStab2 at 15, 20 and 25 m/s. Linear and quadratic gain-scheduling with additional damping term. Rigid wind turbine and steady aerodynamic.

On the other hand when using the *Quad.+Damp.* gain-scheduling, the rotor speed has similar response at the different wind speeds. The overspeed value is different because the sensitivity of the aerodynamic torque to a wind speed variation changes with the wind speeds. The shape of the response is simply scaled by a factor indicating similar frequency and damping of the regulated mode.

B. High-order model

In this section the performances of the gain-scheduling methods are compared closing the loop with a high-order model. The model is obtained with HAWCStab2. The model includes a fully flexible turbine, unsteady aerodynamics and a second-order filter of the rotor speed for the PI controller (natural frequency of 0.6 Hz and damping ratio of 0.7). The controller tuning is performed to assign to the regulated pole a frequency of 0.1 Hz and a damping ratio of 0.7, Figure 3 on page 5. Figure 7 on the next page shows the damped natural frequency and the damping ratio of the rotor speed regulator mode for the high-order model. It appears immediately that all the three approaches fail at placing the pole where it is asked with the tuning. The damped natural frequency results at higher values while the damping at lowers. When using only the aerodynamic gain in the gain-scheduling (*Lin.* and *Quad.*) the natural frequency grows linearly with the wind speed. The addition of the aerodynamic damping, *Quad.+Damp.* improves the location of the pole reducing the dependency on the wind speed and reducing the minimum value. The opposite happens for the damping. The *Lin.* and *Quad.* approaches have a lower damping in the whole wind speed range compared to the more complex method. The *Quad.+Damp.* approach seems more capable at pulling up, closer to the reference value, the damping for increasing wind speeds. For the full model the situation is critical at the beginning of the operational region. Here indeed the damping ratio drops considerably approaching 0 % instead of the desired 70 %. The more detailed gain-scheduling approach *Quad.+Damp.* is able to increase the damping compared to the simple one *Lin.* but, still, the value of the damping is significant lower than the desired one. At low wind speeds the scheme *Quad.* achieves the same performances of the more complex method *Quad.+Damp.*. The reason of this poor performance of all the approaches is partially due to the presence of the second-order rotor speed filter. Figure 8 on the following page shows the effect of the second-order filter on the damped frequency and the damping ratio of the rotor speed regulator mode. When

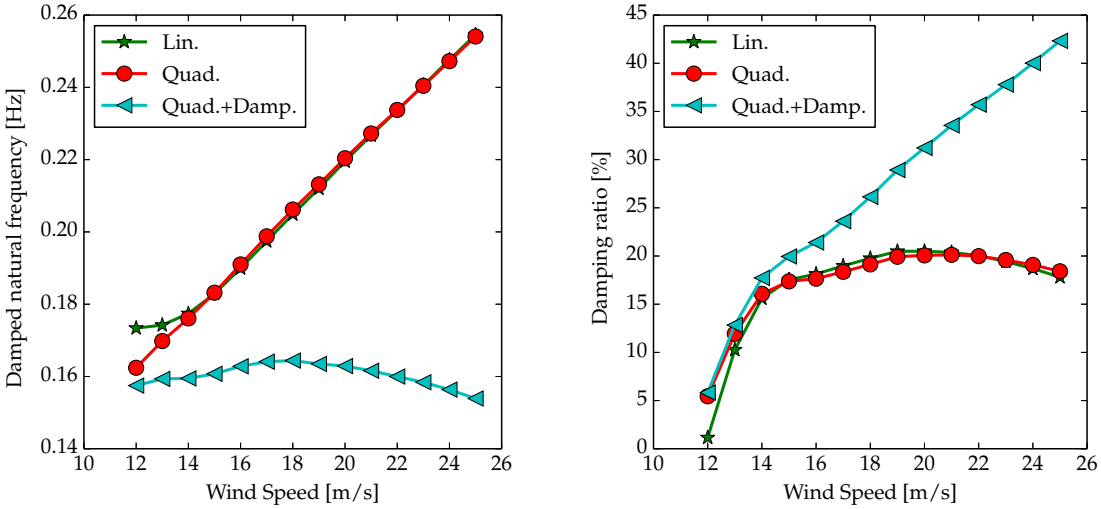

a) Damped natural frequency. *b) Damping ratio.*

Figure 7. Damped natural frequency and damping ratio of the rotor speed regulator mode using a high-order model of the wind turbine. Comparison of the three gain-scheduling schemes.

removing the filter the damped natural frequency of the regulator mode decreases in all the range except at 12 m/s. The maximum difference occurs in the central part of the operational region when a reduction of approximately 6 % occurs. The damping ratio shows significant differences when removing the filter. The minimum value goes from approximately 5 % to 30 %. Since it is not possible to remove the rotor speed filter for real application, because the drivetrain mode would be excited by the pitch action, a significant care must be taken when deciding its cut-off frequency.

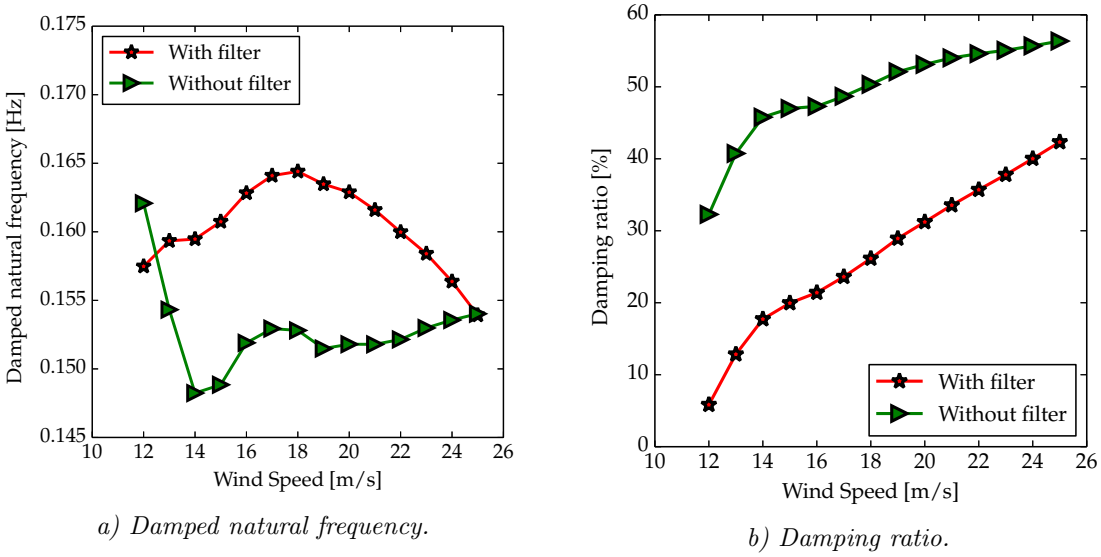

a) Damped natural frequency. *b) Damping ratio.*

Figure 8. Damped natural frequency and the damping ratio of the rotor speed regulator mode using a high-order model of the wind turbine. Comparison of the influence of the second-order rotor speed filter when using the gain-scheduling that includes the aerodynamic damping *Quad.+Damp.*.

1. Comparison of the linear and non-linear model

In this section the systems obtained with the high-order linearized model are compared with results computed with a non-linear model obtained with HAWC2. Figure 9 shows the comparison between HAWCStab2 and HAWC2 results of the rotor speed response to a wind speed step. The wind speeds are 15, 20, and 25 m/s. Only the *Lin.* and *Quad.+Lin.* gain-scheduling methods are compared. The comparison shows a similar behavior in both models. In the time responses it is possible to identify three different modes that are excited by the wind speed steps the regulator mode, the drivetrain mode, and the first lateral tower mode. The regulator mode is the dominant one. The drivetrain mode can be noticed close to the maximum overspeed as a high frequency variation. The first lateral tower mode can be noticed once the regulator mode oscillations are damped out. The frequency and the damping of the regulator mode are in a satisfactory agreement between the two models. For both gain-scheduling methods the damping increases for increasing wind speed, as shown in the previous section.

2. Effects on the wind turbine aeroservoelastic modes

Figure 10 on the following page shows the effect of the gain-scheduling method on the closed-loop aeroservoelastic wind turbine modes. The only modal damped natural frequency that is affected is the first longitudinal tower mode. When using the *Quad.+Damp.* method the frequency of the first longitudinal tower mode decreases for increasing wind speeds. At 25 m/s the first longitudinal tower frequency is almost coinciding with the first lateral tower mode. When looking at the first modes it also appears that when the aerodynamic gain is neglected, the speed regulator damped frequency increases with the wind speed and it approaches the first tower modes. This reduction in the frequency gap could be a problem when the tower has a lower frequency or when a more aggressive speed regulation (i.e. higher natural frequency of the speed regulator mode) is required. In these cases the two modes might coincide and high loads due to tower excitation could occur. Hence, taking into account also the aerodynamic damping in the gain-scheduling reduces the risk of running into tower excitation problems. Figure 11 on the next page shows the effect of the gain-scheduling

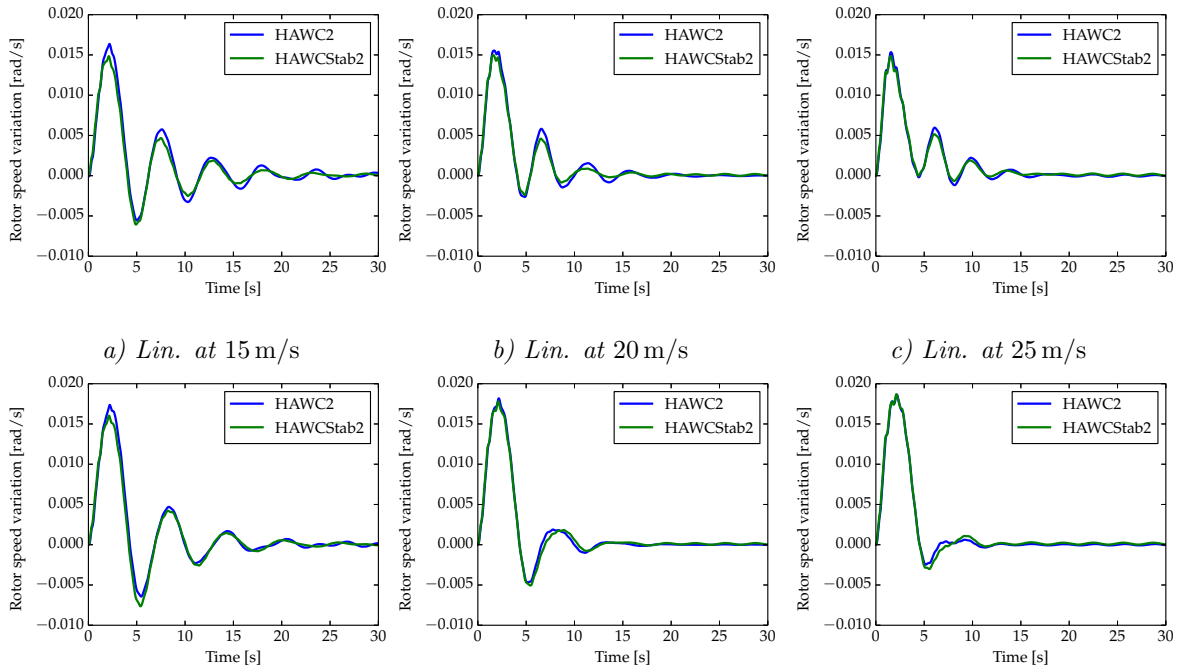

Figure 9. Rotor speed response to a wind speed step. Comparison between HAWC2 and HAWCStab2 at 15, 20 and 25 m/s. Linear and quadratic gain-scheduling with additional damping term. Fully flexible wind turbine and unsteady aerodynamic

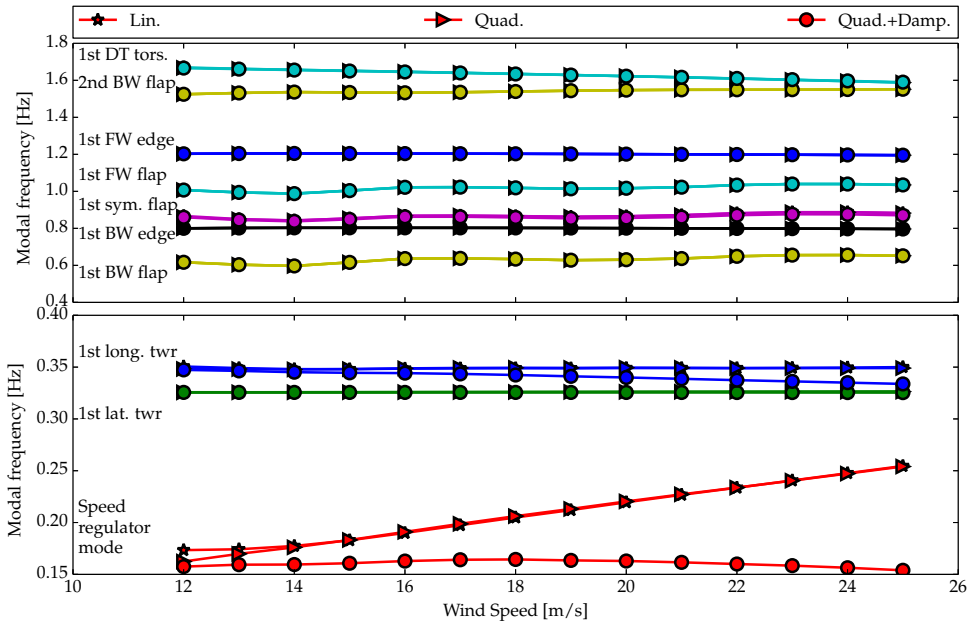

Figure 10. Closed loop aeroservoelastic damped natural frequencies of the first 10 turbine modes. Comparison between the gain-scheduling methods.

methods on the damping ratio of the first ten closed-loop aeroservoelastic wind turbine modes. Other than the speed regulator mode the first longitudinal tower mode appears to be affected by the different gain-scheduling schemes. As for the frequency, when using the method *Quad.+Damp.* the damping decreases with increasing wind speed, going from 15 % to 10 %. The first drivetrain mode is also affected. At low wind speeds the damping ratio is slightly higher when using *Quad.+Damp.* compared to *Lin.*. This increase can

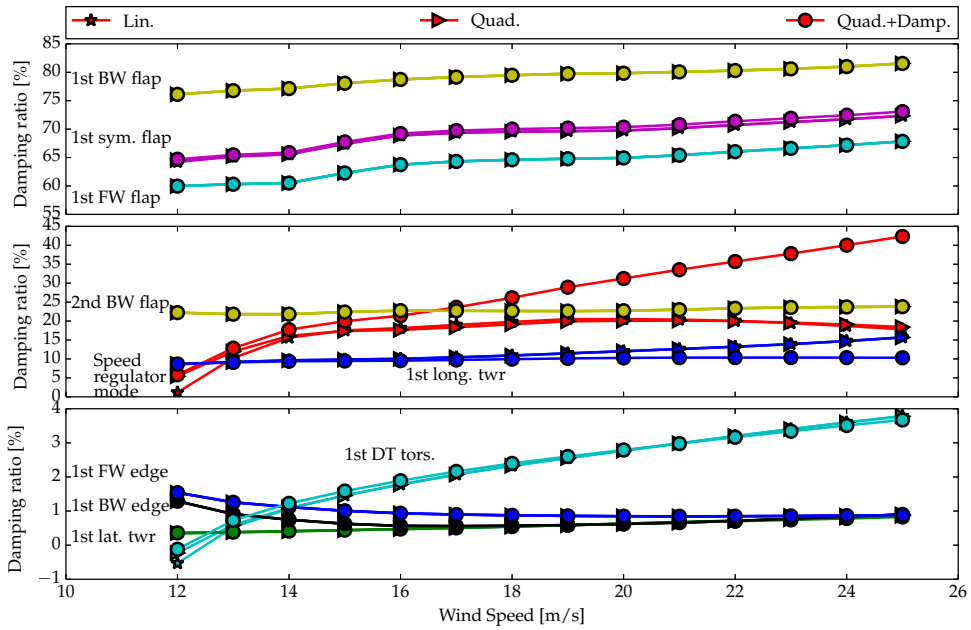

Figure 11. Closed loop aeroservoelastic damping ratios of the first 10 wind turbine modes. Comparison between the gain-scheduling methods.

be important since the mode is low damped close to the switching between the operational regions. In the case under evaluation the mode even results negatively damped. None of the other first ten wind turbine modes seems to be noticeably affected by the choice of the gain-scheduling method.

C. Effects on the loads

In this section the gain-scheduling schemes are compared looking at their effects on wind turbine loads. The loads are computed with turbulent wind simulations performed with HAWC2. Three different wind speeds are analyzed 12, 15, and 25 m/s. The turbulence intensity at each wind speed is set according to the wind turbine class II-B.[12] Figure 12 shows the variation with respect to the *Lin.* scheme of the standard deviation of the rotor speed and tower base longitudinal bending moment. The rotational speed has a higher standard deviation for both methods (*Quad.* and *Quad.+Damp.*) at all the wind speeds. The reason for this increase is due to the different location of the regulator mode. Since a lower frequency of the regulator mode means that the controller action is less aggressive, higher rotor speed variations are expected. The *Quad.* method has a lower frequency compared to *Lin.* at low wind speeds, see Figure 10 on the previous page, and that justifies the 5 % increases in the rotor speed standard deviation seen in Figure 12 *a)*. For higher wind speeds the difference in the frequency is minimal and therefore no significant variation in the standard deviation is present. With the *Quad.+Damp.* scheme the regulator frequency is always lower compared to the method *Lin.* and the gap increases with the wind speed. Hence, the increasing standard deviation for increasing wind speed when using the *Quad.+Damp.* method. A controller with a lower regulator frequency is more likely to generate less loads on the tower since less thrust variations are present and there is less tower excitation due to the higher gap between the controller frequency and the tower frequency. The lower load can be seen in Figure 12 *b)* where the standard deviation of the tower base longitudinal moment decreases when using the *Quad.+Damp.* scheme compared to the *Lin.* and *Quad.*.

V. Conclusions

A comparison of different gain-scheduling schemes for a pitch regulated wind turbine PI controller has been performed. A new gain-scheduling has been derived and introduced. The new approach also takes into account the dependency of the aerodynamic torque on the rotational speed. When using a high-order linear model the placement of the regulator mode is modified by the other wind turbine modes. The damping of the regulator decreases and it gets close to negative values at to the beginning of the above-rated region. The regulator mode frequency is shifted at higher values compared to the designated one. The new gain-scheduling improves the placement of the regulator pole guaranteeing an almost constant mode frequency and a higher damping compared to the traditional methods. The lower regulator frequency leads to a less

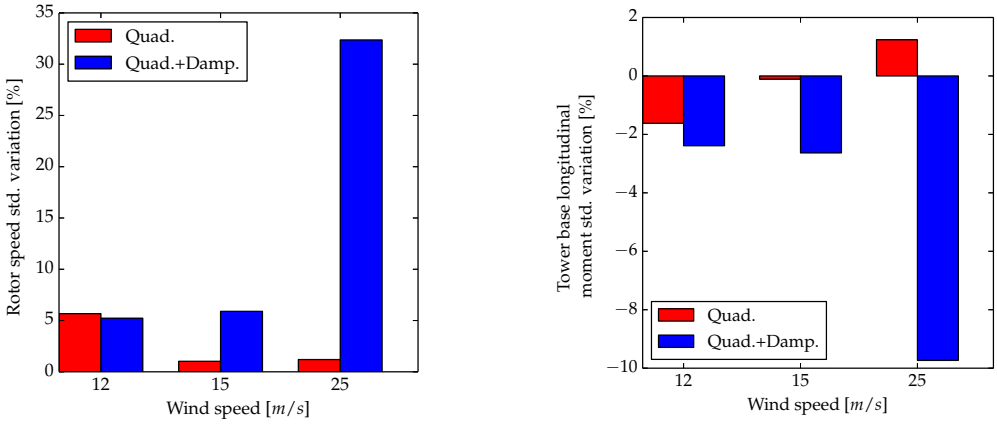

a) Rotor speed *b) Tower base long. moment*

Figure 12. Percentage increase with respect to the *Lin.* case of the standard deviation of the rotor speed and tower base longitudinal bending moment.

aggressive rotor speed regulation and hence to higher rotor speed variations. On the other hand it appears that the standard deviation of the loads at the tower base is reduced.

References

[1]Hansen, M. H., Hansen, A., Larsen, T. J., Øye, S., Sørensen, P., and Fuglsang, P., "Control design for a pitch-regulated, variable speed wind turbine," Tech. Rep. Risø-R-1500(EN), Risø National Laboratory, Roskilde, Denmark, 2005.

[2]Wright, A. D. and Fingersh, L. J., "Advanced Control Design for Wind Turbines; Part I: Control Design, Implementation, and Initial Tests." Research Report TP-500-42437, NREL, 2008.

[3]Bossanyi, E. A., "The Design of closed loop controllers for wind turbines," *Wind Energy*, Vol. 3, No. 3, 2000, pp. 149–163.

[4]Hansen, M. H., "Aeroelastic Optimization of MW Wind Turbines," Tech. Rep. Risø-R-1803(EN), Risø National Laboratory, Denmark, 2011.

[5]Riziotis, V. A., Politis, E. S., Voutsinas, S. G., and Chaviaropoulos, P. K., "Stability analysis of pitch-regulated, variable-speed wind turbines in closed loop operation using a linear eigenvalue approach," *Wind Energy*, Vol. 11, No. 5, 2008, pp. 517–535.

[6]Larsen, T. J. and Hansen, M. A., "How 2 HAWC2, the user's manual," Tech. Rep. Risø-R-1597(ver. 3-1)(EN), Risø National Laboratory, Denmark, 2007.

[7]Jonkman, J., Butterfield, S., Musial, W., and Scott, G., "Definition of a 5-MW Reference Wind Turbine for Offshore System Development," Tech. Rep. NREL/TP-500-38060, NREL/NWTC, 2009.

[8]Hansen, M. H., "Aeroelastic stability analysis of wind turbines using an eigenvalue approach," *Wind Energy*, Vol. 7, No. 2, 2004, pp. 133–143.

[9]Hansen, M. H., "Aeroelastic Properties of Backward Swept Blades," American Institute of Aeronautics and Astronautics, Orlando, Florida, 2011, p. 119.

[10]Sønderby, I. and Hansen, M. H., "Open-loop frequency response analysis of a wind turbine using a high-order linear aeroelastic model," *Wind Energy*, 2013, pp. n/an/a.

[11]Hansen, M. H. and Henriksen, L. C., "Basic DTU Wind Energy controller," Tech. Rep. E-0028, DTU Wind Energy, 2013.

[12]IEC/TC88, *IEC 61400-1 Ed.3: Wind turbines - Part 1: Design requirements*, 2005.

Article V: Investigation of the Dependency of Wind Turbine Loads on the Simulation Time

The article was presented at the *European Wind Energy Association* conference in Barcelona, Spain, 10-13 March 2014.

Investigation of the dependency of wind turbine loads on the simulation time

C Tibaldi*, L C Henriksen* and C Bak*
tlbl@dtu.dk

* DTU Wind Energy,DK-4000 Roskilde, Denmark

Abstract

In this work the dependency of several wind turbine parameters with respect to the length of simulations used for their evaluation is investigated. The analysis is performed by computing the parameters with a different number of turbulent wind simulations, therefore simulation time, and repeating the computation with different turbulence realizations. The repetition of the computation is performed to identify the scatter of the parameters for a given number of turbulent seeds due to the different turbulence realization. The dependency on the simulation time of load variations due to changes in the collective pitch controller tuning is also investigated. Results show a significantly high dependency of the parameters and their variations on the turbulent wind realization. This dependency makes the use of turbulent wind simulation results not reliable for numerical optimization purposes.

1 Introduction

To improve the design of wind turbines holistic numerical optimization has become a useful tool [1–3]. An optimization procedure allows taking into account different design variables and constraints in an automated process, avoiding more time consuming manual iterations. An important problem related with numerical optimization is the selection of a cost function. The cost function should be representative of the model physics and should capture the effects of design variables changes on the system. Depending on the objective of the design the cost function can be different and its formulation can vary from very simple to complex. When wind turbine design is performed, several parameters have to be investigated to evaluate the goodness of the solution, e.g. annual energy production, maximum loads and fatigue loads. If several parameters need to be evaluated and to be included in the cost function, the selection of the cost model can become non-trivial and complex. When a detailed cost model is missing or the optimization is based on a model without enough detail to give the required informations, the cost of energy can be converted into changes of loads and performances computed during simulations. Using this approach the parameters have to be linked together, e.g. with constant weights, to obtain a scalar cost function. Alternatively a multi-objective Pareto front optimization can be performed. When the cost model is a function of parameters computed from a set of simulations, the design obtained is restricted to the specific case analyzed. Hence, it is required to investigate if the solution obtained is also valid for life time conditions. To improve the reliability of this approach it is necessary to understand how the loads computed in simulations and used in the cost function are representative of the wind turbine life time loads and within which limits the designer can rely on the obtained results. To obtain a reliable design a sufficiently large set of wind conditions must be taken into account to consider all the possible scenarios. When turbulent wind simulations are used to compute the loads, parameters might require different simulation time before settling to a value. Hence a cost function, based on these parameters, might be more or less sensitive to the number of turbulent wind conditions included in the computation. If the turbulent wind time series are fixed during the optimization procedure and they are not generated for every cost function evaluation the stochastic effect of the wind is reduced. Using the same wind boxes fixes a specific wind condition, but any change in the design would lead to a different wind turbine response and therefore to a different wind seen by the structure.

In this work we want to investigate the dependency of several wind turbine parameters with respect to the length of the turbulent wind simulations used for their evaluation. The increase in simulation time is obtained increasing the number of turbulent seeds used for the load evaluation. The dependency of the parameters is also investigated looking at their variation with respect to changes in the collective pitch proportional integral (PI) controller tuning.

This paper is divided as follows. First the methods used for the analysis are explained. In a following section the results of the parameters dependency and the parameters variations dependency on the simulation time are shown. The paper ends with some considerations and conclusions.

2 Method

All the analysis showed in this work is based on sets of multibody aeroservoelastic simulations performed with the code HAWC2 [4]. The simulations are performed for normal turbulent conditions with a turbulence intensity selected according to the standard [5] for a class B. The wind turbine selected for the investigation is the NREL reference 5 MW wind turbine [6]. The controller used to regulate the wind turbine is described in [7].

2.1 Dependency of parameters

The parameters analyzed in this investigation are the damage equivalent load (DEL), the standard deviation (STD), the mean value (MN), and the maximum value (MAX). These parameters are evaluated in different location of the wind turbine in order to have a description of the different components. The loads are the bending moments at the blade root (flapwise, edgewise and resultant), at the tower base (longitudinal, lateral and resultant), and at the end of the shaft on the generator side (torsional). All the loads, except the ones depending on maximum values, depend on the mean wind speed. Hence, to obtain a single parameter, they are weighted with a Weibull probability function to obtain the lifetime expected value.

A set of 2100 simulations is initially generated (100 turbulent seeds for 21 mean wind speeds each) for normal operation of power production. The simulations are then combined and post processed to obtain the parameters analyzed. The simulations that are post-processed together to lead to a single parameter are divided in sets with increasing number of turbulent seeds. The number of turbulent seeds goes from 1 to 20. Each set with a fixed number of turbulent seed is repeated 5 times, changing the wind speed realization. This division leads to 100 different simulation sets. For each of the 100 sets, 21 mean wind speeds, from 5 m/s to 25 m/s, are used for each turbulent seeds. Hence, the five sets that are composed by one turbulent seed include 21 simulations, while the five sets with 20 turbulent seeds are composed of 420 simulations (21 mean wind speeds times 20 different turbulent seeds). Figure 1 shows a visualization of how the simulations are combined into the sets. In the graph the 100 sets are shown on the coordinate axis, while on the ordinate axis all the simulations at one mean wind speed are represented. Each of the 100 sets is post processed independently to compute the performances and the parameters at the different wind turbine locations.

All the parameters shown in the investigation are normalized with respect to the same parameter computed with 21 mean wind speeds and 100 turbulent seeds

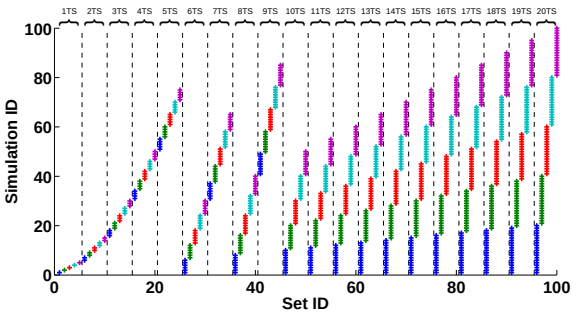

Figure 1: Visualization of sets used for the postprocessing.

2.2 Dependency of parameter variations

The parameters analyzed in this investigations are the damage equivalent load (DEL) and the standard deviation (STD) of the blade root flapwise bending moment and of the tower base longitudinal bending moment. Also the standard deviation of the rotational speed is investigated.

The analysis of parameter variations is performed only at the wind speed of 15 m/s. Two sets of simulations are generated.The two sets are formed by 100 simulations with 100 different turbulence realizations. The two sets differs on the type of gain scheduling used [8]. A linear gain scheduling is used for the first controller setting while a quadratic, that includes both aerodynamic gain and aerodynamic damping, is used for the second. The different gain-scheduling schemes lead to a difference in the regulator mode frequency and damping. One controller has a lower regulator mode frequency. The difference in the regulator mode frequency is about 12 %. Since one controller has lower frequency, this controller leads to a less aggressive regulation, hence higher rotational speed variations and lower tower base bending moments. Two analysis of these sets are performed. First the variation of the parameters is evaluated using only one wind realization for both the controller settings. This investigation shows how the loads are sensitive to the wind turbulence even when using the same wind realization. Secondly the variation is evaluated while increasing the number of turbulence seeds used for the evaluation of the parameters. With this analysis it is expected to evaluate how many turbulence seeds are required in order to get a parameter variation that is consistent and independent of the set of simulations considered.

3 Results

3.1 Dependency of parameters

In this section the dependency of the parameters is analyzed with respect to the increasing number of turbulent seeds used for their evaluation.

Figure 2 shows the mean power and the DEL of the blade root flapwise bending moment computed from all the simulations. It appears clearly how the parameters at the same mean wind speed are scattered due to the different turbulence seeds. Each turbulent box leads to a different load value and the scatter at the same mean wind speed can be significant.

Figure 3 shows how blade root DELs and STD change when increasing the number of turbulent seeds. The standard deviation of the 5 samples for each number of turbulent seed is shown in Figure 3 b. The scatter of the samples decreases faster within the first five seeds. The standard deviation of the parameters in the edgewise component after five seeds is not significantly reduced. In the flapwise direction a reduction of the scatter is still present after ten seeds but at a non monotonic and slower rate. The DELs seem to have lower scatter compared to the STD.

Figure 4 shows how the MAX load and the MN load at the tower base are affected by the number of turbulence seeds. As expected the MAX value, since it is a non linear function and does not depend on integrals, shows a large spread of the samples for the three loads. This scatter in the data shows clearly

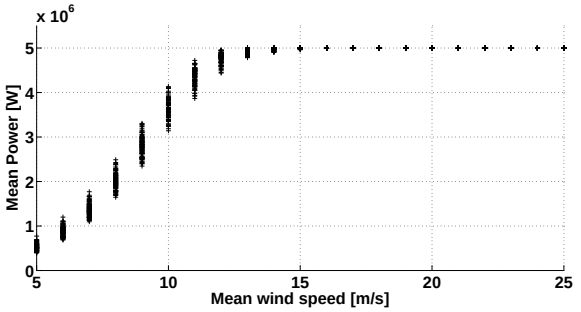

a) Mean power.

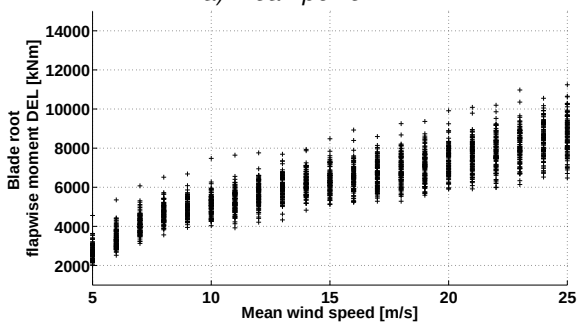

b) Blade root flapwise moment DEL.

Figure 2: Example of scatter of loads computed for 100 different turbulent seeds for each mean wind speed.

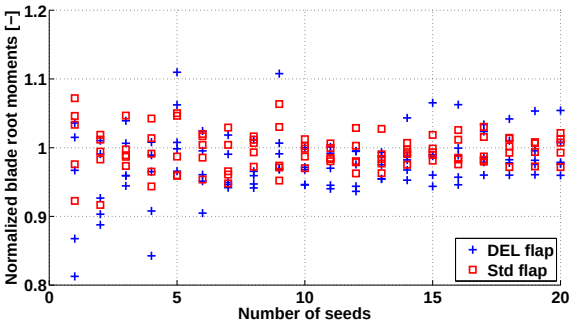

a) Samples.

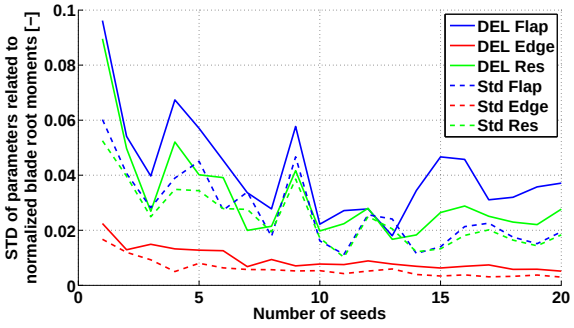

b) Standard deviation.

Figure 3: Dependency of blade DELs and standard deviations on the number of turbulent seeds. Samples and their standard deviations.

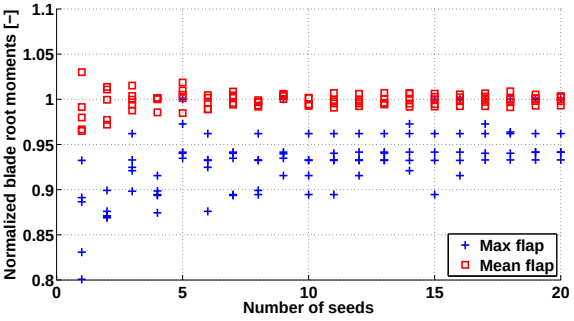

a) Samples.

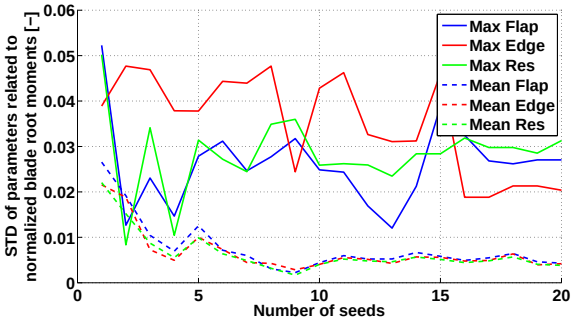

b) Standard deviation.

Figure 4: Dependency of blade DELs and standard deviations on the number of turbulent seeds. Samples and their standard deviations.

that to identify the maximum value of a load, with a good fidelity level, a very large number of simulations is needed. The MN value samples have a lower standard deviation. The scatter of the MN value samples does not change significantly after ten turbulent seeds.

Figure 5 shows the dependency of the resultant of the bending moments at the tower base. The standard deviation, Figure 5 b, of all parameters but the maximum value decreases for an increasing number of turbulent seeds. The scatter of the DEL is lower than the one of the STD for most of the cases, but the STD seem to decrease constantly while the DEL, after five turbulent seeds, seems not to reduce the scatter any longer.

Figure 6 shows the dependency of the shaft torque. The accuracy of the DEL samples appear to be higher on the shaft compared to the other components. Already with five turbulent seeds the standard deviation is lower than 1%. Also in this case the standard deviation of the STD decreases more slowly and less smoothly compared to the DEL. Also in this case it is necessary to include many simulations in the computation of the loads to capture the maximum value.

These results show the sensitivity of wind turbine parameters on the length of the simulation used to evaluate them. Even with a very high number of turbulent seeds the dependency can be considerably high.

3.2 Dependency of parameters variation

In this section the dependency of the variation of wind turbines parameters is evaluated. First the variations are compared using one seed at the time and looking at their dependency on the wind realization. After the dependency on the number of turbulent seeds is evaluated.

Figure 7 shows the variation of the blade root flapwise bending moment DEL and STD (a), of the tower base longitudinal bending moment DEL and STD (b), and of the rotor rotational speed standard deviation (c). The loads variations are shown for each of the 100 turbulent seed at a wind speed of 15 m/s. From the figure it appears that a large scatter of the variations is present. The different turbulent wind leads to load variations that differs significantly from each other. For both blade and tower loads and both DEL and STD, positive and negative values are present. The blade loads variations range between $\pm 11\,\%$ while tower loads between $-14\,\%$ and $5\,\%$. This behavior means that when changing a parameter the evaluation of its effect on the loads can be hidden and dominated by the wind realization. For the tower load an overall reduction can be noticed but the scatter has the same range as the mean value of the

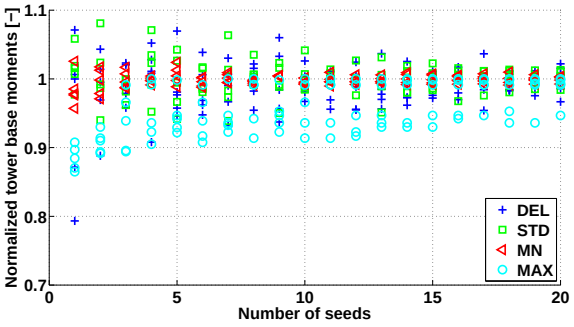

a) Samples.

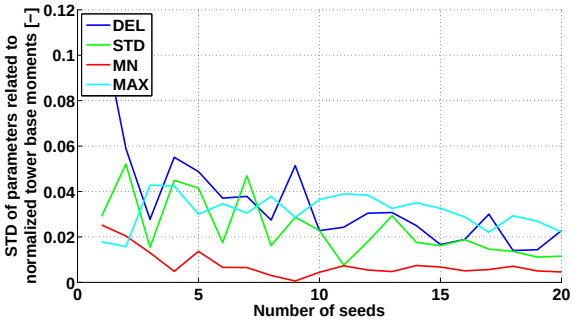

b) Standard deviation.

Figure 5: Dependency of tower DELs, standard deviations, mean and maximum values on the number of turbulent seeds. Samples and their standard deviations.

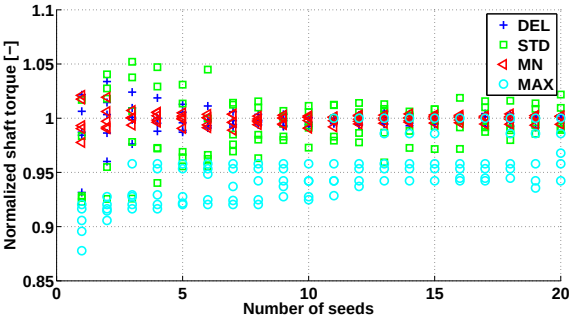

a) Samples.

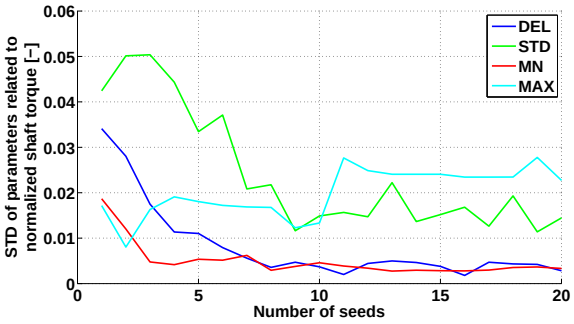

b) Standard deviation.

Figure 6: Dependency of shaft torque DELs, standard deviations, mean and maximum values on the number of turbulent seeds. Samples and their standard deviations.

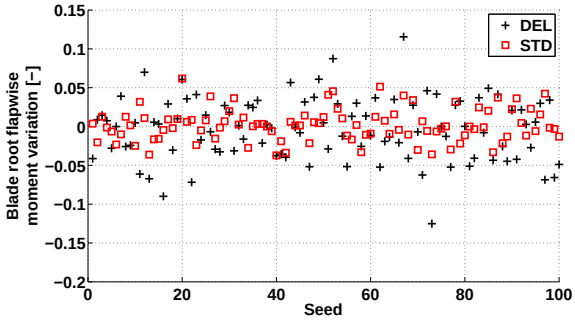

a) Blade root flapwise bending moment.

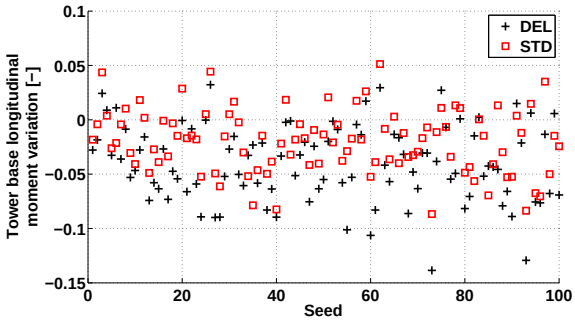

b) Tower base longitudinal bending moment.

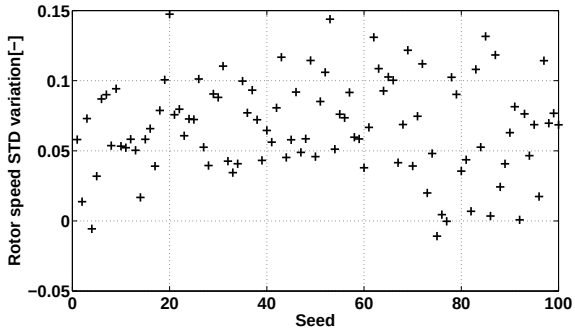

c) Rotor speed standard deviations.

Figure 7: Dependency of DELs and standard deviations variations on the turbulent seed. Wind speed of 15 m/s.

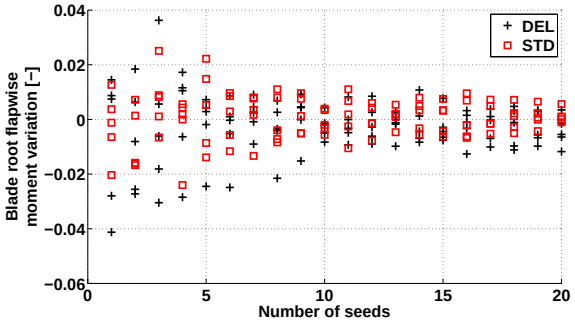

a) Values.

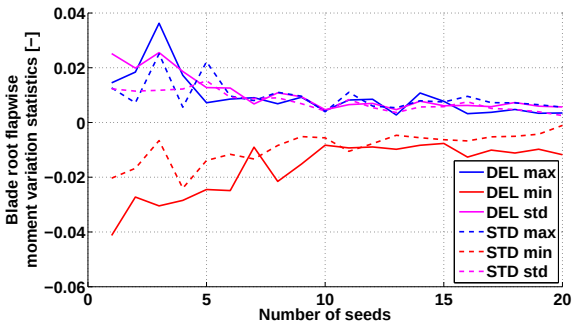

b) Statistics.

Figure 8: Dependency of blade root flapwise bending moment DELs and standard deviations variations on the number of turbulent seed. Wind speed of 15 m/s.

samples. The rotor speed standard deviation variation appears to be mostly increasing, only few wind realization lead to a negative value. An estimation of the effect of one wind turbine parameter on the rotor speed standard deviation is completely dominated by the turbulent wind effects. These results show that when evaluating loads variations with only one turbulent seed the results obtained are dominated by the turbulent wind load variations effects.

Figure 8 shows the dependency of blade root flapwise bending moment DEL and STD variations on the number of turbulence seeds used for their evaluation. The figure shows both values and statistics of the variations. Increasing the number of turbulent seeds a reduction in the scatter of the variations appears. The range of the samples decreases but non monotonically. The blade flapwise moment standard deviation variation scatter is lower compared to the one associated with the DEL, especially when using few turbulent seeds. Even with 20 turbulent seeds the scatter appears to be too large for numerical applications where a numerical gradient evaluation is required.

In Figure 9 the dependency of the tower base longitudinal bending moment DEL and STD is shown. Also in this case the values and the statistics are shown. At the tower base the variation becomes always negative when using 2 or more turbulent seeds. Despite the consistency in the load reduction the variations ranges of 2 % even when using 20 turbulent seeds. The scatter of the values is of the same amplitude as the mean value of the variations, especially for the standard deviation.

Figure 10 shows the dependency of the rotor speed standard deviation variation on the number of turbulent seeds. Values and statistics are shown. The rotational speed standard deviation variation has a scatter of almost 2 % even when using 20 turbulent seeds. These variations are always consistently positive if using more than one turbulent seed. Again the variations do not converge monotonically towards a value but oscillations are presents when increasing the length of the simulation.

From this analysis it appears that the variation of the parameter analyzed due to a change in the controller settings is differently affected by the turbulent wind realization. If the parameter is not very sensitive to the controller settings a scatter around zero

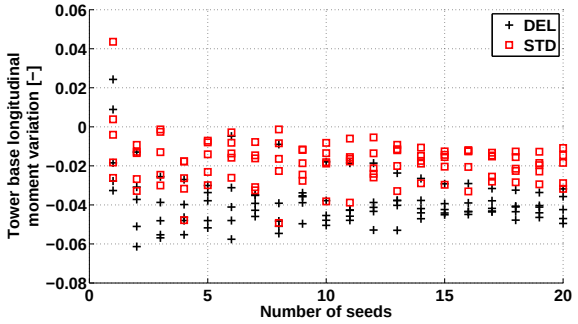

a) Values.

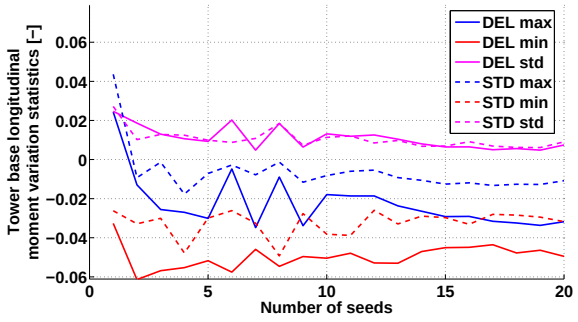

b) Statistics.

Figure 9: Dependency of tower base longitudinal bending momen DELs and standard deviations variations on the number of turbulent seed. Wind speed of 15 m/s.

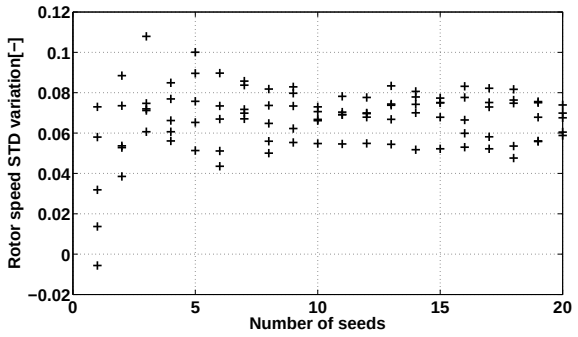

a) Values.

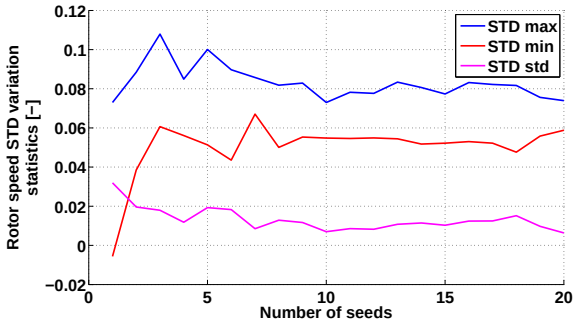

b) Statistics.

Figure 10: Dependency of rotor speed standard deviations variations on the number of turbulent seed. Wind speed of 15 m/s.

is present due to the wind. In numerical optimization this variation would be interpreted as a setting dependency and therefore it would mislead the optimization algorithm. If the parameter is more sensitive to the settings then it is always possible to obtain a consistent direction of variation but many turbulent seeds might be needed. In this case a misinterpretation of the actual value of the gradient would be anyway present even with many wind realizations.

4 Conclusions

From this investigations it appears that even with a high number of turbulent wind simulations, wind turbines loads depend on the turbulence realization that is used for their evaluation. When variations in the loads due to changes in parameters are evaluated the effect of the parameter itself can be comparable with the changes due to the different wind seen by the wind turbine. This behavior can be problematic when performing numerical optimization. Changes in the loads due to the wind seen by the wind turbine can be attributed to changes in the design variables. This attribution would lead to a wrong estimation of the dependency of the cost function from the design parameters. Hence the optimization would not converge or it would but not to a significant minimum point for the design. Caution must be taken when evaluating loads and parameters from turbulent wind aeroelastic simulations.

References

[1] C Tibaldi, MH Hansen, and L Henriksen. Optimal tuning for a classical wind turbine controller. Proceedings of *Torque 2012*, The science of making torque from wind. 2012

[2] CL Bottasso, F Campagnolo, A Croce, and C Tibaldi Optimization-based study of bend-twist coupled rotor blades for passive and integrated passive/active load alleviation. *Wind Energy*, Vol. 16, No. 8, 2013, pp. 1149–1166.

[3] CL Bottasso, F Campagnolo, and A Croce Multidisciplinary constrained optimization of wind turbines Vol. 27, No. 1, 2012, pp. 21–53

[4] T. J. Larsen and M. A. Hansen. How 2 HAWC2, the user's manual. Technical Report Risø-R-1597(ver. 3-1)(EN), Risø National Laboratory, Denmark, 2007.

[5] IEC/TC88. *IEC 61400-1 Ed.3: Wind turbines - Part 1: Design requirements*. 2005.

[6] J Jonkman, S Butterfield, W Musial, and G Scott. Definition of a 5-MW reference wind turbine for

offshore system development. Technical Report NREL/TP-500-38060, NREL/NWTC, 2009.

[7] MH Hansen and LC Henriksen. Basic DTU wind energy controller. Technical Report E-0028, DTU Wind Energy, 2013.

[8] C Tibaldi, LC Henriksen, MH Hansen, and C Bak. Effects of gain-scheduling methods in a classical wind turbine controller on wind turbine aeroservo-elastic modes and loads. In *32nd ASME Wind Energy Symposium*. American Institute of Aeronautics and Astronautics, 2014.

Article VI: Concurrent Aeroservoelastic Design of a Wind Turbine Operating in Partial Load Region

This article was presented at the *8th PhD seminar on Wind Energy in Europe* in Zurich, Switzerland, in September 2012.

Proceedings of 8th PhD Seminar on Wind Energy in Europe
September 12-14, 2012, ETH Zurich, Switzerland

CONCURRENT AERO-SERVO-ELASTIC DESIGN OF A WIND TURBINE OPERATING IN PARTIAL LOAD REGION

C. Tibaldi*, M. H. Hansen and L. C. Henriksen
Wind Energy, DTU
Roskilde, Denmark
*e-mail: tlbl@dtu.dk

ABSTRACT

In this work a method to perform concurrent aero-servo-elastic design of a wind turbine operating in the partial load region is presented. The blade sweep and the controller parameters are optimized, with a numerical optimization, to improve the wind turbine performances and reduce the loads. The method and the cost function used for the investigation are presented. The cost function is based on loads computed during simulations and it describes the cost of energy. Results show that it is possible to reduce the cost of energy of a wind turbine operating in the variable speed region. A reduction of the cost of energy of 12% *is achieved with eight iterations for the case study here presented.*

NOMENCLATURE

Abbreviations

ADC	actuator duty cycle
AEP	annual energy production
DEL	damage equivalent load
DLC	design load cases

INTRODUCTION

One of the most used strategy to control pitch-torque controlled wind turbines in the variable rotational speed region is to select the torque proportionally to the square of the rotational speed. This approach allows the tracking of a constant tip-speed-ratio. To maximize the power production in a steady condition, the tip-speed-ratio λ and the pitch angle β have to be selected to maximize the power coefficient C_p. However, due to turbulence and large rotor inertia, the controller actions is not quick enough to keep the tip-speed-ratio constant after a change in the wind speed. Variations in the tip-speed-ratio mean that, if λ and β are selected to maximize the power coefficient, the operating point will drop on one side of the $C_p(\lambda)$ curve creating a drop in power production. Moreover, if the tip-speed-ratio decreases for an increase in the wind speed while operating at the top of the C_p curve the flow on the blade will stall and the turbine may risk stall-induced vibrations.

To improve the power capture Johnson [1] suggests to operate at a higher tip-speed-ratio. At a higher rotational speed the operational point moves at a lower power coefficient but it tracks better the tip-speed-ratio in response to wind changes. Johnson shows that is possible to increase the power capture by 0.5% increasing the tip-speed-ratio by 3.5%.

In this paper an approach to improve the regulation in the variable speed region by mean of a swept-back blade is presented. Here the swept-back blade is exploited to reduce the rotor speed variations and to help the controller tracking a constant tip-speed-ratio. Lower rotor speed variations decrease the risk of stall, hence of stall induced vibrations. Moreover the controller can operate closer to the maximums power coefficient, improving the power capture. In this work the amount of sweep and the controller parameters are changed to minimize a cost function based on loads computed during simulations. To perform the concurrent aero-servo-elastic design a method based on a numerical optimization is presented. The concurrent design of the blade and the controller is a key point to identify the best configuration that minimizes the costs.

The swept blade is selected for this investigations because it showed good ability in reducing the operating loads and reliability during field tests. In the investigation performed at Sandia National Laboratories [2] the performances obtained with a swept-back blade are compared with the ones obtained with a conventional smaller rotor. Despite the larger rotor the swept blade showed lower loads and the same power capture as the smaller conventional rotor. A detailed investigation of the effects on the loads due to the blade sweep are shown in the work by Verelst and Larsen [3]. In their investigation the loads generated during simulations with turbulent wind are computed and compared for different blade sweep configurations.

Results of the work here presented show that with concurrent aero-servo-elastic design it is possible to reduce the cost of a wind turbine when operating in the variable speed region.

In the following section the controller used for the investigation and how the swept-back blade is modeled are described. The numerical optimization and the cost function are then introduced. Finally the results of an optimization are shown and commented.

CONTROLLER DESCRIPTION AND SWEPT-BACK BLADE

The controller used here is inspired by Bossanyi [4]. It is divided into four different sub controllers, each for a different operational region. The four regions are:

1. constant minimum rotor speed variable torque;
2. variable rotor speed, variable torque region;
3. constant rated rotor speed, variable torque region;
4. constant rated rotor speed, constant power region.

In the following only the controller for the variable rotor speed region is described because the investigation is performed only at low wind speeds. The techniques of switching between regions are not described. It follows the ideas of Bossanyi [4] and is not part of the optimization problem.

For the regulation in the variable rotor speed the pitch is kept constant at the angle β^* and the generator torque is used to control the rotational speed Ω to track a constant tip-speed-ratio. The value of the torque is set to $Q_{ref} = k\Omega^2$ to balance the aerodynamic torque. The constant k can be computed as

$$k = \eta \frac{1}{2} \rho \pi \frac{R^5}{\lambda^{*3}} C_p(\beta^*, \lambda^*), \tag{1}$$

where ρ is the air density, R is the rotor radius, β^* and λ^* are the pitch angle and the tip-speed-ratio that maximize the power coefficient C_p, and $\eta \leq 1$ is an efficiency factor used to increase the tip-speed-ratio. Setting $\eta = 1$ the torque balance will ensure optimal tip-speed-ratio λ^* in steady state.

The advantage of using a swept-back blade is due to the coupling between the aerodynamic loads and the torsional rotation of the sections. When sweeping a blade the aerodynamic center is moved backward with respect to the elastic axis of inner blade sections. Hence the lift occurring in the outer part of the blade generates a moment about the elastic axis that induce a rotation of the blade sections. This coupling can have beneficial effects when a sudden change in the wind speed occurs, e.g. due to turbulence. When the wind suddenly changes the lift in the outer part of the blade increases. This variation increases the torsional moment generating a rotation of the blade sections. This rotation reduces the angle of attack and hence the loads. A detailed description of this aeroelastic behavior can be found in [5]. The sweep of the blade is obtained changing the position of the half chord point of each blade section. The half chord point is translated in the rotor plane, without modifying the distance from the hub. The sweep is modelled with an exponential function,

$$x(z) = x_0(z) + b\left(\frac{z - z_s}{R - z_s}\right)^{\alpha} \tag{2}$$

where x_0 is the position of the half chord point for the unswept blade, z is the radial position along the blade, z_s is the position along the blade where the sweep start, R is the blade length, and b and α are coefficient that describe the shape of the swept blade. The coefficient b indicates the sweep at the blade tip, and α indicates the curvature of the sweep. Figure 1 shows three different blade planforms changing the parameter b.

OPTIMIZATION PROBLEM

Figure 2 shows a route diagram of the numerical optimization procedure. Simulations are performed with the multi-body aero-servo-elsastic code HAWC2 [6] according to the IEC standards [7] for a given set of controller and sweep parameters. When the simulations are terminated a post processing procedure extracts the equivalent fatigue loads, the ultimate loads and the power production performances. These values are used to compute a scalar cost function and evaluate the fulfillment of the constraints, which goes into the optimization routine that computes new design variables. A gradient based optimization algorithm implemented in the Matlab function `fmincon` [8] has been used here. The procedure can be easily adapted to other

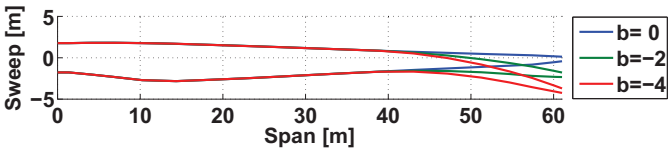

FIGURE 1. Different swept blade for different values of b.

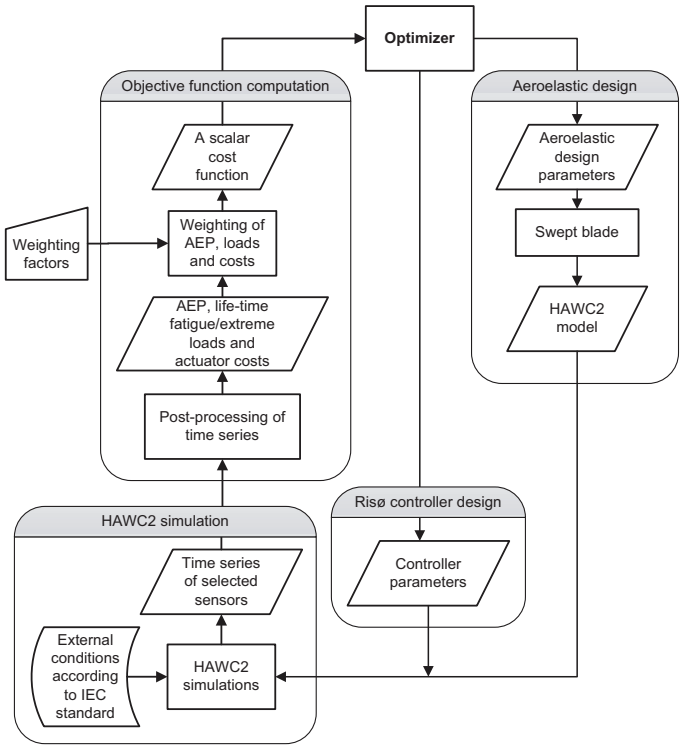

FIGURE 2. Route diagram of the numerical optimization procedure.

algorithms and optimization platforms.

The cost function is based on loads l computed during simulations:

$$J = \sum_i w_i c_i(l) \tag{3}$$

were $c_i(l)$ are the costs of the wind turbine components and w_i are weights. The cost of the blade, the tower and the drivetrain are computed with an average between fatigue and ultimate loads divided by the annual energy production AEP, while the cost of the pitch system (mechanism and bearings) is computed as the ratio between the normalized actuator duty cycle ADC and the AEP.

$$c_i = \frac{1}{2}\frac{\hat{l}_{fatigue} + \hat{l}_{ultimate}}{\widehat{AEP}} \tag{4}$$

$$c_{pitch} = \frac{\widehat{ADC}}{\widehat{AEP}} \tag{5}$$

where $\hat{l}_{fatigue}$ is the normalized life-time damage equivalent load DEL, $\hat{l}_{ultimate}$ is the normalized maximum load computed during the simulations, $\widehat{ADC}$ is the normalized actuator duty cycle and $\widehat{AEP}$ is the normalized annual energy production. The parameters $\hat{l}_{fatigue}$, $\hat{l}_{ultimate}$, $\widehat{ADC}$ and $\widehat{AEP}$ are normalized with respect to the corresponding value of a reference solution. The loads used for the tower and the blade are the resultant of the root section in-plane moments. The load used for the drivetrain is the torque on the shaft at the generator side. The ADC is defined as

$$ADC = \sum_j F(V_j)\frac{1}{T}\int_0^T \frac{\dot{\beta}(t,V_j)}{\dot{\beta}_{max}}dt \tag{6}$$

where $F(V_j)$ is the value of the life time Weibull probability function for the wind speed V_j, T is the length of a simulation, $\dot{\beta}$ is the pitch rate and $\dot{\beta}_{max}$ is the maximum allowable pitch rate. The weights used in Equations (3) are shown in Table 1. These values are computed dividing an estimated cost of the component by an estimated cost of the wind turbine. The estimated costs are obtained using the method showed in [9].

To ensure tower-blade clearance a constraint on the maximum amount of sweep is set equal to 4 m.

The simulations used to compute the loads are in accordance with the DLC 1.2 [7] but they only cover the variable speed region. Four different mean wind speeds are selected (4 , 5 , 6 and 8 m/s), and four different turbulent seeds are used for each of the mean wind speeds. To weight the effect of each wind speeds on the life time loads a Weibull distribution function is used.

For this investigation the optimization variables selected are the pitch angle β, the efficiency coefficient η and the sweep parameter b.

All the results presented in the next sections are shown with respect to a reference solution for the 5MW NREL reference wind turbine. This solution is obtained tuning the controller to track maximum power coefficient $\eta = 1$ and using a straight blade.

The starting solution required by the gradient based algorithm is obtained with a controller tuned to maximize the power coefficient and a blade with a backward sweep of 1 m.

TABLE 1. Cost function weights, w.

Component	c
Blade	0.311
Tower	0.122
Drivetrain	0.231
Pitching system	0.042

RESULTS

Figure 3 shows the variation of the total cost function for the first eight iterations. The total cost is reduced by almost 12% compared to the cost of the reference solution. Figure 4 shows the wind turbine components cost variation. The blade, the tower and the pitch system are subject to lower loads, while the drive train shows higher loads. The changes of the optimization variables at the different iterations are shown in Figure 5. The reduction of the loads on the tower at the second iteration, Figure 4, is due to the reduction of the efficiency parameter η, Figure 5. Reducing the value of η the mean value of the rotational speed increases. A higher rotational speed increases the gap between the 3P frequency and the tower first natural frequency reducing the tower vibrations, hence the fatigue loads. For example, an efficiency factor of 80% increases the distance between the 3P and the first tower natural frequency by 7%. The higher loads on the drive train that occur from the second iteration are due to the switch of the operative region. Because the turbine is operating at a higher rotational speed, lower η, the switch between the variable speed region and the constant speed region occurs for lower wind speeds. In the constant rotational speed the torque

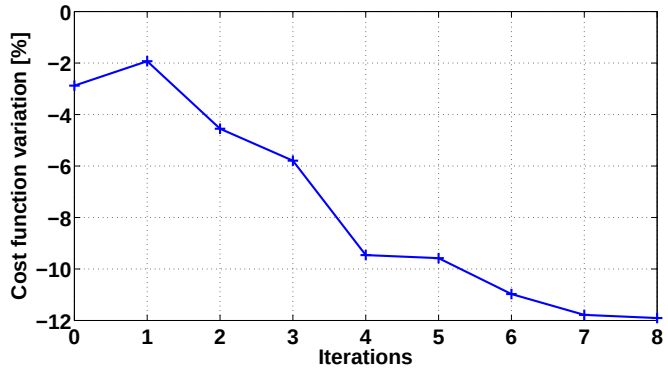

FIGURE 3. Total cost variation.

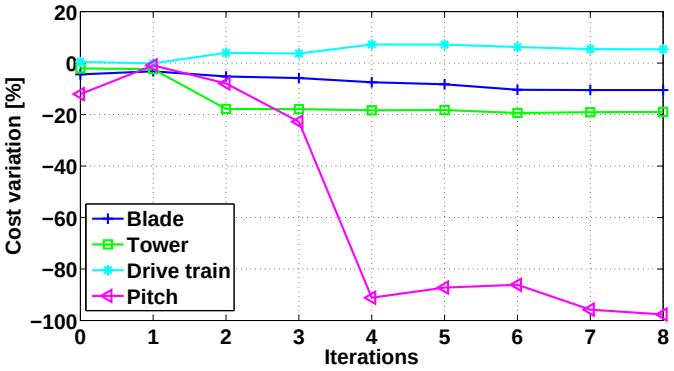

FIGURE 4. Component-cost variation.

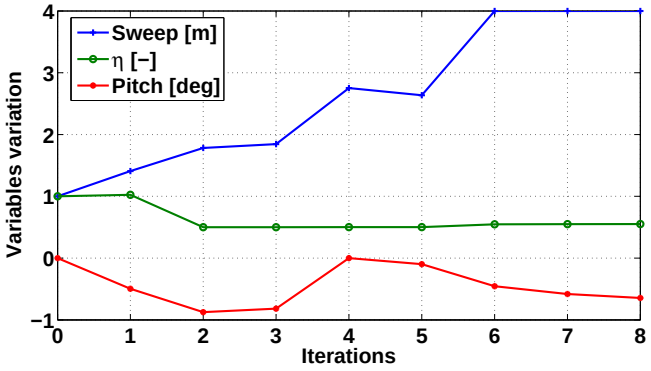

FIGURE 5. Optimization variables variation.

controller is more aggressive, hence the higher drive train fatigue loads. The sweep of the blade increases at each iteration and it reaches the maximum allowed value. This may show that the cost model used for this investigation is not good enough to limit the amount of sweep. A possible solution to this problem is to include in the cost model the torsional moment at the blade root. Indeed when increasing the sweep the torsional moment increases. During the optimization the algorithm is always reducing the pitch angle except at the fourth iteration. A pitch angle lower than the one of the straight blade is required to compensate the static rotation of the blade sections due to the sweep. Indeed with a swept-back blade, the outer part of the blade operates at a lower aerodynamic angle of attack due to the torsional coupling of the blade, hence the blade generates a lower power coefficient. To compensate this effect and to restore the original power coefficient it is necessary to operate at a lower pitch angle. The variations of the pitch system cost are extremely high because in the partial load region the actuator duty cycle is null due to the constant pitch strategy. Hence a pitch variation due to a switch in the operative region can generate a large variation in the cost.

CONCLUSIONS

In this work a method to perform concurrent aero-servo-elastic design using a numerical optimization has been presented. The results from the numerical optimization have shown that is possible to improve the wind turbine performances in the variable speed region leading to a lower cost of energy. In eight iterations the cost of the energy has been reduced by almost 12%. The cost reduction has been achieved reducing the loads on the blade and on the tower. The blade sweep has been increased while the controller efficiency factor has been reduced to increase the tip-speed-ratio. The pitch angle is reduced to compensate the reduction in power production due to the sweep of the blade. Further investigations should focus on repeating the

numerical optimization including in the cost function the blade torque to limit the sweep. Future works may also focus on the selection of a more suited optimization algorithm. A more realistic cost function could give more reliable and factual results while a more advanced algorithm, e.g. based on global optimization, could further improve the cost reduction identifying the global minimum.

REFERENCES

[1] Johnson, K., Fingersh, L., Balas, M., and Pao, L., 2004. "Methods for increasing region 2 power capture on a variable speed wind turbine". *Journal of Solar Energy Engineering,* ***126***, pp. 1092–1100.

[2] Ashwill, T. D., 2010. Sweep-twist adaptive rotor blade: Final project report. Tech. Rep. SAND2009-8037, Sandia National Laboratories, USA.

[3] Verelst, D. R. S., and Larsen, T. J., 2010. Load consequences when sweeping blades - a case study of a 5MW pitch controlled wind turbine. Tech. Rep. Risø-R-1724(EN), Risø National Laboratory, Denmark.

[4] Bossanyi, E., 2009. Controller for 5MW reference turbine. Tech. Rep. GH report 11593/BR/04, Garrad Hassan and Partners Limited report.

[5] Bisplinghoff, R. L., Ashley, H., and Halfman, R. L., 1996. *Aeroelasticity*. Dover Publications.

[6] Larsen, T. J., and Hansen, M. A., 2007. How 2 HAWC2, the user's manual. Tech. Rep. Risø-R-1597(ver. 3-1)(EN), Risø National Laboratory, Denmark.

[7] IEC/TC88, 2005. *IEC 61400-1 Ed.3: Wind turbines - Part 1: Design requirements*. International Electrotechnical Commission (IEC), 8.

[8] MATLAB, 2011. *Version 7.13.0*. Natick, Massachusetts: The MathWorks Inc.

[9] Fingersh, L., Hand, M., and Laxson, A., 2006. Wind turbine design cost and scaling model. Tech. Rep. NREL/TP-500-40566, National Renewable Energy Laboratory, USA.

Article VII: Aeroelastic Optimization of a 10 MW Wind Turbine

The article was presented at the *33rd ASME Wind Energy Symposium* during the *SciTech 2015* conference organized by the American Institute of Aeronautics and Astronautics in Kissimmee, Florida, USA, 5-9 January 2014 .

I was responsible for the Test Case 3 and 4 in sections *V.C* and *V.D*.

Aero-Elastic Optimization of a 10 MW Wind Turbine

Frederik Zahle*, Carlo Tibaldi †, David Robert Verelst ‡
Christian Bak§, Robert Bitsche¶, José Pedro Albergaria Amaral Blasques‖
Technical University of Denmark, Wind Energy Department, 4000 Roskilde, Denmark

This article presents the multi-disciplinary wind turbine analysis and optimization tool HawtOpt2 that is based on the open-source framework OpenMDAO, and interfaces to several state-of-the art simulation codes, which allows for a wide variety of problem formulations and combinations of models. In this article simultaneous aerodynamic and structural optimization of a 10 MW wind turbine rotor is carried out with respect to material distribution and outer shape. A set of optimal designs with respect to mass and AEP are presented, which shows that an AEP biased design can increase AEP with 1.5% while a mass biased design can achieve mass savings of up to 20% compared to the baseline DTU 10MW RWT. A newly developed frequency-domain based fatigue model is used to minimise fatigue damage, which achieves up to 8% reduction in the tower bottom fore-aft fatigue damage, with only limited reductions of the aerodynamic performance or increased mass.

I. Introduction

The size of modern wind turbines continues to increase and with this comes challenges to the designers to reduce the overall cost of energy. To meet this challenge it is becoming increasingly important to design the turbine considering the inherent couplings between the different disciplines involved in the design at an early stage in the design process. It is widely recognized that multi-disciplinary optimization can be used to systematically evaluate and balance the trade-offs between conflicting objectives, and thus reach better designs.

In the recent years several frameworks have been present to perform wind turbine multi-disciplinary optimization design. Among these there are the works by Fuglsang et al.,[1] Bottasso et al.,[2] Ashuri et al.,[3] Merz et al.,[4,5] Fischer,[6] Ning.[7]

In this work an optimization framework was developed to enable concurrent optimization of the structure and outer shape of a wind turbine blade, which was named HawtOpt2. This tool builds on the experience gained with the HawtOpt code,[1] but is otherwise a completely new codebase written in the Python programming language, and based on the open source framework OpenMDAO,[8] which is used to define the optimization problem, and handle the data and workflow. Different tools have been interconnected within the framework to resolve the different levels of the problem. The finite element cross sectional tool BECAS[9–11] is used to predict the structural and mass properties and to retrieve stresses along the blades. The aeroservoelastic tool HAWCStab2[12] is used to predict aerodynamic performance and deflections of the rotor, modal properties of the turbine, and retrieve a linearized model of the turbine. A method to evaluate fatigue damage loads in the frequency domain is also used.

The overall objective of the paper is to apply the HawtOpt2 framework to design a 10 MW wind turbine rotor for the existing DTU 10MW RWT platform, where both the outer shape of the blade as well as the structural design of the blade are optimized concurrently. Different test cases are presented, each addressing a specific aspect of the design problem. Firstly, a pure structural optimization is presented, in which the outer

*Senior Scientist, DTU Wind Energy, 4000 Roskilde, Denmark.
†PhD student, DTU Wind Energy, 4000 Roskilde, Denmark
‡Post-doctoral Researher, DTU Wind Energy, 4000 Roskilde, Denmark
§Senior Scientist, DTU Wind Energy, 4000 Roskilde, Denmark.
¶Senior Scientist, DTU Wind Energy, 4000 Roskilde, Denmark.
‖Post-doctoral Researher, DTU Wind Energy, 4000 Roskilde, Denmark.

shape is unaltered. Secondly, a series of optimal designs are made with a series of aeroelastic optimizations to identify a trade off between the annual energy production (AEP) and the blade weight. Finally, two further designs are obtained, one limiting the design space to avoid resonance conditions of the blade edgewise modes and one to lower the tower base longitudinal fatigue damage. The DTU 10MW RWT[13,14] is used as the baseline design for all optimizations. Although the diameter of a wind turbine rotor is one of the primary variables for increasing AEP, the diameter of the existing platform is maintained to limit the design space and simplify the analysis of the resulting designs.

II. Models and framework

The HawtOpt2 framework uses OpenMDAO (Open-source Multidisciplinary Design, Analysis, and Optimization Framework)[8,15–17] to handle the definition of the optimization problem, workflow, dataflow and parallelization of simulation cases. OpenMDAO provides an interface to PyOpt[18] which has wrappers for several optimization algorithms, and in this work, the gradient-based sequential quadratic programming optimizer SNOPT is used. The development of the HawtOpt2 framework is part of a larger effort to design an entirely open-source systems engineering platform for wind turbine plants with the aim of enabling a larger degree of uniformity and versatility for users of the many wind plant analysis tools available in open source and under license. This framework is developed as a collaboration between NREL and DTU Wind Energy and is named Framework for Unified Systems Engineering and Design of Wind Turbine Plants (FUSED-Wind).[19] While in its present form HawtOpt2 does not interface fully to FUSED-Wind, the aim is to provide this interface to allow users to combine the tools made available in HawtOpt2 with tools made available by other developers using FUSED-Wind.

Interfaces have been developed to connect the optimization framework to the finite element cross sectional tool BECAS and to the aeroelastic tool HAWCStab2, that form the core of the state-of-the art analysis capability provided by the tool.

BECAS[9–11] allows for the evaluation of the cross sectional structural and mass properties of the blade. The tool is based on a 2D finite element formulation that allows for an exact geometrical description of the section. Different regions with different material and different thicknesses can be specified enabling the description of different layups.

The linear high-order aeroservoelastic model implemented in HAWCStab2[12] uses an unsteady blade element momentum (BEM) model of the rotor and a geometrically non-linear finite beam element model to compute steady-state aerodynamic states, structural deflections and linearized models of the wind turbine. A detailed description of the model is provided by Hansen.[20,21] An extensive validation and analysis of the open-loop performances of the tool are provided by Sønderby and Hansen.[22]

A method to evaluate fatigue damage based on a linear model is used in one of the test cases. The method is frequency based and does therefore not require time domain simulations, which for gradient-based optimization is central, since the stochastic nature of time-domain simulations with turbulence does not allow for accurate evaluation of gradients of objectives and constraints with respect to the design variables. The method is described in details by Tibaldi et al.[23]

The present work makes use of a gradient based optimizer, and since none of the participating solvers at present have the capability of providing analytically derived gradients, a finite difference approximation of the objective and constraint gradients is used, which is computed by OpenMDAO and provided to SNOPT.

III. Blade Paramerization

To enable optimization of both the structure and aerodynamic shape of the blade, a suitable parameterization of the geometry has to be chosen. The parameterization is on the one hand required to be general enough to not limit the design space, while on the other hand be as simple as possible in order to limit the number of design variables required. In this work so-called free-form deformation (FFD) splines based on Bezier curves are favoured over direct splines of the actual quantities of interest, since the number of design variables and the complexity of the resulting shape are decoupled.

The blade planform is described in terms of distributions of chord, twist, relative thickness and pitch axis aft leading edge, the latter being the distance between the leading edge and the blade axis. The lofted shape of the blade is generated based on interpolation of a family of airfoils with different relative thicknesses.

The internal structure is defined from a number of regions that each cover a fraction of the cross-sections

along the blade. Each region consists of a number of materials that are placed according to a certain stacking sequence. Figure 1 shows a cross section in which the region division points (DPs) are indicated. The DP curves are described by a smooth spline as function of span that takes values between s=-1 and s=1, where s=-1 is located at the pressure side trailing edge, s=0 is at the leading edge, and s=1 is located at the trailing edge suction side. Shear webs are associated to two specific DPs on the pressure and suction side, respectively, and will move according to these points.

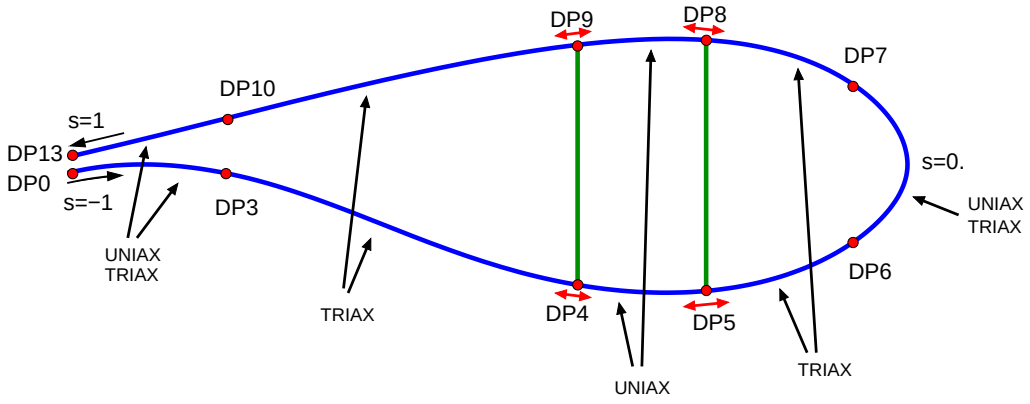

Figure 1. Region division points (DP) definition: red points indicate division points between regions; their positions are defined as curve fraction from pressure side TE (s=-1) to LE (s=0) to suction side TE (s=1).

The composite layup is likewise described by a series of smooth splines describing the thicknesses of individual layers. Figure 2 shows the composite layup of the DTU 10MW RWT for regions 0 to 6. Note that the layup of the DTU 10MW RWT has the same material distributions on the suction and pressure sides.

Also indicated in Figure 1 are the materials in the blade, which in this work are included as design variables. This includes both uniax and triax material in the trailing edge, biax in the trailing panel, uniax in the spar caps, and triax and uniax in the leading edge panels. As for the baseline design, all material thicknesses are varied symmetrically between pressure and suction side of the blade.

IV. Problem formulation

The numerical optimization problem that is solved is defined as:

$$\begin{aligned} \underset{\mathbf{x}_p,\,\mathbf{x}_s}{\text{minimize}} \quad & f(\{\mathbf{x}_p,\,\mathbf{x}_s\},\mathbf{p},w) \\ \text{subject to} \quad & \mathbf{g}(\mathbf{x}_p) \leq \mathbf{0}, \\ & \mathbf{h_g}(\mathbf{x}_s) \leq \mathbf{0}, \\ & \mathbf{h_s}(\mathbf{x}_s) \leq \mathbf{0}, \\ & \mathbf{k}(\{\mathbf{x}_p,\,\mathbf{x}_s\}) \leq \mathbf{0} \end{aligned} \tag{1}$$

A scalar cost function f is minimized, subject to several nonlinear constraints. The cost function depends on a set of design variables $\{\mathbf{x}_p,\,\mathbf{x}_s\}$, a set of constant parameters $\mathbf{p}$, and a weight w. The design variables can be divided into two sets: the planform variables $\mathbf{x}_p$ and the structural variables $\mathbf{x}_s$. The planform variables define the outer shape of the blade. These variables are the chord, the twist, and the relative thickness distributions. The structural variables define the internal geometry of each blade blade section. These variables include thicknesses of the different material layups and position and width of the spar caps. The design variables, together with the parameters $\mathbf{p}$, define the entire wind turbine. The design variables are all normalized such that when they are equal to zero they correspond to the value of the baseline.

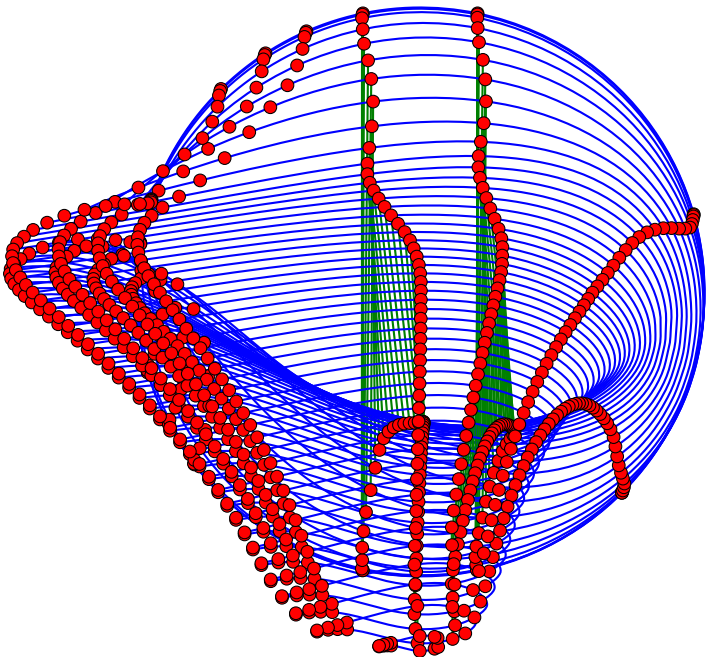

Figure 2. Non-rotated cross sections along the blade showing the region DPs and shear webs. CHANGE TO TWISTED BLADE PLOT.

The cost function is defined as

$$f(\{\mathbf{x}_p,\, \mathbf{x}_s\}, \mathbf{p}, w) = \frac{W(\{\mathbf{x}_p,\, \mathbf{x}_s\}, \mathbf{p})}{W(\{\mathbf{0},\, \mathbf{0}\}, \mathbf{p})} + w\frac{AEP(\{\mathbf{0},\, \mathbf{0}\}, \mathbf{p})}{AEP(\{\mathbf{x}_p,\, \mathbf{x}_s\}, \mathbf{p})} \tag{2}$$

where W is the blade weight, AEP is the annual energy production. $W(\{\mathbf{0},\, \mathbf{0}\}, \mathbf{p})$ and $AEP(\{\mathbf{0},\, \mathbf{0}\}, \mathbf{p})$ are the blade weight and annual energy production of the baseline design.

Three different type of constraints are defined depending on the variables they depend on. Constraints $\mathbf{g}$ depend only on planform parameters. They include bounds on the chord and relative thickness. Constraints $\mathbf{h_g}$ depends only on structural parameters. These constraints include bounds on the material thicknesses and on the position and widths of the spar caps. Constraints $\mathbf{h_s}$ denote the limits on the maximum allowable stresses in the structure. For simplicity and to reduce computational time, stresses are evaluated based on a fixed set of loads, obtained from non-linear time marching simulations performed on the baseline wind turbine using the HAWC2 code.[24] Therefore, they only depends on the material thicknesses. This simplification of the solution of the optimization problem is likely to have an impact on the final designs, particularly the very mass-biased ones where significant amounts of material are removed. In this work, constraints on buckling of the composite surface panels are not computed, and will have to be considered as a next step in the design process of the blade. The constraints $\mathbf{k}$ depend on both the planform and structural variables. These constraint are obtained from steady-states analysis with a fully flexible rotor. Two sets of cases are considered: normal operation and idling in storm conditions. During normal operation maximum tip deflections, thrust, and lift coefficient are limited. In the storm case maximum tip deflection, thrust, and integrated forces along the blade are also limited. The constraints $\mathbf{g}$ include also bounds on the position of the aeroelastic wind turbine edgewise frequencies, to avoid resonances during operation, and constraints

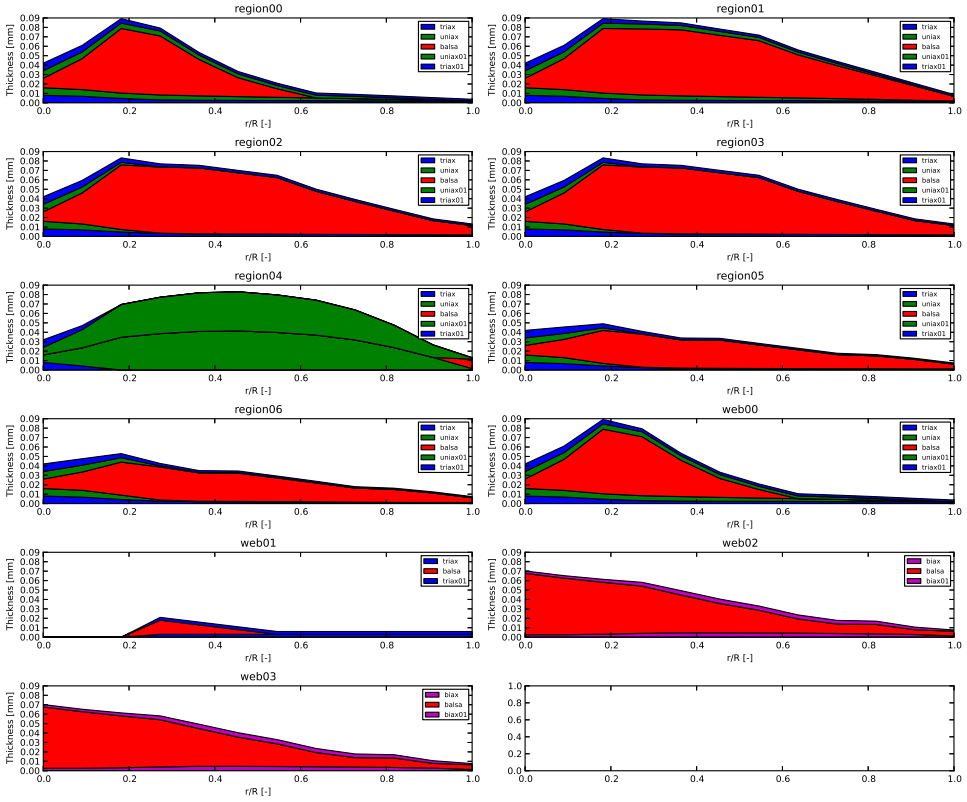

Figure 3. Baseline composite layup of the regions.

on the fatigue at the tower base bottom in the longitudinal direction. The constraints on the frequencies and on the fatigue are only used in the test cases where it is explicitly specified. Figure 4 shows a so-called extended design structure matrix diagram[25] of the workflow in HawtOpt2.

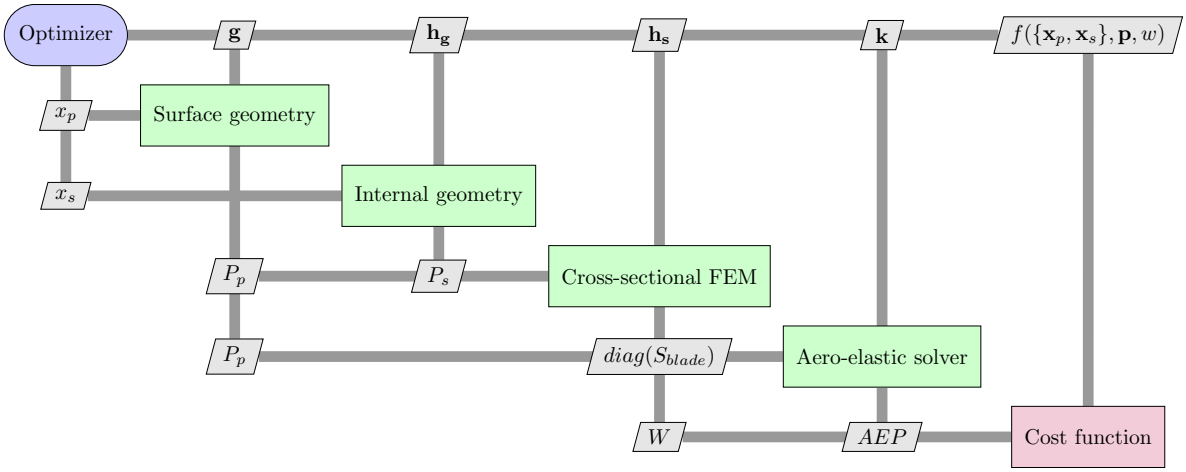

Figure 4. Extended Design Structure Matrix diagram of the workflow of HawtOpt2.

Tables 1 and 2 provides a summary of design variables and constraints used in this study.
Table 3 summarises the key parameters for the DTU 10MW RWT used as the baseline platform in this

Parameter	Spanwise distribution	# of DVs	Comment
Chord	[0, 0.2, 0.4, 0.6, 0.8]	5	Tip chord fixed
Twist	[0.2, 0.4, 0.6, 0.8, 1.]	5	Root twist fixed
Relative thickness	[0.2, 0.4, 0.6, 0.8]	4	Root and tip thickness fixed
Trailing edge uniax	[0, .2, .40, .75, 1.]	5	Pressure/suction side
Trailing edge triax	[0, .2, .40, .75, 1.]	5	Pressure/suction side
Trailing panel triax	[0, .2, .40, .75, 1.]	5	Pressure/suction side
Spar cap uniax	[0, .2, .40, .75, 1.]	5	Pressure/suction side
Leading panel triax	[0, .2, .40, .75, 1.]	5	Pressure/suction side
Leading edge uniax	[0, .2, .40, .75, 1.]	5	Pressure/suction side
Leading edge triax	[0, .2, .40, .75, 1.]	5	Pressure/suction side
DP4	[(0, .2), .40, .75]	3	Inner CPs grouped, tip position fixed
DP5	[(0, .2), .40, .75]	3	Inner CPs grouped, tip position fixed
DP8	[(0, .2), .40, .75]	3	Inner CPs grouped, tip position fixed
DP9	[(0, .2), .40, .75]	3	Inner CPs grouped, tip position fixed
Total		61	

Table 1. Free form deformation spline (FFD) design variables used in the optimizations.

work. As described above, only the rotor is optimized in this work leaving all other parameters unaltered. Although the outer shape is controlled by the optimizer, the cross sectional shape is, as described in Section III, based on an interpolation between the FFA-W3 airfoil series, and as such, the aerodynamic characteristics of the airfoils are unchanged. At this stage, the 3D corrections applied on the airfoils based on the initial design are used, although these in principle should be recomputed for every pertubation of the outer shape. The error associated with this simplication is however not considered to be considerable compared to the uncertainty associated with 3D correction engineering models.

V. Results

V.A. Test case 1: Pure Structural Optimization with Fixed Outer Shape

The objective of the first set of test cases was to in one case minimise blade mass and in the next case to minimise blade mass moment subject to the constraints described in Section IV. Since AEP was not part of the objective this corresponds to a weight $w = 0.$ in the objective defined in Equation 2. The outer shape of the blade was fixed while the material thickness distributions, spar cap positions and widths were design variables, see Figure 1. This resulted in a total of 47 design variables. Stress analysis was conducted using load cases based on the six most severe load cases computed for the DTU 10 MW RWT.

The mass optimized blade mass was 35.3 tonnes which is an 17.7% reduction in mass relative to the baseline mass of 42.8 tonnes. The mass moment optimized design achieved a 13% reduction in mass moment, and a mass of 39.4 tonnes which is a 9.2% reduction.

Figure 5 shows plots of the structural properties of the two optimized designs relative to the baseline. While the two objectives are similar in that they achieve an overall mass reduction, the resulting distributions of mass are very different. While the mass optimization focuses on removing mass from the root of the blade, while actually increasing mass by 10% on the outer part of the blade, the mass moment optimization does not remove mass from the root, but achieves a 10% reduction in mass on the outer part of the blade. This is also clearly reflected in the thickness distribution of the spar cap, shown in Figure 6, where the mass optimized design removed material from the root, while adding material on the outer part of the blade, and oppositely, the mass moment optimization added material at the root and removed material from the outer part of the blade.

Constraint	Value	# of Cons	**Comment**
max(chord)	< 6.2 m	1	Maximum chord limited for transport.
min(relative thickness)	> 0.24	1	Same airfoil series as used on the DTU 10MW RWT.
min(material thickness)	> 0.0	78	Ensure FFD splines do not produce negative thickness.
$t/w_{sparcap}$	> 0.08	24	Basic constraint to avoid spar cap buckling.
max(Flapwise tip deflection)	$<$ ref value	1	Operational tip deflection cannot exceed that of the DTU 10MW RWT.
max(Flapwise tip deflection)	$<$ ref value	1	Extreme wind standstill tip deflection cannot exceed that of the DTU 10MW RWT.
max(Edgewise tip deflection)	$<$ ref value	1	Extreme wind standstill tip deflection cannot exceed that of the DTU 10MW RWT.
Rotor thrust	$<$ ref value	1	Operational rotor thrust cannot exceed that of the DTU 10MW RWT.
Blade flapwise load	$<$ ref value	1	Extreme wind standstill loads cannot exceed that of the DTU 10MW RWT.
Blade edgewise load	$<$ ref value	1	Extreme wind standstill loads cannot exceed that of the DTU 10MW RWT.
Lift coefficient @ $r/R = [0.5 - 1.]$	< 1.35	5	Limit operational lift coefficient to avoid stall.
Ultimate strain criteria	< 1.0	66	Material failure in each section for six load cases.
Tower bottom long. fatigue	$<$ [5%, 10%]	2	Fatigue reduction, only in test case 3.
Blade rotor speed fatigue	$<$ ref value	2	Fatigue reduction, only in test case 3.
abs((Edgewise FW mode frequency)/6P)	$> 7\%$	2	Frequency constraint, only in test case 4.
min(Edgewise BW mode damping)	$> 1\%$	2	Frequency constraint, only in test case 4.
Total		189	

Table 2. Non-linear constraints used in the optimizations.

Parameter	Value
Wind Regime	IEC Class 1A
Rotor Orientation	Clockwise rotation - Upwind
Control	Variable Speed Collective Pitch
Cut in wind speed	4 m/s
Cut out wind speed	25 m/s
Rated wind speed	11.4 m/s
Rated power	10 MW
Number of blades	3
Rotor Diameter	178.3 m
Hub Diameter	5.6 m
Hub Height	119.0 m
Drivetrain	Medium Speed, Multiple-Stage Gearbox
Minimum Rotor Speed	6.0 rpm
Maximum Rotor Speed	9.6 rpm
Maximum Generator Speed	480.0 rpm
Gearbox Ratio	50
Maximum Tip Speed	90.0 m/s
Hub Overhang	7.1 m
Shaft Tilt Angle	5.0 deg.
Rotor Precone Angle	-2.5 deg.
Blade Prebend	3.332 m
Rotor Mass	227,962 kg
Nacelle Mass	446,036 kg
Tower Mass	628,442 kg
Airfoils	FFA-W3

Table 3. Key parameters of the DTU 10 MW Reference Wind Turbine.[13,14]

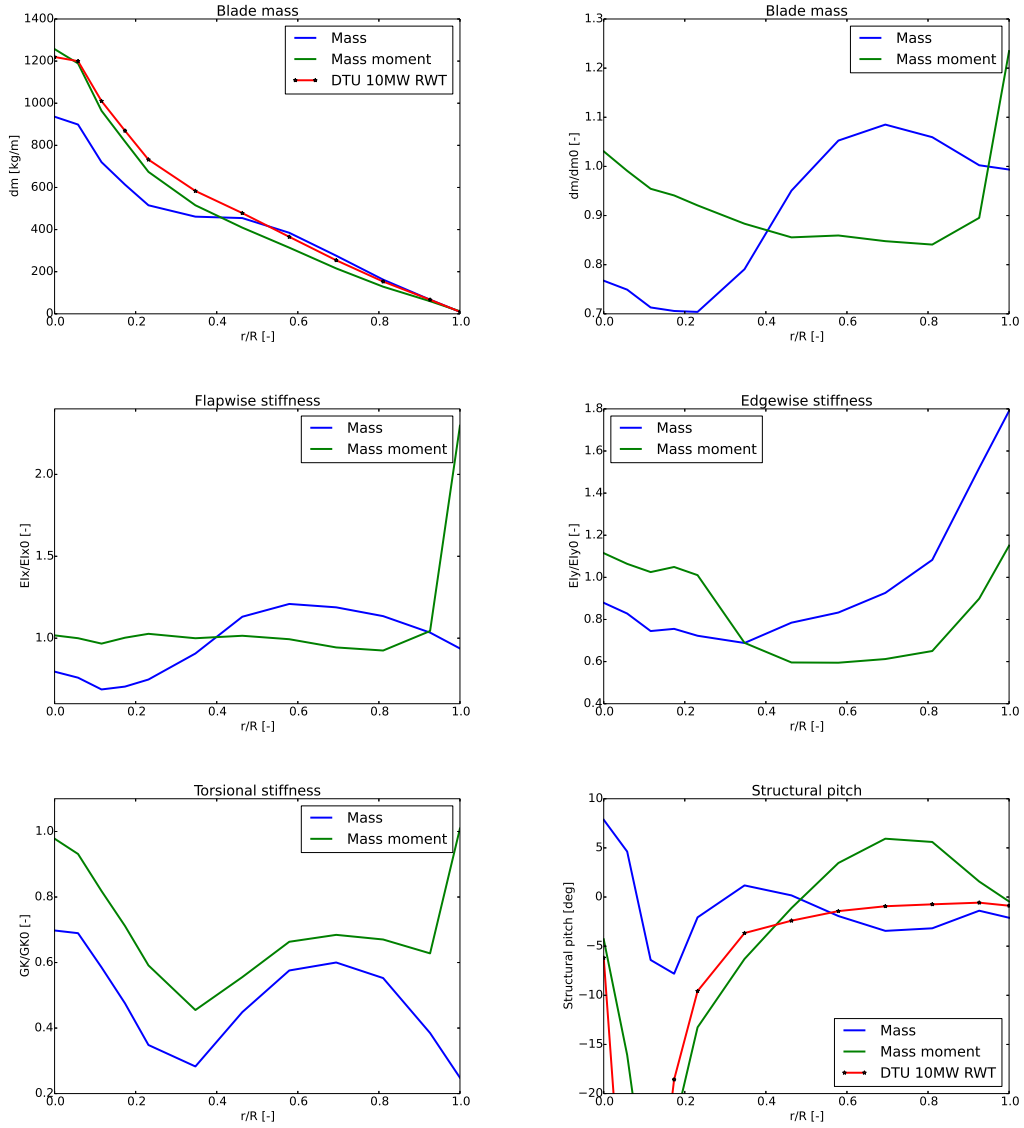

Figure 5. Blade structural properties for the structure only optimizations.

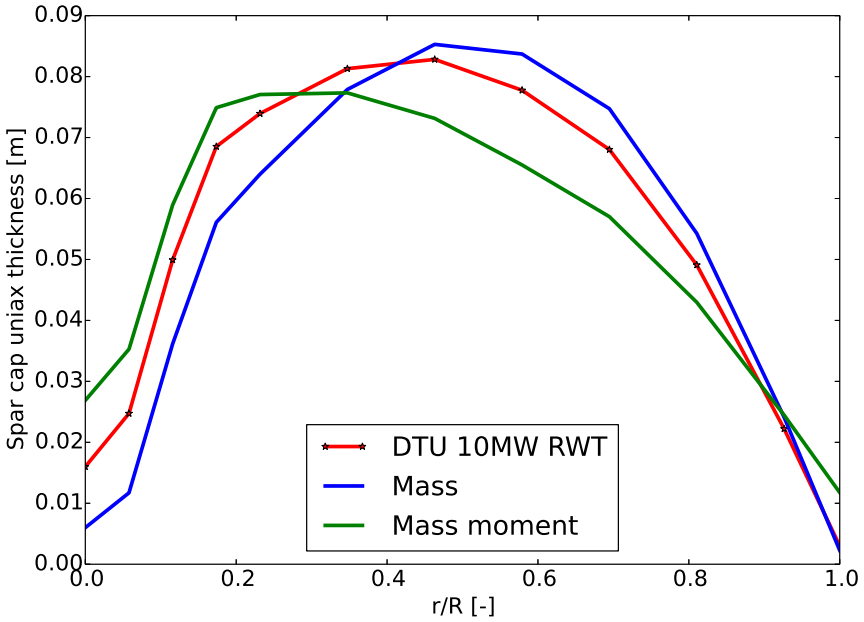

Figure 6. Blade spar cap thickness distribution for the structure only optimizations.

V.B. Test case 2: Shape and structural Optimization for Mass and AEP

For this test case, the objective was a compound objective consisting of both mass and AEP as defined in Equation 2 where the weight w was varied in the range w=[0.8, 0.95, 0.9, 0.925, 0.95, 0.975], resulting in a series of designs with varying bias towards either mass (low w) or AEP (high w). As opposed to the previous test case both the internal structural layout and the blade shape were included in the design variables. Allowing the chord, twist and relative thickness to vary added another 15 design variables to the problem, totalling 61 design variables as listed in Table 1.

Figure 7 shows the resulting optimal designs plotted with the resulting AEP vs mass points. As expected, the different designs are placed on a pareto front according to the bias in the respective objective functions. The most mass biased design denoted AEP0.8 achieves a mass reduction of approximately 20% with no improvement in AEP, whereas the most AEP biased design denoted AEP0.975 achieves an AEP increase of 1.7%, but at the cost of an increase in mass of 11%. The design AEP0.9 does not appear to be on the pareto front, indicating that it could have gotten stuck in a local minimum. The AEP0.925 design moved onto the pareto front with bias on AEP, but moved along this front downwards towards a more mass biased final design, resulting in a slight improvement of the objective function. It appears that an AEP to mass bias of 0.9-0.925 results in designs with significant mass savings combined with an increase in AEP, whereas designs with more bias towards mass do not achieve significantly lower mass, but only a reduction in AEP.

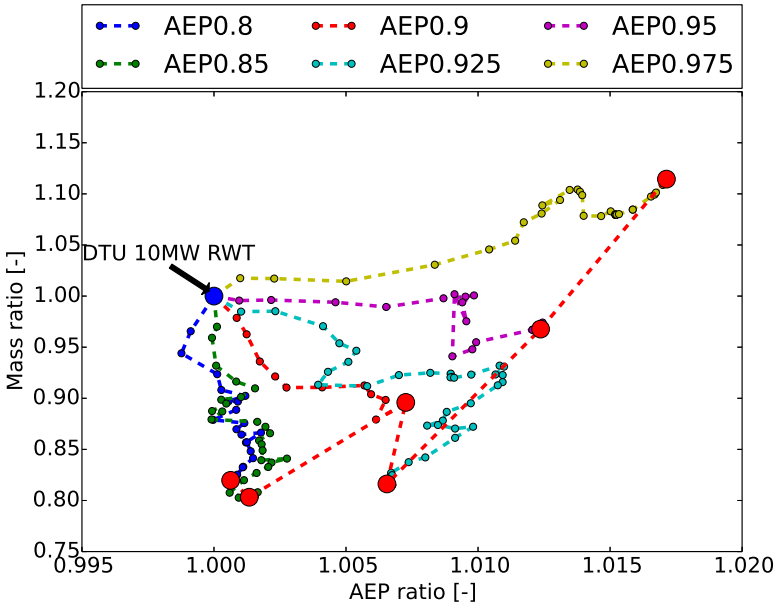

Figure 7. Pareto optimal design for the massAEP designs.

Figure 8 shows the optimized planforms for the pareto optimal designs. The primary coupling variables between the aerodynamics and the structure is the thickness and chord distributions. Common to all the designs is that the chord is reduced considerably on the mid and outer part of the blade of up to 15%, with a corresponding adjustment of the twist, with the highest reduction for the AEP biased designs. The constraint on maximum chord is active for most of the designs. The distribution of relative thickness is, however, very different for the six designs, with a radical reduction in thickness for the AEP0.975 design and oppositely a large increase in relative thickness for the AEP0.8 design. Common to the designs compared to the baseline design, however, is an increase in thickness on the mid part of the blade, which allows for removal of thickness and mas from the inner part of the blade, resulting in a larger overall reduction in mass, at the price of reduced aerodynamic performance on the outer part of the blade, which is compensated for on the inner part of the blade.

Looking at the aerodynamic loads on the blades shown in Figure 9, all designs increase the loading on

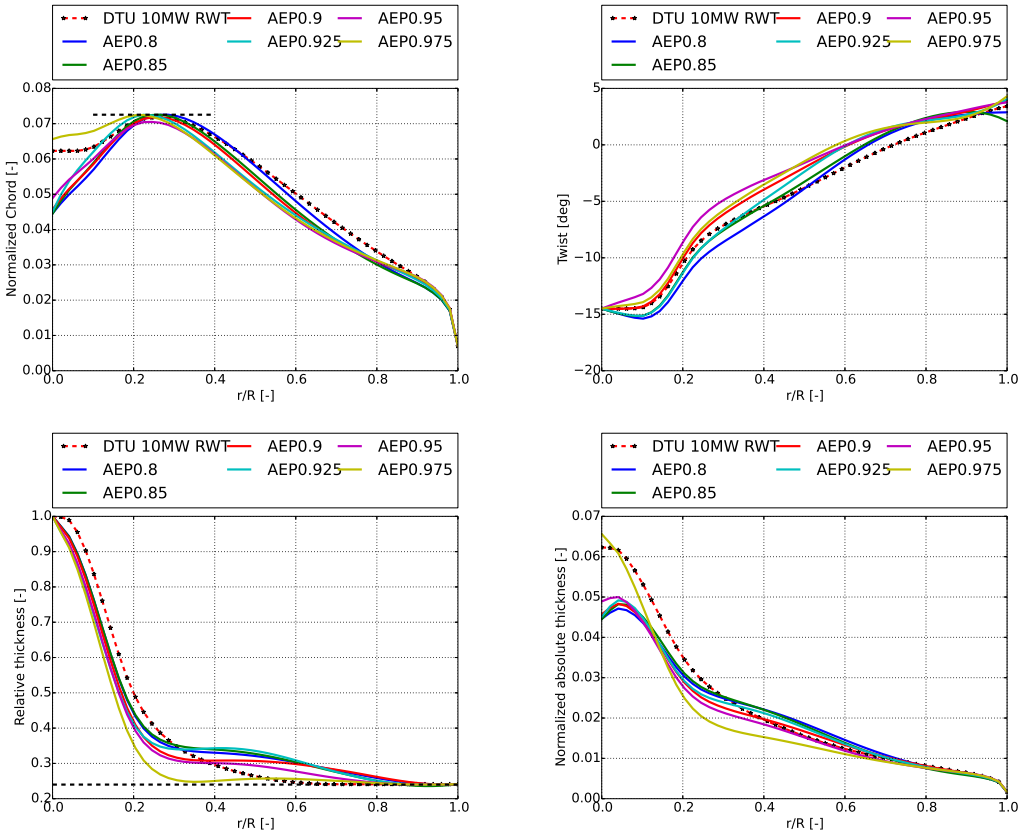

Figure 8. Optimized blade planform for test case 2.

the mid part of the blade, and either increase or decrease the loading at the tip for bias towards AEP or mass, respectively. All designs activate the constraint on maximum allowed operational lift coefficient of 1.35. This constraint is in place to ensure ample distance to the maximum lift coefficient of the aerofoils, since the rotor can easily experience variations of ± 4 degrees angle of attack under operation in turbulent or sheared inflow conditions. Except for the AEP0.975 design, the tendency is to compromise aerodynamic performance on the mid part of the blade in order to increase thickness, which is somewhat compensated for by an increase in performance further in-board on the blade.

The structural properties of the mass/AEP optimized designs are plotted in Figure 10. All the designs have a large reduction in flapwise, edgewise and torsional stiffness in the root, while the flapwise stiffness is increased at around mid-span and kept reasonably unchanged on the outer part of the blade. The edgewise stiffness is reduced from mid span and outwards, with the highest reduction at 80% span of 40%. Turning to the mass distribution, it is evident that the objective to reduce mass is most easily achieved by removing mass from the root, similar to the result for the structure only optimization discussed in Section V.A. From a fatigue perspective, this tendency is perhaps not desirable since edgewise fatigue is driven primarily by gravity loads, suggesting that the use of mass moment in the objective would be better suited for achieving designs with overall lower fatigue loads.

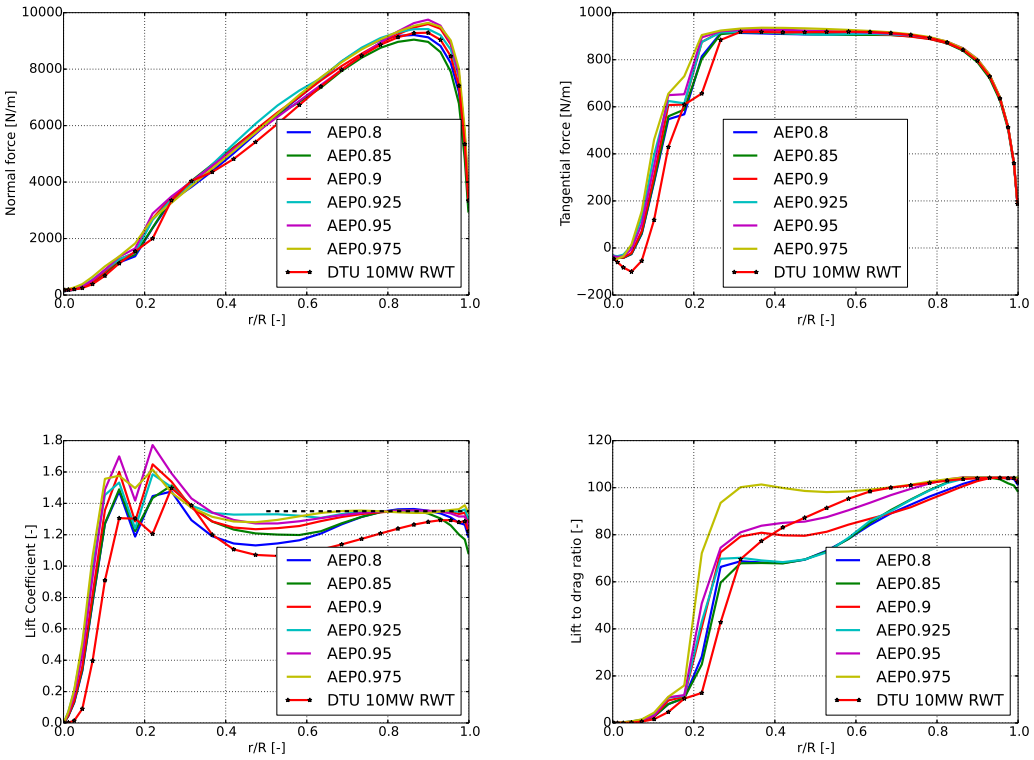

Figure 9. Optimized blade planform for test case 2.

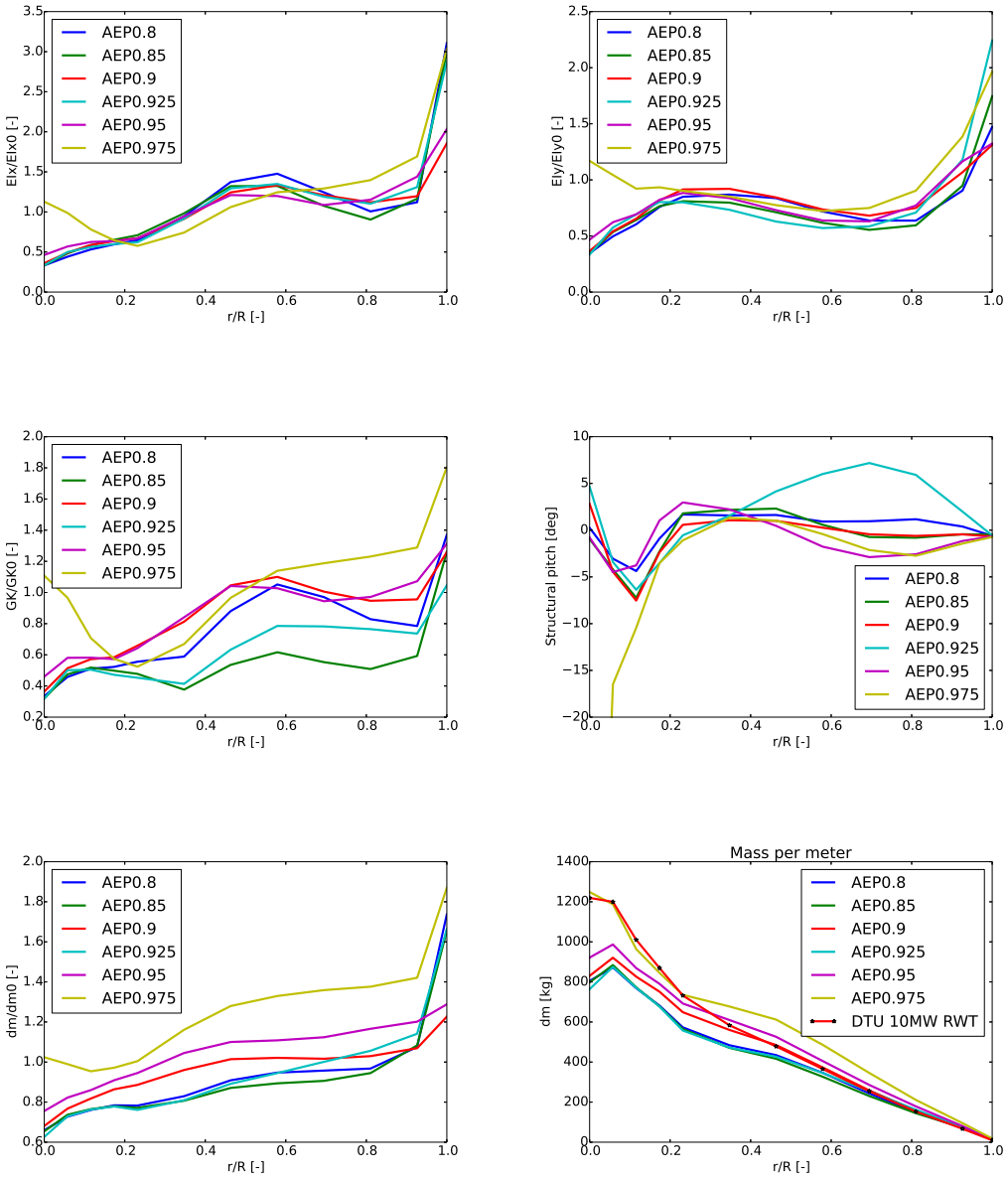

Figure 10. Optimized blade planform for test case 2.

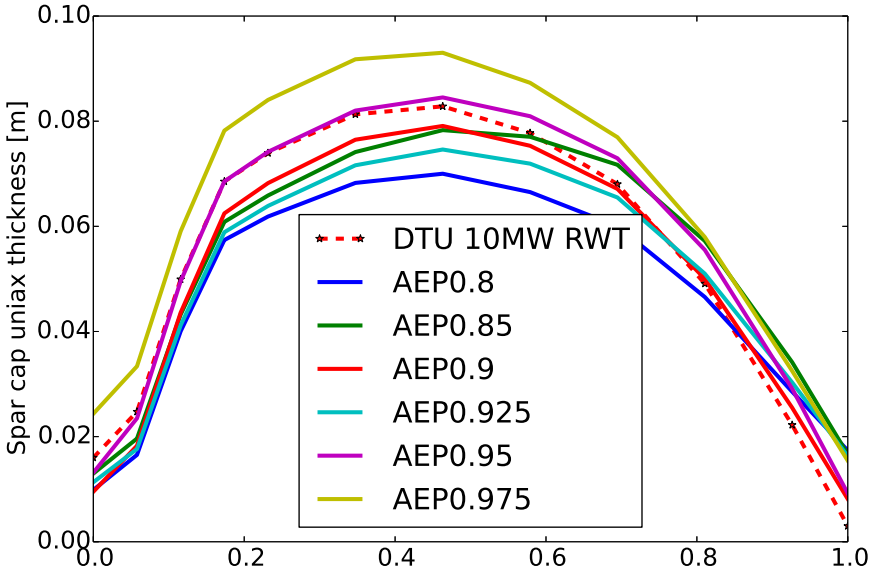

Figure 11. Blade spar cap thickness distribution for the test case 2 designs.

V.C. Test case 3: Shape and structural Optimization with Fatigue Constraints

This test case is based on the optimization problems presented in test case 2, therefore it includes both shape and structural design variables. This case has two additional constraint, one on the fatigue damage of the tower bottom longitudinal bending moment and one on the fatigue damage of the rotor speed. A reduction of the tower base load can be beneficial for the design of an off-shore wind turbine sub-structure and therefore it can reduce the cost of energy. The constraint on the fatigue of the rotor speed is included to avoid that the rotor speed variations increase. The fatigue constraint on the tower load imposes a lower fatigue damage than the one of the baseline design, therefore it is violated at the beginning of the optimization. The fatigue has been added as a constraint so that the cost function is not modified and a better comparison of the designs obtained can be performed. However, this choice undermine the optimization problem because the optimization algorithm has to find first a feasible solution, leading to a slower convergence. The fatigue is estimated based on a spectral method and a linear model computed with HAWCStab2. The linear model is in closed-loop configuration therefore it includes the wind turbine controller. In this test case the tuning of the controller is not modified, and the tuning of the reference model is used throughout the optimization. Two cases are tested with two different level of fatigue damage reduction for the tower base, 5% and 10%. the constraint on the rotor speed is set so that it does not increase compare to the reference design one. These cases are labeled *Fatigue 5%* and *Fatigue 10%* respectively. The fatigue is constrained only at 11 and $14m/s$. Both cases have $w = 0.9$ because in test case 2 it appeared to be a good compromise between AEP and blade mass.

Figure 12 shows the evolution of the optimizations both in term of objectives and constraints. Figure 12a) illustrates the variations at each minor iteration of the AEP and the mass with respect to the Pareto front computed in Test case 3. The results of AEP0.925, *Fatigue 5%*, and *Fatigue 10%* are shown. Both designs with the fatigue constraint fall inside to the Pareto front, showing that when the fatigue constraint is included it is more challenging to push the design towards lower mas or increase in AEP. *Fatigue 5%* has lower mass and lower AEP compared to *Fatigue 10%*, as all the designs of the Pareto front with a weight that favors the structural design to the aerodynamic one. Figure 12b) shows the reduction of the tower base longitudinal bending moment at each major iteration. Both optimizations terminate before the target fatigue constraint is achieved, however the error is lower than 1.5% in both cases.

Figure 13 shows the planforms of the optimized blades. Chord, twist, relative thickness and absolute thickness of the optimized models are plotted. Both designs with the fatigue constraints show a reduction of the chord in the outermost $20m$ of the blade, both compared to the reference design and the AEP0.925 case. This reduction in the chord length reduces the loading at the blade tip and therefore the thrust. In the central part of the blade *Fatigue 5%* has higher chord compared to the other optimized models. This is probably achieved to obtain high absolute thickness and therefore higher stiffnesses with lower mass. At the blade root all the models have a consistent blade chord reduction. The twist angle of all the models with the fatigue constraint is increased. *Fatigue 10%* has a surprising increase of the twist angle in the first half of the blade. This increase is obtained to achieve high lift coefficient in the inner part of the blade and compensate the reduction in loading at the blade tip. In the outer half of the blade all the optimized models reached

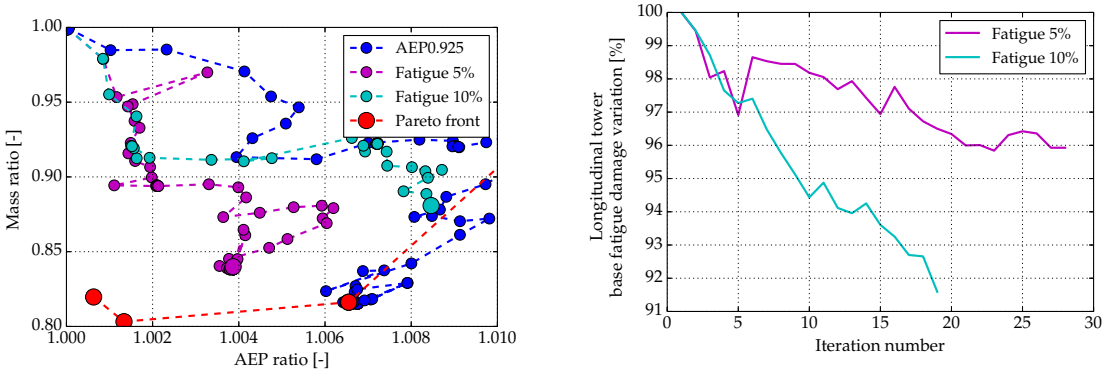

a) AEP and blade mass in the Pareto front.

b) Tower base longitudinal bending moment fatigue damage variation.

Figure 12. Iterations of Test case 3 optimizations.

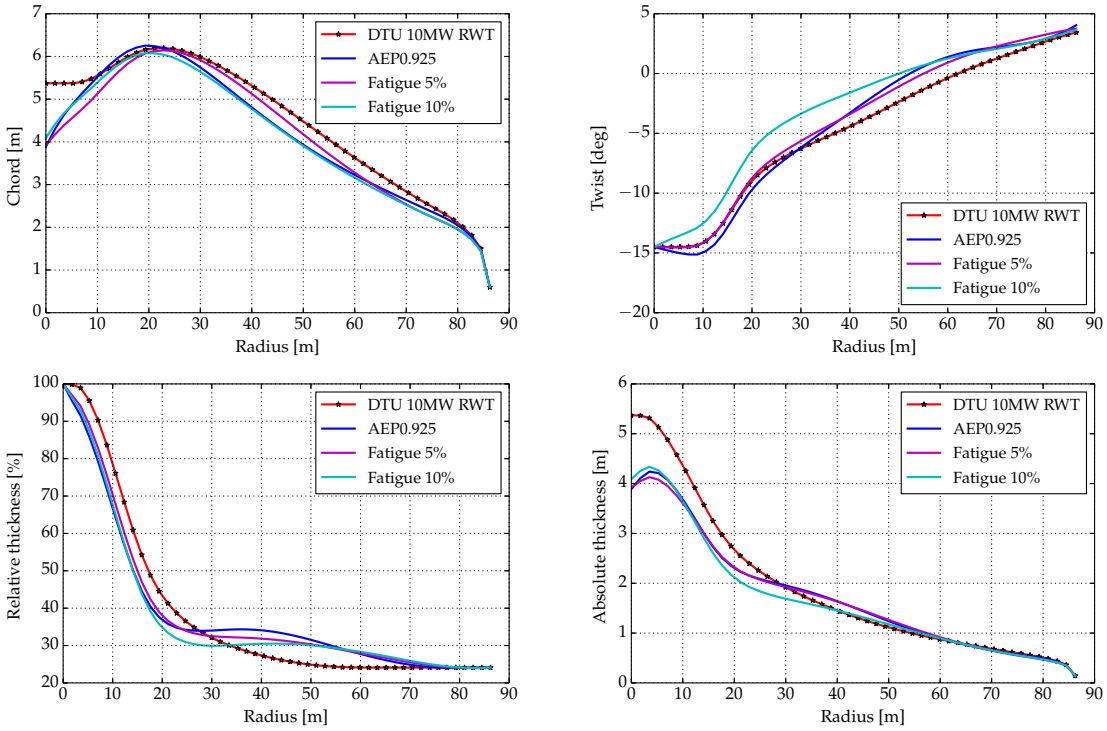

Figure 13. Optimized blade planforms for test case 3. Chord (up-left), twist (up-right), relative thickness (down-left), and absolute thickness (down-right).

higher relative thicknesses. The optimization favors thicker airfoils to increase the sectional stiffnesses and reduce mass. Among the optimized models, *Fatigue 10%* has the highest mass and lowest relative thickness, while AEP0.925 has lowest mass and highest relative thickness.

Figure 14 shows the blade steady-state loading of the reference and optimized models at $10.5m/s$. As noticed before, there is a tendency to move the blade loading from the tip to the root of the blade to reduce the fatigue loading. This tendency is clear from the normal forces and the tangential forces. Also AEP0.925 has a reduced maximum normal force. This reduction is achieved to satisfy the constraint on the maximum tip deflection when removing material from the layups and therefore mass. The tangential force is significantly increased in the first $25m$ of the blade in the optimized models. It appears that all the AEP increases are obtained thanks to higher performances in the inner half of the blade. The lift coefficients that are achieved in the inner part of the blade are significantly high. These values belongs to the airfoils polar but are unlikely to be achieved in normal operations, therefore lower performances are expected than here estimated.

Figure 15 shows the blade structural properties normalized with respect to the reference design. The flapwise stiffness is moved towards the central part of the blade in all the designs. Large reductions are obtained at the root due the the reduction in the chord. Between 20 and $50m$ the optimized model with higher stiffness correspond to the one with higher absolute thickness and the one with lower stiffness has the lower absolute thickness. Model *Fatigue 5%* and AEP0.925 have similar absolute thickness in this region, therefore the overall stiffness difference has to be obtained with a difference in the material layups. All the models show a reduction in the edgewise stiffness due to the reduction in the blade chord that reduces the moment of inertia. A consistent reduction of the torsional stiffness and the mass distribution are also obtained.

To verify the validity of the method here used to evaluate the fatigue damage a set of cases during normal operation are evaluated with the nonlinear aeroelastic code HAWC2.[24,26] Nine different wind speed between 10 and $26m/s$ are evaluated. For each wind speed three yaw angles are considered: 0, -10, and $10deg.$. For each yaw angle six turbulent seeds are evaluated. From these simulations the fatigue damage of the tower base longitudinal bending moment ad of the rotor speed are evaluated with the Rainflow counting method.

Figure 16 shows the reduction of the fatigue damage of the longitudinal tower base bending moment

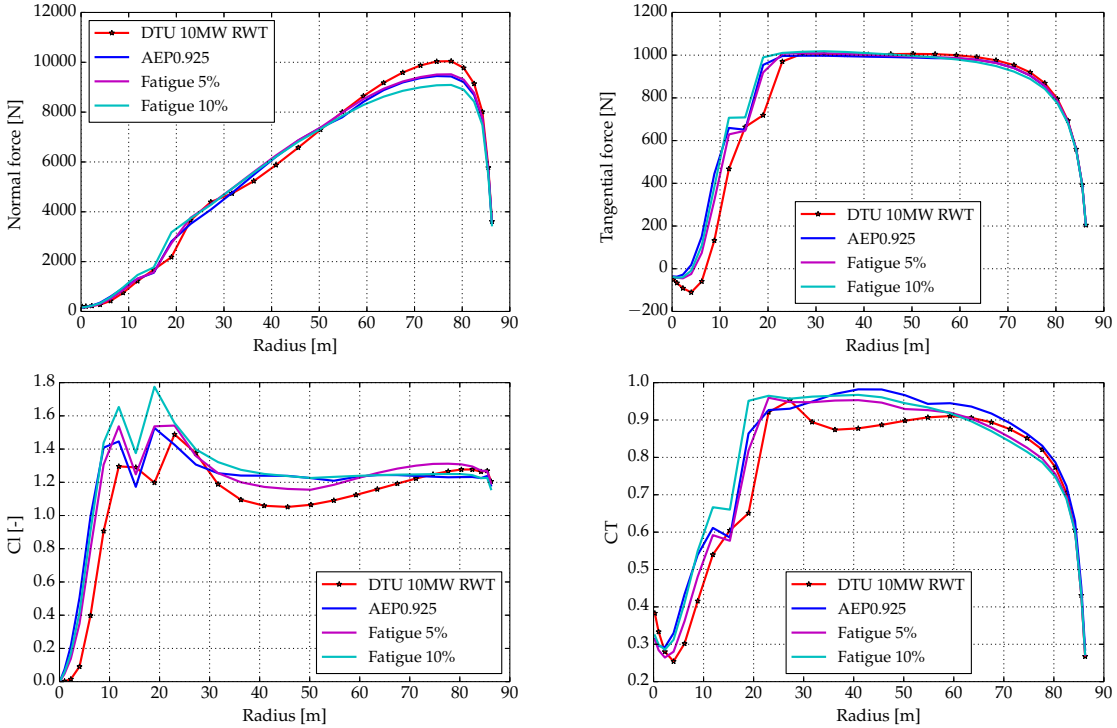

Figure 14. Optimized blade steady-state loading at 10.5m/s for test case 3. Normal force (up-left), tangential force (up-right), lift coefficient (down-left), and thrust coefficient (down-right).

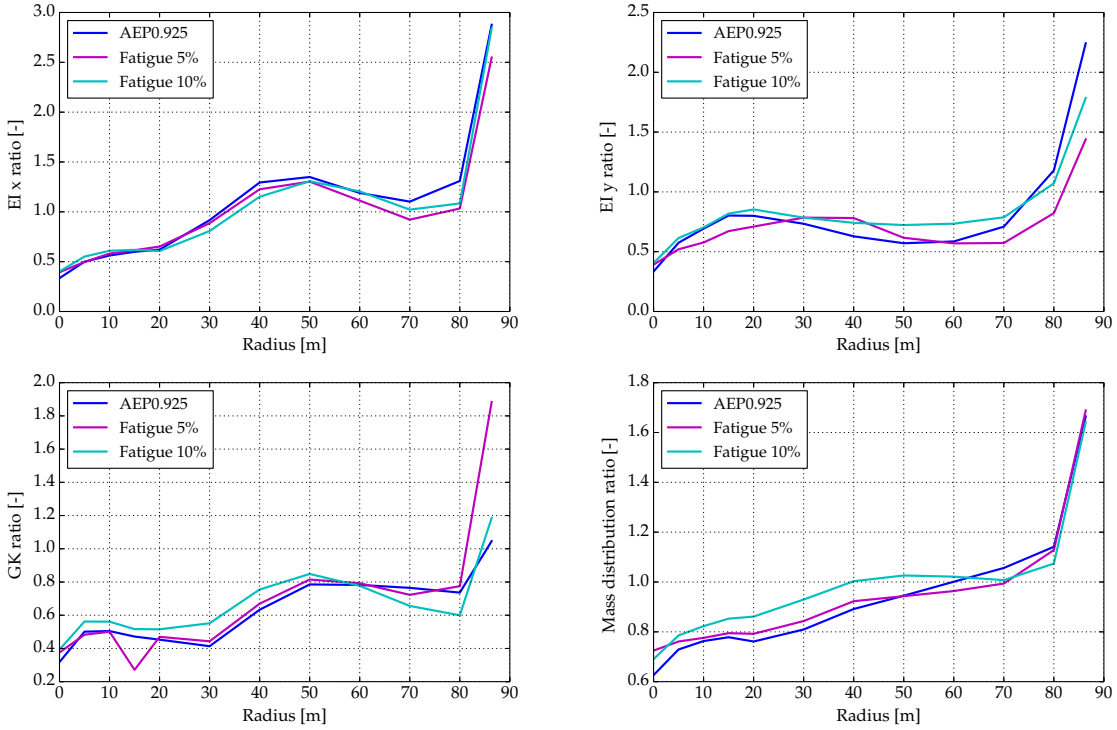

Figure 15. Optimized blade structural properties normalized with respect to the reference design for test case 3. Flapwise stiffness (up-left), edgewise stiffness (up-right), torsional stiffness (down-left), and distributed mass (down-right).

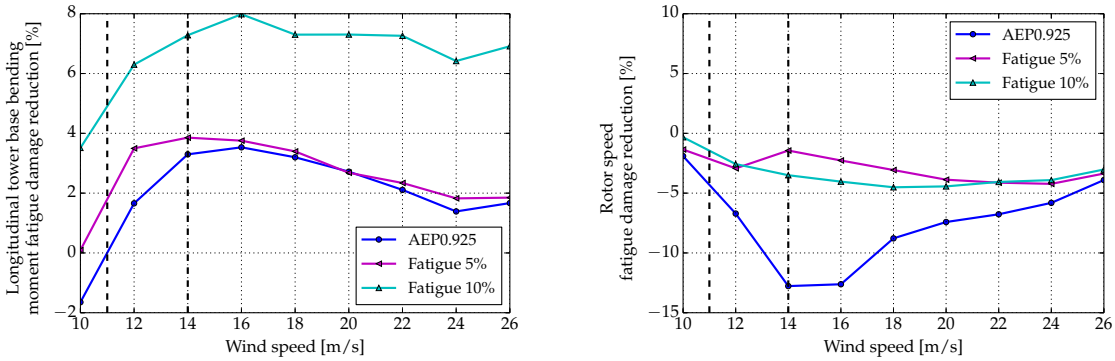

Figure 16. Fatigue damage equivalent load reduction with respect to the reference design. Tower base longitudinal bending moment and rotor speed. Values evaluated with nonlinear time domain simulations. Dashed vertical lines indicate the wind speed where the constraint is present in the optimization.

evaluated with time domain nonlinear simulations. The values shown in the plot confirm what was estimated with the simplified method used in the optimization framework. The figure shows also the variation of the rotor speed. It appears that the design without constraint on the fatigue has a significant increase of the rotor speed variation, on the other hand the designs where this parameter is constrained not to exceed the initial value the increase does not exceed 5%.

V.D. Test case 4: Shape and structural Optimization with Frequency Constraint

This final test case includes both shape and structural design variables. This case has an additional constraint on the position of the first forward whirling (FW) edgewise mode, to avoid resonance conditions with the external excitations, and a constraint on the minimum damping of the backward whirling (BW) edgewise mode. All the designs obtained in test case 2 show a significant reduction of the blade frequencies. In some cases the FW edgewise frequency coincides with the 6P external excitation. This condition should be avoided since can lead to high blade edgewise vibrations. A constraint on the aeroelastic frequencies can ensure that the final design will not be subject to resonant conditions and therefore the final design will not experience high blade loading. The constraint is implemented as a minimum distance that the frequency of the FW edgewise mode has to have from the 6P external excitation frequency. The target distance is 7%. The constraint on the mode damping is included to avoid designs with a very low damped edgewise mode that would lead to high fatigue damage loading. The damping ratio is set to be higher than 1%. Both constraints are applied at 14 and $25 m/s$. Also in this case the weight in the objective function is equal to 0.9. The obtained solution is denoted *Freq. constr.*.

Figure 17 shows the evolution of the optimization with respect to the Pareto front of test case 2. This new design locates far from the Pareto front but still it reaches a 10% reduction of the blade mass, and does not compromise the AEP.

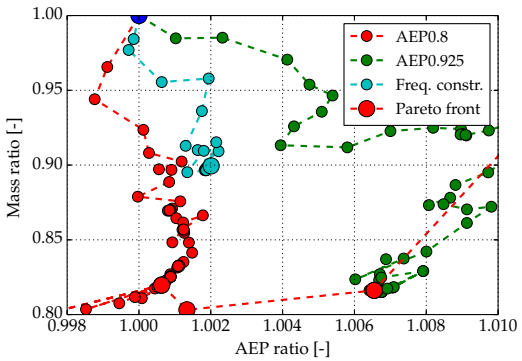

Figure 17. Iterations of Test case 4 optimizations.

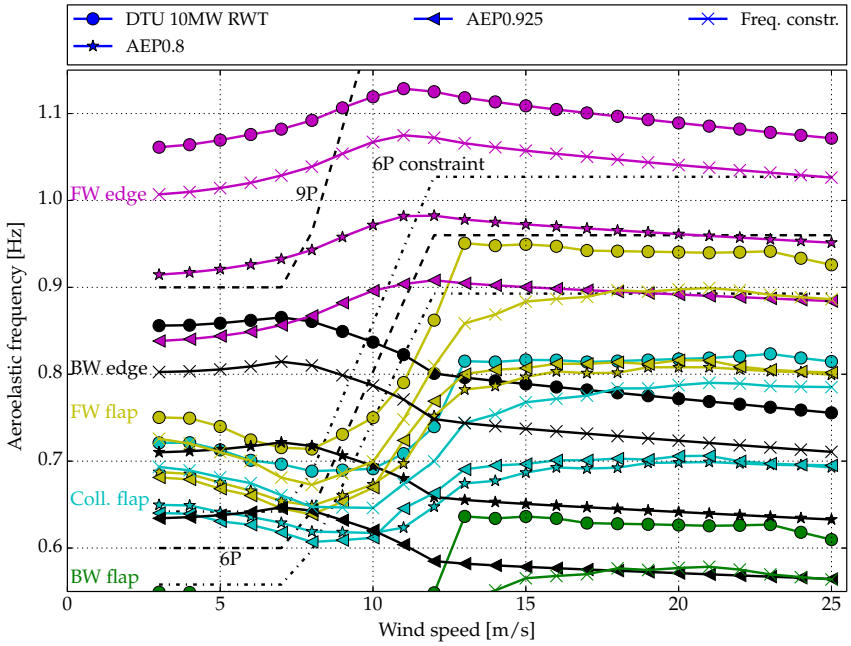

Figure 18. Wind turbine aeroelastic frequencies close to the 6P external excitation. Comparison between DTU 10MW RWT, AEP0.8, AEP0.925, and *Freq. Contr.*.

Figure 18 shows the wind turbine aeroelastic frequencies close to the 6P external excitation of designs DTU 10MW RWT, AEP0.8, AEP0.925, and *Freq. constr.*. The designs AEP0.8 and AEP0.925 are also included because they represent significant limits on the Pareto front. In the plot the first collective flapwise mode (Coll. flap.), the first FW flapwise mode (FW flap.), and the first FW and BW edgewise modes (FW edge and BW edge) can be seen. All the optimized models have a significant reduction in the values of the aeroealstic frequencies compared to the reference design. The frequency of the FW edgewise mode of AEP0.8 is overlapping the frequency of 6P external excitation above rated wind speed. AEP0.925 has the frequency of the FW edgewise mode that is sufficiently reduced to be lower than the 6P frequency. The frequency of *Freq. Constr.* hits the constraint at $25m/s$ and it is not further reduced.

Even if the constraint is based on the distance between the mode and the excitation frequency, and therefore it does not impose the mode frequency to be higher than the 6P frequency, the algorithm is not able to find a solution with a frequency lower than the 6P. This limitation is intrinsic of a gradient based algorithm. To further improve the design a different formulation of the constraint should be identified, or a the design with $w = 0.8$ should be started from the design of $AEP0.925$, so that the frequency is already lower than the 6P frequency.

Figure 19 shows the wind turbine aeroelastic damping ratio of the first edgewise backward and forward whirling modes. Above $15m/s$ the damping ratios of the BW edgewise mode of AEP0.8 and AEP0.925 are lower than the values of the reference model. The constraint on the damping of *Freq. Contr.* is active at $25m/s$. Between 15 and $24m/s$ the damping is lower than 1%, but in this region the constraint is not implemented.

The main advantage of constraining the position of the wind turbine aeroelastic frequencies and dampings is that it allows changing the wind turbine dynamic to control the fatigue loads during operations without evaluating nonlinear time domain simulations. A blade that has a higher damping or that has its blade edgewise mode frequencies sufficiently far from external excitations frequencies is likely to have lower fatigue loads. However in this investigation the design obtained is not evaluated with time domain simulations to verify the loading levels.

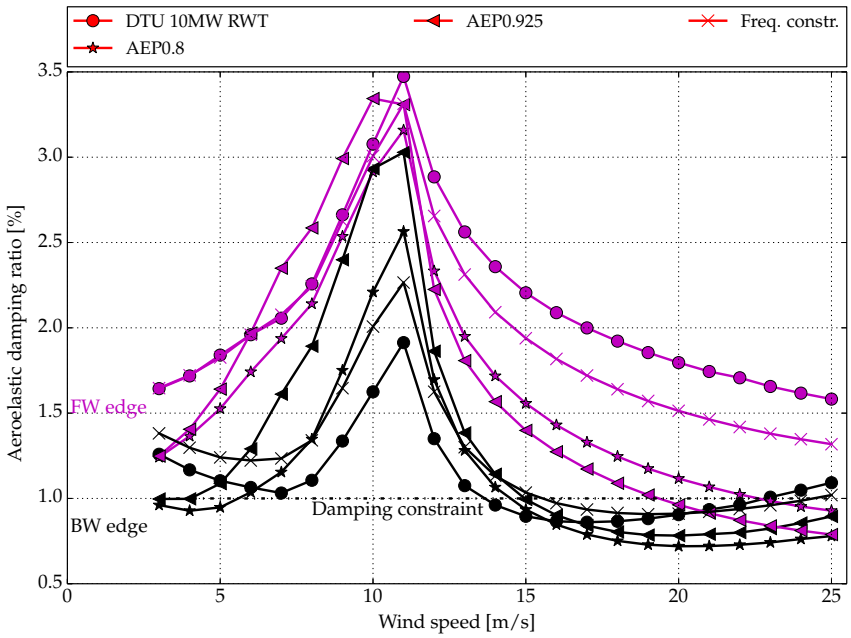

Figure 19. Wind turbine aeroelastic damping ratios of the first edgewise whirling modes. Comparison between DTU 10MW RWT, AEP0.8, AEP0.925, and *Freq. Contr.*.

VI. Discussion

The present results demonstrate the capabilities of the newly developed optimization framework, HawtOpt2 to enable concurrent optimization of both structure and aerodynamics of a wind turbine rotor as part of the conceptual design phase of a rotor. Compared to the sequential and manual design process used for the DTU 10MW RWT, the tool replaces a work cycle involving several people in charge of the aerodynamic, structural and aero-elastic design aspects, respectively, allowing for a much more comprehensive exploration of the complex aero-structural design space of a wind turbine rotor. A fully coupled optimization strategy thus efficiently helps map the inherent trade-offs between mass and AEP for the rotor, and produce conceptual designs that are significantly closer to a feasible design point than a traditional sequential approach would allow for. The ability to additionally place critical eigen frequencies and explicitly target fatigue reductions already in the conceptual design phase, presents a significant advancement over traditional sequential design processes.

Although the coupled designs vary according to the specific objectives and constraints specified, they have a number of common traits. All designs have a reduced chord and operate at higher lift coefficients than the baseline design, hitting the constraint of maximum allowable operational C_l. This tendency is likely to have been driven by the standstill extreme load case, for which loads and deflections are directly proportional to the chord. In fact, the fatigue constrained designs presented in Section V.C, reduce the chord even further, since also fatigue loads are proportional to the chord. This tendency suggests that airfoils with high relative thickness and high operational lift coefficient are desirable along the entire span of the blade. As shown by Bak et al.,[27] the FFA-W3 airfoils have relatively low design lift and are structurally biased with a large area for the spar cap. Bak concludes that high lift coefficient, low chord designs need to be designed with smaller structural box to achieve equivalent performance to the low lift alternatives. Using high lift airfoils in connection with the present design methodology would thus most likely enable further fatigue and extreme load reductions.

Except for the very AEP biased design *AEP0.975*, the coupled designs achieved significant weight savings in the root of the blade, reducing stiffness on the inner part of the rotor, while they all converged towards a higher flapwise stiffness at around mid-span, achieved primarily by increasing the thickness of the blade. Compared to the baseline DTU 10 MW RWT, the new designs thus employ airfoils of higher relative thickness across most of the mid and outer span, but achieve lower relative thickness on the inner part of the blade, regaining some of the efficiency lost on the mid part of the blade.

For the structure only optimizations presented in Section V.A, optimization towards a reduction of either mass or mass moment were shown. These results show that the two objectives lead to quite different designs, where the mass moment design leads to lower mass of the outer part of the blade, whereas the mass design focuses primarily on removing mass from the root. Although not demonstrated in this paper a mass moment objective is likely to be superior to the mass objective in relation to edgewise fatigue since these are driven by gravitational loads. It remains to be shown in future work that this is in fact true.

Results presented in Section V.C show the validity of employing the simplified method to evaluate the fatigue damage within a design procedure. The level of estimated fatigue of the final design is indeed confirmed with nonlinear aeroelastic simulations.

There are two important caveats to the present results which are:

1. Buckling is not taken into account in the structural design: This could mean that material would have to be reintroduced in the blade to overcome local buckling, although buckling is typically primarily overcome by adjusting the core thickness in the panels, which would not significantly increase mass.

2. All test cases use "frozen" extreme load cases corresponding to those from the baseline blade: Time dependent aeroelastic simulations were not carried out as part of the optimization. This means that the computed stresses only reflect the changes in thickness and not the changes in cross-sectional shape and assumes that the optimized designs will not exhibit significant increases in extreme loads.

These two points remain subjects of future work.

VII. Conclusions anf Future Work

This article presented a newly developed multi-disciplinary optimization tool for wind turbines named HawtOpt2, which enables simultaneous optimization of both structure and outer geometry of a wind turbine rotor. The framework interfaces to a number of state-of-the-art analysis codes, which allows for conceptual design exploration to a very high level of fidelity and feasibility.

A series of test cases were presented in which different aspects of the design problem were explored.

As the most simple case, Section V.A presented two optimized designs of the baseline DTU 10MW RWT for which the internal structure was optimized for minimum mass and minimum mass moment, respectively. This study showed that while optimizing for mass leads to an 18% lighter blade, the mass was primarily removed from the root, whereas optimizing for mass moment tends towards removing mass further out board, which is favourable for reducing fatigue loads. The latter design achieved a 13% reduction in mass moment and a mass reduction of 9%.

In the second set of test cases both outer shape and internal structure were optimized for achieving both a reduction in mass as well as an increase in AEP, which are conflicting objectives. A pareto study showed that a reduction in mass of 20% is achievable relative to the DTU 10MW RWT, achieving an increase of 0.6% in AEP. Further decrease in mass were only marginal at the expense of significant reductions in AEP. Oppositely, an increase in AEP could be achieved up to 1.7% at the cost of increase in mass of 10%. The overall tendency of these designs was to increase relative thickness and design operational lift coefficients, resulting in a more slender design.

The third test cases showed that when including fatigue constraints in the design achieved is modified. The fatigue constraint limits the blade mass reduction to 15% and 12%, and it leads to different AEP levels. The fatigue reduction targets are not fully achieved but significantly improvements are obtained. The fatigue load reductions are also confirmed with nonlinear time domain simulations on the final design.

The fourth test case showed that when limiting the positions of the wind turbine aeroelastic frequencies a lower blade mass reduction is achieved. The constraint limit the blade mass reduction to 10% but it ensures that a resonance condition does not occur. A different formulation of the constraint should be identified to allow the constrained wind turbine frequency to jump on the opposite side of the avoided frequency range.

References

[1]Fuglsang, P., Bak, C., Schepers, J. G., Bulder, B., Cockerill, T. T., Claiden, P., Olesen, A., and van Rossen, R., "Site-specific Design Optimization of Wind Turbines," *Wind Energy*, Vol. 5, No. 4, 2002, pp. 261–279.

[2]Bottasso, C. L., Campagnolo, F., and Croce, A., "Multi-disciplinary constrained optimization of wind turbines," *Multibody System Dynamics*, Vol. 27, No. 1, Jan. 2012, pp. 21–53.

[3]Ashuri, T., Zaaijer, M. B., Martins, J. R. R. A., van Bussel, G. J. W., and van Kuik, G. A. M., "Multidisciplinary design optimization of offshore wind turbines for minimum levelized cost of energy," *Renewable Energy*, Vol. 68, Aug. 2014, pp. 893–905.

[4]Merz, K. O., "Rapid optimization of stall-regulated wind turbine blades using a frequency-domain method: Part 1, loads analysis," *Wind Energy*, July 2014, pp. n/a–n/a.

[5]Merz, K. O., "Rapid optimization of stall-regulated wind turbine blades using a frequency-domain method: Part 2, cost function selection and results," *Wind Energy*, March 2014, pp. n/a–n/a.

[6]Fischer, G. R., Kipouros, T., and Savill, A. M., "Multi-objective optimisation of horizontal axis wind turbine structure and energy production using aerofoil and blade properties as design variables," *Renewable Energy*, Vol. 62, No. 0, 2014, pp. 506 – 515.

[7]Andrew Ning, S., Damiani, R., and Moriarty, P. J., "Objectives and Constraints for Wind Turbine Optimization," *Journal of Solar Energy Engineering*, Vol. 136, No. 4, June 2014, pp. 041010.

[8] "http://openmdao.org," 2012.

[9]Blasques, P., "User s Manual for BECAS A cross section analysis tool for anisotropic and inhomogeneous beam sections of arbitrary geometry e Pedro Blasques," 2012.

[10]Blasques, J. P. and Stolpe, M., "Multi-material topology optimization of laminated composite beam cross sections," *Composite Structures*, Vol. 94, No. 11, 2012, pp. 3278 – 3289.

[11] "http://becas.dtu.dk/," .

[12] "http://hawcstab2.vindenergi.dtu.dk/," .

[13]Bak, C., Zahle, F., Bitsche, R., Kim, T., Yde, A., Henriksen, L. C., Andersen, P. B., Natarajan, A., and Hansen, M., "Design and Performance of a 10 MW Wind Turbine," *To be submitted*, July 2013.

[14] "http://dtu-10mw-rwt.vindenergi.dtu.dk/," .

[15]Moore, K., Naylor, B., and Gray, J., "The Development of an Open-Source Framework for Multidisciplinary Analysis and Optimization," *10th AIAA/ISSMO Multidisciplinary Analysis and Optimization Conference*, AIAA, Victoria, Canada, Aug. 2008, AIAA 2008-6069.

[16]Gray, J. S., Moore, K. T., and Naylor, B. A., "OPENMDAO: An Open Source Framework for Multidisciplinary Analysis and Optimization," *13th AIAA/ISSMO Multidisciplinary Analysis and Optimization Conference, Fort Worth, TX, AIAA, AIAA-2010-9101*, AIAA, Fort Worth, Texas, Aug. 2010.

[17]Heath, C. M. and Gray, J. S., "OpenMDAO: Framework for Flexible Multidisciplinary Design, Analysis and Optimization Methods," *8th AIAA Multidisciplinary Design Optimization Specialist Conference (MDO)*, Honolulu, Hawaii, 2012, pp. 1–13.

[18] "http://pyopt.org/," .

[19] "http://fusedwind.org/," .

[20]Hansen, M. H., "Aeroelastic stability analysis of wind turbines using an eigenvalue approach," *Wind Energy*, Vol. 7, No. 2, 2004, pp. 133–143.

[21]Hansen, M. H., "Aeroelastic Properties of Backward Swept Blades," American Institute of Aeronautics and Astronautics, Orlando, Florida, 2011, pp. 1–19.

[22]Snderby, I. and Hansen, M. H., "Open-loop frequency response analysis of a wind turbine using a high-order linear aeroelastic model," *Wind Energy*, Vol. 17, No. 8, 2014, pp. 1147–1167.

[23]Tibaldi, C., Henriksen, L. C., Hansen, M. H., and Bak, C., "Wind turbine fatigue damage evaluation based on a linear model and a spectral method," *Under review*, 2014.

[24] "http://www.hawc2.dk/," .

[25]Lambe, A. B. and Martins, J. R. R. A., "Extensions to the Design Structure Matrix for the Description of Multidisciplinary Design, Analysis, and Optimization Processes," *Structural and Multidisciplinary Optimization*, Vol. 46, 2012, pp. 273–284.

[26]Larsen, T. J. and Hansen, A. M., "How 2 HAWC2, the user's manual," Tech. Rep. Ris-R-1597(ver. 4-5)(EN), Ris National Laboratory, 2014.

[27]Bak, C., Gaudern, N., Zahle, F., and Vronsky, T., "Airfoil design: Finding the balance between design lift and structural stiffness," *Journal of Physics: Conference Series (Online)*, Vol. 524, 2014, Content from this work may be used under the terms of the Creative Commons Attribution 3.0 licence. Any further distribution of this work must maintain attribution to the author(s) and the title of the work, journal citation and DOI. Published under licence by IOP Publishing Ltd.

Report I: Methods for Automatic Tuning of Wind Turbine Controllers

DTU Wind Energy

Methods for systematic tuning of wind turbine controllers

Department of Wind Energy Report 2015

Carlo Tibaldi, Morten Hartvig Hansen and Frederik Zahle

DTU Wind Energy E-0100

December 2015

DTU Vindenergi
Institut for Vindenergi

Author(s): Tibaldi C, Hansen MH, Zahle F
Title: Methods for Automatic Tuning of Wind Turbine Controllers
Institute: Department of Wind Energy

Summary (max. 2000 char.):
Automated methods for wind turbine controller tuning can be useful to obtain a first estimation of the controller gains. Furthermore, these techniques can be employed within a multidisciplinary design procedure allowing for concurrent aeroservoelastic design. This report presents two methods to systematically tune the gains of the PI pitch controller of the Basic DTU Wind Energy Controller. The first method is based on pole-placement technique and the second on fatigue loads reduction. Both methods require linear models of a wind turbine that are obtained with HAWCStab2. These techniques are solved with numerical optimization.
The frequency placement method shows improvements compared to the state-of-the-art method but only when the model complexity is low. Tuning with load based method shows that different compromises between tower loads and rotor speed regulations can be achieved.

Report Number: DTU Wind Energy E-0100
Publication Date: December 2015

ISBN: 978-87-93278-56-1

Pages: 22
Tables: 2
Figures: 7
References: 24

Technical University of Denmark
DTU Wind Energy
Frederiksborgvej 399
4000 Roskilde
Denmark

Contents

1 Introduction

Tuning of wind turbine controllers is an important and delicate step of the controller design. This process is often performed with manual trial and error iterations where the gains are changed until the response of the controlled system satisfies the requirements. Automated methods can be useful to obtain a first estimation of the controller tuning of a new wind turbine design since they do not require manual iterations and a detailed knowledge of the controller and of the effect of the gains on the response. Furthermore, systematic techniques can be employed within a multidisciplinary design procedure allowing for concurrent aeroservoelastic design.

In wind energy applications, a method to tune a wind turbine proportional integral PI controller with a pole-placement technique is presented by Øye [1]. This method can be used to tune the PI pitch controller and the PI generator torque controller. In this approach, the wind turbine is represented with a single degree of freedom model of the rigid body rotor rotation. The reduced turbine model is then connected with a simple model of the PI controller obtaining a formulation of the closed-loop system. The gains of the controller are then selected to obtain a desired frequency and damping of the mode associated with the controlled rotor rotation, the regulator mode. Because the model is represented by a second order equation, a closed system can be derived to obtain the gains analytically at one wind speed. In the case of the PI pitch controller, the gains are then modified with a gain-scheduling technique to account for the changes in the aerodynamic properties of the rotor when the wind speed changes. The gain-scheduling parameters can be obtained by polynomial fitting of aerodynamic properties of the rotor as function of the pitch angle. This method has the advantage of retrieving a controller tuning with a direct approach and no iterations. However, the simplified model sets some limits. As shown in the works by Hansen [2] and Tibaldi et al. [3], when the tuning obtained with the single degree of freedom model is used on a high-order wind turbine model, the position of the regulator mode does not satisfy the target requirements. The interaction with other wind turbine components leads, indeed, to a drift of the regulator mode frequency and a reduction of its damping. The filter on the rotor speed feed-back is largely responsible for the latter.

One of the main drawbacks of pole-placement techniques is that they require the selection a priori of the frequency and damping of the regulator mode. The former has to be selected somewhere below the first tower modes frequencies, the latter is usually selected close to a damping ratio of 70 %. To obtain a method to tune a controller that is free from parameters chosen a priori, a procedure based on loads minimization can be employed. The tuning of a PI pitch controller involves the identification of a balance between tower loads and rotor rotational speed variations. The rotor speed should be as constant as possible to guarantee a regular power output. To achieve this quality in power production a high pitch activity is required to react quickly to the changes of the wind speed. On

the other hand, a high pitch activity affects also the aerodynamic thrust that is the main responsible for the longitudinal tower loadings. Therefore, an aggressive tuning has small rotor speed variations but high tower loading and a soft tuning leads to higher rotor speed variations and lower tower loads.

Two different methods for systematic controller tuning are here presented and discussed: a pole-placement technique of the regulator mode based on high-order models, and a method for fatigue loads reduction.

Both methods are based on linear high-order models of the wind turbine, therefore they do not require time domain simulations. The linearized models used in this investigation are obtained with the aeroservoelastic code HAWCStab2 [4]. Numerical optimization techniques need to be used in both approaches to obtain the set of tuning gains. The optimizations are all performed with a framework developed with OpenMDAO [5].

In the fatigue method, the load is evaluated in frequency domain from the transfer function of the linear model at different operational points. The technique to evaluate the fatigue is described in details by Tibaldi et al. [6].

The DTU Wind Energy 10 MW Reference Wind Turbine [7, 8, 9] is used throughout the investigation.

2 Methods and Models

This section contains a description of the methods and models used in this investigation.

2.1 Controller Gains

This investigation focuses on the gains of the proportional integral (PI) pitch controller on the rotor speed feedback of the Basic DTU Wind Energy Controller [10]. However, both methods are general and can be applied to any linearized controller.

The controller gains are defined as:

$$k_P = k_{P,0}\ \eta_K + k_{P,0,\Omega}\ \eta_K\ \eta_{K,\Omega} \qquad\qquad k_I = k_{I,0}\ \eta_K \tag{2.1}$$

where $k_{P,0}$, $k_{P,0,\Omega}$, and $k_{I,0}$ are constant gains, and η_K and $\eta_{K,\Omega}$ are gain-scheduling parameters function of the low-pass filtered measurement of the pitch angle. The gain-scheduling parameters are defined as:

$$\frac{1}{\eta_K} = 1 + \frac{\Theta}{K_1} + \frac{\Theta^2}{K_2} \qquad\qquad \eta_{K,\Omega} = 1 + \frac{\Theta}{K_{1,\Omega}} + \frac{\Theta^2}{K_{2,\Omega}} \tag{2.2}$$

where Θ is the pitch angle and K_1, K_2, $K_{1,\Omega}$, and $K_{2,\Omega}$ are constant.

The parameters K_1, K_2, $K_{1,\Omega}$, and $K_{2,\Omega}$ define the gain-scheduling. The gain-scheduling is required to take into account the changes in the aerodynamic characteristics of the rotor above rated wind speed and to achieve uniform controller performances.

The gain-scheduling parameters can be estimated analytically by fitting of the steady state aerodynamic gain and the aerodynamic damping. The aerodynamic gain is the partial derivative of the aerodynamic torque with respect to the pitch angle, the aerodynamic damping is the partial derivative of the aerodynamic torque with respect to the rotational speed. These derivatives are derived as quasi-steady gradients from the velocity triangles and derivatives of profile coefficients along the blade span, and not from the gradients of the power coefficient surface which would include the slow effect of dynamic inflow [11].

The scheduling technique implemented in the Basic DTU Wind Energy controller follows the one proposed by Øye [1] and extended in Tibaldi et al [3].

2.2 Numerical Pole-placement Technique

When tuning a controller with a pole-placement technique, the frequency and damping of the mode associated with the controlled rotor rotation, the regulator mode, are imposed to specific values, chosen a-priori, adjusting the the controller gains. To achieve this, linear models of the wind turbine in closed-loop are required to compute the frequencies and dampings from the eigenvalues.

This method requires two models, a full high-order model (evaluation model) and a reduced model (tuning model). The full high-order model is used to evaluate the quality of the tuning. The reduced model is employed in the tuning procedure to obtain the gains.

If the reduced model employed is very simple, an analytical formulation of all the controller parameters can be derived. An analytical formulation allows to directly compute the controller gains without iterative methods. However, when the model used for the placement has a higher order, numerical methods need to be used to estimate the gains. Better performances should be achieved on the full high-order model because the differences between the tuning model and the evaluation model are smaller. On the other hand when the tuning model has many states, the identification and selection of the regulator mode among all the modes is not trivial.

2.3 Fatigue-based Method

There are two main drawbacks when performing numerical optimization based on loads evaluated with nonlinear aeroservoelastic simulations: the computational time and the uncertainty of the results due to the stochastic turbulent wind. Time domain simulations are usually very time consuming to be integrated in a design procedure, especially if they are performed at each cost function evaluation. Since an optimization can require several hundreds of cost function evaluations, the computational time of the objective should be limited, so that a solution can be achieved within an acceptable time. When loads are evaluated from simulations with turbulent inflow the amount of turbulent seeds that are used can significantly affect the design and alter the convergence of the algorithm. An investigation on the uncertainty of the results is presented by Tibaldi et al. [12].

In this work, the loads are evaluated with a frequency domain method so that the limitations mentioned above are partially overcome. The method utilizes a linear model of the wind turbine in closed-loop configuration to compute the transfer function from the wind input to a desired sensor. The transfer function is then combined with the power spectra of the wind to obtain the power spectra of the output. A spectral method is finally applied to the output to obtain an estimation of the fatigue damage of the sensor. A detailed description of the method is presented by Tibaldi et al.[6]. An application of the method is shown by Zahle et al.[13].

Loads evaluated with this approach should also be verified with nonlinear time domain simulations. In this work the aeroservoelastic code HAWC2 [14, 15] is used for this purpose.

2.4 Linear Models

The open-loop wind turbine models are obtained with HAWCStab2, a tool developed at DTU Wind Energy. HAWCStab2 is an improved version of HAWCStab [16] with a different kinematic formulation. The model is an analytical linearization of a nonlinear finite beam element model using a co-rotational element formulation. The beam model is coupled with an unsteady blade element momentum model of the blade aerodynamics including shed vorticity, dynamic stall, and dynamic inflow [17]. A validation and analysis of the open-loop performances are provided by Sønderby and Hansen [18] for a version of HAWCStab2 without the present dynamic inflow model.

In this investigation, the linearized controller equations are implemented in a Python routine and evaluated each time the controller gains are changed. The controller model is a simplified linearization of the Basic DTU Wind Energy Controller, described by Hansen and Henriksen [10]. A description of the linear controller is presented by Tibaldi et al. [6].

2.5 Optimization Problems

The numerical optimization problems that are solved are defined as:

$$\begin{aligned} \underset{\boldsymbol{x}}{\text{minimize}} \quad & f(\boldsymbol{x}) \\ \text{subject to} \quad & \boldsymbol{g}(\boldsymbol{x}) \leq \boldsymbol{0} \end{aligned} \tag{2.3}$$

A scalar nonlinear cost function f is minimized changing a set of variables $\boldsymbol{x}$. The variables are the normalized gains $k_{P,0}$, $k_{I,0}$, and $k_{P,0,\Omega}$ and the gain-scheduling parameters K_1, K_2, $K_{1,\Omega}$, and $K_{2,\Omega}$. All these variables are normalized by the initial value used in the optimization and obtained with the single degree of freedom model proposed by Øye [1].

The objectives function used for the pole-placement differs from the one used for the fatigue-based tuning.

The objective of the pole-placement is to achieve uniform performances throughout the rated region, therefore the regulator mode is required to have same frequency and damping at all wind speeds. The regulator mode is identified at each wind speed selecting the mode that has the smallest error, defined as:

$$e_i = \sqrt{\left(\frac{\boldsymbol{\omega}_i - \tilde{\omega}}{\tilde{\omega}}\right)^2 + \left(\frac{\boldsymbol{\xi}_i - \tilde{\xi}}{\tilde{\xi}}\right)^2} \tag{2.4}$$

where ω_i and ξ_i are the system modes frequency and damping ratio at the wind speed with index i and $\tilde{\omega}_i$ and $\tilde{\xi}_i$ are the target regulator mode frequency and damping ratio. Before computing the error e_i, the modes with a damping ratio higher than 98 % are removed from the set of the system modes.

The objective function f is defined as the norm of the frequency and damping error with respect to the target values

$$f = \sqrt{\sum_{i}^{n}\left(\frac{\omega_i - \tilde{\omega}}{\tilde{\omega}}\right)^2 + \sum_{i}^{n}\left(\frac{\xi_i - \tilde{\xi}}{\tilde{\xi}}\right)^2} \tag{2.5}$$

where ω_i and ξ_i are the regulator mode frequency and damping ratio at the wind speed with index i and $\tilde{\omega}_i$ and $\tilde{\xi}_i$ are the target regulator mode frequency and damping ratio. No weight is considered between the errors on the frequencies and the damping ratios because they are here considered of equal importance.

The objective of the fatigue-based optimization is to minimize the fatigue damage load of the tower base longitudinal bending moment.

$$f = \sqrt{\frac{1}{n}\sum_{i}^{n}\left(\frac{del_i}{\tilde{del}_i}\right)^2} \tag{2.6}$$

where del_i is the damage fatigue load at the wind speed with index i, and $\tilde{del}_i$ is the load of the same sensor of the initial design.

The pole-placement problem does not contain any constraints. The fatigue-based optimization has a constraint that bounds the variations of the rotor speed standard deviation not to increase compared to the reference initial value, and a constraint to avoid the damping ratio of the regulator mode to be higher than a fixed value. The damping ratio is evaluated on a single degree of freedom model of the wind turbine. The constraints are added to avoid the optimization to increase excessively the damping of the regulator mode, that would lead to a slow rotor speed regulation.

2.6 Optimization Framework

The optimizations performed in this investigation are carried out with a framework based on the open-source tool OpenMDAO (Open-source Multidisciplinary Design, Analysis, and Optimization framework) [5, 19, 20, 21]. OpenMDAO provides an interface and tools to help setting up MDAO problems, managing directly data and work flows.

The framework is coupled with the optimization package PyOpt [22] that includes a large variety of optimization algorithms, here the algorithm SNOPT [23, 24] is used.

An application of the framework used to interface OpenMDAO with HAWCStab2 is described by Zahle et al. [13].

3 Results

3.1 Pole-placement

This section shows results of the pole-placement obtained with five different models with increasing order. The five models used for the tuning are:

SDOF single degree of freedom or two states model of the rigid rotor rotation as described by Øye [1];

Model 1 twelve states model including: the rigid rotor rotation, the second-order low pass filter on the rotor speed feedback, the second order band stop filter on the drivetrain frequency, and three second order models of the pitch actuators;

Model 2 same as *Model 1* with the addition of degrees of freedom for blade flexibility;

Model 3 same as *Model 2* with the addition of state variables for the unsteady blade aerodynamics;

Model 4 same as *Model 3* with the addition of state variables for dynamic inflow.

All the gains are computed numerically, except for *SDOF* model. All the linearized models are obtained at the same steady operational conditions that are evaluated including blade deflection. In the case of models *SDOF* and *Model 1* the degrees of freedom associated with the blades deformations are removed after the computation of the steady states, i.e., the blades are deflected in the stationary steady state in an assumed uniform inflow, but vibrations about this mean operational state are neglected.

The target value of the natural frequency is 0.06 Hz and of the damping ratio is 70 %. The frequencies and dampings are evaluated at five wind speeds in the objective function (Equation (2.5)), 11, 14, 17, 20, and 23 m/s.

The size of the models used in the tuning differs significantly due to the different order. Therefore, the computational time required to reach a solution is different from model to model. The computations with models *Model 1* and *Model 2* last few seconds and 30 minutes respectively. On the other hand, the larger models *Model 3* and *Model 4* take approximately 2 and 3 hours, respectively.

Table 3.1 shows the variation of the controller gains obtained from the pole-placement method with the different models. The gains are normalized with respect to the gains obtained with the model *SDOF* that correspond to the initial solution of the optimization.

Figure 3.1 illustrates the proportional and integral gains of the controller obtained with the pole-placement method with the different models. The plotted gains are the actual PI

Table 3.1: Controller gains variation with respect to those obtained with model *SDOF*. *Model 1* (rigid turbine and filters), *Model 2* (filters and flexible rotor), *Model 3* (filters, flexible rotor, and unsteady aerodynamic), and *Model 4* (filters, flexible rotor, unsteady aerodynamic, and dynamic inflow).

	$k_{P,0}$	$k_{I,0}$	$k_{P,0,\Omega}$	K_1	K_2	$K_{1,\Omega}$	$K_{2,\Omega}$
SDOF	1.000	1.000	1.000	1.000	1.000	1.000	1.000
Model 1	0.883	0.750	0.772	0.937	9.874	0.350	1.396
Model 2	0.631	0.465	0.582	2.484	1.630	0.298	1.290
Model 3	0.620	0.420	0.788	1.729	1.413	0.897	0.985
Model 4	0.570	0.580	0.689	1.435	1.349	1.196	1.052

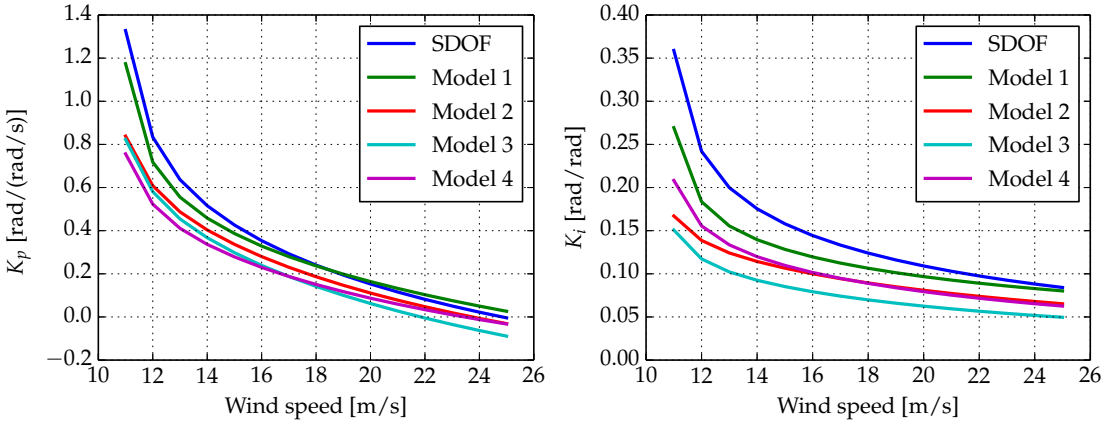

a) Proportional gain. *b) Integral gain.*

Figure 3.1: Proportional and integral gains. Comparison between the different models used for the tuning *SDOF* (rigid turbine), *Model 1* (rigid turbine and filters), *Model 2* (filters and flexible rotor), *Model 3* (filters, flexible rotor, and unsteady aerodynamic), and *Model 4* (filters, flexible rotor, unsteady aerodynamic, and dynamic inflow).

gains, described in Equation (2.1), therefore they include the gain-scheduling. For increasing wind speeds the aerodynamic damping increases, therefore, the proportional controller gain has to decrease for increasing wind speed to avoid the regulator mode damping to increase excessively. Similarly, also the integral gain has to decrease to keep the regulator mode frequency close to the desired values. When the model order is increased, the proportional gain is systematically decreased. On the other hand, the integral gain decreases for increasing model complexity except when the dynamic inflow model is included. In this case, the gain is higher than when only the dynamic stall is included (*Model 3*).

Figure 3.2 shows the damped frequency and damping ratio of the regulator mode of the models used for the tuning. The figure includes only the results of models *Model 1*, *Model 2*, *Model 3*, and *Model 4*, where the black dashed line is the target value. The results show the effectiveness of the optimization to minimize the cost function because the model used for the tuning and the evaluation are the same. The plots show that when the model is simple, and it has few degrees of freedom, the optimization finds a tuning that allows

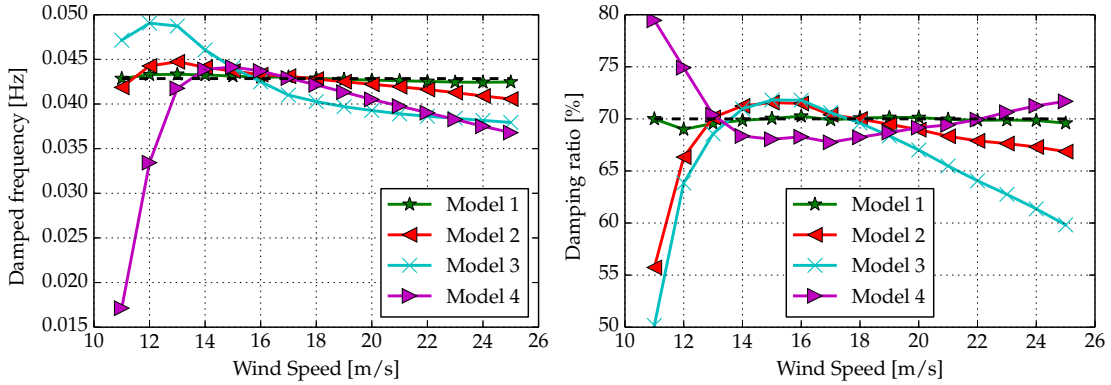

a) Damped frequency. *b) Damping ratio.*

Figure 3.2: Regulator mode frequency and damping evaluated with model used for the tuning. Comparison between the tuning obtained with models *SDOF* (rigid turbine), *Model 1* (rigid turbine and filters), *Model 2* (filters and flexible rotor), *Model 3* (filters, flexible rotor, and unsteady aerodynamic), and *Model 4* (filters, flexible rotor, unsteady aerodynamic, and dynamic inflow). The black dashed lines are the target values.

the regulator mode to coincide with the target one. When the model used for the tuning has a high-order, the discrepancy between the target frequencies and dampings and the evaluated ones increases. *Model 2* is able to achieve a good fitting of the target frequency, however, at low wind speed, the damping ratio obtained is lower than desired. When the unsteady aerodynamic is included (*Model 3*), the maximum difference on the frequency is almost 10 %, and the damping decreases both at low and high wind speeds. These gaps can be related to the inability of the gain-scheduling function to better fit the turbine characteristics. The gain-scheduling assumes a certain shape function to compensate the variations of the wind turbine properties, that apparently is not sufficient to capture the physics of the high-order models. *Model 4* has a different behavior than the other models. The damping of this model is higher than the target one at low and high wind speeds. The higher damping at low wind speeds reduces significantly also the value of the damped frequency.

Figure 3.3 shows the damped frequency and damping ratio of the regulator mode of the full high-order model for different tuning. The figure compares the results of the tunings obtained with models *SDOF*, *Model 1*, *Model 2*, *Model 3*, and *Model 4*. All the models except from *Model 4* have the regulator mode with frequency and damping very different from the one evaluated with the same model as in the tuning (Figure 3.2). These differences illustrate the effects of the different model complexity on the controller dynamic. The tuning obtained with *Model 1* is not able to guarantee the position of the regulator mode once the dynamic is evaluated with the full high-order model. At the lowest wind speed, the frequency is more than twice the target value, and the damping is significantly lower. When the rotor speed filter is included in the model for the tuning, an important improvement is obtained compared to the *SDOF* model. Indeed, the damping increases at all wind speeds. Models *Model 2* and *Model 3* show the effects of considering the blades deflection and the dynamic stall model in the tuning process. Despite these two models are already with a

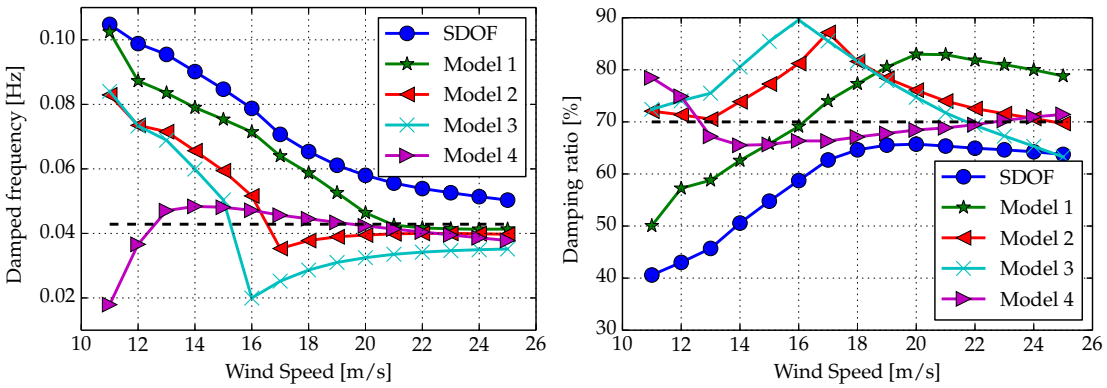

a) Damped frequency. *b) Damping ratio.*

Figure 3.3: Regulator mode frequency and damping evaluated with the full high-order model. Comparison between the tuning obtained with models *SDOF* (rigid turbine), *Model 1* (rigid turbine and filters), *Model 2* (filters and flexible rotor), *Model 3* (filters, flexible rotor, and unsteady aerodynamic), and *Model 4* (filters, flexible rotor, unsteady aerodynamic, and dynamic inflow).

high detail, the placement of the regulator mode is still far from the target values. The main advantage of these models is the increase of the minimum damping ratio. However, the frequency is also reduced, especially when also the dynamic stall model is included, leading to a slow controller dynamic. The frequency and damping of models *Model 2* and *Model 3* are non-smooth between 15 m/s and 17 m/s. Only once a model of the dynamic inflow is included in the tuning procedure, the regulator mode frequency and damping are more uniform.

To have a better understanding of the behavior of the regulator mode, the eigenvalues in its proximity are plotted in Figure 3.4. In the figure, the increasing marker size indicates increasing wind speed, with a wind step size of 0.3 m/s, and the different color distinguish the different tuning models. The regulator modes poles are those with an imaginary part close to 0.04 Hz at high wind speed. All the eigenvalues with an imaginary part lower than 0.005 Hz are associated with the dynamic inflow and dynamic stall models. An additional eigenvalue with an imaginary part close to 0.02 Hz is present. This pole is highly affected by the tuning and the dynamics of the inflow. The real part of the pole varies considerably when the wind speed increases, the mode is not present when frozen wake is assumed, and it is not so isolated from the other aerodynamic poles when the controller is not present. For models *SDOF* and *Model 1*, this eigenvalue has approximately a real part of -0.02 Hz and an imaginary part of 0.02 Hz at low wind speed, and for increasing wind speed its real part increases in absolute value. Interesting is the interaction of this mode with the regulator mode of model *Model 2*. When the real parts of this mode and the regulator mode are close to -0.06 Hz, the two poles attract each other and they separate again at higher wind speed. This interaction leads to the non smooth trend of the regulator mode damping of *Model 2* and *Model 3*, shown in Figure3.3. In the case of *Model 4*, this mode has a different behavior; it starts with a higher frequency and a real part close to -0.09 Hz and for increasing wind speeds its imaginary part decreases. This different behavior, compared with the two other models, raises the doubt on which mode is actually the regulator mode

for this tuning. Further investigations are required to better understand the nature of this additional mode and to identify which of these modes dominate the dynamic of the controller and therefore the dynamic of the rotor speed response.

From the investigation it appears that the dynamic inflow model, highly interacts with the regulator mode, affecting significantly the controller frequency and damping. Furthermore, if the dynamic inflow model is included in the tuning procedure, as for *Model 4*, the identification of the regulator mode among all the aeroservoelastic modes becomes non-trivial. Further effort should be spent to better understand the dynamics of the controller and dynamic inflow interaction and, therefore, better exploit this tuning technique.

3.2 Fatigue-based Method

This section presents the results of two test cases where the fatigue based method is used to tune the PI pitch controller.

The fatigue loads and the damping ratio are estimated and used in the objective function (Equation 2.6) and constraint at the wind speeds of 12, 14, 16, and 18 m/s. The cases have different constraints on the maximum damping ratio of the one degree of freedom model. In the first case, *Tuning 1*, the maximum damping ratio is 80 %, in the second case, *Tuning 2*, it is 95 %. *Tuning 1* achieves a objective function reduction of 1.01 %, *Tuning 2* of 2.06 %. Both solutions have the constraint on the rotor speed variation active at 12 m/s and the one on the damping ratio active at 18 m/s.

The gains obtained from this optimization are shown in Figure 3.5 and Table 3.2. Also the values of a reference tuning, that is the initial guess for the optimization, are illustrated. The reference tuning is obtained with pole-placement of a single degree of freedom model.

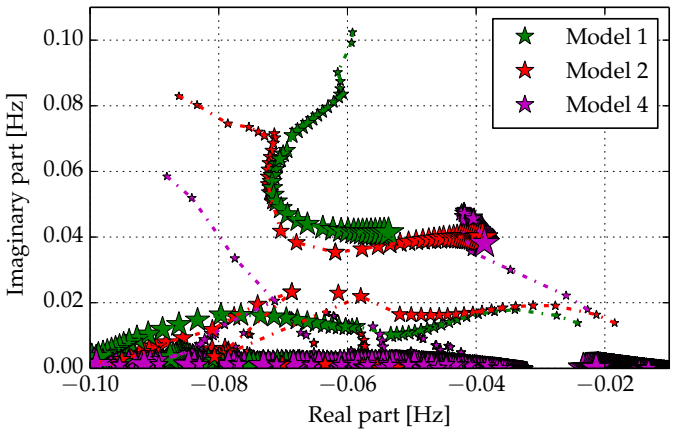

Figure 3.4: Full high-order model poles close to the regulator mode as function of the wind speed. Comparison between *Model 1* (rigid turbine and filters), *Model 2* (filters and flexible rotor), and *Model 4* (filters, flexible rotor, unsteady aerodynamic, and dynamic inflow). Increasing marker size means increasing wind speed. Wind step size: 0.3 m/s.

Table 3.2: Controller gains variation with respect to *Reference*. Comparison of *Tuning 1* and *Tuning 2* obtained with the fatigue-based method.

	$k_{P,0}$	$k_{I,0}$	$k_{P,0,\Omega}$	K_1	K_2	$K_{1,\Omega}$	$K_{2,\Omega}$
Ref.	1.000	1.000	1.000	1.000	1.000	1.000	1.000
Tuning 1	1.140	0.894	0.800	0.934	0.937	1.032	1.119
Tuning 2	11.059	0.702	1.400	0.823	1.858	1.216	1.940

Both proportional gains are higher than the reference one. *Tuning 1* is uniformly higher at all wind speeds. At low wind seed, *Tuning 2* is similar to the reference value and it becomes higher for higher wind speeds. On the other hand, the integral gains are both lower than the reference value.

Figure 3.6 shows the tower base longitudinal bending moment damage equivalent load evaluated with nonlinear time domain simulations. The figure shows the actual values for six different turbulence seeds and their mean values.

Figure 3.7 shows the tower base longitudinal bending moment and rotor speed fatigue damage variation with respect to the reference solution. The loads are evaluated with nonlinear time domain simulations. The variations in the tower loads are small and not uniform. *Tuning 2* achieves a load reduction that on average is 1 %, while *Tuning 1* almost does not affect the loads. On the other hand, the rotor speed variations are more significant. *Tuning 1* satisfies the constraint on the rotor speed in all the operational region, on the other hand *Tuning 2* has higher rotor speed variations in the first part of the region. These increases are not captured by the linear model used for the tuning. *Tuning 1* is faster (it has a lower damping ratio) compared to *Tuning 2* because it has a higher proportional gain, especially below 20 m/s. On the other hand, both tunings, have lower integral gain that means lower frequency of the regulator mode and, therefore, less aggressive regulation. The obtained loads are the result of a balance between these behaviors.

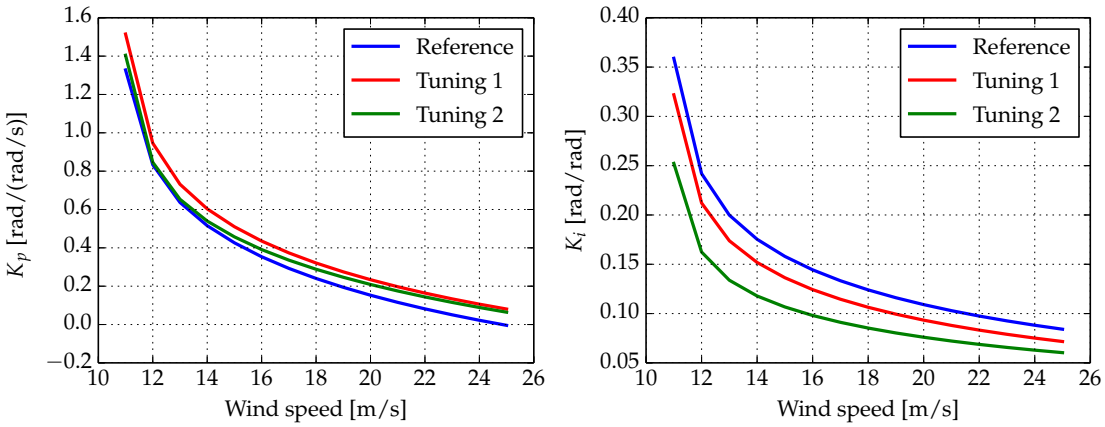

a) Proportional gain. *b) Integral gain.*

Figure 3.5: Proportional and integral gains. *Reference*, *Tuning 1*, and *Tuning 2* obtained with the fatigue-based method.

This investigation should be repeated evaluating the loads also at higher wind speeds. The focus should be on understanding if the loads can be reduced above 20 m/s since the obtained tunings lead to lower rotor speed variations.

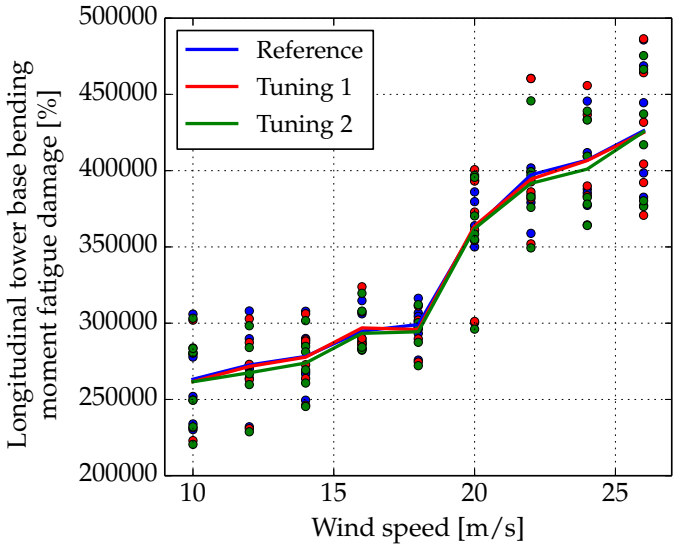

Figure 3.6: Tower base longitudinal bending moment damage equivalent load evaluated with HAWC2. Values and mean. Comparison between the *Reference* tuning, *Tuning 1*, and *Tuning 2*.

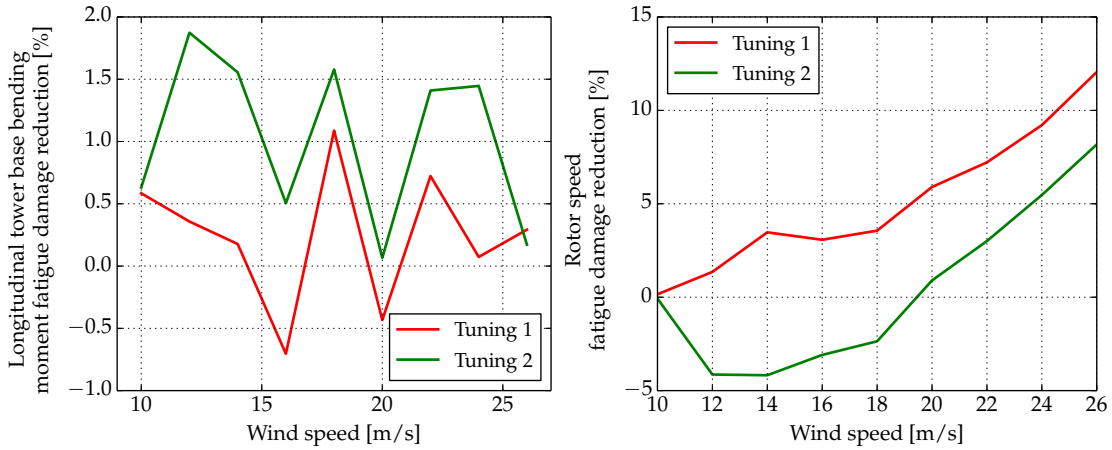

a) Tower base. *b) Rotor speed.*

Figure 3.7: Tower base longitudinal bending moment and rotor speed damage equivalent load evaluated with HAWC2. Load variation of *Tuning 1* and *Tuning 2* with respect to the reference tuning.

4 Conclusion

This report has presented two methods to systematically tune the gains of the PI pitch controller of the Basic DTU Wind Energy Controller. The first method is based on pole-placement technique and the second on fatigue loads reduction. Both methods require linear models of a wind turbine that are here obtained with HAWCStab2. These techniques are solved with numerical optimization.

The frequency placement method shows improvements compared to the state-of-the-art method but only when the model complexity is low. Including the rotor speed low pass filter in the tuning model improves the placement of the mode increasing the damping. However, when the model order increases, no significant improvements are noticed. Further investigations are required to better understand the interaction between the pole associated with the regulator and those associated with the dynamic inflow. Improvements in the gain-scheduling, such as a higher order scheduling function, could allow for better placement of the mode.

The fatigue based method has the advantage that it does not require any parameter decided a priori, since it is load based, therefore, better trade-off between tower loads and rotor speed regulation should be achieved. The tunings obtained with this techniques leads to lower tower loads at the price of compromising the rotor speed regulation in the first part of the operational region. The performances are evaluated by nonlinear time domain aeroservoelastic simulations.

Further analysis with the fatigue based techniques should be performed to identify if the reduction of the rotor speed variations at high wind speed can be limited to further reduce the tower loads.

However, these methods might be too slow to be used extensively for tuning applications. Only the pole-placement technique with the model that includes also the rotor speed filter improves the placement of the pole and gives results within few seconds, therefore it can be employed as a new tuning reference without compromising computational time.

No considerations on the actual load level have been done for the pole-placement technique. New investigations should focus on identifying better strategies than having the regulator mode frequency at the same value throughout the operational region.

Future analysis should focus on the integration of these techniques in a wind turbine optimization design procedure to perform concurrent rotor and controller design.

Bibliography

[1] Hansen MH, Hansen A, Larsen TJ, Øye S, Sørensen P, Fuglsang P. Control design for a pitch-regulated, variable speed wind turbine. *Technical Report Risø-R-1500(EN)*, Risø National Laboratory, 2005.

[2] Hansen MH. Aeroelastic optimization of MW wind turbines. *Technical Report Risø-R-1803(EN)*, Risø National Laboratory, 2011.

[3] Tibaldi C, Henriksen LC, Hansen MH, Bak C. Effects of gain-scheduling methods in a classical wind turbine controller on wind turbine aero-servo-elastic modes and loads. *32nd ASME Wind Energy Symposium*. American Institute of Aeronautics and Astronautics, 2014. doi: 10.2514/6.2014-0873.

[4] HAWCStab2 - Aeroservoelastic Analysis Code.
http://hawcstab2.vindenergi.dtu.dk.

[5] OpenMDAO. http://openmdao.org.

[6] Tibaldi C, Henriksen LC, Hansen MH, Bak C. Wind turbine fatigue damage evaluation based on a linear model and a spectral method. *Wind Energy*, 2014, doi: 10.1002/we.1898.

[7] The DTU 10MW Reference Wind Turbine project site. http://dtu-10mw-rwt.vindenergi.dtu.dk.

[8] Bak C, Zahle F, Bitsche R, Kim T, Yde A, Henriksen LC, Andersen PB, Natarajan A, Hansen MH Design and performance of a 10 MW wind turbine. *To be submitted* 2013.

[9] Bak C, Bitsche R, Yde A, Kim T, Hansen MH, Zahle F, Gaunaa M, Blasques JPAA, Døssing M, Wedel Heinen JJ, Behrens T. Light rotor: The 10-MW reference wind turbine. *Proceedings of EWEA 2012 - European Wind Energy Conference and Exhibition*, 2012.

[10] Hansen MH, Henriksen LC. Basic DTU Wind Energy controller. *Technical Report E-0028*, DTU Wind Energy, 2013.

[11] Henriksen LC, Hansen MH, and Poulsen NK. A simplified dynamic inflow model and its effect on the performance of free mean wind speed estimation. *Wind Energy* 2013; **16**(8): 1213–1224, doi: 10.1002/we.1548.

[12] Tibaldi C, Henriksen LC, Bak C. Investigation of the dependency of wind turbine loads on the simulation time. *proceedings of EWEA 2014*, 2014.

[13] Zahle F, Tibaldi C, Verelst DR, Bak C, Bitsche R, and Blasques JP. Aero-elastic optimization of a 10 MW wind turbine. *33rd ASME Wind Energy Symposium*. American Institute of Aeronautics and Astronautics, 2015.

[14] Welcome to HAWC2!. http://www.hawc2.dk.

[15] Larsen TJ, Hansen MA. How 2 HAWC2, the user's manual. *Technical Report Risø-R-1597(ver. 4-4)(EN)*, Risø National Laboratory, 2014.

[16] Hansen MH. Aeroelastic stability analysis of wind turbines using an eigenvalue approach. *Wind Energy* 2004; **7**(2):133–143, doi: 10.1002/we.116.

[17] Hansen MH. Aeroelastic properties of backward swept blades. *49th AIAA Aerospace Sciences Meeting including the New Horizons Forum and Aerospace Exposition*. American Institute of Aeronautics and Astronautics, 2011, doi: 10.2514/6.2011-260.

[18] Sønderby I, Hansen MH. Open-loop frequency response analysis of a wind turbine using a high-order linear aeroelastic model. *Wind Energy* 2014; **17**: 1147–1167, doi: 10.1002/we.1624.

[19] Moore KT, Naylor B, Gray JS. The development of an open-source framework for multidisciplinary analysis and optimization. *10th AIAA/ISSMO Multidisciplinary Analysis and Optimization Conference*. American Institute of Aeronautics and Astronautics, 2008.

[20] Gray JS, Moore KT, Naylor BA. OPENMDAO: An open source framework for multidisciplinary analysis and optimization. *13th AIAA/ISSMO Multidisciplinary Analysis and Optimization Conference*, American Institute of Aeronautics and Astronautics, 2010.

[21] Heath CM, Gray JS. OpenMDAO: Framework for flexible multidisciplinary design, analysis, and optimization methods. *8th AIAA Multidisciplinary Design Optimization Specialist Conference*, American Institute of Aeronautics and Astronautics, 2012.

[22] Perez RE, Jansen PW, Martins JRRA. pyOpt: a python-based object-oriented framework for nonlinear constrained optimization. *Structural and Multidisciplinary Optimization* 2012; **45**(1), 101–118. doi: 10.1007/s00158-011-0666-3

[23] Gill PE, Murray W, and Saunders MA. SNOPT 7 user's guide. *Technical Report Numerical Analysis Report NA 04-1*, Department of Mathematics, University of California, 2008.

[24] Gill PE, Murray W, Saunders MA. SNOPT: An SQP algorithm for large-scale constrained optimization (reprinted from SIAM journal optimization, vol 12, pg 979-1006, 2002). *Siam Review* 2005; **47**(1):99–131, doi: 10.1137/S0036144504446096.

DTU Wind Energy

DTU Wind Energy is a department of the Technical University of Denmark with a unique integration of research, education, innovation and public/private sector consulting in the field of wind energy. Our activities develop new opportunities and technology for the global and Danish exploitation of wind energy. Research focuses on key technical-scientific fields, which are central for the development, innovation and use of wind energy and provides the basis for advanced education at the education.

We have more than 230 staff members of which approximately 60 are PhD students. Research is conducted within 9 research programmes organized into three main topics: Wind energy systems, Wind turbine technology and Basics for wind energy.

Technical University of Denmark
DTU Vindenergi
Frederiksborgvej 399
Bygning 118
4000 Roskilde
Telefon 46 77 50 85
info@vindenergi.dtu.dk
www.vindenergi.dtu.dk